Final

CR 137528

AVAILABLE TO THE PUBLIC

Final Report

Covering the Period 1 May 1973 to 30 April 1974

STUDY TO DESIGN AND DEVELOP REMOTE MANIPULATOR SYSTEM

By J W HILL D E McGOVERN A J SWORD

Prepared for.

NATIONAL AERONAUTICS AND SPACE ADMINISTRATION
AMES RESEARCH CENTER
MOFFETT FIELD, CALIFORNIA 94035

CONTRACT NAS2-7507

STANFORD RESEARCH INSTITUTE
Menlo Park, California 94025 · U.S.A.

STANFORD RESEARCH INSTITUTE
Menlo Park, California 94025 • U.S.A.

Final Report *May 1974*

Covering the Period 1 May 1973 to 30 April 1974

STUDY TO DESIGN AND DEVELOP REMOTE MANIPULATOR SYSTEM

By. J W HILL D. E McGOVERN A J SWORD

Prepared for

NATIONAL AERONAUTICS AND SPACE ADMINISTRATION
AMES RESEARCH CENTER
MOFFETT FIELD, CALIFORNIA 94035

CONTRACT NAS2-7507

SRI Project 2583

Approved by

EARLE JONES, *Director*
Electronics and Bioengineering Laboratory

BONNAR COX, *Executive Director*
Information Science and Engineering Division

FOREWORD

This report was prepared by Stanford Research Institute under Contract NAS2-7507 monitored by James L. Jones, Ames Research Center, National Aeronautics and Space Administration, Moffett Field, California. The work of Douglas E. McGovern was supported by the Atomic Energy Commission on Sandia Laboratories' Doctoral Study Program at Stanford University. John W. Hill was project leader.

We would like to acknowledge the contributions of Mr. William Olson and Mr. Gerald A. Russell, who made many contributions to the fabrication and electronic assembly of the SRI end effector; Stephen J. Matthews, who was of tremendous help in running the experiments, aiding in the data reduction, and performing as a subject when needed; Antonly F. Ferrera, who helped develop and construct the tactile feedback interface unit, and J. R. Woodbury, who designed the range finder electronics.

ABSTRACT

This report describes several approaches to the modeling of human performance in remote manipulation tasks. The emphasis is on automated procedures using computers to analyze and count motions during a manipulation task. Performance is monitored by an on-line computer capable of measuring the joint angles of both master and slave and in some cases the trajectory and velocity of the hand itself. In this way the operator's strategies with different transmission delays, displays, tasks, and manipulators can be analyzed in detail for comparison. Some progress is described in obtaining a set of standard tasks and difficulty measures for evaluating manipulator performance: The goal of this work is to develop a model from which the difficulty and time required to perform an arbitrary manipulation task can be determined. To explain the degrading effects of control brace and manipulator on continuous tracking tasks, a describing function model of a man-manipulator system is developed that uses a noise generator. Remote sensing systems based both on touch and distance sensing are also described. A touch-sensing system uses proportional force sensors distributed over the remote hand to measure the overall force distribution of objects against the hand. A range sensor uses reflection from infrared light beams to identify the position of objects at a distance of a few centimeters to more than 20 centimeters in front of the hand.

CONTENTS

ILLUSTRATIONS

TABLES

I INTRODUCTION

This report covers a one-year research effort toward the development of (1) measurement techniques and tasks for evaluating man's manipulative performance and (2) remote sensing and display techniques to augment man's manipulative skills. Much of the work is a further development of the manipulator system previously described by Hill and Sword (1973).* The body of this report covers the work toward these objectives. Three papers based on this work have been presented at conferences and are reproduced in Appendices D, E, and F. The remaining five appendices describe techniques and instrumentation for computer-augmented teleoperator control and performance measurement.

The use of several performance indices in the time-delayed manipulation task of Section II and the tactile display evaluation task of Section III was made possible by an automated performance monitoring system developed on this project. Based on the changing joint angles of the master and slave, monitored by a small computer system, several new performance measurements were developed that are many times more stable than task time, the usual performance measure taken in these experiments.

Section II compares seven measures of performance in a time-delayed manipulation task. Preliminary results of the time delay experiment indicate that two new measures, MRATIO and MBAR, defined in the text, are almost an order of magnitude more sensitive than task time, the conventional measure, in determining performance changes in transmission delays in the range from 0.0 to 1.0 second. Taking advantage of the operator's

---

*References are listed at the end of this report.

move-and-wait strategy it is also shown how the energy consumed in carrying out a task can be reduced by a factor of three in the one-second transmission delay case.

In Section III the same seven measures are used to compare performance with and without tactile and visual-tactile displays in the usual master-slave control mode (no time delay). The results are useful in showing the relationship between the new performance measures with no time delay, even though there was little difference in performance with or without the displays.

Section IV describes the concept and implementation of a touch sensing and feedback system for manipulators. The touch sensing system uses proportional force sensors distributed over the hand to measure the overall force distribution of objects against the hand. Proportional force and torque sensors at the wrist measure the resultant of all the forces on the hand.

The compensatory tracking analysis of Section V proves the stability of the describing function approach to modeling human manipulation performance in continuous motion tasks. Results indicate that the linear model for the operator is relatively insensitive to changes in the amplitude and bandwidth of the command signal, and is nearly identical for one-, two-, and three-axis tracking. This last result strongly suggests that a human operator conducts his movements in at least a three-dimensional space and cannot give improved performance when restricted to fewer dimensions. Comparison between direct tracking with the human arm and through the Rancho remote manipulator shows a large change in both the linear model for the operator and his noise spectrum or remnant. The presence of the manipulator can be accounted for by a band-limited white noise of given amplitude in a simple model.

Section VI extends the usefulness of the task difficulty measures attributed to Fitts (1954) to realistic manipulation situations. Experiments carried out with the Rancho and Ames manipulators showed how an index of difficulty could be extended to both arms and two different tasks. The Ames manipulator was found to be 2.5 times faster than the Rancho on tasks of equal difficulty.

In Section VII, we describe a new approach to the measurement of performance in manipulation tasks. A portable performance monitoring system records master and slave joint angles as well as the position and velocity of the end effector in cartesian coordinates. Preliminary results with a set of standard tasks show trajectories of the hand in the work space. The goal of this work is to break down manipulation tasks into a set of fundamental "building block" tasks which can be described by simple difficulty measures. The building block tasks could be used to synthesize and hence predict performance on the more complex tasks that must be done with manipulators.

II COMPARISON OF SEVEN PERFORMANCE MEASURES IN A TIME DELAYED MANIPULATION TASK

A. Introduction

In communication systems with transmission delay, such as those used in exploration of the moon or the planets, direct control by human operators becomes a very slow and laborious process. The problem is that the operator cannot see the results of an action until some later time determined by the transmission delay. During this period, the environment may have changed, or a movement may have overshot the target. The operator is thus forced into a move-and-wait situation in which his moves are cautious and are punctuated with periods of waiting to see the results of his actions. Physical fatigue and frustration may compound the problem.

In experiments with a two-degree-of-freedom master-slave manipulator, Sheridan and Ferrell (1963) and Ferrell (1965) found that open-loop task measurements made with no transmission delay could be used to predict performance times with 1.0-, 2.1-, and 3.2-second time delays using a simple model. Experimenting with a six-degree-of-freedom manipulator, Blackmer et al. (1968) found only fair correspondence between task times with no transmission delay and those with 1-, 3-, and 6-second delays using the Ferrell (1965) model. With a six-degree-of-freedom manipulator, Black (1970) showed a high correlation between task time and the number of moves with a 3.5-second delay.

The preliminary study summarized in this paper was carried out to explore manipulation with a wide range of transmission delays. Shorter delays than those used in the previous studies (0.0, 0.3, and 1.0 second) were included to study the transition from continuous to the interrupted

"move-and-wait" strategy. Delays longer than those used in previous studies (10 seconds) were included to determine the magnitude of the attentive or steadying problems that would develop. Main departures of this work from the previous experiments are (1) that no particular movement strategy was imposed on the subjects, and (2) that an automated, rather than subjective, method of counting and timing moves was used.

B. A Complex Move-and-Wait Strategy

A time history of master moves and the subsequent slave moves is illustrated in Figure 1. A move is defined as the period of time between the beginning of a master move and the beginning of the subsequent master move. Each master move is considered to occur in three phases (Sheridan and Ferrell, 1963): move time, wait time, and reaction time, as defined below.

- M_m --Duration of master move.
- M_w --Time from end of master move to end of slave move.
- M_r --Time while master reacts to the consequences of his move and decides upon a subsequent move.

When a simple move-and-wait strategy is being used, the total task time can be expressed in terms of these times, using the following formula:

$$\text{Task Time} = \sum_{i=1}^{N} \left(M_{mi} + M_{wi} + M_{ri} \right) ,$$

where N is the total number of moves required to complete the task.

A complete description of the situation, however, requires the specification of both the system transmission delay and the slave-movement times defined below that correspond to the previous master move times.

- T_d--Round trip transmission delay
- S_r--Slave reaction time
- S_m--Duration of slave move
- S_w--Same as M_r.

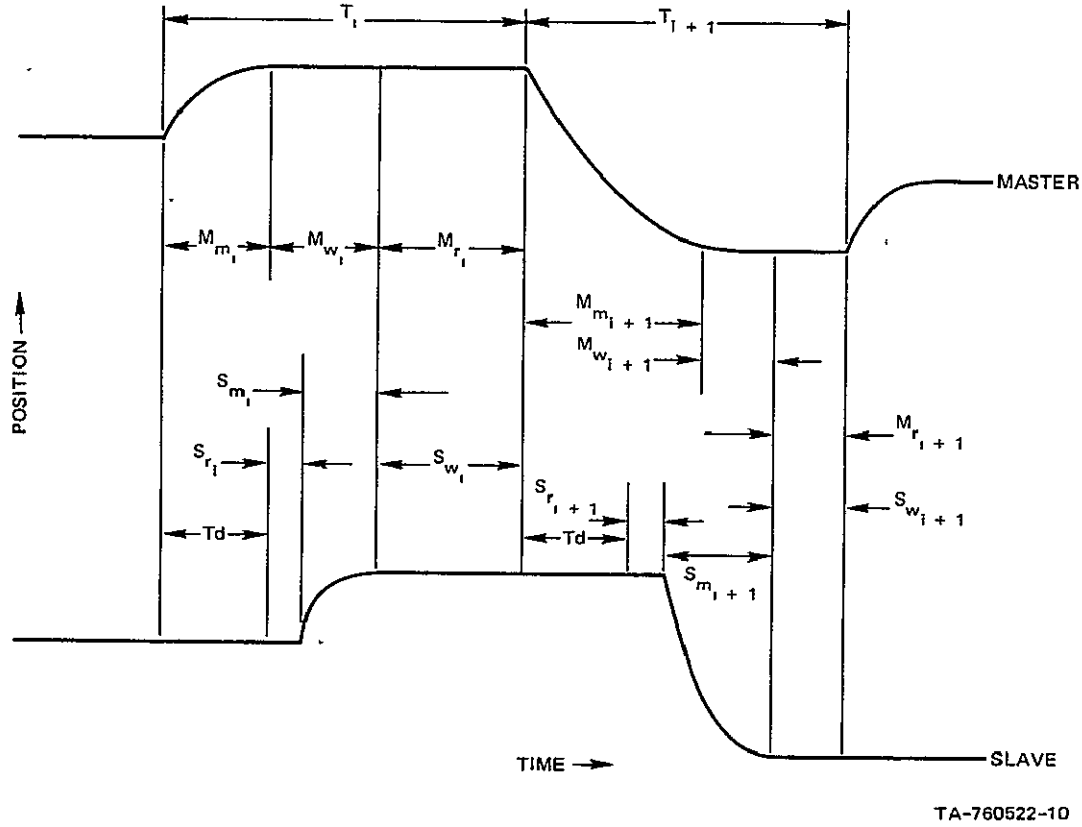

FIGURE 1 TIME HISTORY OF THE i^{th} AND THE $i + 1^{st}$ MOVES FOR A MOVE-AND-WAIT SITUATION

If the master follows a true move-and-wait strategy and does not move again until the slave has finished moving (simple move-and-wait strategy), the relationship shown in Figure 1 exists among the above quantities.

To investigate these quantities and their relationship, the transmission delay simulation of the supervisory control system described by Hill and Sword (1973) was used. Preliminary investigations with delays between

zero and five seconds indicated a considerable deviation from Sheridan and Ferrell's (1963) result; the simple move-and-wait strategy is not always followed. The longer the time delay, the more frequently complex moves are made before the result of the main move is evident. With a five-second time delay, for example, two or three moves are frequently given before their results are seen, as if the operator were impatient to see his results. In other cases, he overreaches his target and makes a second move while the first move is in progress. Examples of both simple and complex moves are indicated in the chart recording of Figure 2, obtained with the chart recorder monitor described by Hill and Sword (1973).

C. Mini-Computer-Based Performance Monitor

A minicomputer-based performance monitor package was created to study (1) the complex move-and-wait strategy, and (2) the movement and waiting times with different transmission delays. A series of computer programs are used to measure and tabulate the movement and waiting times with considerably greater accuracy and reliability than is possible for a human observer with a stop watch.

The performance monitor package consists of an on-line program for data logging and several off-line programs for numerical analysis. During the experimental runs, a high-speed disk memory logs on-line data. After the experiment is completed the data are copied to magnetic tape for permanent storage. Different off-line programs are used to search the log and to extract the desired performance indices.

The on-line performance logger detects the beginning and end of moves by using derivatives of the individual joint angles. In total, 14 derivatives (seven master- and seven slave-joint angles) are updated and digitally filtered every 1/30th of a second. If any of the master or slave joints exceeds a predetermined threshold for motion during a 1/30-second period,

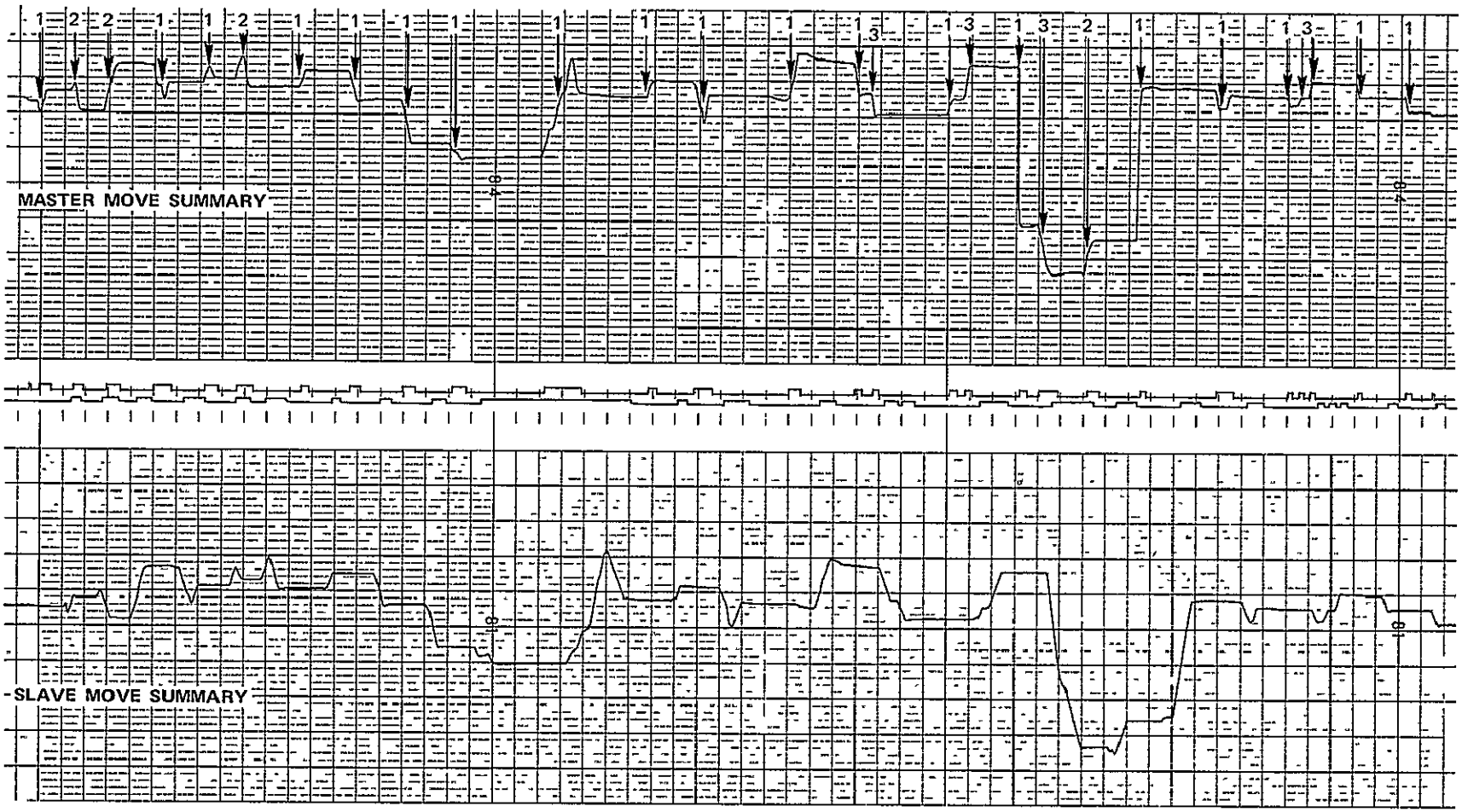

FIGURE 2 RECORD OF MASTER AND SLAVE MOVES WITH THREE-SECOND TIME DELAY

Master moves denoted by arrows are labeled according to slave motion: 1 indicates move while slave stationary (simple move-and-wait), 2 indicates move while slave moving (move-while-moving), and 3 indicates an additional move before result of first move seen (complex move-and-wait) (One time division = 2.5 seconds.)

a note of the fact is made in separate master- and slave-move detection queues. These queues (software shift registers) record whether or not a move was detected during 12 successive 1/30-second intervals. From these intermediate data, decisions are made to determine whether a master or slave move has begun or ended. The criteria for detecting the beginnings and ends of moves that have proved successful are defined below:

- Move criterion. A move begins when the velocity threshold is exceeded during the current 1/30-second interval and will be exceeded on five of the next 12 intervals.
- Done criterion. A move is done when the velocity threshold is not exceeded during the current interval and will not be exceeded more than once in the next 12 intervals.

Two total task measurements are also obtained. The on-line program counts the number of 1/30-second intervals taken to complete a task and logs the total at the end to permit the calculation of task duration. Additionally, it accumulates the current delivered by the 24-volt servo power supply every 1/30th of a second and logs the total at the end of the run to permit calculation of the total energy consumed.

One off-line program searches the data-log to calculate the following seven different measures for each test run:

M-MOVES	Number of master moves
S-MOVES	Number of slave moves
ENERGY	Total task energy consumed
TIME	Total task time
MTIME	Total time during which the master was moving
MRATIO	MTIME/TIME, or the fraction of task time the master was moving
MBAR	MTIME/M-MOVES, or the mean time per move.

A second program can be used to determine the distribution of movement times from a particular set of test runs. Any of the master- or slave-movement times defined in Figure 1 can be analyzed. Details of the on-line and off-line analysis procedures are given by Hill and Sword (1974).

The experiment is arranged in a 3 × 5 × 2 factorial design, as shown in Figure 3. Each cell in the design represents a performance characteristic measured on two subjects in eleven repetitions of the task.

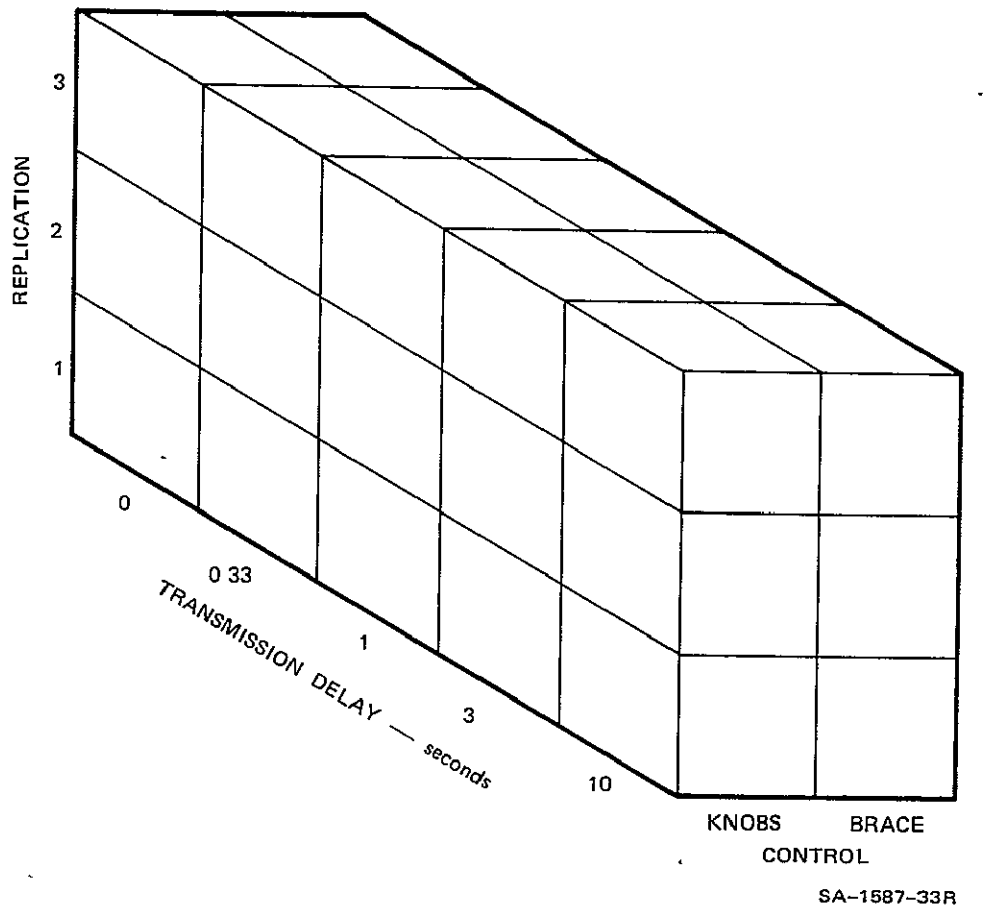

FIGURE 3 DESIGN OF THE PILOT TIME DELAY EXPERIMENT

The experiment variables are (1) manual control mode, (2) transmission delay, and (3) replication, as indicated in Figure 3. The manual

control mode is varied by use of either the Rancho master brace or a bank of six potentiometers. Transmission delays from zero to ten seconds are provided in both control conditions, and in all replications by using the 30-Hz delay line simulation (Hill and Sword, 1973). Direct viewing was used, and audio cues were provided in all experimental cases.

1. Apparatus

The Rancho arm and computer-augmented control system described by Hill and Sword (1973) in Section II of Reference 1 were used for this experiment. The control modes were solely manual, master-slave modes. No sensory feedback other than direct vision was provided to the operator. The task was to pick up a block randomly placed within the arm workspace and deposit it in a small container.

2. Subjects

Two male subjects, LM and SM, were used for this experiment. Both had had considerable experience in using the manual control modes for a pickup task. However, neither subject had ever attempted the task with a transmission delay.

3. Procedure

The on-line performance logger is started by the experimenter when the end effector passes through a plane one foot above the table top on the way down to grasp the object. The experimenter detects the plane crossing by observing a pointer attached to a string running over a pulley on the ceiling attached to the end effector. The task is complete when the object is grasped and deposited in the receptacle about one foot away, and the end effector moves up above the plane. Simultaneously, the experimenter stops the performance logger by typing a letter on the control

teletype. The difficulty of both the pickup and drop tasks is about 3.5 bits.

In a single replication, each subject performed 10 runs consisting of 11 repetitions each. Five runs, each corresponding to one of the transmission delays, were performed, using each of the two control modes. This sequence was repeated three times for each subject (three replications). In all, each subject made 330 individual pickups.

D. Results

The average number of master moves per pickup as a function of transmission delay is shown in Figure 4.

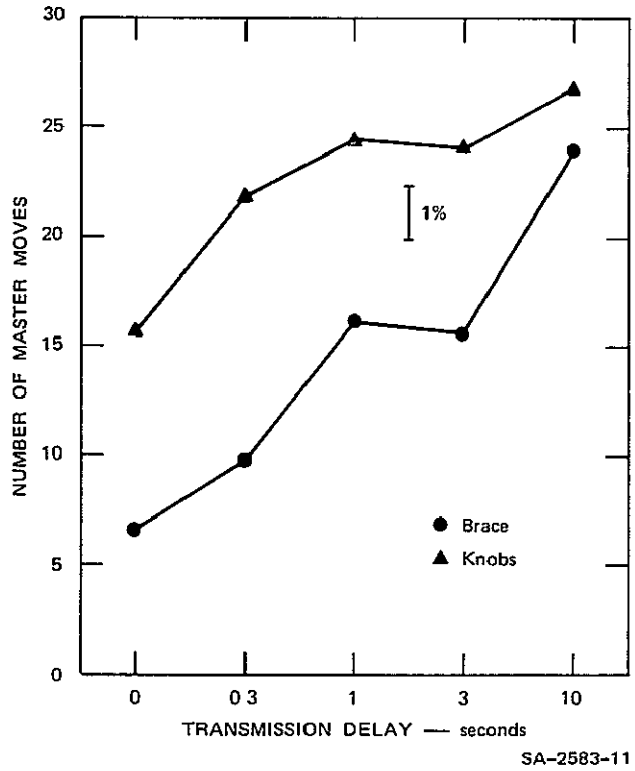

FIGURE 4 NUMBER OF MASTER MOVES IN TIME DELAY EXPERIMENT

The increasing number of moves suggests that in the zero- to one-second time-delay region, the control strategy is being continuously changed from continuous control to the move-and-wait strategy. Between the one- to three-second delay region, the number of moves is constant, suggesting a constant move-and-wait strategy; and at 10-seconds' delay, problems of holding the brace stationary for such a long time cause an increasing, perhaps unintentional, number of brace moves. In going from three to ten seconds, the number of knob-generated moves does not increase as much as the number of brace-generated moves. If the time delay were increased much beyond ten seconds, the knobs would become the preferred control mode. The constant number of moves in the one- to three-second range agrees with the results of Sheridan and Ferrell (1963), and Ferrell (1965), who explored only this range. Outside this range, however, different explanations must hold.

Two other measures, task time and the time spent moving the master, are both shown for comparison in Figure 5. Whereas the task time increases

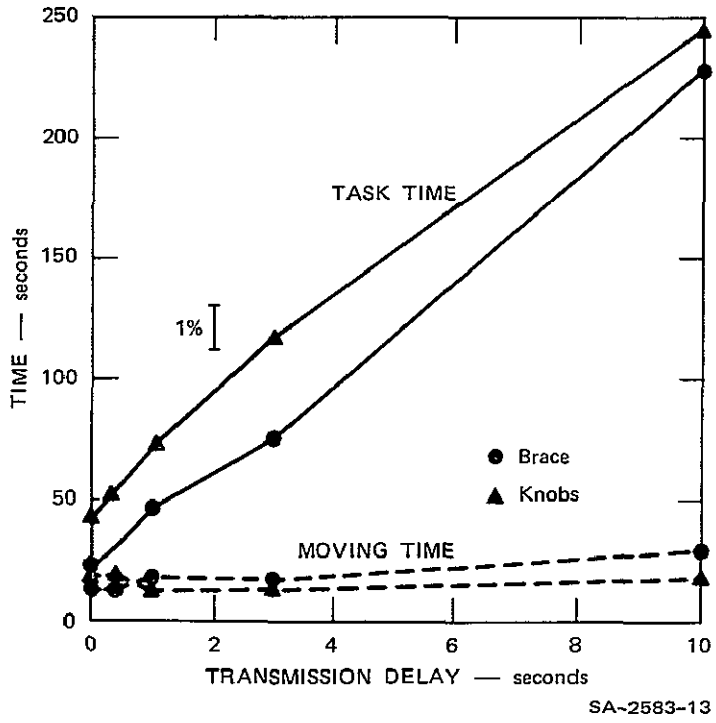

FIGURE 5 TASK TIME AND MOVING TIME IN THE TIME DELAY EXPERIMENT

almost directly with the time delay, the moving time is nearly constant at about 20 seconds, independent of time delay. The task time with the control brace can be simply modeled as a fixed time of 20 seconds plus 20 additional seconds for every second of transmission delay:

$$TIME_b = 20 + 20 \text{ (transmission delay)} \quad . \qquad (1)$$

The additional time (or cost) for using the simpler control source (knobs instead of brace) is roughly 25 seconds, giving:

$$TIME_k = 45 + 20 \text{ (transmission delay)} \quad . \qquad (2)$$

An expanded plot of the relatively constant moving time is given in Figure 6. It can be seen that there is a statistically significant cross-over of moving times between 0.3- and 1.0-second-transmission delay, and very large increase in brace-moving time with the 10-second delay. While the percentage changes in moving time are small compared to the other performance measures, the statistically significant crossover between 0.3- and 1.0-second delay (with less moving time for the brace at small delays, and less moving time for knobs at large delays), may be the result of a changeover from the continuous to the move-and-wait strategy in this range of time delays.

When the moving time is divided by the task time, we have the proportion of time moving; or by multiplying by 100, the percentage of time moving. This ratio, which turns out to be an exceedingly stable measure of performance, is shown for this experiment in Figure 7. In addition to the low variance of this measurement, two surprising results are indicated in Figure 7. Looking at the intercept at zero time delays, we see that only about half of the time is spent moving in this condition.

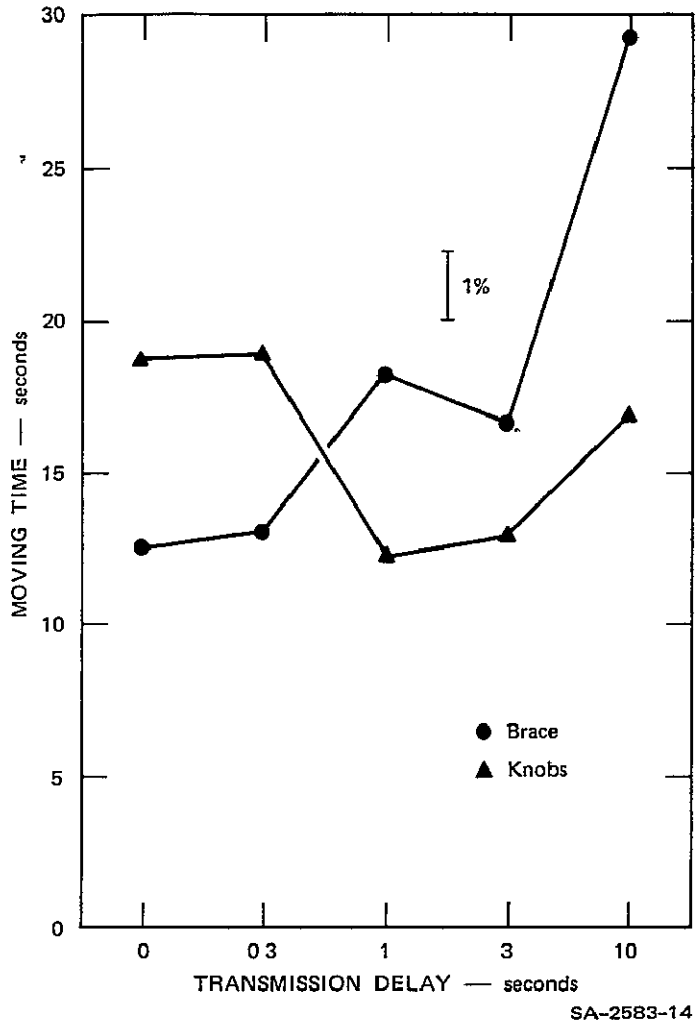

FIGURE 6 TOTAL MOVING TIME IN THE TIME DELAY EXPERIMENT

Previously it has been assumed that in the zero time-delay condition the master brace was continuously moving. The low percentage of time moving (57 percent), together with the fact that there are about five brace moves during the task with zero time delay, tells us that there are several waits and that the waits are nearly as long as the moves. There are several possible alternative reasons for the apparent pauses (move-and-wait strategy) measured at zero-transmission delay. One reason may be inadequacy of the on-line performance logger. In this case, the velocity threshold used to determine whether the master is moving may be too high. Another explanation may be that the master was moved quickly

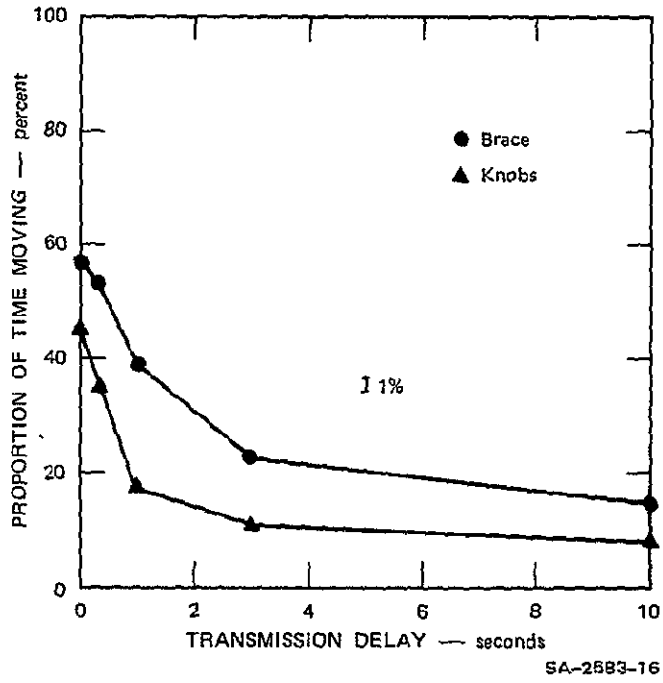

FIGURE 7 PERCENTAGE OF TIME MOVING IN THE TIME DELAY EXPERIMENT

and the slowly responding slave was still moving. In this second case, the operator would be waiting for the slave to come to rest before making another move. A third explanation may be that control with the brace is somewhat more difficult than has been thought, and that there is a time necessary at major-move points during the task, when the operator actually hesitates while deciding which joints to move next to produce the desired action.

Another surprising feature of the moving ratio of Figure 7 is that as the transmission delay increases, the curves do not approach their asymptote as the reciprocal of the delay. The reciprocal relation would be predicted by the simple move-and-wait strategy of Sheridan and Ferrell (1963). The failure to hold with this relation is roughly a factor of two in the moving time ratios shown in Figure 7.

The reductions in the moving ratio with short transmission delays, in three replications of the experiment shown in Figure 8, suggest that

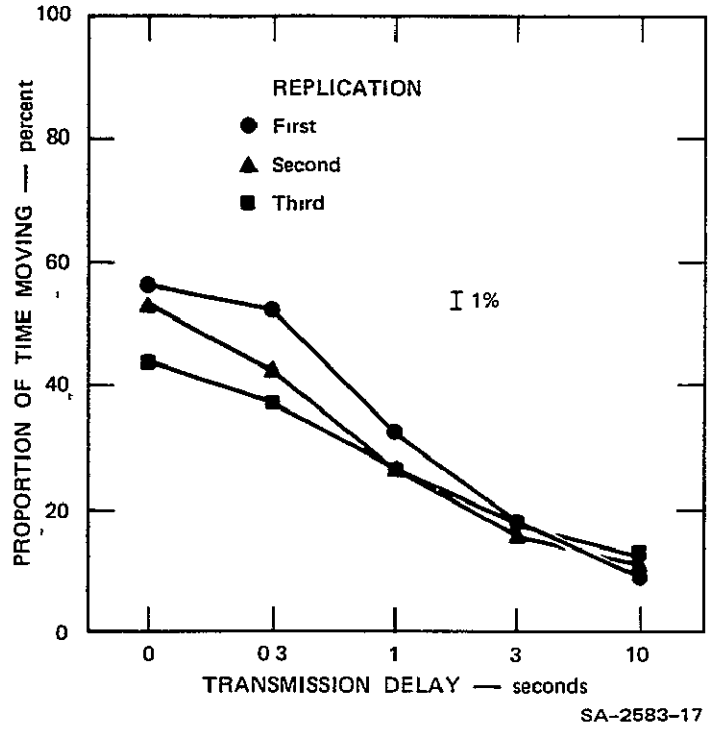

FIGURE 8 PERCENTAGE OF TIME MOVING FOR THE THREE REPLICATIONS OF THE EXPERIMENT

the second of the above-mentioned three reasons explains the low moving ratios observed. Since the moving ratio decreases with practice, and the task time also decreases with practice, the first and third explanations are ruled out. The hypothesis that the long wait times are due to the operator's waiting for the slave to catch up with the master can be tested by further processing of the data taken.

The mean move-time results shown in Figure 9 suggest that the time required to make a single move with the knobs is half that of the control brace, independent of time delay. As was shown previously in Figure 4, however, a larger number of control movements are made with the knobs than the brace. Multiplying movement time by the number of control moves gives the relatively constant total moving time of Figure 6.

For both brace and knobs, the mean time per move decreases as the transmission delay is increased to one second, is constant with one- and three-second delays, and finally begins to increase slightly with ten

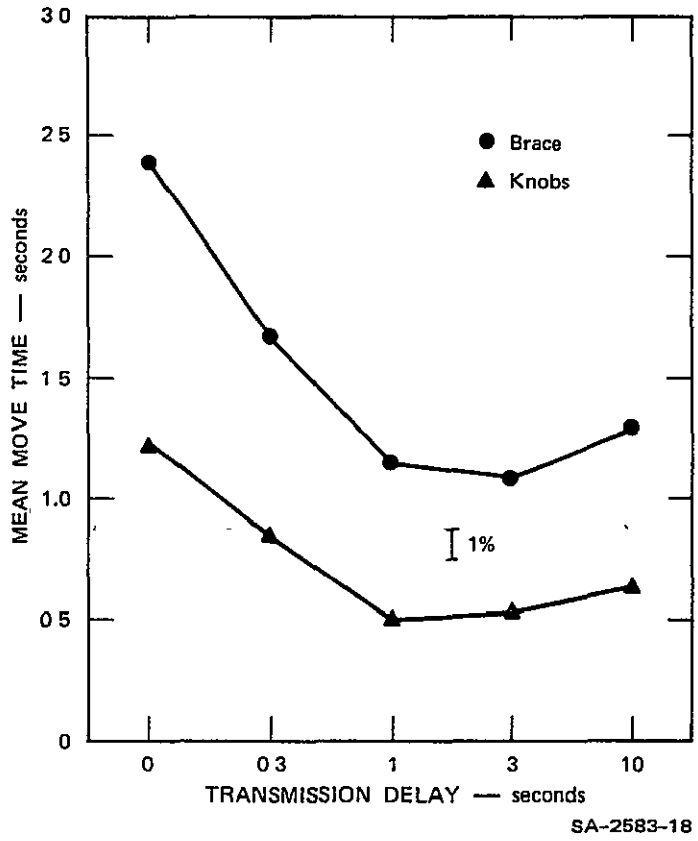

FIGURE 9 MEAN MOVE TIME IN THE TIME DELAY EXPERIMENT

seconds' delay. These changes are very similar to those seen in the number of master moves shown in Figure 7. For both curves, the changes seen over the first second of transmission delay reflect the increasing use of the move-and-wait strategy, and the constancy for delays of one second or longer reflects a fairly consistent move-and-wait strategy.

E. Energy Consumed and a Scheme for Reducing It

The energy consumed by the slave arm in carrying out the pickup task is shown in Figure 10. The energy consumption with increasing time delay is linear for both knob and brace control, and is very similar to the task-time results shown in Figure 3. The crossover between brace and

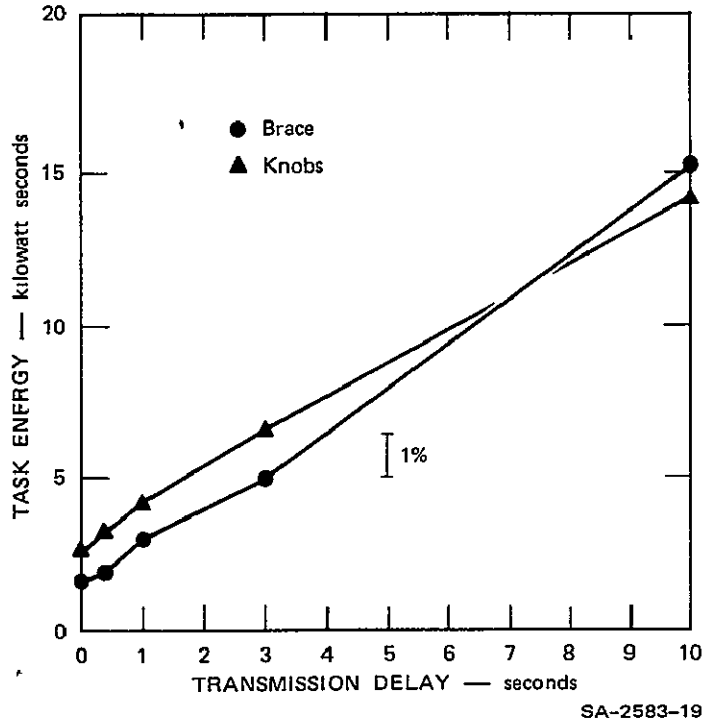

FIGURE 10 ELECTRICAL ENERGY CONSUMED IN THE TIME DELAY EXPERIMENT

knobs at the 10.0-second delay in Figure 9 is not statistically significant, and the energy consumed (in kilowatt seconds) for brace and knob control can be modeled as

$$\text{Energy}_b = 2 + 1.2\ (\text{transmission delay}) \quad . \quad . \qquad (4)$$

$$\text{Energy}_k = 3 + 1.2\ (\text{transmission delay}) \quad . \qquad (5)$$

The price for using the simpler control source (the knobs) is an additional kilowatt second.

Combining the relationship of the task time to transmission delay [Eqs. (1) and (2)] with the very similar relationship of energy to transmission delay [Eqs. (4) and (5)], we may express task energy in terms of task time for brace and knob control as

$$\text{Energy}_b = 0.8 + 0.06 \text{ (task time)} \quad . \qquad (6)$$

$$\text{Energy}_k = 0.3 + 0.06 \text{ (task time)} \quad . . \qquad (7)$$

With the simple master-slave control scheme used in the laboratory, more energy is consumed in carrying out the same task as the transmission delay becomes greater. By using our knowledge that the total moving time for the task is relatively constant, even though the task time increases greatly with transmission delay (the difference between the task and moving time of Figure 3), we may design a remote control system that only requires a fixed amount of energy for a task, no matter what the delay. This can be accomplished by simply cutting off the power at the slave arm whenever it is at rest. Such a modification, taking advantage of the move-and-wait strategy to conserve power, could be implemented with individual threshold circuits on each joint, each circuit capable of turning off the servoamplifier whenever the error was less than a preset level.

F. Distribution of Movement Times

Using the off-line histogram program, we measured and tabulated the durations of the moving times. Ten distributions were obtained, one for each of the five time delays and each of the two control modes, by combining the data of the two subjects and the three replications of the experiment. These results are shown in Figures 11 and 12. The total number of moves under each curve and the mean moving time for each curve is given in Table 1.

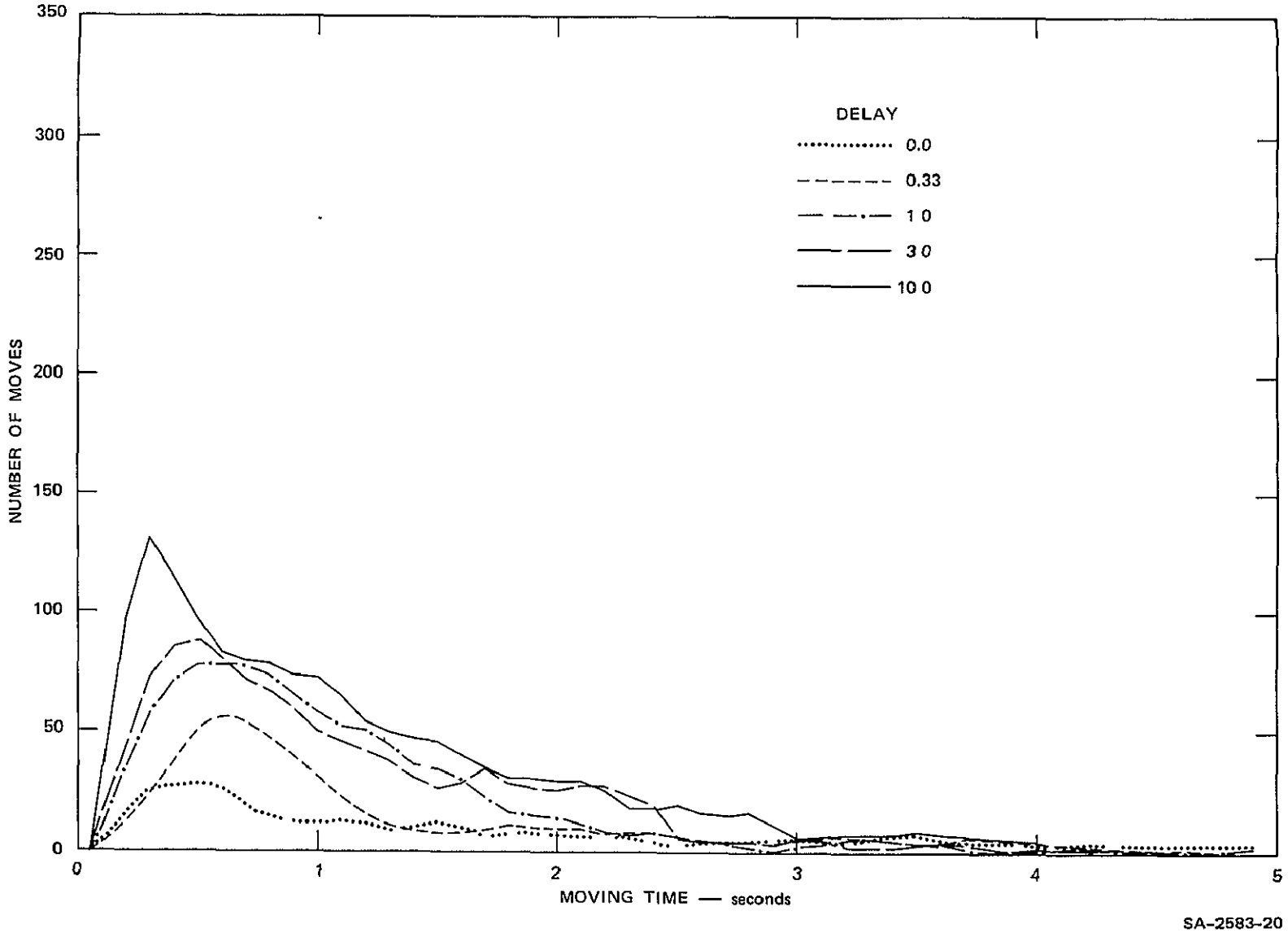

FIGURE 11 DISTRIBUTION OF MOVING TIMES WITH BRACE CONTROL

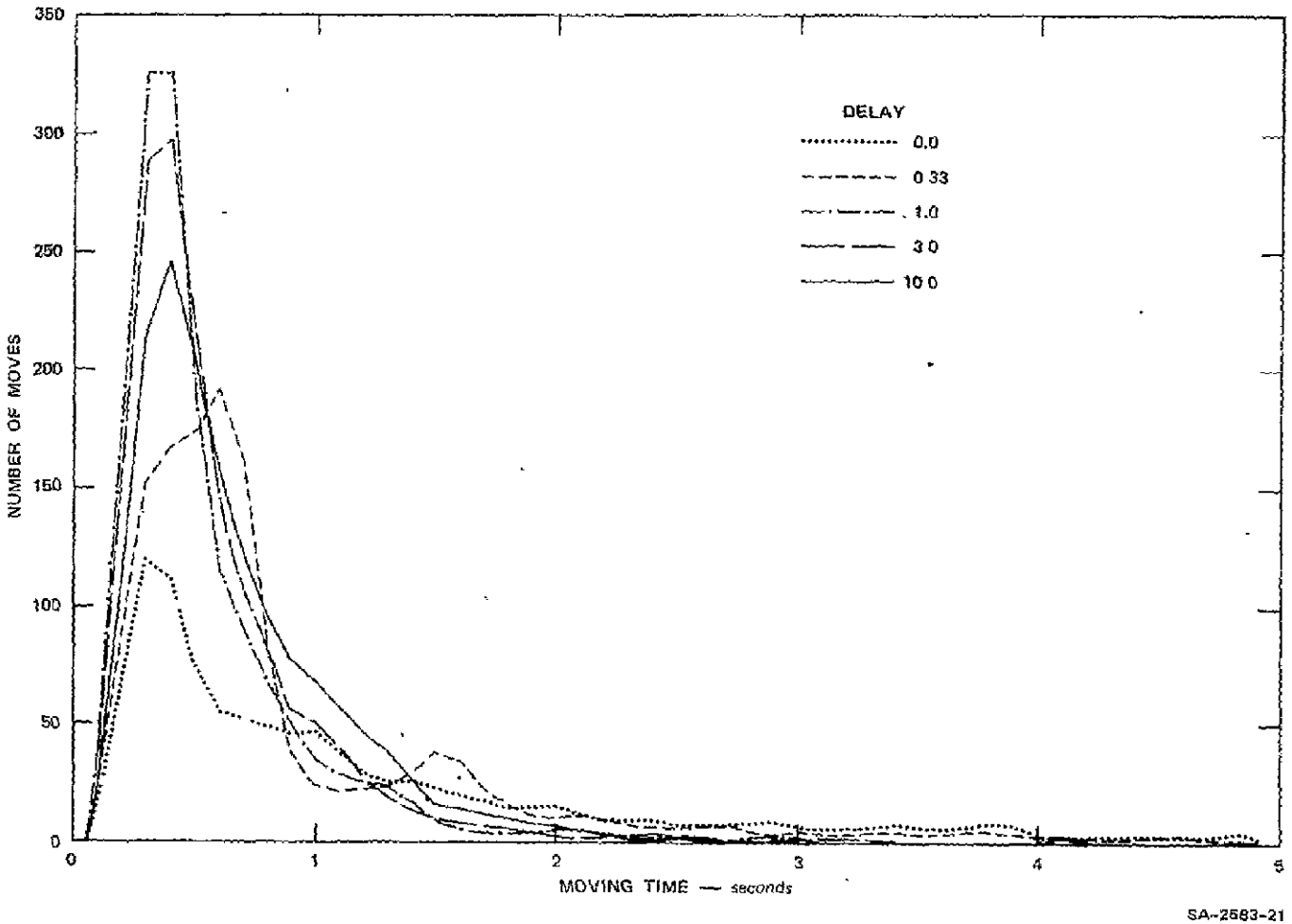

FIGURE 12 DISTRIBUTION OF MOVING TIMES WITH KNOB CONTROL

Table 1

TOTAL NUMBER OF MOVES AND MEAN MOVING TIME
FOR THE PILOT TIME DELAY EXPERIMENT

Control	Delay	Moves	Mean Move Time
Brace	0.0	427	1.938
	0.33	643	1.542
	1.0	1044	1.135
	3.0	1056	1.059
	10.0	1581	1.224
Knobs	0.0	1033	1.188
	0.33	1448	0.861
	1.0	1570	0.505
	3.0	1607	0.532
	10.0	1567	0.630

Several changes are obvious from the curves and data of Table 1. As the transmission delay increases, so does the number of moves of duration shorter than 0.5 second, with both knob and brace control. On the other hand, the number of moves longer than 2.0 seconds decreases with knob control, but increases with brace control, as the transmission delay increases. These differences may be due to the great increase in total moves (270 percent) with brace, and small increase with knobs (52 percent), as the transmission delay goes from 0.0 to 10.0 seconds.

A surprising feature of the brace-moving time distributions is the constancy of the shape of the distribution with increasing time delay. It has been assumed previously that going from continuous to delayed conditions caused the operator to change from continuous moving to abrupt, short moves and ensuing waits. The results of Figure 11, however, show that the moving times are very similar for continuous and time-delayed operation. There is a large proportion of long moves (two seconds or more) for all time delays.

The distribution of knob moves better fits the stereotyped change from continuous to move-and-wait strategy. These distributions (see Figure 12) can be visually broken down into the sum of two distributions, one peaking between 0.4 and 0.5 seconds, and a second continuous, long-tailed distribution similar to that of the brace distribution of Figure 11. As the time delay increases, the area under the peaked distribution greatly increases, while the amplitude of the long-tailed distribution greatly decreases.

G. Comparison of Seven Different Performance Measures

An analysis of variance was made on each of the performance measures to determine their ability to distinguish between the four experimental variables: test subjects, replications, means of control, and time delays. The results of these analyses, summarized in Table 2, show that a large number of the variables and their interactions are statistically significant.

In addition to being a test of the null hypothesis for each variable, the F-ratios given in Table 2 are figures of merit for determining which of the seven measures best indicates changes from a particular variable or combination of variables. For a good performance measure, we want (1) large changes (large variance) in the measure with an experimental variable; and (2) small changes (small variance) in repeated measurements with the same conditions. The F-ratio is the ratio of the variance attributed to an experimental variable divided by the variance in repeated measurements. Thus, the larger the F-ratio, the better a measure distinguishes between experimental variables.

With the F-ratio used as a figure of merit, the largest F-ratio for each of the 15 sources of variation given in Table 2 is marked with a rectangular box. Surveying the seven performance measures indicates that

Table 2

SUMMARY OF SEVEN ANALYSES OF VARIANCE OF THE SEVEN MEASURES TAKEN IN THE PRELIMINARY TIME DELAY EXPERIMENT

Missing entries have F-values less than that given in the rightmost column and are not significant at the 0.01 level.

Source of Variation	df	M-MOVES	S-MOVES	ENERGY	TIME	MTIME	MRATIO	MBAR	$F_{0.01}$
Subjects (S)	1	7.71	--	--	11.50	--	8.97	--	6.63
Replication (R)	2	21.84	14.44	--	21.23	48.88	48.72	37.64	4.61
Control (C)	1	194.03	156.32	--	33.95	18.27	722.25	658.30	6.63
Delay (D)	4	65.99	54.12	194.43	282.21	29.65	897.38	213.34	3.32
S X R	2	--	--	--	--	--	--	--	4.61
S X C	1	--	--	--	--	--	--	--	6.63
S X D	4	--	--	--	4.99	--	5.14	--	3.32
R X C	2	4.83	--	7.58	5.71	5.85	16.76	9.93	4.61
R X D	8	--	--	--	5.71	3.43	16.17	17.83	2.51
C X D	4	6.61	--	--	--	35.66	25.96	13.34	3.32
S X R X C	2	--	--	--	--	--	8.65	--	4.61
S X R X D	8	--	--	--	--	--	--	--	2.51
S X C X D	4	--	--	5.52	5.82	--	--	--	3.32
R X C X D	8	--	2.95	--	--	4.43	4.38	11.23	2.51
S X R X C X D	8	2.87	--	--	--	--	--	--	2.51
Within repetitions	600								

only five rank largest in some source of variation; and of these, only three claim the great majority of the largest F-ratios. The three most important measures, in decreasing rank, are

- Moving ratio
- Total moving time
- Task time.

These results indicate that different measurements should be made, depending on which experimental conditions it is desirable to compare. For example, differences between subjects are best measured with task time (TIME); and differences between control source are best measured with moving time (MTIME), or mean movement time (MBAR).

Another way of ranking the experimental variables is by the total variance attributed to each. This ratio lumps the test conditions and their interactions into one figure of merit and indicates for the experiment as a whole which measurement is best. The resulting variance ratios, given in Table 3, indicate that the MRATIO is clearly the best measurement, and that MBAR and TIME are the second best. For the experiment as a whole, MRATIO, the fraction of time moving, is by far the most sensitive measurement.

H. Correlations Between the Seven Performance Measures

Frequently two or more measures change nearly identically with the experimental variables. For example, the task time and the energy consumed both vary similarly for the different time delays and control sources. To determine the relation between the seven performance measures the pairwise correlation* coefficients based on all 660 measured values of each variable were computed. The results are shown in Table 4 as an

---

*Pearson correlations, $r = \sigma_{xy}/\sigma_x \sigma_y$.

Table 3

TOTAL EXPERIMENTAL VARIANCE
DIVIDED BY ERROR VARIANCE

Variable	Variance Ratio
M-MOVES	12.06
S-MOVES	8.31
ENERGY	14.97
TIME	23.00
MTIME	8.03
MRATIO	81.09
MBAR	28.63

array of correlation coefficients. Some interesting relations between variables shown in the correlation coefficients are mentioned below.

- The number of master and slave moves (M-MOVES and S-MOVES) are, as we might expect, highly correlated (r = 0.961); and we may consider that either of these two variables measures changes in the other. We recommend selecting the number of master moves as a performance measure and not being concerned with the number of slave moves.

- Task time and energy consumed are also highly correlated (r = 0.913), and we may similarly choose either of these variables as representative of the changes measured by the other. As time has been measured in these experiments as a matter of course, and is easy to measure without sophisticated equipment, we think time is a better measure of performance than energy. It is possible to express energy in terms of time, using the equations given previously in the discussion of energy.

- The last three variables, MTIME, MRATIO, and MBAR, correlate poorly with each other and with the other variables in the experiment.

- The total moving time, MTIME, does not correlate statistically with MRATIO or MBAR ($p > 0.01$), which indicates that the total moving time measures a performance characteristic that is independent of these other two variables.

This analysis shows that the number of performance measures can be reduced because of high correlations between some of the measures. Both the number of slave moves and the energy consumed may be omitted because of their high similarity to other measures. Taking the two measures

Table 4

CORRELATION COEFFICIENTS BETWEEN VARIABLES IN THE PRELIMINARY TIME DELAY EXPERIMENT

Coefficients not significant at the 0.01 level are designated by 0.

Variable	S-MOVES	ENERGY	TIME	MTIME	MRATIO	MBAR
M-MOVES	0.961	0.645	0.721	0.663	-0.525	-0.521
S-MOVES	--	0.645	0.707	0.607	-0.514	-0.491
ENERGY	--	--	0.913	0.532	-0.548	-0.240
TIME	--	--	--	0.530	-0.598	-0.289
MTIME	--	--	--	--	0	0
MRATIO	--	--	--	--	--	0.716

M-MOVES and TIME together with any one of the remaining three (MTIME, MRATIO, and MBAR), we may reproduce any of the others. This is true because of the relations between the variables as they are defined on the first page of this section. Because of its low variation, the choice of MRATIO (MTIME divided by TIME) as the third variable to complement M-MOVES and TIME seems a natural choice. As a consequence, three measurements, M-MOVES, TIME, and MRATIO are recommended as a complete description of time-delayed performance.

I. Choice of Measures for Future Experiments with a Transmission Delay

Though the range of delays used in this experiment varied from 0.0 to 10.0 seconds, the main purpose in analyzing it was to determine the ranges and usefulness of several performance measures in the transmission delay range from 0.0 to 1.0 second. These results will be used to design the main transmission-delay experiment, which will have a finer gradation of delay within this range.

To compare the seven different performance measures in the delay range from 0.0 to 1.0 second, certain measurements obtained with the control brace for two subjects are given in Table 5. The table presents in successive columns measurements taken with no delay and with 1.0 second delay; the percentage change of the measurements in going from 0.0 to 1.0 second delay, and the change measured in standard deviations in going from 0.0 to 1.0 second delay. A desirable feature of a performance measure is a large percentage change in going from one case to another. A more valuable feature, however, particularly for statistical comparison and hypothesis testing, is the change measured in standard deviations.

On the basis of the previous correlation analysis and the change in standard deviations from Table 5, the following conclusions may be made regarding measurements to be taken on the main transmission-delay experiment.

- M-MOVES is a better measure than S-MOVES (both are highly correlated), because of the greater change in standard deviations.
- TIME is a better measure than ENERGY (both are highly correlated), for the above reason.
- Neither TIME nor ENERGY is a really good statistical measure of performance, because of their low change in standard deviations over this delay range. TIME should be included in the analysis for comparison with results of past experiments.
- Of the last three new measures, MRATIO and MBAR are most reliable of all, showing larger changes (measured in standard deviations) than any of the other variables.
- MBAR, the mean move time, is by far the best measure, showing an overall change of more than two to one (the highest, except for M-MOVES), and by far the most reliable, with a change of 26 standard deviations.

Table 5

COMPARISON OF SEVEN DIFFERENT MEASURES OF PERFORMANCE WITH THE CONTROL BRACE AT ZERO AND ONE SECOND DELAY

Variable	$\Delta T = 0$	$\Delta T = 1$	Percentage Change	Change in Standard Deviations
M-MOVES	6.47	16.22	150	10.4
S-MOVES	5.47	13.53	147	8.9
ENERGY (kW-s)	1.56	3.05	95	2.8
TIME (s)	22.56	46.76	107	3.4
MTIME (s)	12.49	18.22	45	6.4
MRATIO	0.56	0.39	-31	-22.1
MBAR (s)	2.40	1.14	-52	-26.3

III EXPLORATORY EVALUATION OF A TOUCH FEEDBACK SYSTEM

To evaluate the usefulness of the touch sensing and feedback system reported by Hill and Sword (1973), the experiment described in this section was carried out. The experiment is designed to answer questions about the value of touch feedback under different viewing conditions. We would like to find objective performance indices of the savings in task time, or the reduction of drops and fumbles that would occur in a given situation.

A. Experimental Method

1. Design

In conjunction with the on-line performance measuring system described in Appendix G, a factorial design with three feedback and three viewing conditions was used. The three tactile display conditions are:

- F_o--No feedback. No information from the touch sensors is presented to the operator.
- F_t--Tactile feedback. The tactile display system consisting of two bimorph displays and an air-jet contact display is provided to the operator.
- F_v--Visual feedback. The CRT moving jaw display of the touch sensors is provided to the operator.

The three viewing conditions of this experiment are:

- V_d--Direct viewing. The operator views the scene directly from a position about two meters away.
- V_{tv}--TV viewing. A closed-circuit, broadcast-quality TV system is interposed.
- V_{tv+n}--Noisy TV viewing. Same as T_{tv}, except that a white noise is added to the video (S/N = 0 dB).

2. Subjects

Two male subjects were paid for their services. Both subjects practiced all conditions of this task until their task completion times stabilized. Each subject participated in this experiment approximately two hours per day.

3. Procedure

The three viewing conditions and three feedback conditions define a 3 × 3 factorial experimental design, as shown in Figure 13. Each cell of the design, representing a single viewing and feedback condition, consists of 10 repeated block pickups. The operator's task in each case is to pick up an object (a block or latch) and move it away. Performance measurements are made using the capabilities of the LINC-8 performance monitor described in Appendix G. To ensure that the order in which these nine conditions are carried out minimizes the bias on the experimental results because of continuously improving performance, the conditions are ordered using a Graeco-Latin square technique. In this way, gradual effects will not bias any viewing or feedback condition.

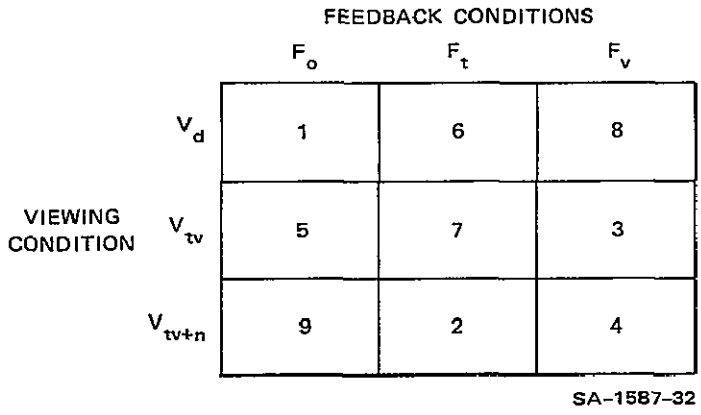

FIGURE 13 DESIGN FOR TOUCH FEEDBACK EXPERIMENT

Two replications of the design shown in Figure 13 were made by each subject. The first replication was made with the conditions ordered as the cell numbers of Figure 13; the second replication was made with the reverse order.

When the viewing and feedback conditions are set up, the experimenter starts the on-line performance monitor as described in Appendix G. When the computer has initialized the appropriate file and is ready, a bell is rung signaling the subject to begin. When he has successfully retrieved the block and brought it back past a marker post, the experimenter signals the computer to stop monitoring and to print out run time and power consumed.

Because of the great deal of processing time taken by the computer-generated CRT-display of tactile information, the performance monitor and CRT display could not be run simultaneously. Therefore, task times measured with a stopwatch were taken throughout the experiment to compare the CRT display, tactile display, and no display conditions. The stopwatch measurements are given a 3×3 factorial analysis in Part B of this section. In the automated measurements (Parts C, D, and E of this section, only the presence and absence of the tactile display are compared in 2×3 analyses.

B. Analysis of the Stopwatch Times for the Complete Experiment

The stopwatch task times were given an analysis of variance to determine how they were influenced by the four control variables. The summary of the results is given in Table 6. There is insufficient evidence to show that the results depend on other than a few variables or combinations of variables. A first examination of Table 6 shows that the task times do not depend on the test subject nor the display condition. A close look at Table 6 indicates that all the significant

Table 6

SUMMARY OF ANALYSIS OF VARIANCE OF THE STOPWATCH TASK TIMES MEASURED IN THE TACTILE DISPLAY EXPERIMENT

Source of Variation	df	Mean Square	F	Significance
Subjects (S)	1	45.6	--	--
Run (R)	1	1474.2	51.9	$p < 0.001$
Display (D)	2	35.4	--	--
Viewing (V)	2	374.4	13.19	$p < 0.001$
S × R	1	10.0	--	--
S × D	2	22.7	--	--
S × V	2	13.8	--	--
R × D	2	33.9	--	--
R × V	2	140.7	4.95	$p < 0.01$
D × V	4	99.6	3.51	$p < 0.01$
S × R × D	2	26.9	--	--
S × R × V	2	15.5	--	--
S × D × V	4	4.2	--	--
R × D × V	4	165.7	5.81	$p < 0.001$
S × R × D × V	4	16.7	--	--
Within repetitions	252	28.4	--	--

differences observed in the experiment will be observed in a plot of the run-by-display-by-viewing (R × D × V) interaction, as shown in Figure 14.

The combined results of both S's are given in Figure 14, and each data point represents the average task time from eight repeated pickups by each S. One of the main results of this experiment is seen by comparing the corresponding data of Replications I and II. While there are significant differences between both viewing and display conditions in Replication I, there are no significant differences in Replication II.

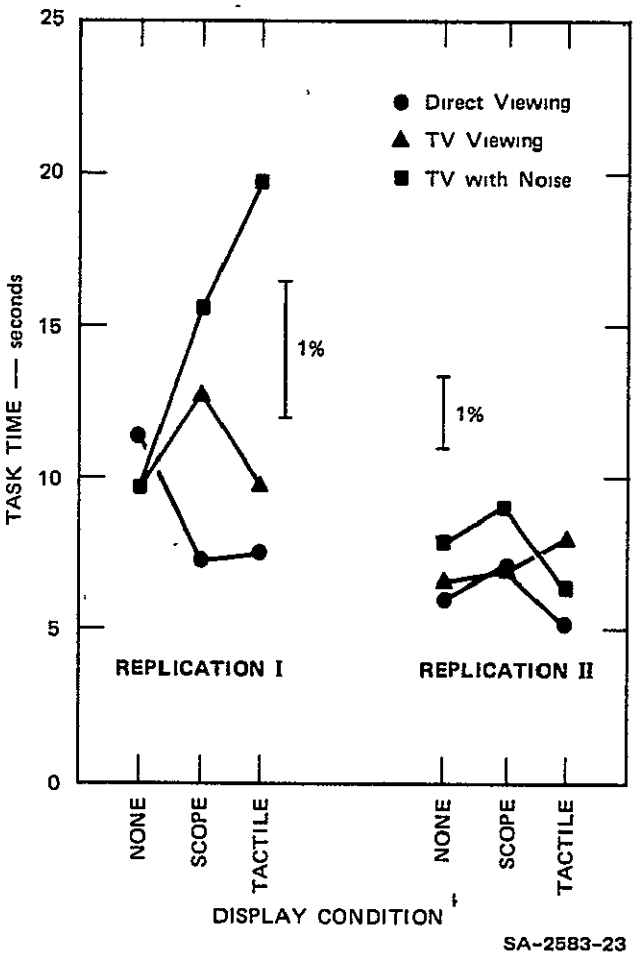

FIGURE 14 TASK TIME AS A FUNCTION OF DISPLAY CONDITION

In other words, after the 72 pickups of Replication I, the practiced S can do the task almost blindfolded, and needs few tactile or visual cues. All that can be said for Replication II is that the practiced task time for picking up a one-inch block with the Rancho Arm, starting from a position one foot above the block, has a mean of 6.96 seconds and standard deviation of 3.46 seconds.

The large differences of performance seen in Replication I must be taken with a degree of skepticism, because of the quickly changing practice effects. The best information obtained from this preliminary display evaluation experiment is about how future experiments should be

designed. The task should be varied to extend the learning effect; and experimental variables should be mixed within a run, rather than blocked into large runs.

C. Results Shown by the Seven Different Performance Measures

An analysis of variance was made on each of the seven performance measures in order to determine their ability to distinguish between the four experimental variables (test subjects LM and SM; Replications I and II; tactile display off and on; and viewing directly, via TV, and via noisy TV). Note that the portion of the experiment with the CRT presentation of the tactile display is not included, because no performance data were logged in this case. The results of these analyses, summarized in Table 7, indicate that only a few of the experimental variables or combinations of experimental variables significantly influenced the results. Only four of the performance measures depend on either viewing or display conditions. The strikingly similar results of these four measurements are shown in Figure 15.

The results of all four measurements show that, with the tactile display off, there is little change in performance with viewing conditions. With the display on, there is an apparent improvement with direct viewing, no change with TV viewing, and an apparent degradation with noisy TV viewing. These changes in performance are difficult to explain and may be due to the quick learning process pointed out in the task-time analysis (Subsection A of this section). We hope further analysis of the learning curves or the number of fumbles made in the experiment will explain this reversal under conditions of increasingly difficult viewing.

D. Correlations Between the Seven Performance Measures

The near similar results from the experiment, plotted in terms of the four performance measures in Figure 15, indicate that the four measures are highly correlated. To determine the relationship between the seven

Table 7

SUMMARY OF ANALYSES OF VARIANCE OF F-STATISTIC IN THE PRELIMINARY TACTILE DISPLAY EXPERIMENT

Missing entries have F values less than that given in the rightmost column and are not significant at the 0.01 level.

Source of Variation	df	M-MOVES	S-MOVES	ENERGY	TIME	MTIME	MRATIO	MBAR	$F_{0.01}$
Subjects (S)	1	--	--	--	--	--	--	--	6.85
Replications (R)	1	32.92	41.17	20.70	28.33	17.91	--	--	6.85
Display (D)	1	--	--	--	--	--	--	--	6.85
Viewing (V)	2	--	7.66	6.38	--	--	--	--	4.79
S X R	1	--	--	--	--	--	--	--	6.85
S X D	1	--	--	--	--	--	--	--	6.85
S X V	2	--	--	--	--	--	--	--	4.79
R X D	1	--	--	--	--	--	--	--	6.85
R X V	2	--	--	9.20	--	--	--	--	4.79
D X V	2	7.81	12.34	10.87	6.84	--	--	--	4.79
S X R X D	1	--	--	--	--	--	--	--	6.85
S X R X V	2	--	--	--	--	--	--	--	4.79
S X D X V	2	--	--	--	--	--	--	--	4.79
R X D X V	2	7.94	10.89	12.62	9.41	--	--	--	4.79
S X R X D X V	2	--	--	--	--	--	--	--	4.79
Within runs	168								

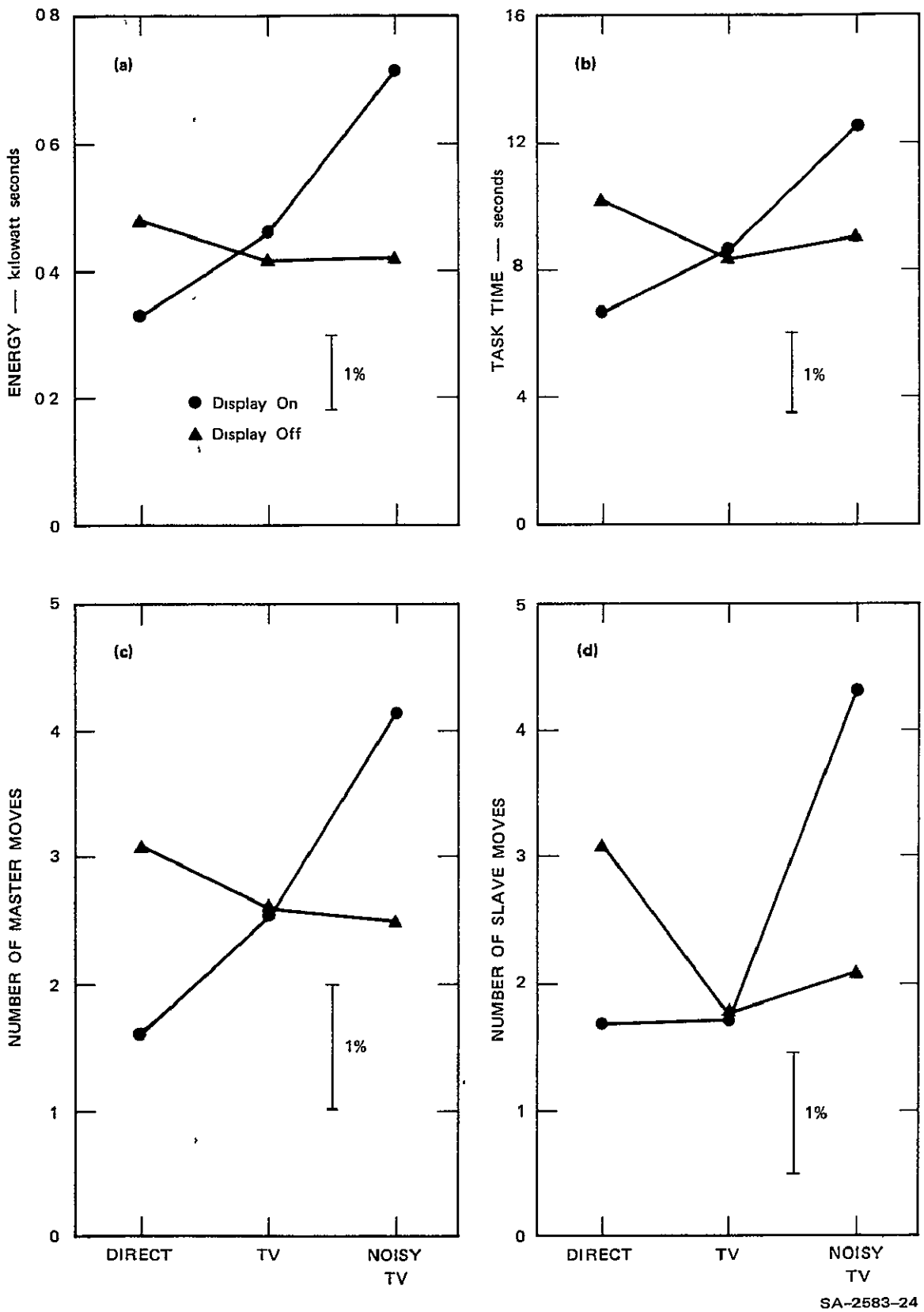

FIGURE 15 RESULTS OF THE PILOT DISPLAY EVALUATION EXPERIMENT

measurements, the pairwise correlation coefficients were calculated. The results are shown as a correlation coefficient matrix in Table 8.

Table 8

CORRELATION COEFFICIENTS BETWEEN PERFORMANCE MEASUREMENTS IN THE TACTILE DISPLAY EXPERIMENT

Zero indicates coefficient not significant at the 0.01 level.

Variable	S-MOVES	ENERGY	TIME	MTIME	MRATIO	MBAR
M-MOVES	0.888	0.839	0.882	0.742	0	-0.413
S-MOVES	--	0.879	0.901	0.774	0	-0.221
ENERGY	--	--	0.968	0.911	0	0
TIME	--	--	--	0.932	0	0
MTIME	--	--	--	--	0.322	0
MRATIO	--	--	--	--	--	0.643

Comparison of these correlation coefficients indicates that the first five measures have large positive correlation coefficients, and must vary similarly in the experiment. The correlations between the variables in this experiment are generally the same as the corresponding correlations of the time delay experiment previously shown in Table 4. The last two variables, MRATIO and MBAR, are not highly correlated with the first five. In particular, there is insufficient evidence to show that MRATIO depends on the first four performance measures. This is different from the high negative correlations between MRATIO and these four measures found in the pilot time-delay experiment. This difference strongly suggests that MRATIO, and to a lesser degree, MBAR, primarily measure performance changes with different time delays. The strong positive relationship between the first four measures is the same in both experiments, suggesting that this is a general result. MTIME correlates much more highly with TIME and ENERGY in this experiment than in the previous time-delay experiment. This is true because of the unchanging

MRATIO measured in relation to the experimental variables in the analysis of variance (Table 7), and in relation to the other performance measures in the correlation analysis (Table 8).

The relationships between a selected set of the performance measures are shown in Figure 16. In the scattergrams two measurements of performance are plotted for each of the 192 block pickups of the experiment. This is the same data from which the correlation coefficients were computed. The relation between task time (TIME) and moving time (MTIM) is shown with a least-mean-squares fitted regression line in Figure 16(a). The high correlation coefficient, 0.932, together with the inverse slope of the line, 0.70, indicates that the results may be described by a constant moving ratio of 70 percent.

The two variables with the highest correlation are shown in Figure 16(b). The equation of the regression line, ENERGY = -0.005 + 0.051 TIME, may be simplified to

$$\text{ENERGY} = \text{TIME}/20 \qquad (8)$$

because the intercept at zero is not statistically significant.

Both of the remaining plots of Figure 14 show how the number of master moves relate to the two other most highly-correlated measures. Though both of these correlations are very high ($r = 0.88$), there is sufficient deviation from a straight line in the plots to suggest that other, unknown factors significantly influence the relationship. The slopes of the regression lines of Figure 16(c) and Figure 16(d) indicate respectively that there are 1.1 slave moves per master move, and an average time of 2.8 seconds per master move.

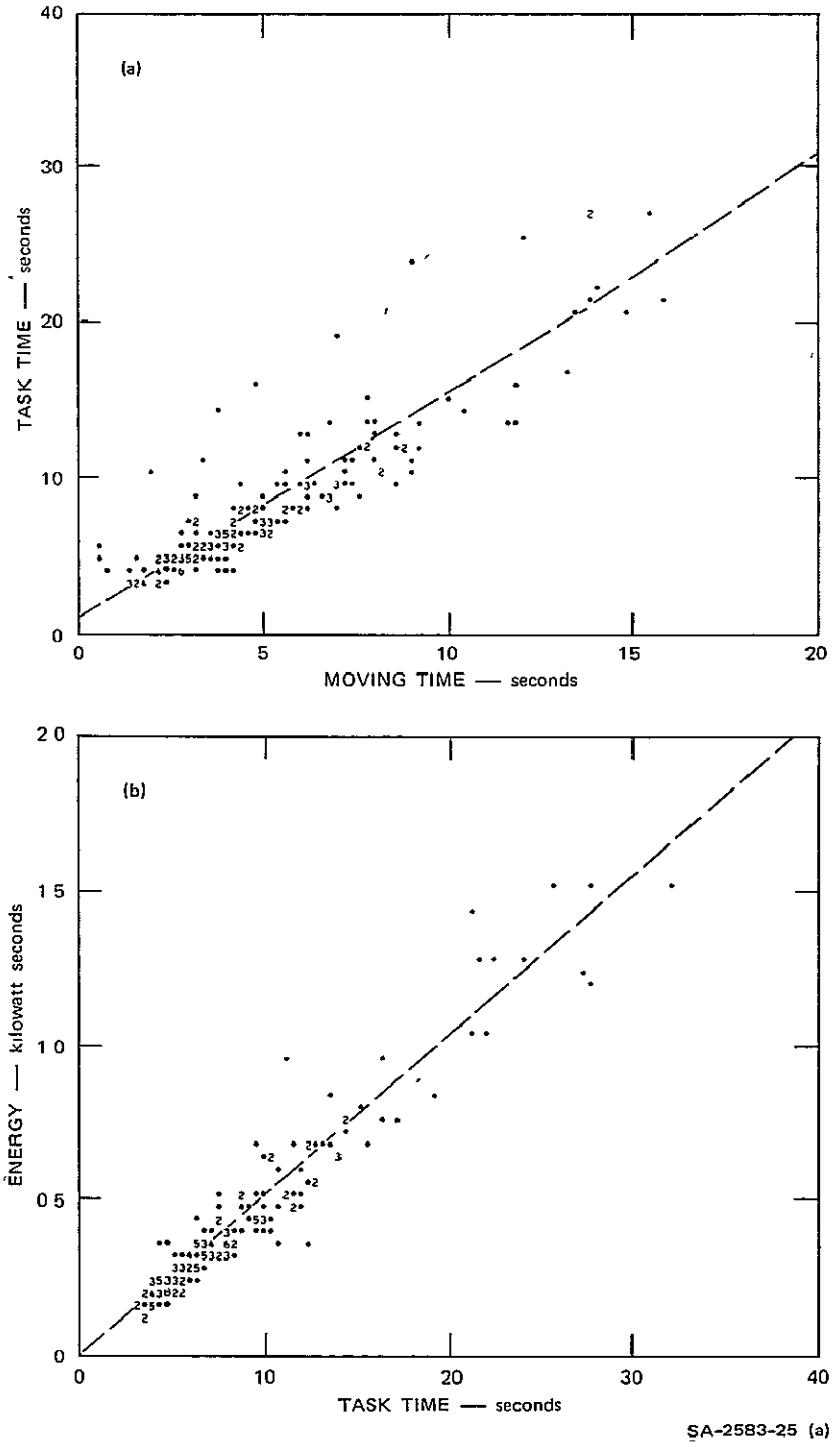

FIGURE 16 SCATTERGRAMS FOR THE DISPLAY EXPERIMENT
Asterisks represent data points and numbers represent the number of data points in a quantization interval
Regression lines are shown dashed

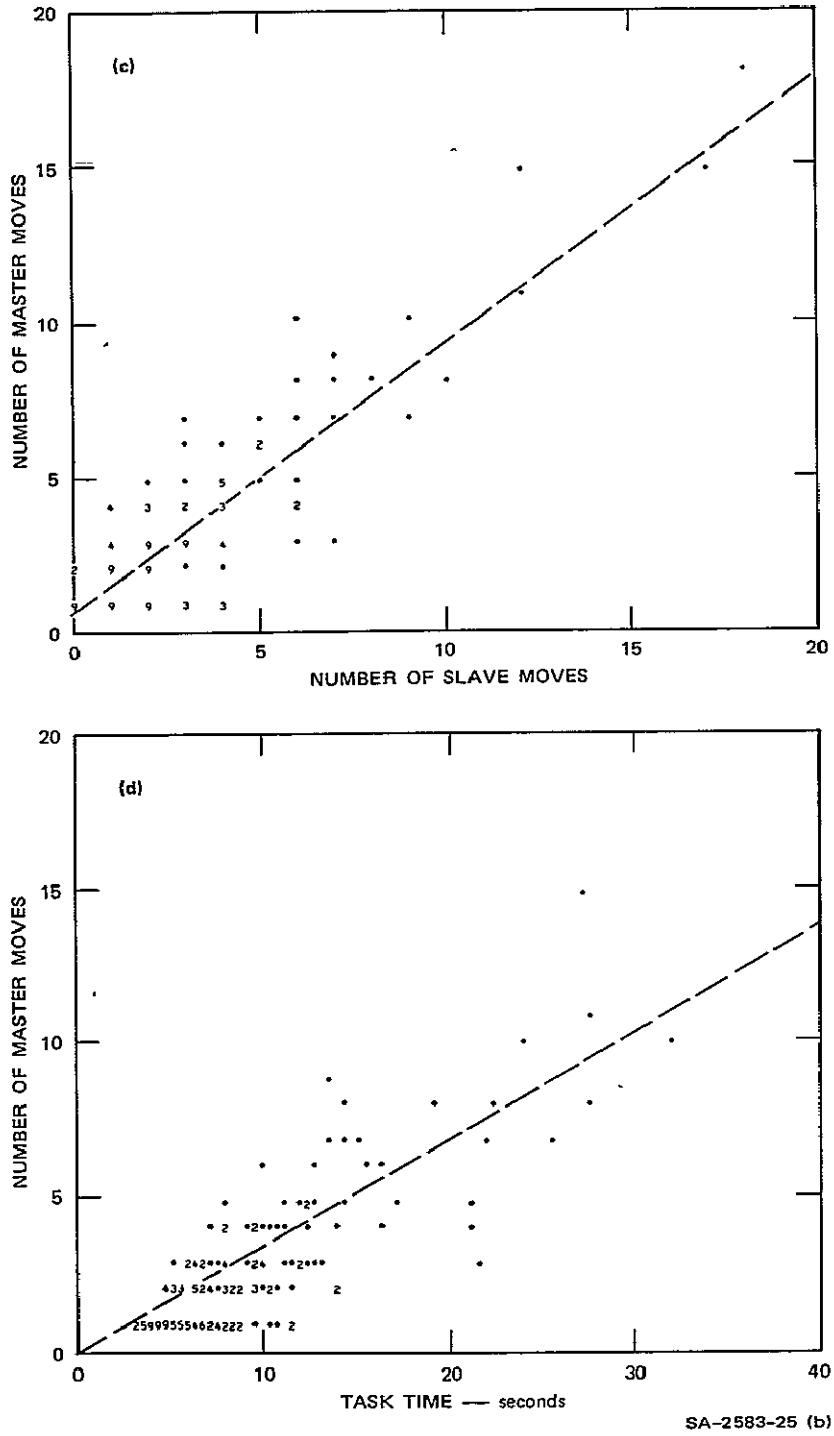

FIGURE 16 SCATTERGRAMS FOR THE DISPLAY EXPERIMENT (Concluded)

Asterisks represent data points and numbers represent the number of data points in a quantization interval. Regression lines are shown dashed.

E. Distribution of Movement Times

Using the "Off-Line Histogram Program" described in Part D of Appendix G, we obtained distributions of movement times to compare the main experimental variables. For each variable, the entire data of the experiment were divided into two or three parts, each of which represented all the data available within a given experimental condition. These moving time distributions, broken down to show the differences between the three different viewing conditions, two display conditions, two test subjects, and two replications, appear in Figure 17. Each of the four plots thus represents all the data of the experiment.

A Chi-square test for equality of the three viewing condition distributions [Figure 17(a)] indicates that the differences are statistically significant [Chi square (18) = 63.9, $p < 0.01$]. The primary area of difference between the three curves is the larger number of short moves (moves of less than one second's duration) in the noisy TV viewing situation. The larger number of moves in this situation (about 25 percent more than direct or TV viewing) suggests that the difference between noisy TV and the other conditions is primarily an increase in the number of short moves.

Differences in moving time distributions with the two tactile display conditions [Figure 17(b)] and the two test subjects [Figure 15(c)] are statistically significant [Chi square (20) = 46.32 and 77.50, respectively, $p < 0.01$], even though differences between these two curves are small. The largest accumulation of Chi square is with short moving times in the range from 0.3 to 1.0 second.

The major difference observed in the moving time distributions is that between Replication I and II [Chi square (20) = 235.90, $p < 0.01$] shown in Figure 17(d). Here, the obvious change brought about by practice is the great reduction in the number of short moves. The number of long

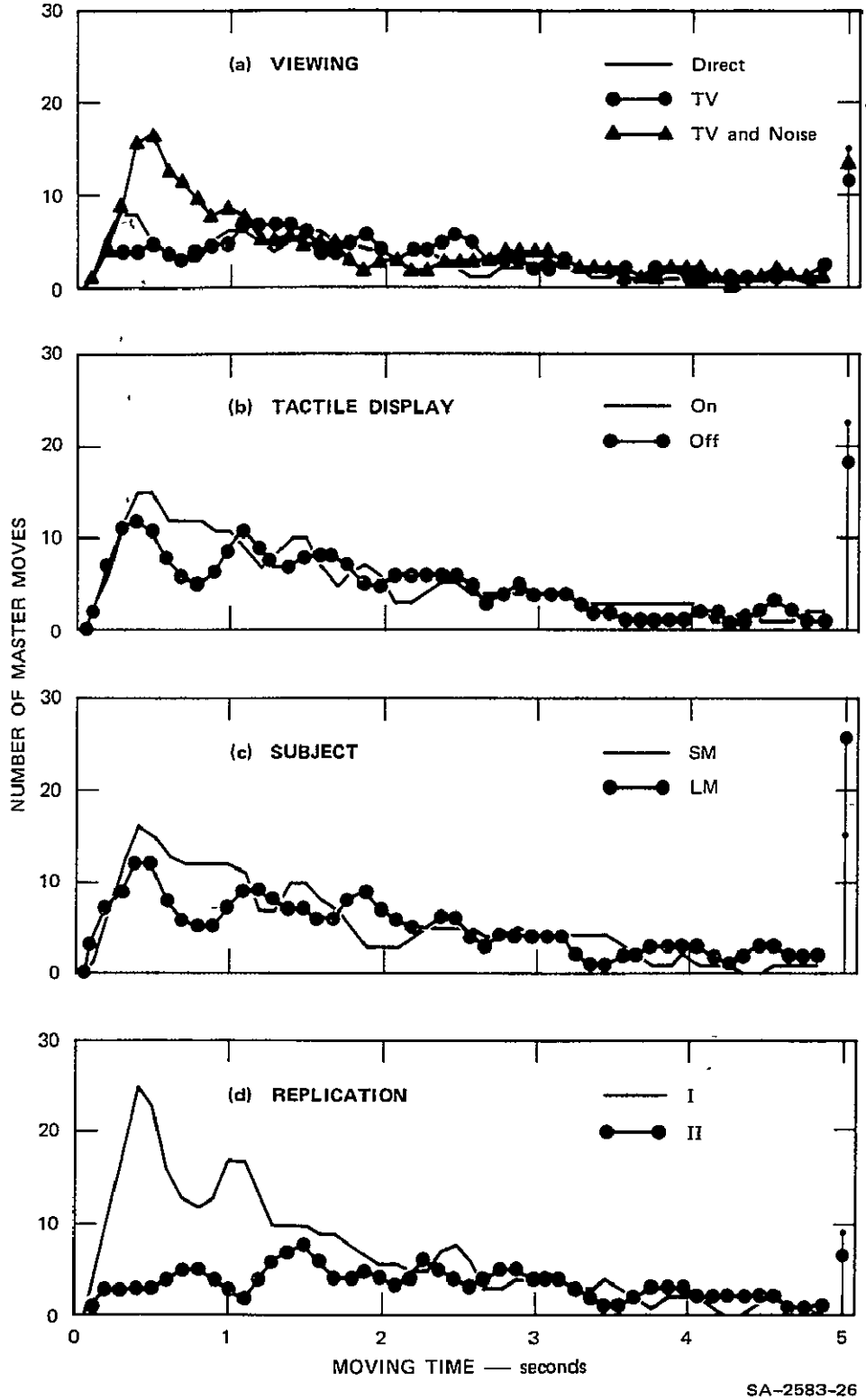

FIGURE 17 MOVING-TIME DISTRIBUTIONS FOR THE PILOT DISPLAY EVALUATION EXPERIMENT

The vertical lines on the right represent the total number of moves with durations 5 seconds or longer.

moves (more than 2 seconds' duration) does not change appreciably for any of the four experimental variables shown in Figure 17.

In conclusion, it seems that changes in moving times with practice, as evidenced by the changes in Figure 17(d), may have strongly influenced the results of the other experimental variables because of the design of the experiment. The design of similar experiments should include a greater alternation of experimental variables, particularly at the beginning of the experiment, where performance is quickly changing.

IV RUGGED TOUCH SENSING AND FEEDBACK SYSTEM

A. Background

From May to November 1972, SRI began to develop a touch sensing and feedback system for the Space Nuclear Systems Office under Contract SNSN-63. The goal of this work was to design a system to provide, through a teleoperator, the touch information normally used by man in directly manipulating objects with his hands. The basic results of this work are given in Part B of this section. More detailed results, such as the design of the sensors, are given in Appendix D.

During the last year, development of the hand has continued under support from both the National Aeronautics and Space Administration under Contract NAS2-7504 and the National Science Foundation under Grant GI-38100X. The hand that has evolved from this work at SRI is described in Part C of this section and in the second half of Appendix D. In addition to the hand with sensors, the electronics for a ten-channel tactile display unit has been built under Contract NAS2-7504. The only missing component in the tactile feedback system at this point is the tactile display with solenoid actuators, pushrods, and control handle.

B. Tactile Feedback Considerations

Designs for a touch sensing system should consider (1) individual sensors and actuators, (2) the optimum encapsulation of the sensors in the end effector, and (3) the arrangement of particular sensors on the tongs. The handgrip of the controller should (1) serve as a handle for transmitting six degrees of force to the arm controller, (2) display

tactile quantities to the hand, and (3) provide one degree of freedom for opening and closing the end effector. The important touch quantities in this control situation is shown integrated in Figure 18.

Based on our feasibility studies (surveys of sensor and actuator technologies), the requirement of fitting the system to the Navy end-effector described by Rechnitzer and Sutter (1972), and the MIT hand controller (Draper Labs Report, 1972), we have several recommendations for a tactile sensing system.

Primarily, the system should convey two types of touch information to the human operator. One of these is contact or touch with a high spatial resolution based on a matrix of sensors on the jaw surfaces and a corresponding matrix of position reproducing actuators on the palmar surfaces of the human finger and thumb. The other type is contact or touch with low resolution for relaying touch quantities from the exterior of the end-effector to the man's hand as force reproducing actuators on the backs, sides, and tips of the human finger and thumb.

The high resolution system should have at least a 3×6 matrix of sensor buttons that cover the end effector gripping surfaces almost completely. The low resolution system should have two sensitive surfaces (uniformly sensitive to force over the entire surface) on each exterior surface of the tongs.

Eventually, two commonly used prehension quantities, force feedback and slippage feedback, should be included in a tactile sensing system. The role and implementation of these quantities is suggested in Figure 18 and implementation of them into the system would give man nearly complete "feel" of the remote environment.

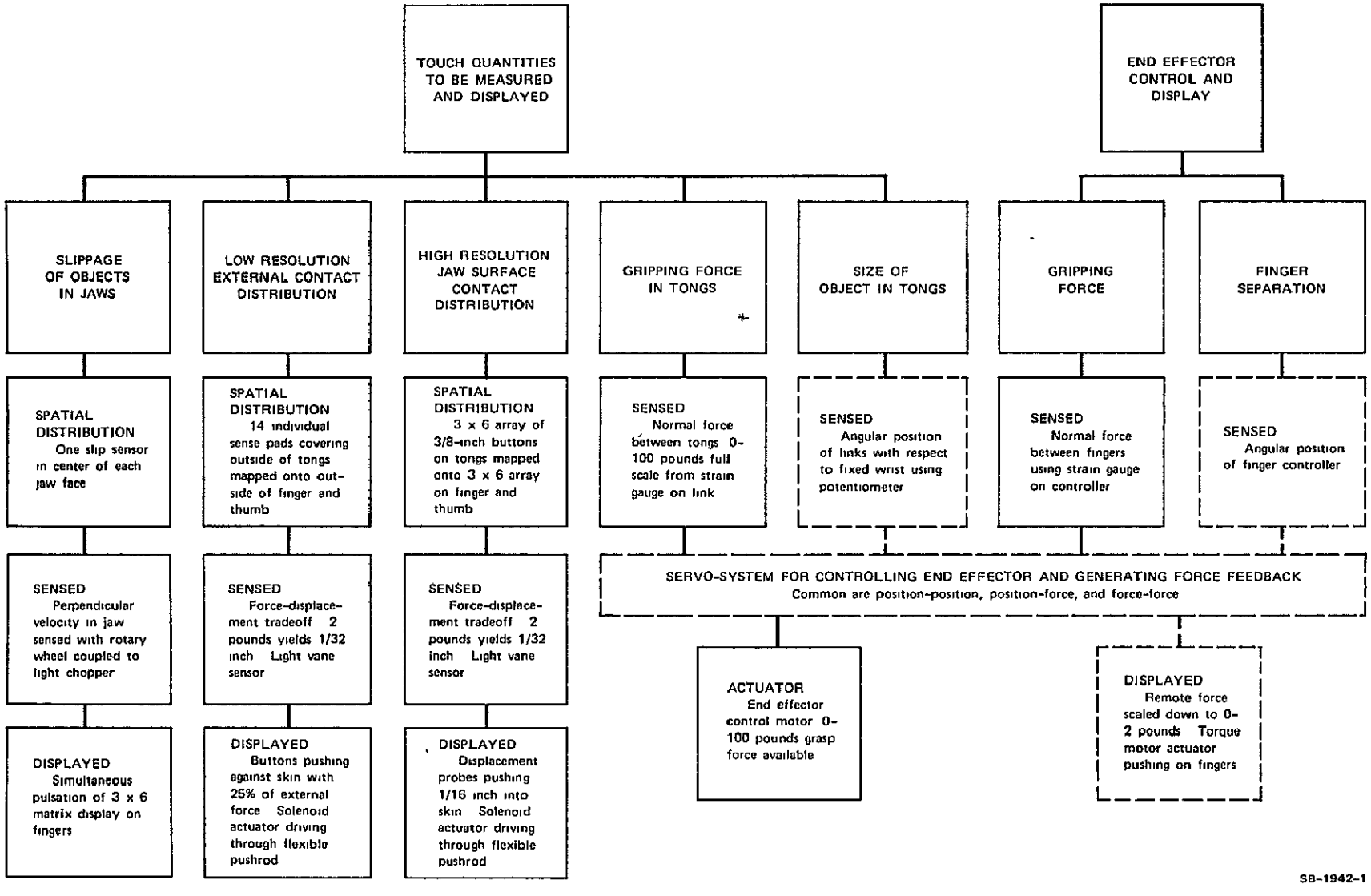

FIGURE 18 SENSING, CONTROL, AND DISPLAY OF TACTILE INFORMATION Touch quantities commonly used by man in prehension are sensed on the end effector and anthropomorphically displayed on the hand controller Dashed boxes are not to be considered in this study

C. General Description of the SRI End Effector

The SRI Tactile/Force End Effector is a general purpose, highly flexible experimental tool that may be used to determine what aspects of tactile and force sensing are most useful in performing tasks via remote manipulation. The tactile/force signals may be used to provide feedback to a human operator, or to a computer for somewhat more automatic operation. Furthermore, feedback to both a human operator and a computer may result in a more useful combination than to either one alone.

The objective in designing this end effector was to provide an integrated sensory system that was rugged enough to withstand occasional encounters with fixed objects, and at the same time provide as much force and tactile information as was thought could be useful.

The system is highly flexible in that it may be used to simulate many end effectors with less sensing capability and, at the same time, it can be used to determine the extra margin of performance gained with increased sensory abilities. It may also be used to determine what specific sensory capabilities are required for an anticipated task, thus providing valuable information to those who are faced with the requirement to design an end effector to meet special needs.

The end effector consists of the following integrated parts.

- Six-axis wrist sensor
- Parallel operating motor driven links
- External touch sensing plates
- Jaw sensor matrices
- T-handle tool holder.

These parts are shown in Figure 19. More detailed interior and assembly views are given in Appendix A.

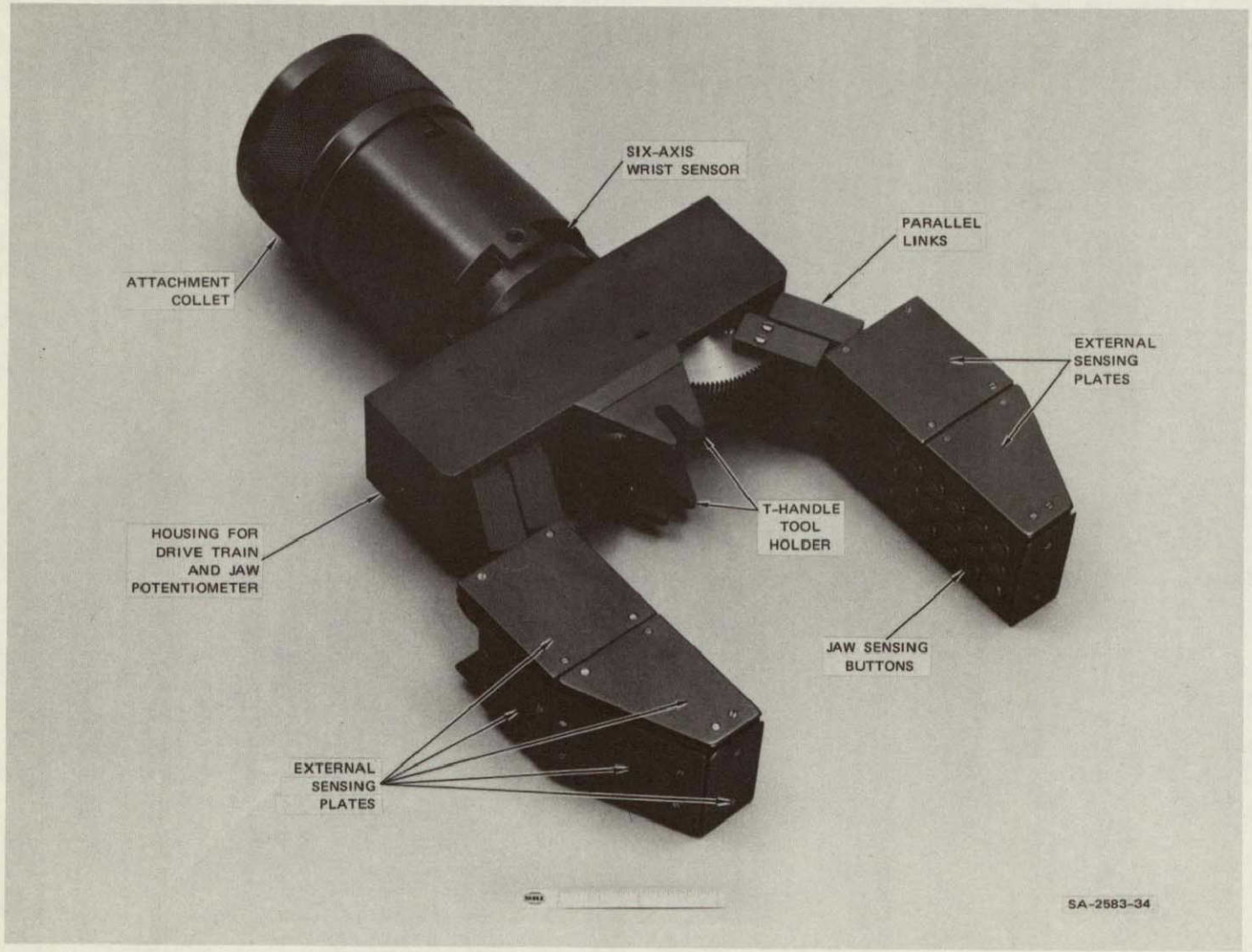

FIGURE 19 END EFFECTOR WITH PROPORTIONAL TACTILE AND SIX-AXIS WRIST SENSORS

The six-axis wrist sensor* is capable of sensing the forces along three axes and the torques about the same three axes. The designed maximum force load is 20 lb. However, since the wrist senses small angular and rotational displacements resulting from forces and torques acting on four removable compliant space members, different force ranges may be obtained by replacing those members. The forces may be displayed on meters or used to provide force feedback to a human operator. Using feedback to a human operator, both time-delayed and non-time-delayed experiments may be performed to determine the limits of usefulness of force feedback. By using the signals to drive meters, or alternatively a chart recorder, it may be determined just what forces are critical to the completion of a task; thus, the development of a specific task algorithm would be greatly simplified.

The parallel links are driven through a gear train by an electric servo motor and can be back driven by external forces. The jaws go from fully open to fully closed in approximately one-half second. The size of the grip with the present links is over four inches. However, this can be increased by replacing the links with longer ones. The gripping force developed through the drive train mechanism is about 20 lb in low torque mode and over 30 lb in high torque mode.

The external touch sensing plates are designed to provide sensing capability over the entire external surface of the jaws. Furthermore, each sensing plate is easily removable so that it may be replaced with any desired, special purpose, sensing plate. In addition, the compliant elements may be easily changed to provide different force sensing ranges.

---

*The wrist sensor of the SRI end effector was developed under National Science Foundation Grant GI-38100X to Stanford Research Institute. It is described in this report along with the rest of the hand because of its integral function in the hand's structure.

The jaw sensor matrices are composed of 18 individual proportional sensors each, and are located on the inside of the jaws in a position anthropomorphically equivalent to the finger pads of human fingers. Each row of sensing buttons has compliant elements of a different stiffness, resulting in a gradation of sensitivity that varies from very sensitive near the jaw tip to insensitive near the base.

The tool holder at the base of the jaw has been provided to accept a "T" shaped handle. This allows a variety of tools which have been fitted with "T" handles to be firmly grasped. By so grasping tools, the forces on the tool can be sensed by means of the six-axis wrist sensor and the jaw sensor matrices.

V AN EVALUATION OF TELEOPERATOR PERFORMANCE USING COMPENSATORY TRACKING

A. Introduction

Several aspects of manipulation tasks resemble compensatory tracking. The operator frequently must move the end effector along a particular path, avoid a series of obstacles, capture a moving object, or work from a moving vehicle. The display being viewed provides information on the relative error between the desired object and the position of the end effector. These situations are basically compensatory tracking tasks.

Powerful tools exist for studying compensatory tracking. One is the describing function or linear model of a nonlinear dynamic system of McRuer et al. (1965). Another is the operator's equivalent time delay, a stable and useful performance indicator determined by Jex, McDonnell, and Phatak (1966).

At first glance, the "critical" task of Jex et al. could be used to characterize a man-arm system. By having the man manipulate a joystick with a mechanical arm, one could measure his equivalent time delay, t_e. The procedure, however, only applies to human control of an integrating vehicle. Including a particular arm "vehicle" in series with the operator and the integrating vehicle of the task complicates the situation and renders the Jex et al. algorithmic computation of t_e invalid for teleoperators.

A more general approach to the problem is that of measuring the entire operator-arm describing function in a compensatory tracking task. From these data, the equivalent operator-arm time delay can be correctly determined. The four experiments described in this section were carried

out to determine the generality of the describing function approach by extending the one-axis results obtained by Hill and Sword (1973) to three-axis tracking. For the first three experiments, variations in the amplitude, bandwidth, and number of orthogonal axes are used to determine the sensitivity of the operator describing function to changes in the command signal. For the fourth experiment, three-axis describing functions are obtained to compare performance with and without the Rancho arm.

The compensatory tracking task was implemented on a small digital computer (LINC-8 with 8K of memory). The computer generated the sum-of-sines command signal and performed the Fourier analysis of the error and response signals on-line. The block diagram of the control situation for each of the three axes is shown in Figure 20. The calculations carried out by the computer, as described in Appendix B, follow the general procedure described by McRuer et al. (1965).

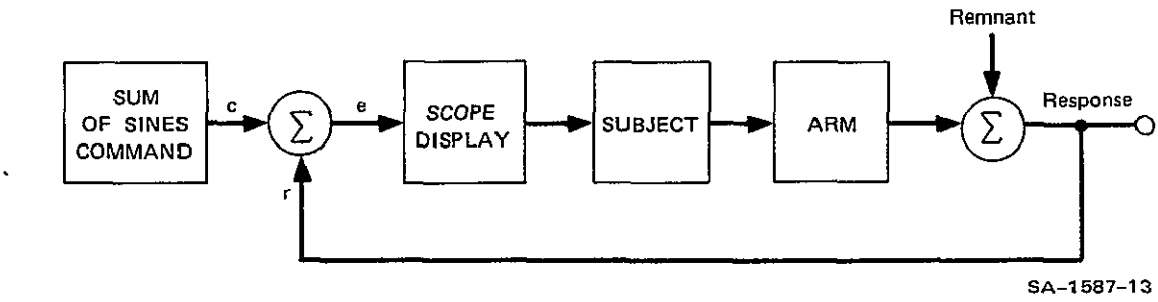

FIGURE 20 COMPENSATORY TRACKING SITUATION

B. Experiment I--Variation in Command Amplitude

Tracking tasks were carried out with three different command signal amplitudes.

1. The Basic Command Signal

The command signal is composed of three independent sum-of-sine command signals, one for each coordinate axis. On each axis, the command signal consists of a sum of ten sine waves, each with a different frequency, amplitude, and initial phase. The frequencies of each of the ten sine waves in each command signal are given in Table 9. The numbers represent the number of full cycles in the 273-second test runs. A warm-up time of 17 seconds was given in which the command was generated and the operator began tracking before the data collection began.

Table 9

FREQUENCIES USED TO GENERATE THE BASIC THREE-AXIS COMMAND AND TO DETERMINE THE REMNANT SPECTRUM
(Cycles per Run)

X-Axis	Y-Axis	Z-Axis	Remnant
5	4	6	3
8	9	11	7
13	17	15	14
20	25	23	19
35	41	37	29
47	67	57	49
83	111	97	93
133	177	154	168
251	273	289	269
440	587	527	549

The amplitides of the lowest six frequencies in the basic command signal were 5.43 cm on the x- and z-axes, and 2.94 cm on the y-axis. The amplitudes of the highest four frequencies were one-tenth of the low frequency amplitudes. This produced a three-dimensional command signal

with root mean square (rms) deviation of 14.4 cm on the x- and z-axes and 7.8 cm on the y-axis. The y-axis amplitude was half the x- and z-axis amplitudes to accommodate the limited human reaching range in the Y direction. The spatial configuration of the basic command signal within the reaching range of the Rancho arm is shown in Figure 21. The average bandwidth of the command signal as defined by McRuer, et al. (1965) is 0.25 Hz (1.55 radians per second).

2. Three-Dimensional Position Sensing

To measure end-effector position, we designed a position sensor. Three of these sensors can be mounted in line with the three orthogonal axes (one sensor per axis). Each is attached to the end effector via a control string, as illustrated in Figure 22.

The control string is provided with a constant return force by a direct-current motor acting as a negator spring. The motor is coupled to the pulley via a belt drive. To provide a velocity measurement in each of the three directions, a tachometer is mounted on the belt drive. Each sensor has a suction-cup base, and movable and fixed control string guides to facilitate mounting. The position and velocity sensor is illustrated in Figure 23.

3. Three-Dimensional Compensatory Display

To do tracking experiments, where the operator is required to trace a path in space, a three-dimensional display is required. The operator must be able to look at the display and quickly assess his position error along x, y, and z coordinates.

A display suitable for this task consists of a movable circle and dot on an oscilloscope screen and a set of fixed, cross lines as

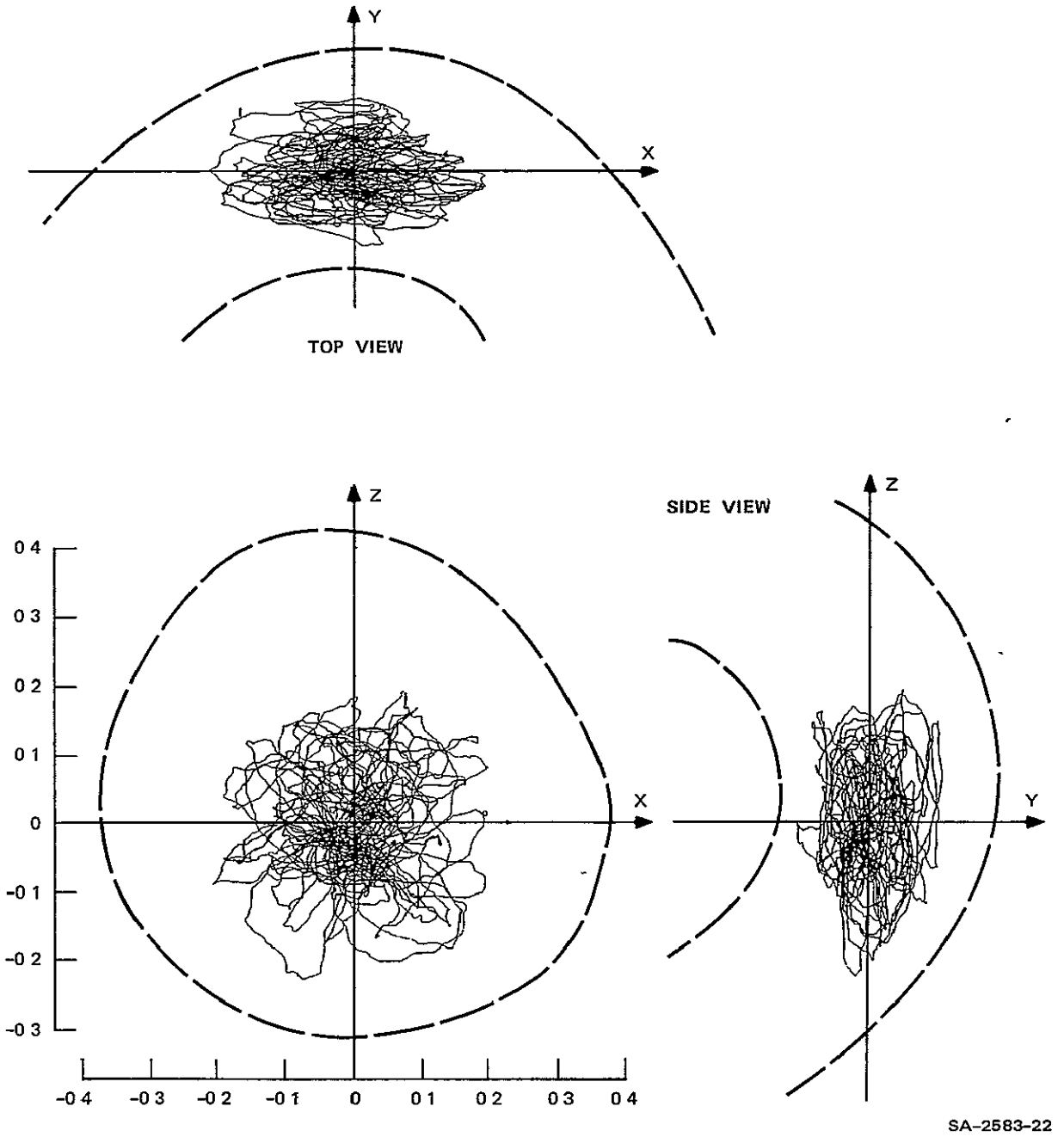

FIGURE 21 THREE VIEWS OF THE TRACKING COMMAND SIGNAL

Dashed lines represent the reaching limits of the Rancho Arm
The scales show distance in meters.

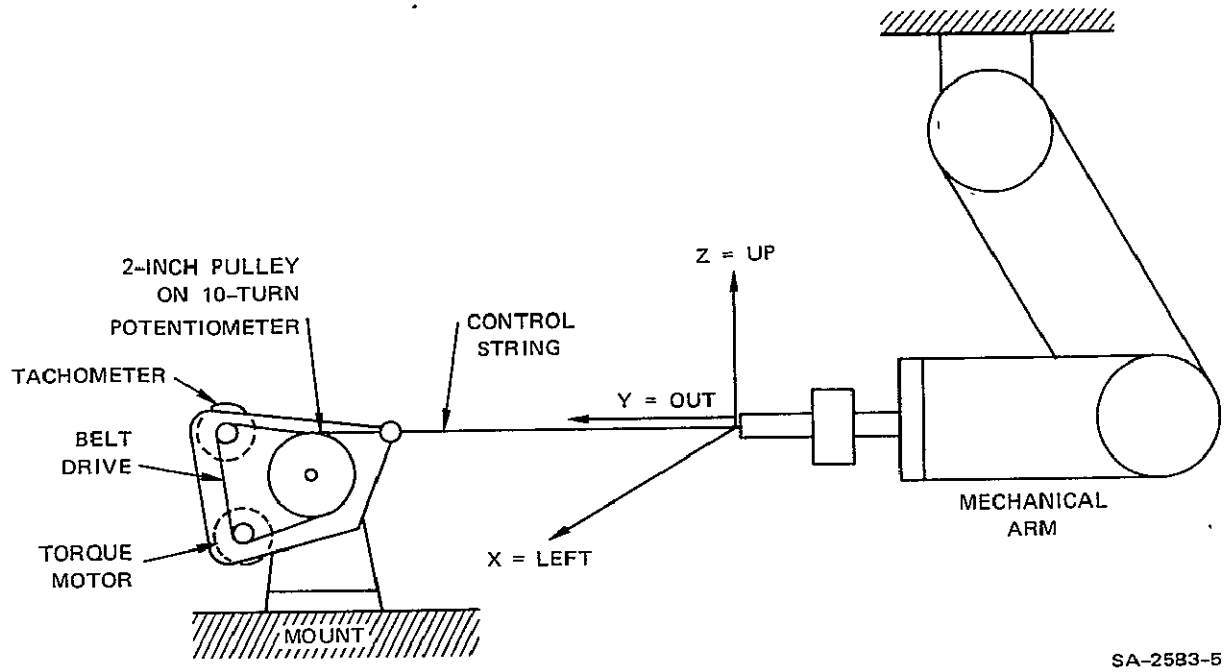

FIGURE 22 MEASURING THREE COORDINATE POSITIONS OF THE END EFFECTOR
(Only the Y-Axis sensor is shown)

shown in Figure 24. The circle and dot can quickly be visualized as an arrow pointing either into or out of the oscilloscope screen. With x and y errors, both the circle and dot move left and right or up and down in unison; with z errors the circle moves up and down with respect to the dot.

4. Subjects

Two male college students participated in the experiments. Both had had about fifteen hours tracking experience with the same equipment before the experiment began.

5. Procedure

Tracking runs were made with three different amplitudes of the basic command signal previously described. The basic command signal was

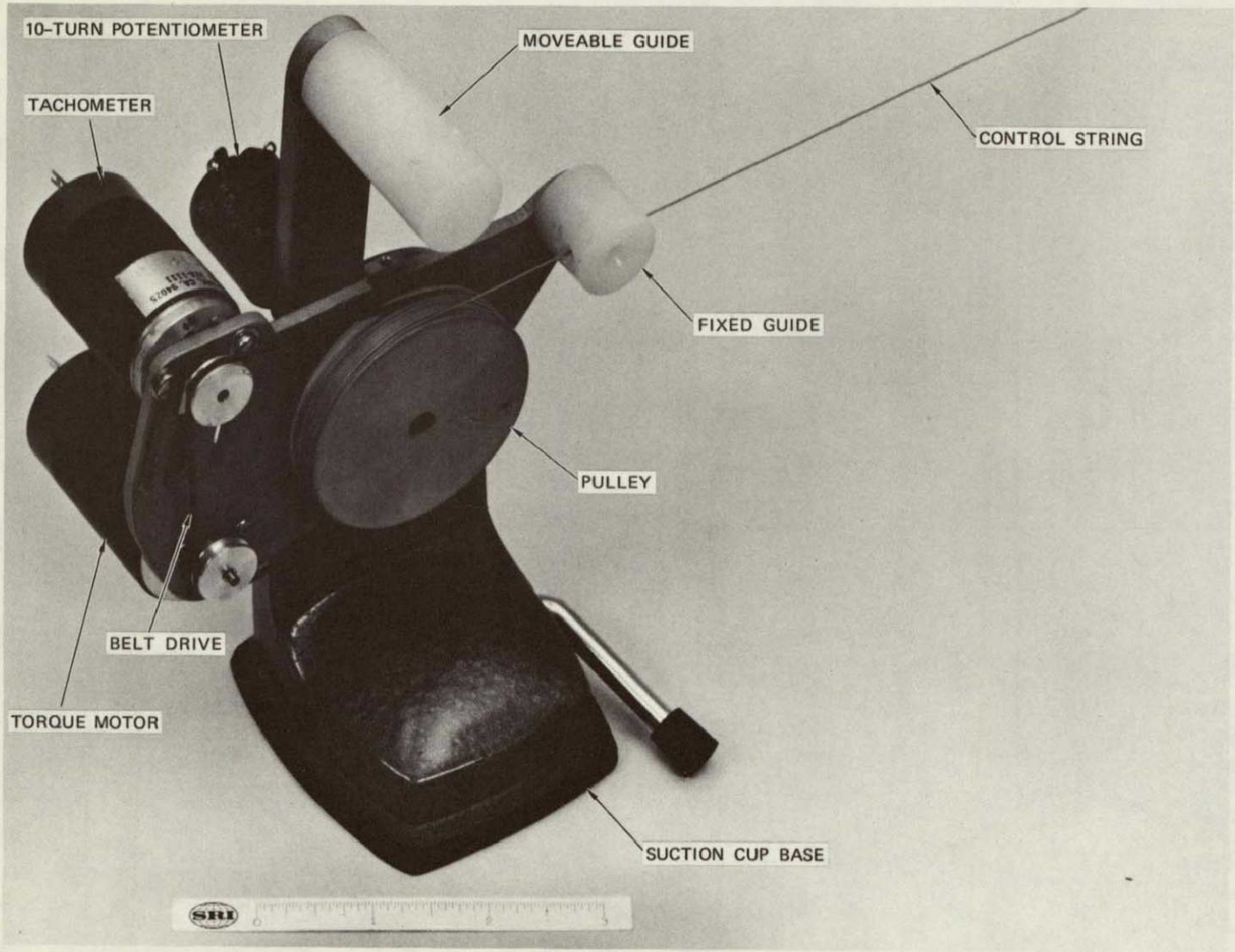

SA-2583-6

FIGURE 23 POSITION AND VELOCITY SENSOR

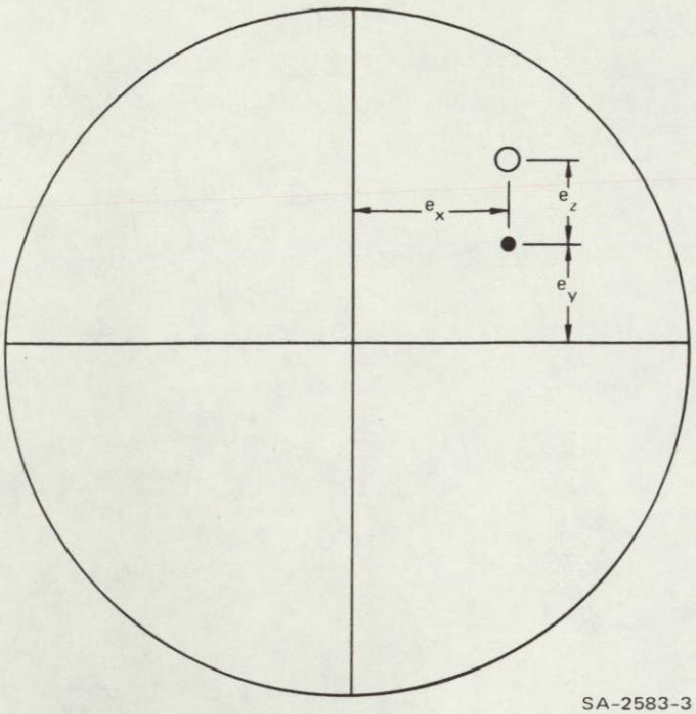

FIGURE 24 TRACKING DISPLAY

used by itself and was also scaled up by 33 and 100 percent by decreasing the voltage on the response-sensing potentiometers. This method left the amplitude of the command seen on the display unchanged but required greater ranges of movement to compensate for the error. The amplitudes of the three composite command signals of the experiment are given in Table 10.

Each of the two subjects performed six tracking runs in an ABCCBA sequence, where A, B, and C correspond to large, medium and basic (small) amplitude commands, respectively. This scheme compensates for learning trends during the experiment.

In addition to analyzing the response at the 10 frequencies of each command signal to determine magnitude and phase lift of the linear part of the operator's (subject's) describing function, the responses on

Table 10

RMS AMPLITUDES OF THE THREE COMMAND SIGNALS OF EXPERIMENT I (Centimeters)

Command	X-Axis	Y-Axis	Z-Axis
Basic	14.4	7.8	14.4
Medium	19.2	10.4	19.2
Large	28.8	15.6	28.8

all three axes were analyzed at the ten remnant frequencies shown in Table 9 to determine the spectrum of the operator's response not correlated with the command signals.

6. Results

Operator describing functions along the three orthogonal axes for the three amplitudes of command are given in Figure 25. Tracking results along each of the axes are similar. Gain increases and remnant decreases as the amplitude of the command signal becomes smaller. There is little difference between the medium and small amplitude describing functions, and we may assume that there is a performance plateau with these moderate amplitude commands. The small amplitude commands were within reach of the human arm as well as the Rancho Arm and thus were used in the tracking experiments to be described herein.

The x, y, and z describing functions obtained with the basic command signal are all shown in Figure 26 for comparison. The small differences suggest that manual tracking is slightly better (with highest gain, lowest remnant) along the x-axis (left and right motion of extended hand) than along the other axes. All three sets of curves are similar, however, with seldom more than 5-dB difference between gains and 10-dB

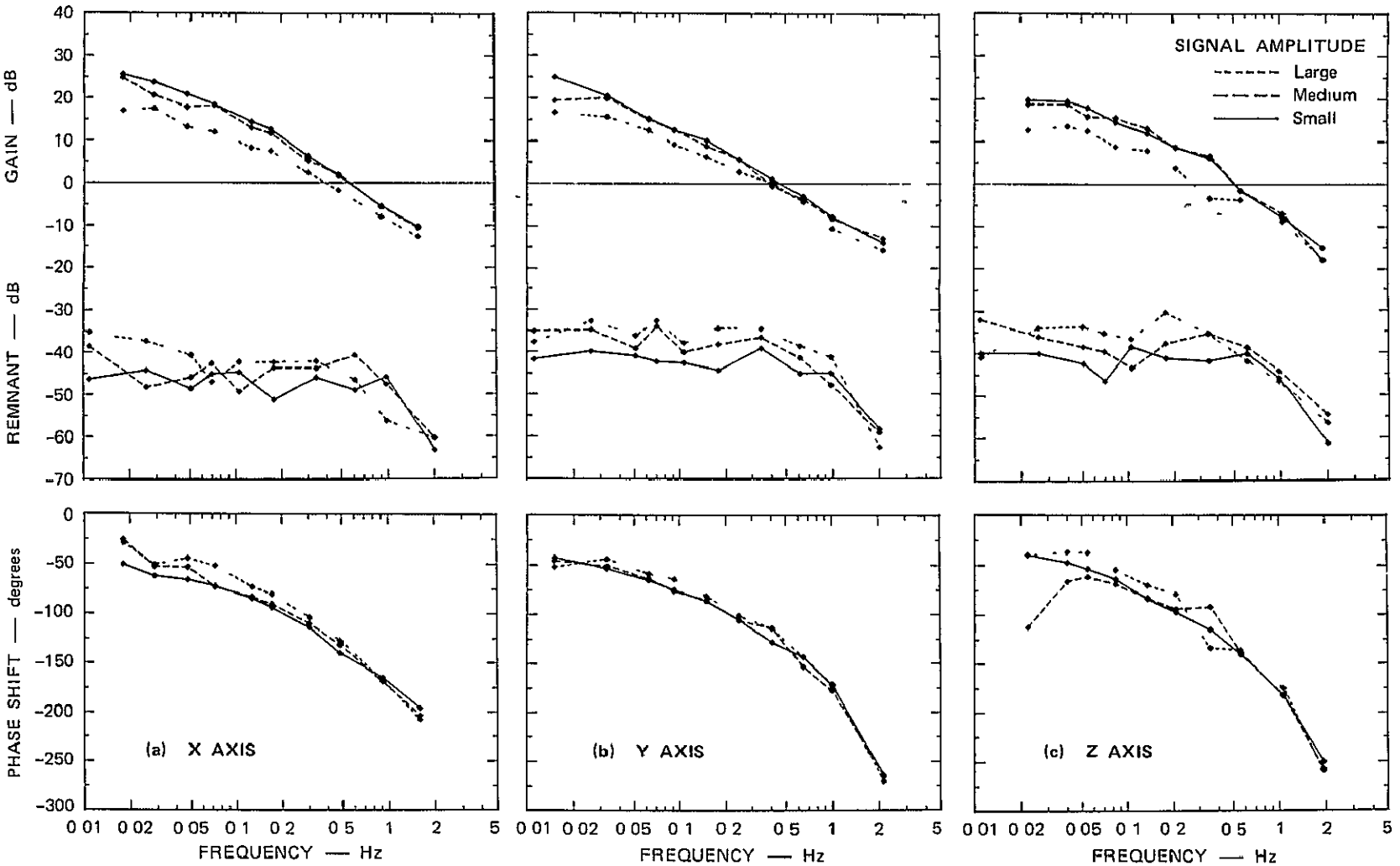

FIGURE 25 THREE-AXIS OPERATOR DESCRIBING FUNCTIONS FOR EXPERIMENT I

Similar changes in performance are seen along all three axes as the command amplitude changes

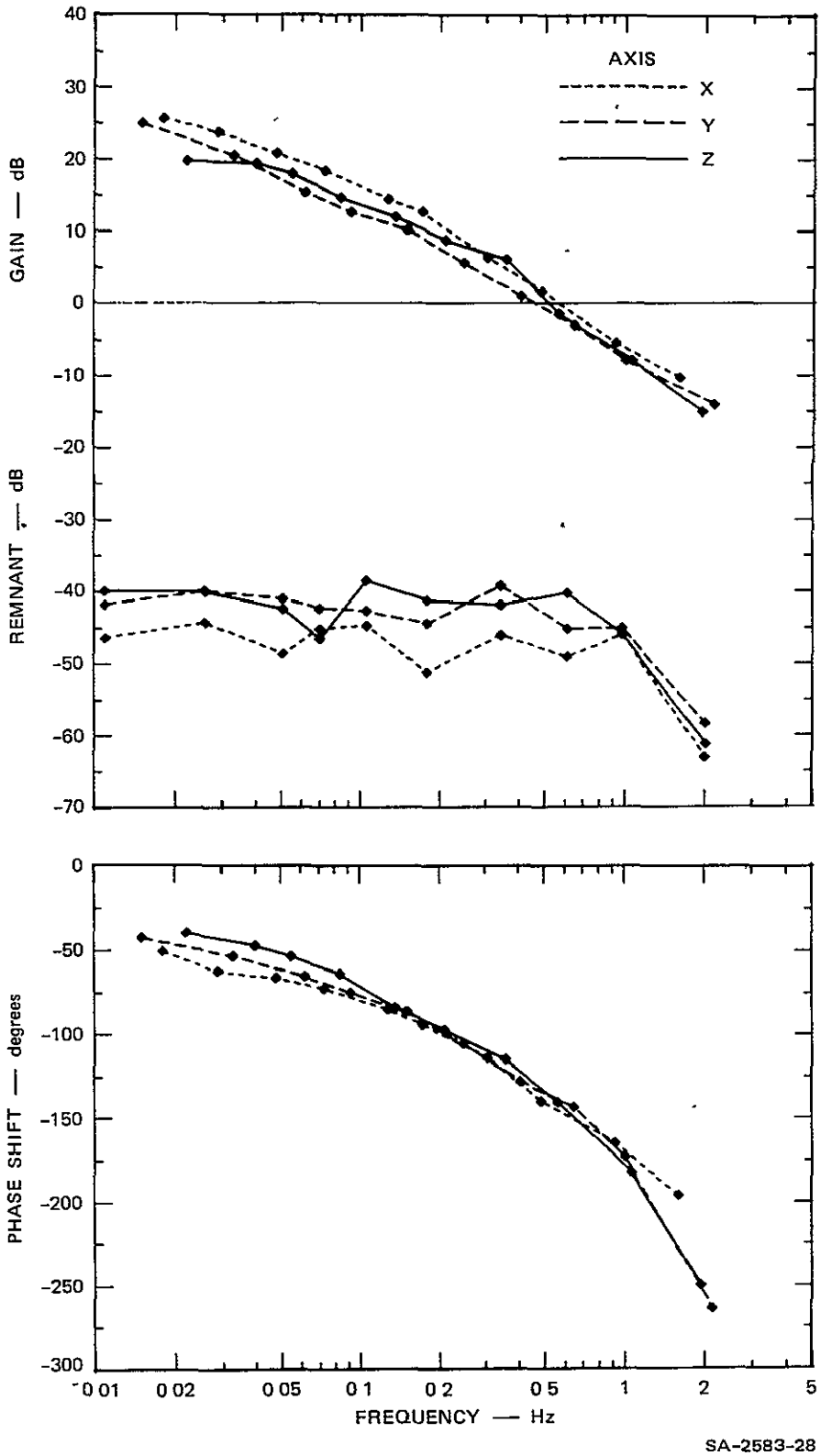

FIGURE 26 COMPARISON OF THE X, Y, AND Z DESCRIBING FUNCTIONS WITH THE BASIC (SMALL AMPLITUDE) COMMAND

difference between remnants. This similarity is an unexpected result, considering the subjectively greater difficulty in following the z-axis as presented on the display than in following the x- and y-axes. The results suggest isotropic moving and reaching characteristics of the human arm.

C. Experiment II--Bandwidth Variations

In this experiment, tracking tasks were carried out with the basic command signals of Experiment I and two additional command signals having both lower and higher bandwidths. The bandwidth of the basic command was increased and decreased by about 50 percent by changing the amplitudes of the individual frequency components following the method of McRuer et al. (1965).

1. Procedure

The low, medium, and high bandwidth commands used in the experiment were composed of the same frequencies shown in Table 9. The amplitude distributions, however, were modified as shown in Table 11. The medium bandwidth command is the same as the basic command described in Experiment I. These amplitude distributions correspond to average bandwidths of 0.16, 0.25, and 0.41 Hz. Wave forms produced by the three command signals are shown in Figure 27.

The two test subjects of Experiment I each made six tracking runs in ABCCBA sequence, with A, B, and C corresponding to low, medium, and high bandwidth, respectively. In each experimental condition, the results of the two subjects on two runs were averaged together.

2. Results

Operator describing functions for the three command signals on the x-axis are shown in Figure 28 and are typical of the results obtained

Table 11

AMPLITUDE DISTRIBUTION OF THE THREE COMMANDS
OF EXPERIMENT II
(Percent)

Frequency Component	Low Bandwidth	Medium Bandwidth	High Bandwidth
1 (lowest)	100%	100%	100%
2	100	100	100
3	100	100	100
4	100	100	100
5	100	100	100
6	10	100	100
7	10	10	100
8	10	10	10
9	10	10	10
10 (highest)	10	10	10

on all three axes. As the command bandwidth was increased there was a small increase in the gain at high frequencies and a decrease in phase lag at all frequencies. There was surprisingly little difference in the describing functions considering the large subjective difficulty reported in tracking the waveform as reported by the test subjects. If we were to rate the medium bandwidth command as "difficult," then the high bandwidth command might take a "panic" rating and the low bandwidth might be considered "easy." In this light, we may consider the describing functions of Figure 28 as largely independent of bandwidth.

Though there is little change in the describing function with command bandwidth, there is considerable change in the size of the tracking errors, as seen in Table 12. Changes in the z-axis tracking error with bandwidth are statistically significant [$F(2,3) = 85.5$, $p < 0.005$] while changes in the other axes are not. Tracking error increases regularly and monotonically with bandwidth on all three axes,

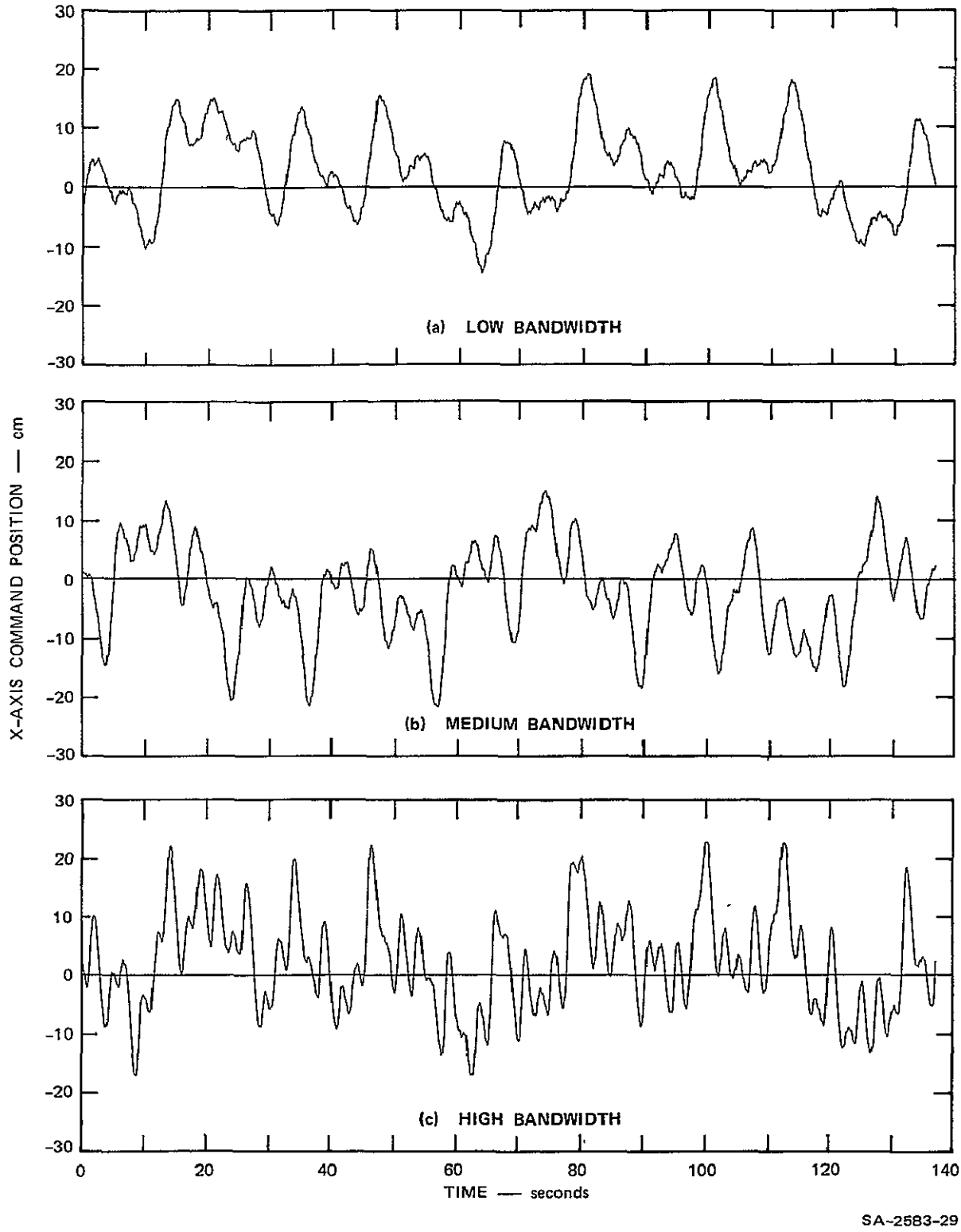

FIGURE 27 COMMAND SIGNALS PRESENTED TO SUBJECT AS A FUNCTION OF TIME

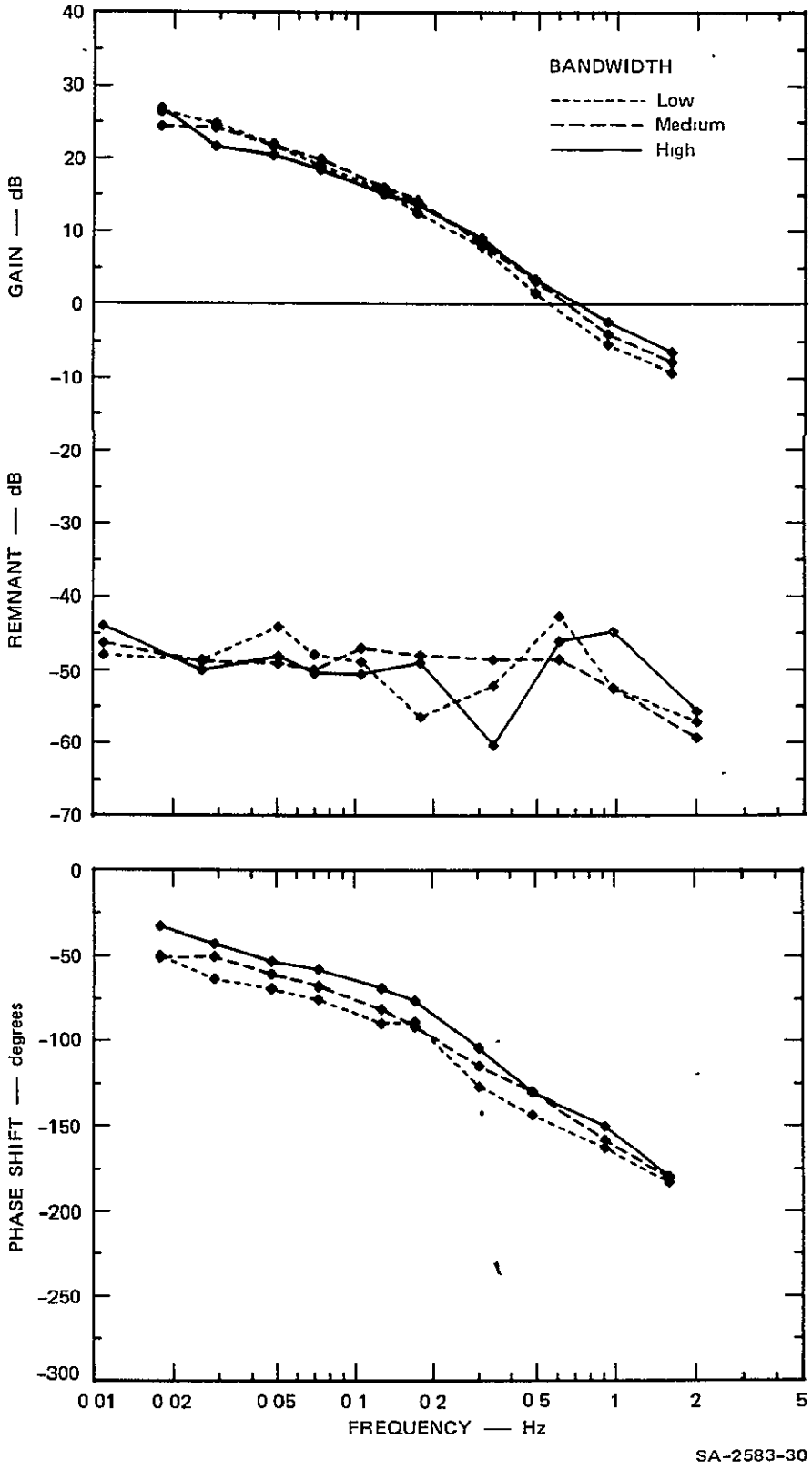

FIGURE 28 X-AXIS DESCRIBING FUNCTIONS FOR CHANGES IN THE BANDWIDTH OF THE COMMAND

Table 12

STANDARD DEVIATIONS OF THE TRACKING ERROR
AS A FUNCTION OF BANDWIDTH
(Centimeters)

Bandwidth	σ_x	σ_y	σ_z	σ
High	3.67	3.70	5.38	7.49
Medium	2.59	2.55	3.54	5.07
Low	2.29	1.95	2.77	4.09

the increase being nearly two-to-one for a two-to-one increase in bandwidth. With the relatively constant gain and remnant characteristics, the increase in error with bandwidth corresponds to the high frequency components of the command not being attenuated by the operator.

D. Experiment III--Number of Axes Tracked

The design of this experiment is similar to the previous experiments except that the three experimental conditions are tracking with only a single-axis, a two-axis, and a three-axis command signal.

1. Procedure

The same test subjects that were used in Experiment I made six tracking runs with the basic command signal described under Experiment I, above. The runs were made in ABCCBA order, where A, B, and C stand for one-, two-, and three-axis tracking, respectively. For two- and one-axis tracking, either one or two axes were turned off by disconnecting the error signal from the display. Thus, the subject could not see his error on the deenergized axes and he was not penalized for any of those errors. In one-axis tracking, for example, only left-right motions were required, and the subject was free to hold his arm at any vertical elevation or

reaching distance in front of him without changing the display. The tracking was normal with the three tracking strings attached to a hand grip held in his hand. One-axis tracking involved only the x-axis, and two-axis tracking involved both x- and y- axes.

2. Results

The describing functions obtained for the three experimental conditions are shown in Figure 29. X-axis tracking results were obtained under all three conditions.

The surprising feature of these curves is the fact that they are nearly superimposed! It suggests that two- or three-axis tracking is no more difficult than one-axis tracking. This is contrary to the idea that, compared to a one-axis tracking task, a two-axis task represents an additional, independent amount of work that will degrade the operator's performance from what he could accomplish on each task independently. We had expected performance to be best with one-axis tracking, and to degrade as the number of axes was increased.

The similar one-, two-, and three-axis results suggest that in a single view of the display the subjects can comprehend the error and compensate for it in a single move. Thus, we should consider one- and two-dimensional moves as subsets of three-dimensional moves. These moves of reduced dimension must require as many decisions to be made by the human as a more general three-dimensional move. These simple results, however, may not hold when the operator is encumbered with a control brace or a master-slave manipulator.

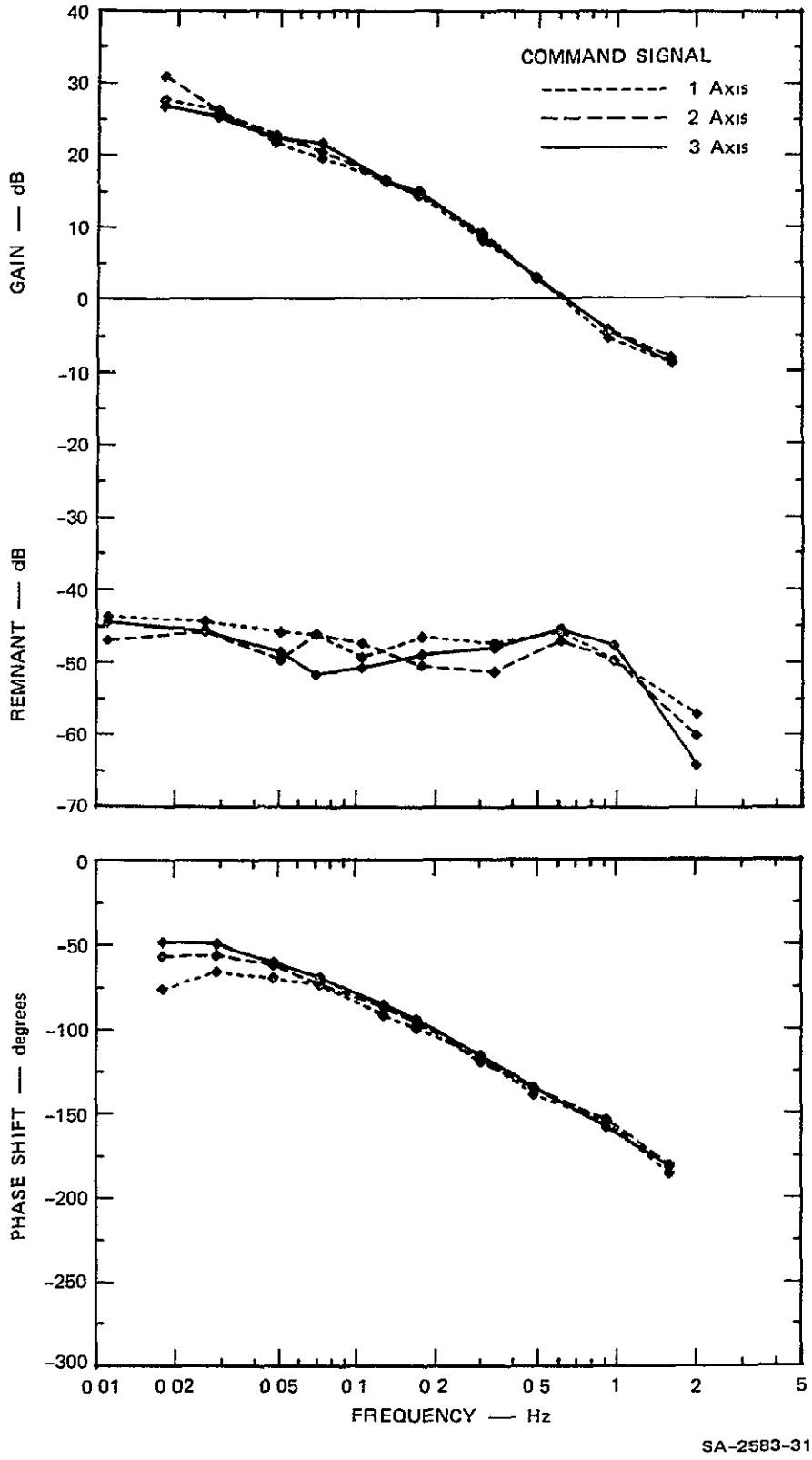

FIGURE 29 X-AXIS DESCRIBING FUNCTIONS IN ONE-, TWO-, THREE-AXIS TRACKING

E. Experiment IV--Controlled Vehicle Variation

In this experiment, the three experimental conditions were tracking with the position strings attached to (1) a hand grip held in the subject's hand, (2) the end of a control brace worn by the subject, or (3) the Rancho Arm. In this last case, the arm was controlled from the control brace. These experimental conditions are referred to as normal, brace, and Rancho, respectively, in the description of the results.

1. Procedure

The basic command of Experiment I was tracked under the three manipulative conditions in six tracking runs by the same two subjects who participated in Experiment I. The ABCCBA sequence of test runs was used, with the A, B, and C conditions corresponding to response of the normal arm, the brace, and the Rancho Arm controlled by the brace, respectively.

2. Results

The describing functions obtained from the x-axis tracking are shown in Figure 30; they typify the results obtained on all the axes. In general, as the brace and then the Rancho Arm are included in the control loop, (1) the gain decreases, (2) the remnant increases, and (3) the phase lag increases. These changes, along with some additional ones, are listed in Table 13. Similar changes were noted in a one-axis tracking experiment (Hill and Sword, 1973) using the Rancho Arm and control brace. The significance level for each variable shown in Table 13 is based on an analysis of variance of the measurements made under each of the three experimental conditions.

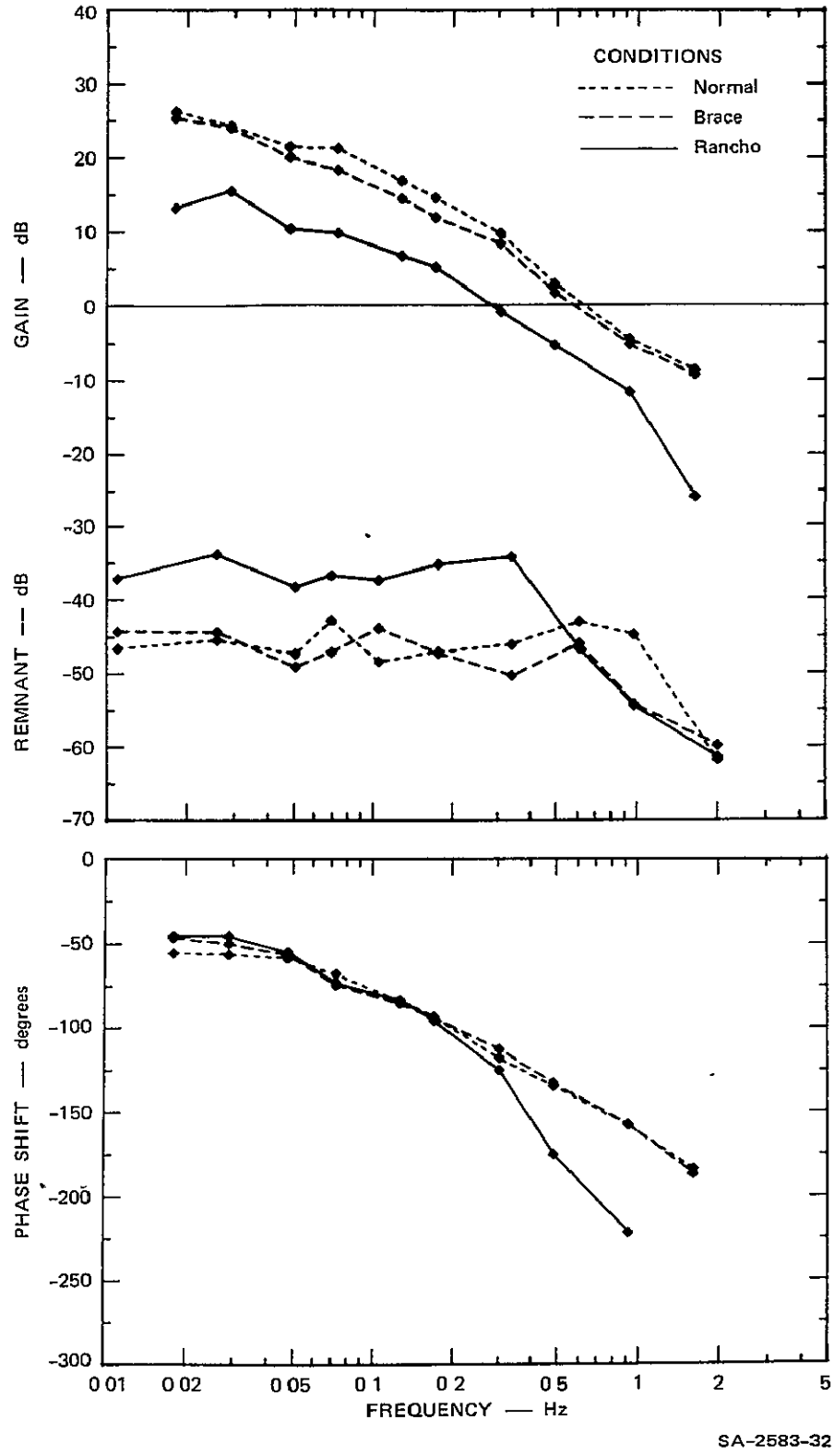

FIGURE 30 X-AXIS OPERATOR/VEHICLE DESCRIBING FUNCTIONS UNDER DIFFERENT MANIPULATIVE CONDITIONS

Table 13

SUMMARY OF KEY VARIABLES IN EXPERIMENT III

Variable	Normal Tracking	Brace Tracking	Rancho Tracking	Units	Significance
X-Error (σ_x)	2.59	2.95	6.49	cm	0.025
Y-Error (σ_y)	2.60	2.78	5.37	cm	0.05
Z-Error (σ_z)	3.50	4.13	8.64	cm	0.01
Gain change	0.0	-1.36	-10.5	dB	0.005
Crossover frequency	0.674	.605	.285	Hz	0.025
Equivalent time delay	0.178	.179	.416	Seconds	Not significant

F. Summary and Conclusions

In Experiment IV the gain decreased and the phase lag increased with the encumbrance of first the control brace and then the Rancho Arm. Similar but less clear-cut results were obtained on the one-axis, higher bandwidth tracking task previously reported (Hill and Sword, 1973). In Experiment IV little reduction in gain (1.4 dB) was found with brace tracking compared to the larger reduction (4.4 dB) found previously. With the additional load of the control brace little change in phase or remnant was recorded in either this or the previous experiments. Where these results and the previous results differ, however, the current results should be accepted for several reasons. These are mainly (1) the greater amount of tracking experience of the subjects, (2) the greater stability of the new data, and (3) the balanced ABCCBA order of the experimental conditions.

In the previous preliminary experiment, the remnant decreased when going from normal to Rancho Arm tracking, whereas the remnant in the current experiment increases in the results shown in Figure 6. This is due to the different way of calculating the remnant in the two experiments and the fact that the tracking error is much larger with the Rancho Arm than with normal tracking. In the previous measurements the remnant magnitudes were obtained by dividing the Fourier amplitudes at the remnant frequencies by the root mean square (rms) error, whereas these amplitudes were divided by the rms command amplitude in the current measurements. The change was made to conform to the more meaningful convention used by McRuer et al. (1965).

The remnant has a flat frequency distribution for all of the control conditions. It may thus be modeled by low pass filtered white noise introduced (added) into the operator's response. The corner of the low pass filter is about 0.3 Hz for the Rancho Arm tracking, 0.6 Hz for normal tracking, and 1.0 Hz for brace tracking. The initial slope of the filter is about 40 dB per decade for all tracking conditions. This shape for the filter would be obtained from a force generator (a muscle) working in a position control loop with a given mass. Changes in the corner frequency suggest that an increasing effective mass may account for the changes in remnant spectrum as the brace, and then the manipulator, are included. The increase in remnant amplitude with the Rancho Arm tracking suggests that a second source of positioning noise may be attributed to the vehicle. A simple model describing this situation is shown in Figure 31. Amplitudes of these noise generators for each controlled vehicle are given in Table 14.

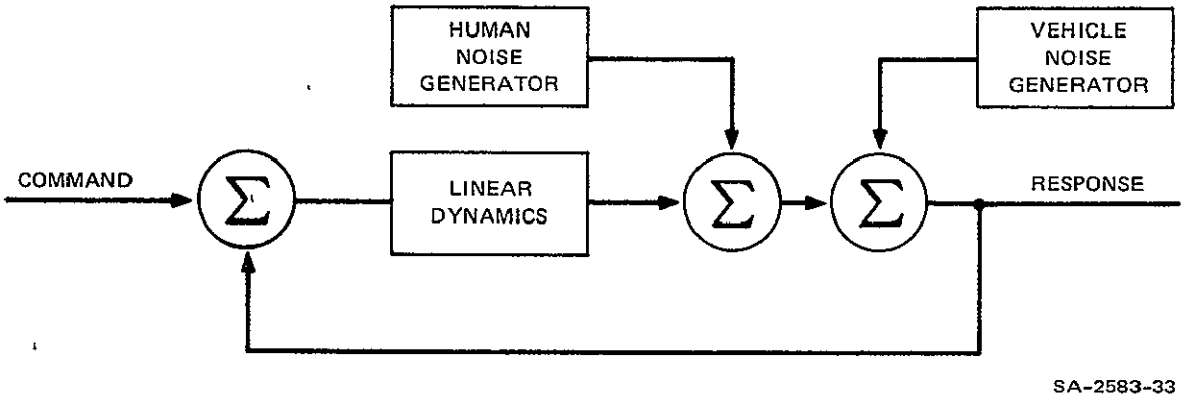

FIGURE 31 A SIMPLE MODEL FOR THE REMNANT IN MANIPULATOR TRACKING TASKS

Table 14

RMS AMPLITUDES OF THE NOISE GENERATORS
OF FIGURE 31
(Centimeters)

Source	X-Axis	Y-Axis	Z-Axis
Basic human noise generator	1.55	1.42	2.06
Additional brace noise generator	0.00	0.89	1.64
Additional brace and manipulator noise generator	3.87	2.75	5.23

VI COMPARISON OF TWO MANIPULATORS USING A STANDARD TASK OF VARYING DIFFICULTY

A. Introduction

Manual control performance can be evaluated using two types of task definitions that differ in levels of complexity. Standard, rather elaborate tasks, characteristic of the projected manipulator usage, such as those of Fornoff and Thornton (1972) and Blackmer (1968), can be adopted. These are perhaps most useful for qualitative comparison of manipulator systems. Performance on these tasks can be used to predict performance on other tasks only in a limited way, however. The validity of such extrapolations is based on similarities between standard and nonstandard tasks. If one aspect of the task changes in difficulty, there is no direct method for modifying the performance results other than rerunning the entire performance evaluation.

A further complication in establishing performance levels in these tasks is that exact description of the task space is required. For instance, it would be difficult to duplicate the results of Blackmer's (1968) experiment without knowing such things as the size of the peg and receptacle and their placement with respect to the manipulator.

Alternatively, a set of task elements can be defined that can be used to synthesize any possible task. Motion-time studies of industrial workers are an example of the usefulness of this type of task definition. Blackmer (1963) used some of these definitions in analyzing the results from his experiment.

Fitts (1954), in a study of human motor response, proposed a task difficulty index, I_d, which allowed task geometry to be represented as a single number. For a block grasping task, I_d is expressed as:

$$I_d = \log_2\left(\frac{2 \times \text{distance moved}}{\text{final tolerance}}\right)$$

where I_d is in information units (bits) and the geometry is as shown in Figure 32.

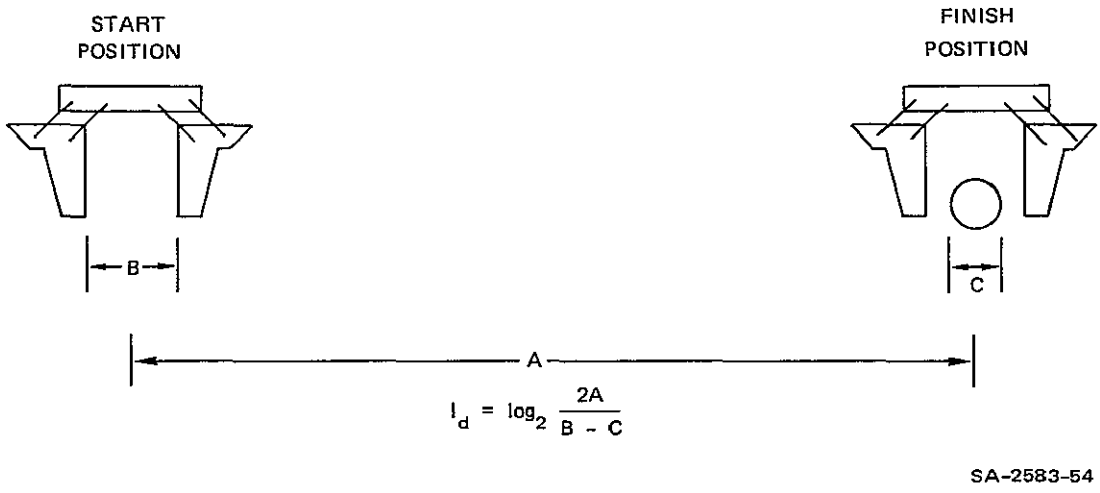

FIGURE 32 DEFINITION OF INDEX OF DIFFICULTY, I_d

Ferrell (1965) used this difficulty index to correlate task completion times to numbers of moves in time delayed manipulation. I_d proved to be a useful way of describing the task requirements.

The investigation reported here was carried out to answer the following questions:

(1) What are the effects of movement distance and task accuracy requirements on task completion time for a simple block grasping task using a remote manipulator?

(2) Is the difficulty index used by Ferrell a valid quantifier for task difficulty for manual control using a manipulator with more than two degrees of freedom?

(3) What are the effects of different operators and different task modes on task completion times?

(4) What is the effective difference between two manipulator systems of significantly different accuracy and precision?

The experiment discussed here was conducted in two parts. In the first part, the Rancho arm located at SRI was used and in the second part, the Vykukal designed arm at Ames Research Center was used. The experiments of these manipulators are described in the following paragraphs.

B. Description of the Rancho Manipulator Experiment

A six-degree-of-freedom arm, based on a Rancho orthotic brace design, was used in this experiment. A description of the arm and its peripheral equipment can be found in Hill and Sword (1973). The slave arm task space was laid out such that the major motion required was a radial movement of the shoulder joint. The operator stood approximately six feet from the slave arm. Figure 33 illustrates the experimental setup.

Two task types were considered as shown in Figure 34. In the HAND task (H task), the empty jaws were moved to grasp the block. Task time extended from a starting signal, given by an observer, until the jaws started to close. The RECEPTACLE task (R task) differed in that the jaws carried a block from a starting position and inserted it in a receptacle. Task time was measured from the start signal until the block just entered the receptacle. These task types differed in that the H task moved a "hole" to contain a stationary block and the R task moved a block to a hole.

Blocks were sized and the distance moved was adjusted so that five H tasks and five R tasks could be accomplished at difficulty levels of

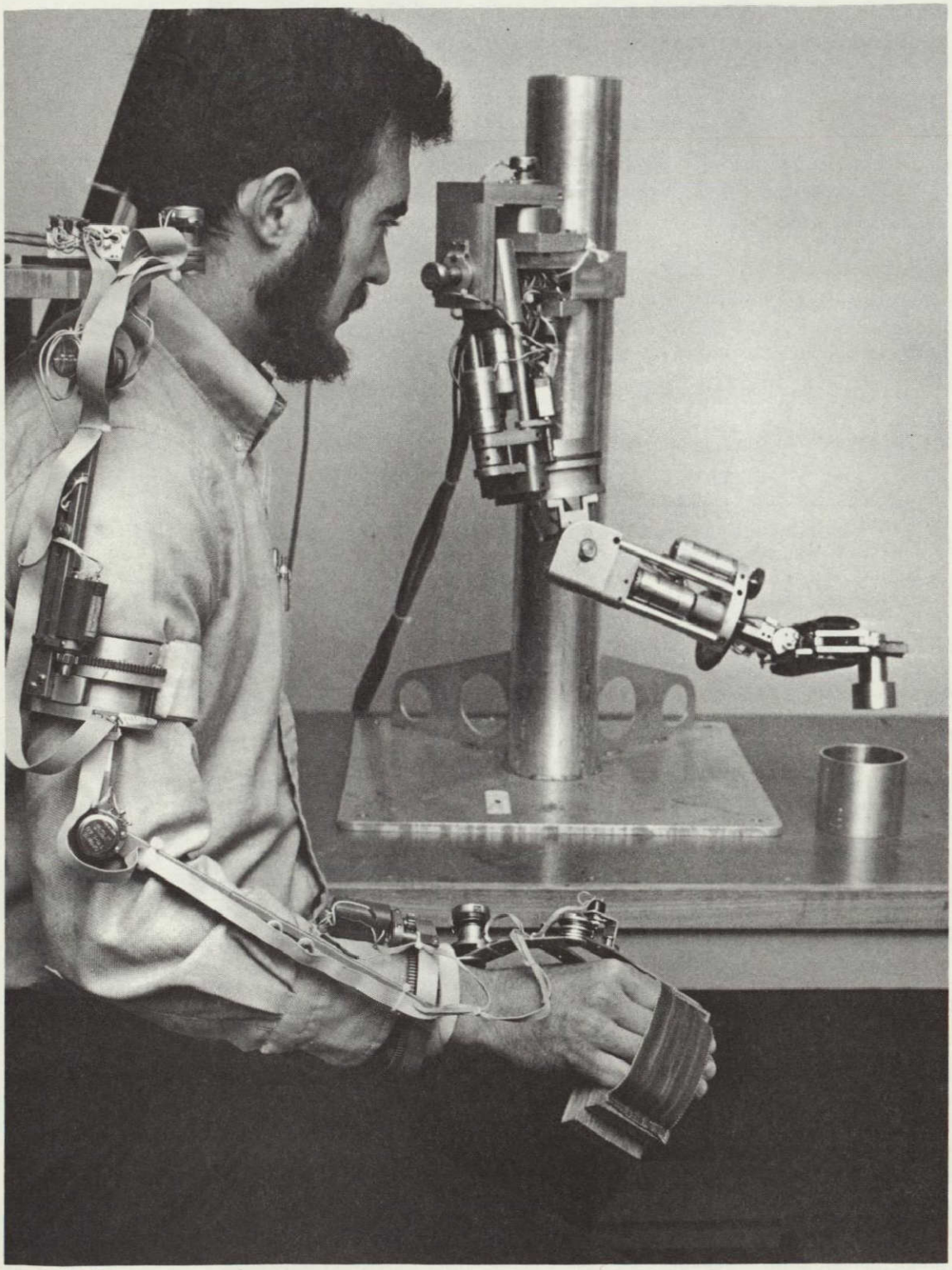

FIGURE 33 RANCHO MASTER-SLAVE MANIPULATOR

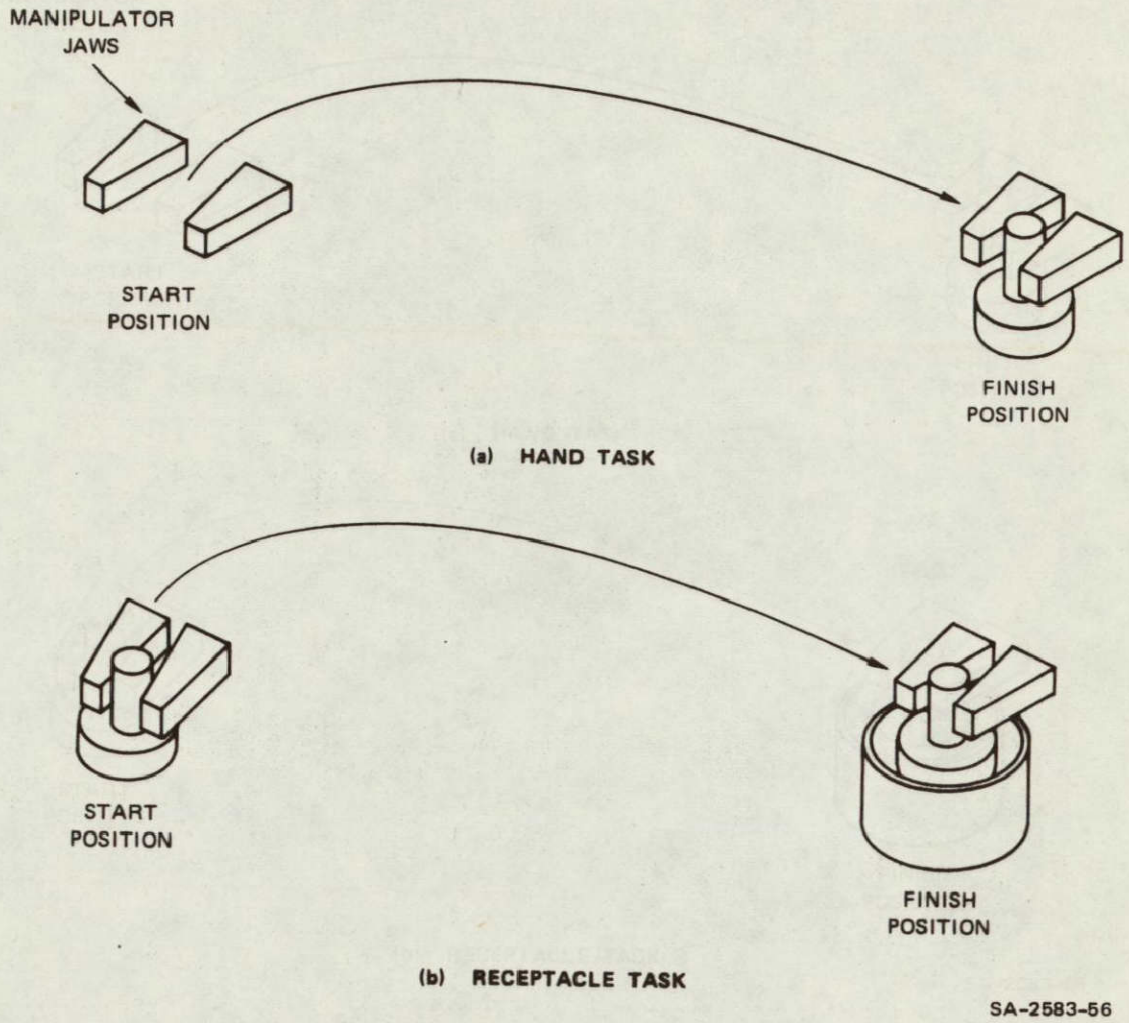

FIGURE 34 HAND AND RECEPTACLE TASK DESCRIPTION

4 and 5 bits. Figure 35 shows the blocks and receptacle. Table 15 lists the respective block sizes and movement distances. The successive sizes of H and R blocks were fastened together to form five blocks to be manipulated. The R blocks were larger to provide a convenient base for the H blocks.

Each experimental session lasted for approximately 25 minutes and consisted of two successive trials at each of the conditions of H tasks and R tasks (five block sizes and two I_d values each). An H task was

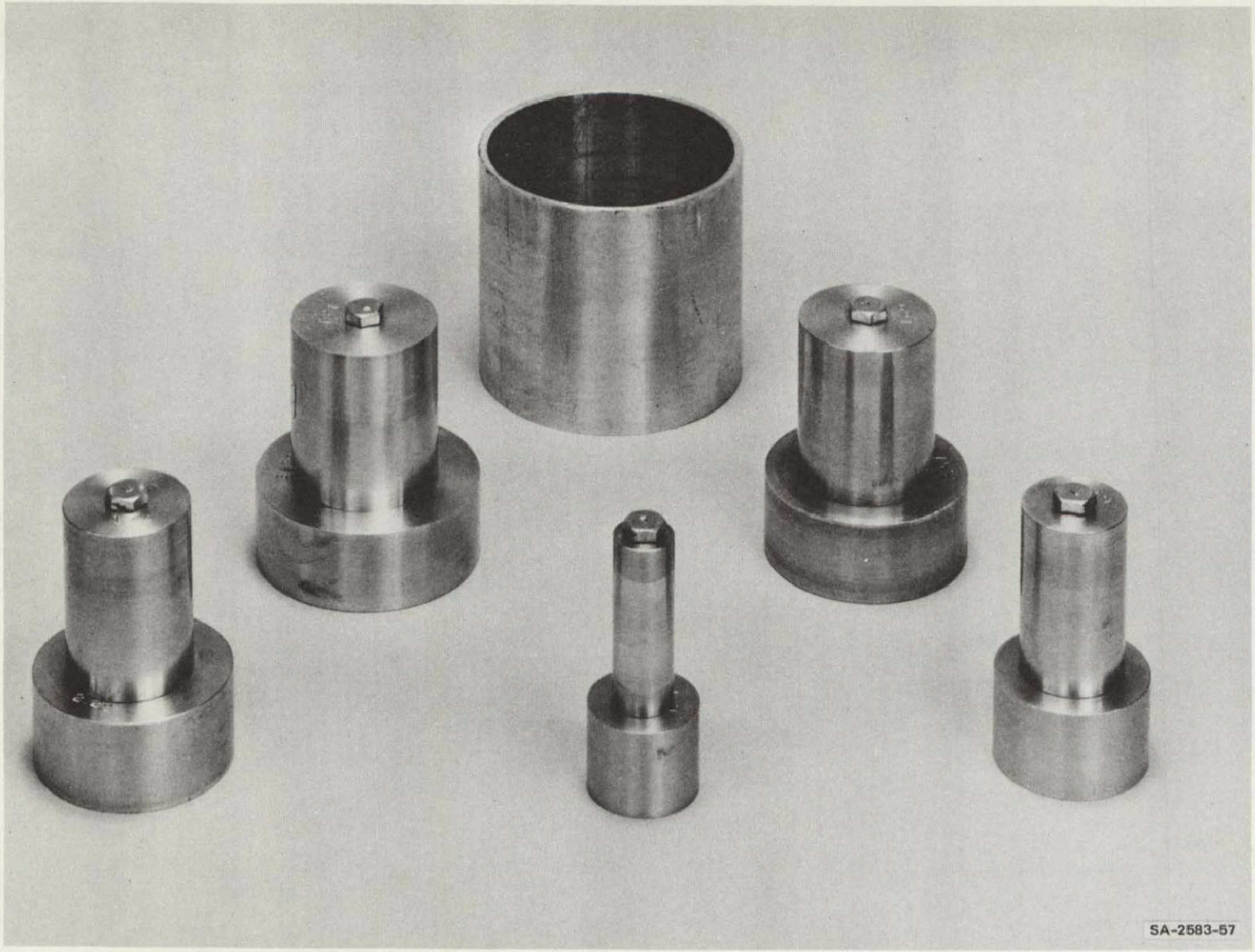

FIGURE 35 TASK BLOCKS AND RECEPTACLES

followed by the corresponding R task. Table 15 shows the correspondence between tasks. The order of presentation of the conditions was randomized and different for each session.

Table 15

TASK NUMERICAL DESCRIPTION
(RANCHO MANIPULATOR)

Computations are based on a jaw opening of 5.56 cm and receptacle inside diameter of 8.31 cm. Blocks of each row are connected.

Hand Task			Receptacle Task		
Block Diameter (cm)	Distance Moved (cm)	I_d (bits)	Block Diameter (cm)	Distance Moved (cm)	I_d (bits)
1.75	30.48	4	3.23	40.64	4
3.02	20.32	4	4.52	30.48	4
3.66	15.24	4	5.79	20.32	4
4.29	10.16	4	6.38	15.24	4
4.60	7.62	4	7.06	10.16	4
1.75	60.96	5	3.23	81.28	5
3.02	40.64	5	4.52	60.96	5
3.66	30.48	5	5.79	40.64	5
4.29	20.32	5	6.38	30.48	5
4.60	15.24	5	7.06	20.32	5

A two-day practice period (about two hours total practice for each operator) was followed by two days of data taking. Three sessions were run each day, with each session starting with several minutes of practice. The first session of the first day was considered as further practice and the data were discarded. A total of ten trials were made at each of the twenty sets of conditions by two subjects.

C. Results of the Rancho Manipulator Experiment

Considerable difficulty was evidenced in extending the arm to the distances required in the 24-inch H task and the 32-inch R task. The data for these distances were therefore discarded. From the remaining data, a regression analysis of the completion time versus movement distance was made with the conditions of operator, type of task, and index of difficulty held constant. The results of the regression are a linear equation describing times as a functional distance and an analysis of variance of the data within each group of times, and of the group means about the regression line. The hypothesis is that completion time should not vary for different movement distances for each condition of operator, task type, and value for I_d. That is, the changes in tolerance required to keep I_d constant as the required movement distance changes offsets the effect of changing the distance.

For the data in this experiment, the derived regression lines were linear (to a significance level of 0.05) and the slopes could be considered zero (to a significance level of 0.05) in all but one case.

A Bartlett test performed on the combined body of data (all operators, distances, and tolerances) rejects the hypothesis that it is from a common distribution at a significance level greater than 0.001. The same test on the $I_d = 4$ data and the $I_d = 5$ data accepts the hypothesis of a common distribution for each of these groupings (significance level less than 0.30). This supports the hypothesis that I_d acts as a quantifier for task difficulty.

A regression performed on the data using the index of difficulty, I_d, as the independent variable and task completion time as the dependent variable is shown in Figure 36 as well as the mean of each set of trials at each experimental condition.

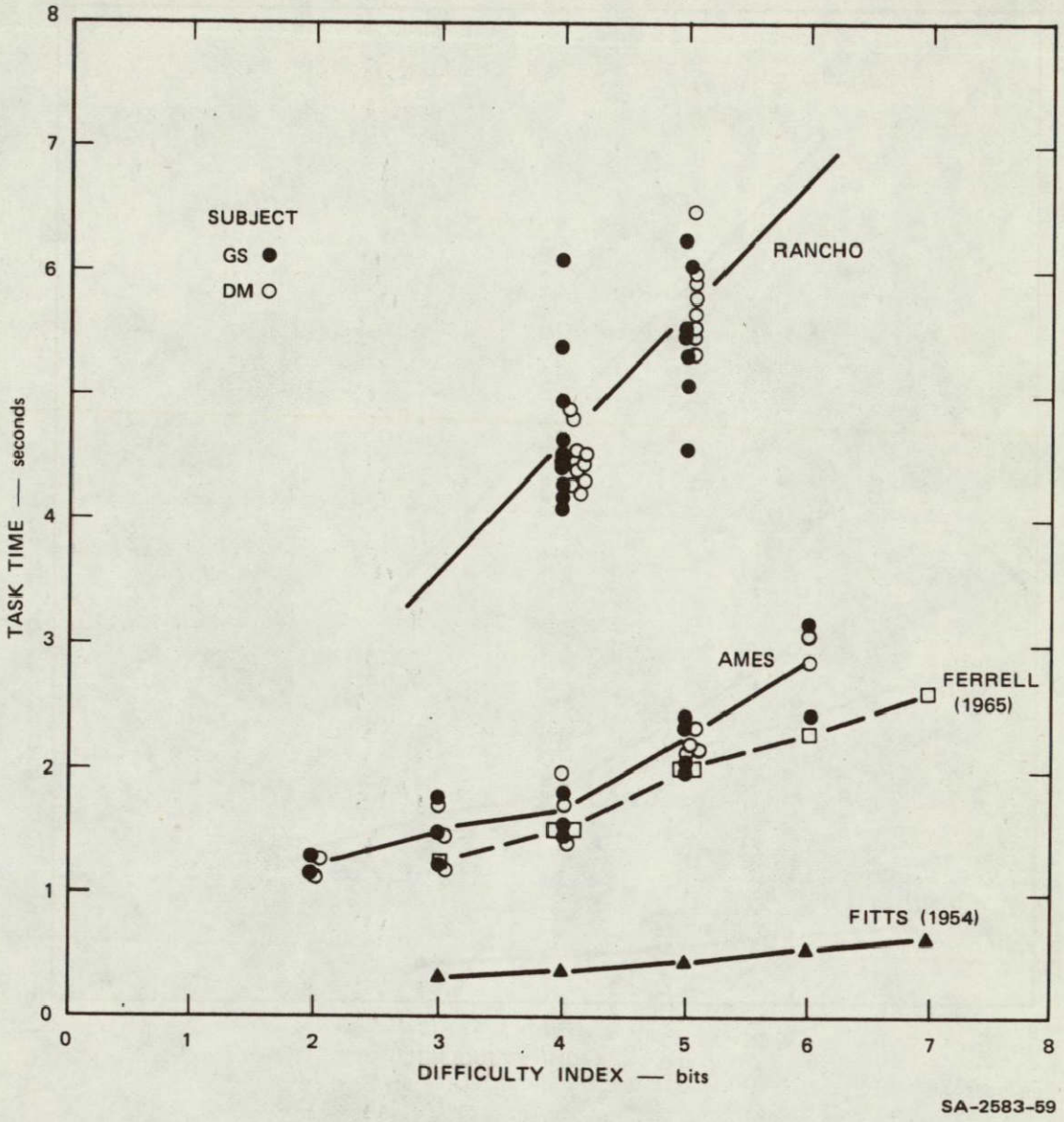

FIGURE 36 TASK TIME VERSUS DIFFICULTY

D. Description of the Ames Manipulator Experiment

A seven degree of freedom manipulator used in this experiment is described in detail by Vykukal, King, and Vallotton (1972). The experimental setup is shown in Figure 37 with the operator seated about five feet from the slave arm.

The end effector of the Ames manipulator, which was supplied by MBA Associates, does not have parallel jaws and was not well suited to the

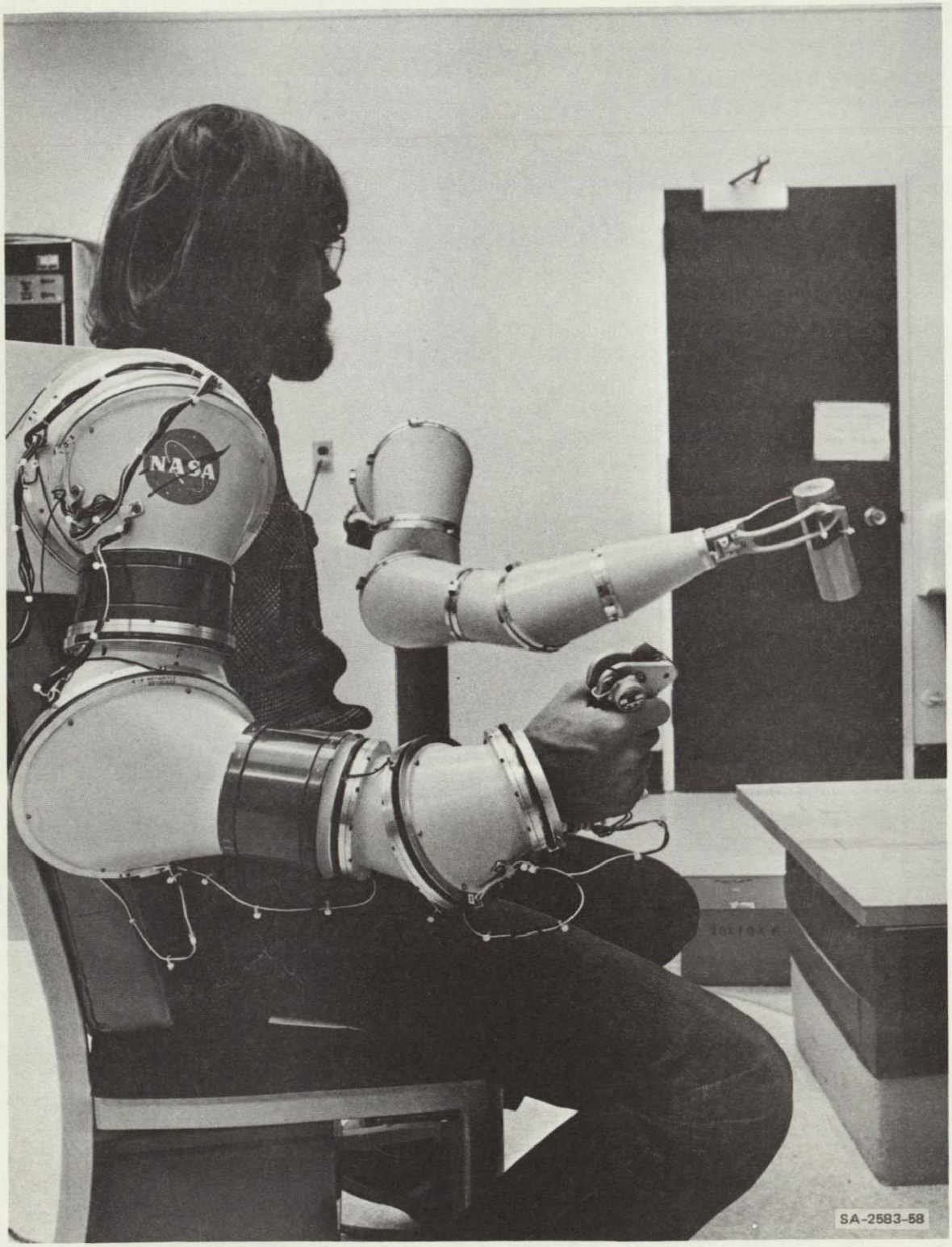

FIGURE 37 AMES MASTER-SLAVE MANIPULATOR

H task. To grasp an object, this end effector requires much more precision in extension or flexion than a parallel-jaw end effector. Results from the previous experiment with the Rancho Arm indicated that the H and R tasks were essentially equivalent. It was therefore decided to do only RECEPTACLE tasks since these did not require end effector alignment on a block as part of the timed task.

Blocks were sized and the distance moved was adjusted so that a wider range of difficulty could be provided. Table 16 lists the respective block sizes and movement distances. The block was grasped and positioned at the proper starting distance by the operator. Task time extended from a starting signal, given by an observer, until the block just entered the receptacle.

Each experimental session lasted for approximately five minutes and consisted of one trial at each of the 15 conditions listed in Table 16. The order of presentation of the conditions was randomized and different for each session. Ten trials were made at each of the 15 conditions.

The same operators were used in this experiment as in the Rancho manipulator experiment. An initial practice period of 20 minutes was allowed. Each session was started with several practice trials, and all data were gathered in one day.

E. Results of the Ames Manipulator Experiment

The data were treated as being from a common source with task completion time, t_c, as the dependent variable and index of difficulty, I_d, as the independent variable. An analysis of variance on these data indicated that a linear relationship is not a good fit to the data (significance less than 0.001). Figure 36 plots the average of the means of all the trials at each difficulty level as a function of difficulty level.

Table 16

TASK NUMERICAL DESCRIPTION (AMES MANIPULATOR)

Computations are based on a receptacle inside diameter of 8.31 cm

Block Diagram (cm)	Distance Moved (cm)	I_d (bits)
3.02	10.16	2
3.23	10.16	2
5.79	10.16	3
4.52	15.24	3
3.23	20.32	3
6.38	15.24	4
5.79	20.32	4
4.52	30.48	4
3.23	40.64	4
7.06	20.32	5
6.38	30.48	5
5.79	40.64	5
4.52	60.96	5
7.06	40.64	6
6.38	60.96	6

F. Conclusions

The major conclusion drawn from these experiments is that the index of difficulty defined by Fitts and used by Ferrell is a valid measure of task difficulty that can be extended to six or seven degree-of-freedom manipulators over at least a small range of operation. Thus, with I_d as a task descriptor, graphs like Figure 36 can be constructed to show task

time as a function of difficulty and to show relative differences between manipulator systems.

Included on Figure 36 are data from Ferrell (1963), using a minimal manipulator with two degrees of freedom, and from Fitts (1954), using a human hand to move pegs from one hole to another. The proximity of Ferrell's data to that derived from experimentation on the Ames manipulator should be noted. It is interesting to conjecture a manipulator "insertion loss" that adds a proportionate amount of difficulty regardless of the manipulator design. More experimentation will refine these data and perhaps lead to a method to quantize these differences.

Close inspection of both the component data and the overall results reveals the limitations of the above statements. Graphing time versus distance for constant I_d and operator indicates the existence of a weak functional relationship between time and distance. Insufficient results are at hand to plot a complete graph of this relationship but the trend is obvious from the data. In the movement range of six to sixteen inches the time required for completion of tasks of equivalent difficulty is almost constant. Out of this range, the time increases.

The equivalence of the tasks of moving an empty hand to a block and moving the block to a receptacle is inferred from the regression analysis on each value of I_d. If these tasks had differed significantly, results would not have been as good. Likewise, the difference in performance of different operators is shown to be not significant. This last result was anticipated from the results seen in previous manipulator experiments in which the difference between operators was shown to be not significant. It is most likely that in more complex tasks this will not be the case.

The superiority of the Ames manipulator over the modified Rancho manipulator is clearly shown. Not only is it quicker by a factor of two and one half, it results in far less variance in repeated trials. Operator fatigue was reduced as well.

VII DEVELOPMENT OF A PORTABLE PERFORMANCE MEASURING SYSTEM

A. Introduction

The experiments discussed in a previous chapter led to the conclusion that tasks can be described by an appropriate difficulty index. A closer appropriate inspection of the details of manipulation lead to a more detailed interpretation. Annett, Golby, and Kay (1958) in an investigation of human motor response, noted that even though the Fitts (1954) description quantized the total task of putting pegs in holes, it did not reflect the actual detailed response of the operator. In their experiments, motion picture analysis indicated two regions of motion. For 15/16ths of the total distance traveled, the travel time was essentially constant, regardless of the size of the target. Requirements on precision were reflected by motion in the last 1/16th of the distance.

This result does not invalidate Fitts' result but illustrates a closer scrutiny of the process of putting pegs in holes and a lower level of defined task complexity.

As applied to augmentation of manipulation, Fitts' definition would provide the human performance level the computer subroutine would have to exceed if it were to replace all of the task. If only a partial augmentation was to be used, the results of Annett, Golby, and Kay would have to be considered.

B. Preliminary Experimentation

Surveys of projected manipulator usage have shown that the major portion of manipulator operation is involved in positioning. This type

of task is then the most important to investigate in detail. This detail allows comparisons of the body of literature on both human and manipulator performance.

The previous experiments did not allow for detailed analysis of motion. A new set of experiments is being undertaken to provide this detail and to refine the earlier data.

Experimental hardware was fabricated to reflect two types of positioning. A peg-in-the-hole experiment provided a standard task with variable precision and a multiple DOF (degree-of-freedom) experiment provided a variable alignment task with fixed precision.

1. Standard Tasks

The peg in the hole experiment (Figure 38) used a task board with marked starting locations and a two-inch diameter receptacle. By varying the clearance between the peg and the hole and the required movement distance, tasks of differing difficulty (in the sense provided by Fitts' difficulty index) can be performed. Table 17 lists the peg diameters, task distances, and associated difficulties.

The starting locations are established with microswitches, giving an electrical timing signal when the peg is initially moved. The receptacle is instrumented with a linear potentiometer which is depressed by the peg entering the hole. This potentiometer provides a record when the peg enters the hole and a continuous record of depth in the hole.

The multiple-DOF task board shown in Figure 39 has three receptacles each requiring a further alignment of a working tool. The large (two-inch) square plate places few requirements on angular alignment or on lateral position. Depression of the plate triggers a microswitch to indicate completion.

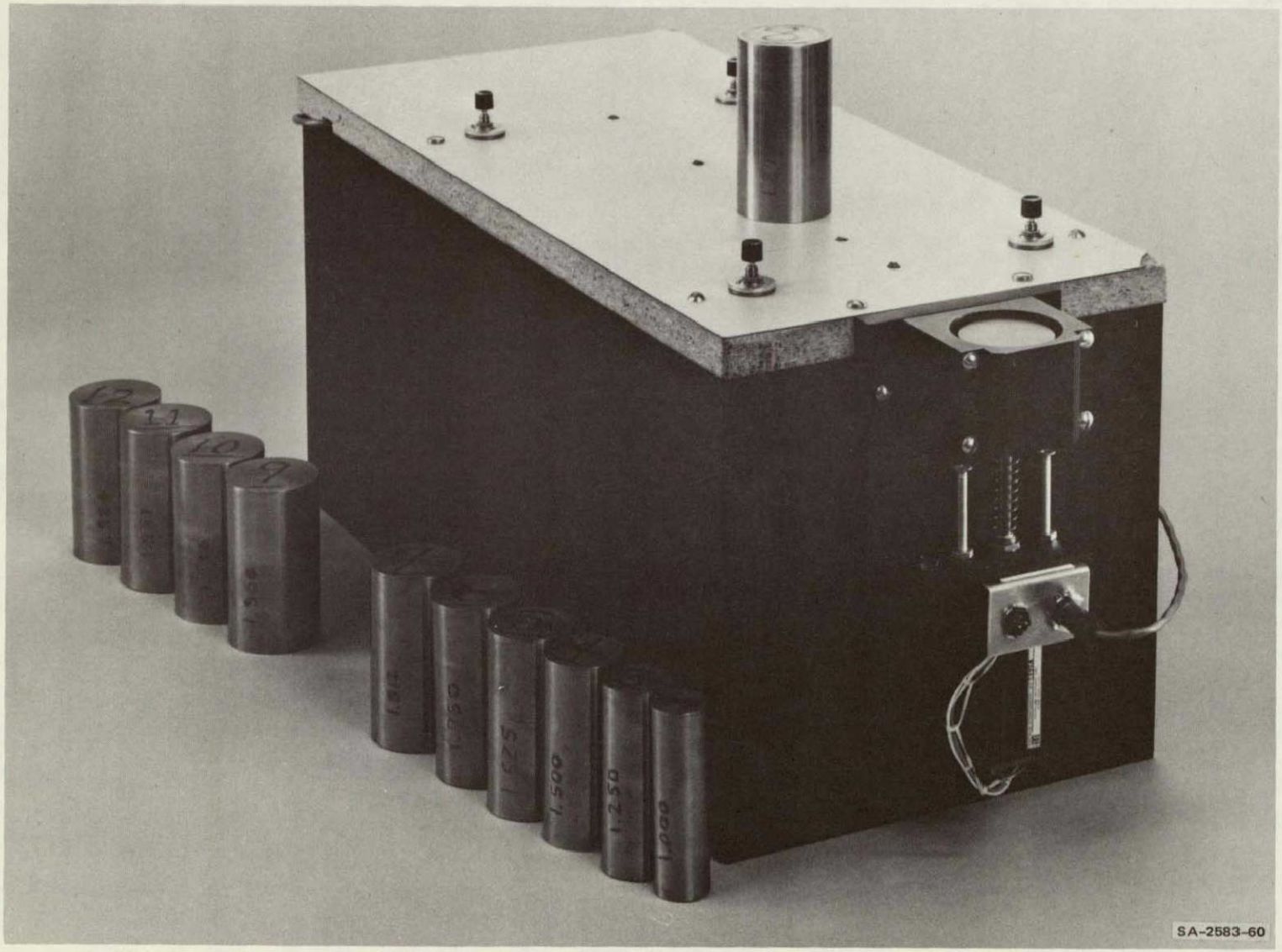

FIGURE 38 PEG-IN-HOLE TASK BOARD

Table 17

PEG-IN-HOLE BLOCK SIZES

(Receptacle inside diameter is 2.000 inches.)

Block Diameter (inches)	At Distance (inches)	I_d (bits)
1.00	16	5
1.25	12	5
1.50	8	5
1.625	6	5
1.750	4	5
1.750	16	7
1.812	12	7
1.875	8	7
1.906	6	7
1.938	4	7
1.938	16	9
1.969	8	9
1.984	4	9
1.984	16	11
1.992	8	11
1.996	4	11

The rectangular plate requires alignment in one lateral direction but little alignment in the other direction or in angular alignment. Again, a microswitch indicates when the plate has been depressed.

The small square plate requires more precise lateral alignment and, depending on tool configuration, varying amounts of angular alignment.

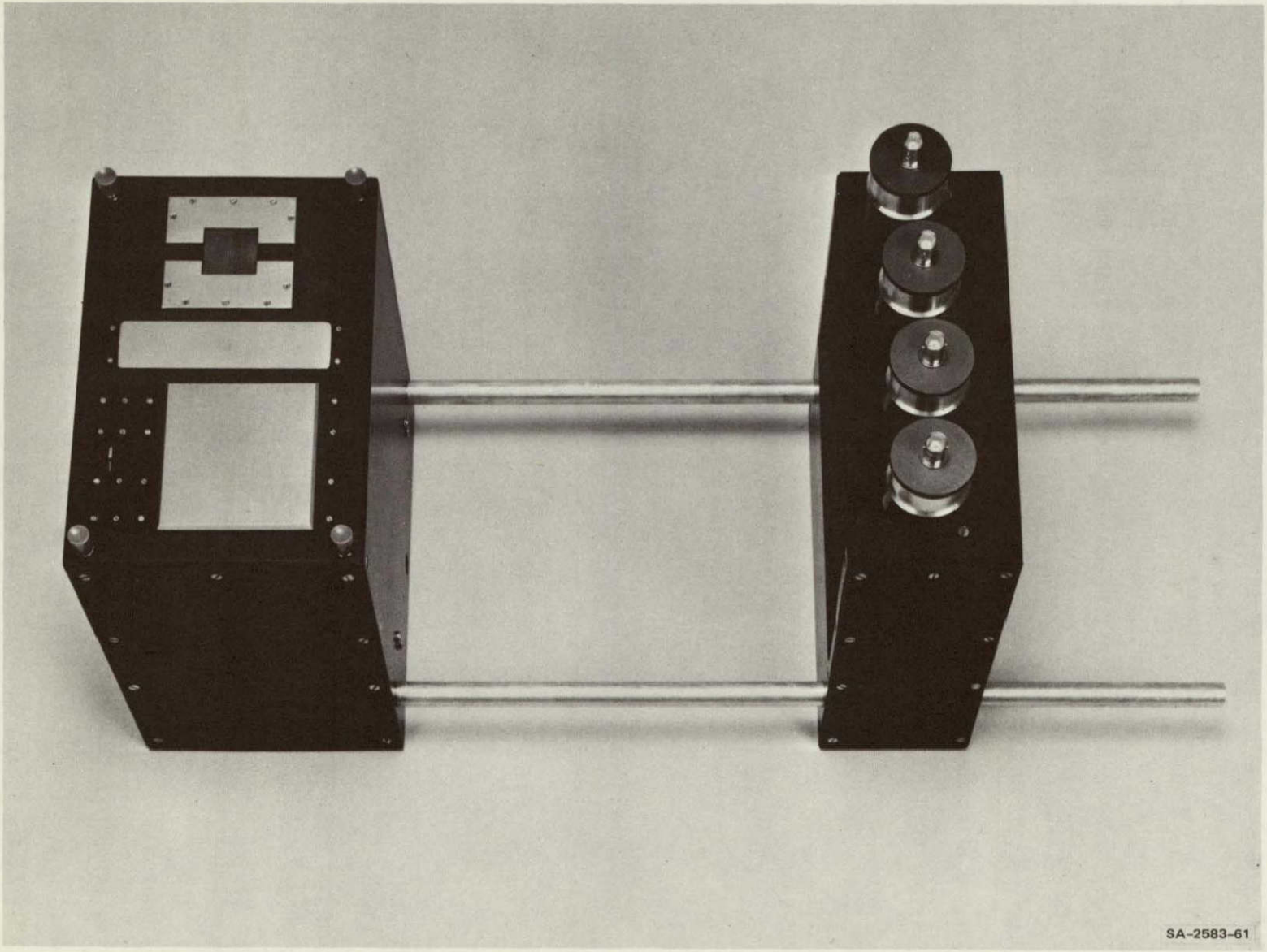

FIGURE 39 MULTIPLE DOF TASK BOARD

This plate is instrumented with a linear potentiometer similar to that on the receptacle in the peg in the hole task board.

The tools used for this task are shown in Figure 40. They are grasped at the large cylindrical end. The sphere is used to depress the large square plate and the rectangular plate for the two least constrained tasks. When the sphere is used to depress the small square plate, little angular alignment is required, as illustrated in Figure 41(a). The sphere, with projections, is used in the small square hole and is restricted in angular alignment by the slot that the projections must enter. The other two angular alignments are unrestricted [Figure 41(b)].

The cylinder with projections is restricted in one more alignment [Figure 41(c)] and the cube is totally restricted [Figure 41(d)]. Tolerances are provided such that a small amount of misalignment is allowed, enabling the completion of this task with a manipulator.

As in the peg-in-the-hole experiment, a microswitch is provided at the starting location so task initiation can be electrically sensed. The microswitches at the various receptacles furnish a task termination signal.

2. Data Gathering Equipment

A comprehensive data taker/performance monitor was developed to allow recording of many variables during a manipulation experiment. This system, shown in Figure 42, was used to sample 23 channels of analog information at 10 hertz. The information was digitized in a 12-bit analog-to-digital convertor and recorded on half-inch 7-track magnetic tape by a Kennedy digital tape recorder. A NOVA 1210 computer provided the interface between the digitized signal and the tape recorder and allowed alphanumeric information to be recorded as a header record (title) to each data run.

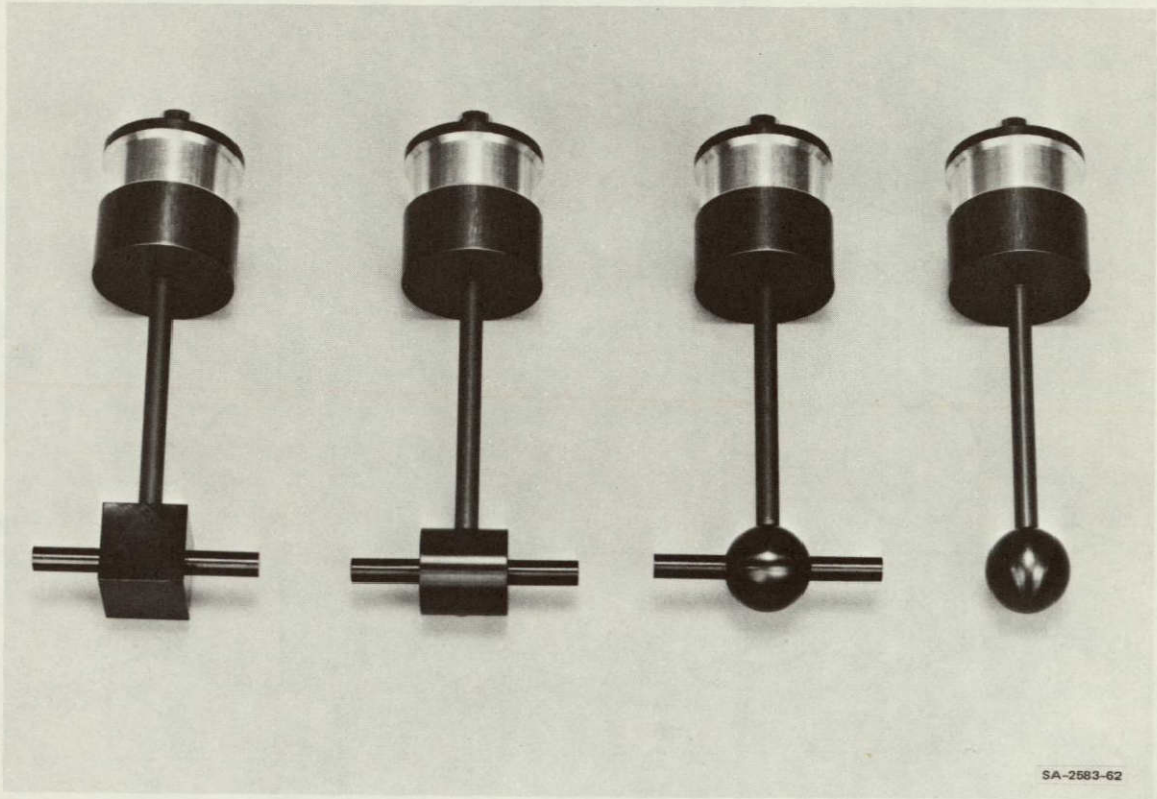

FIGURE 40 TOOLS FOR MULTIPLE DOF TASK BOARD

The system recorded master and slave joint angles (16 channels), real-time position and velocity information (6 channels), and timing information from the task board microswitches (1 channel). The position sensing was through a set of three tensioned strings connected to the peg or tool. Figure 43 illustrates a typical experimental setup. The position and velocity of each string was provided by a ten-turn potentiometer and a tachometer driven by the string, as described in Section V.

3. Data Reduction

A computer program was developed for the CDC 6400 computer to convert the digitized signals from the data taker magnetic tape into

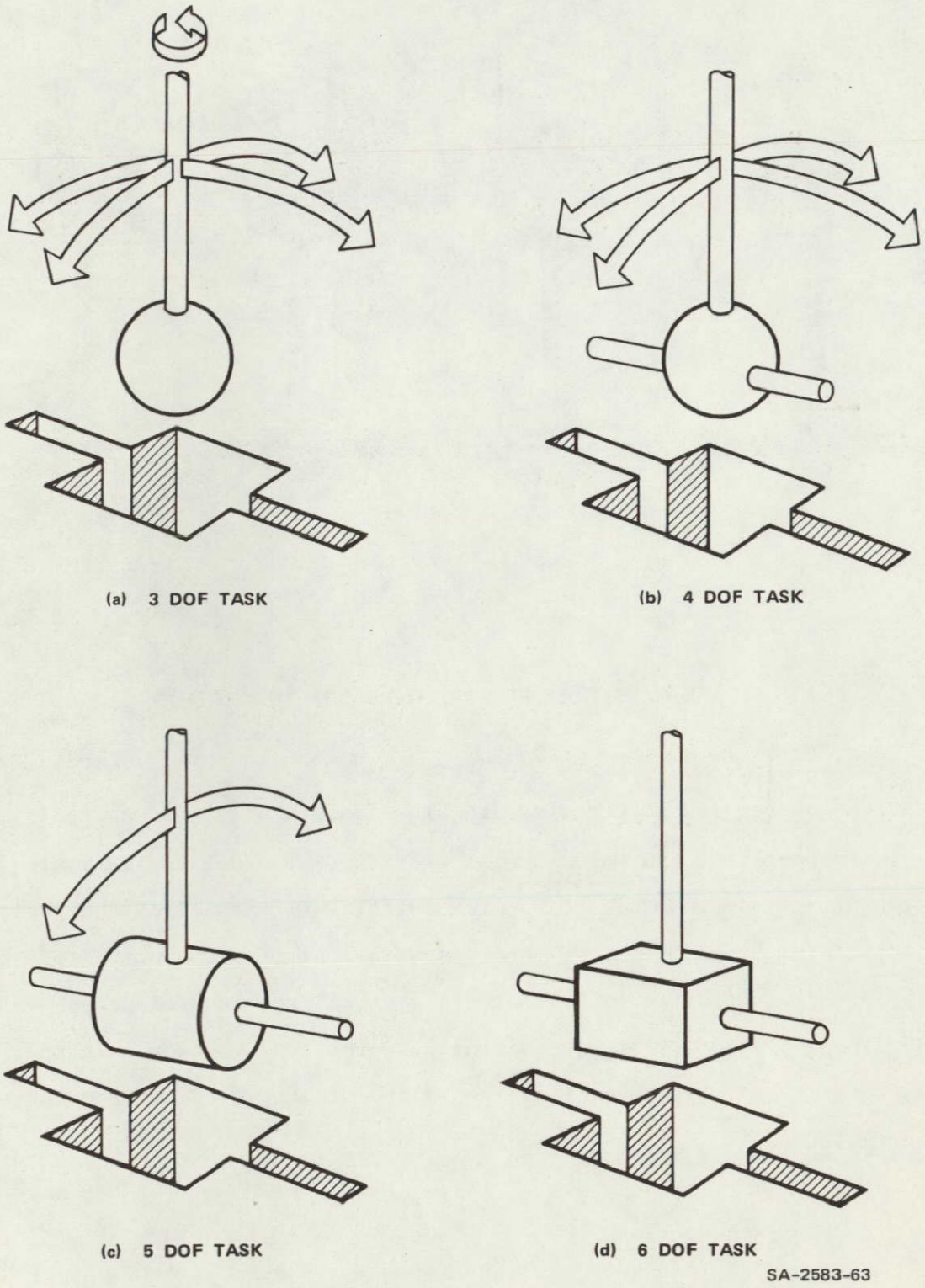

FIGURE 41 FITTING MULTIPLE DOF TOOLS INTO SPECIAL HOLE

Arrows indicate free angular alignments.

FIGURE 42 PORTABLE DATATAKER

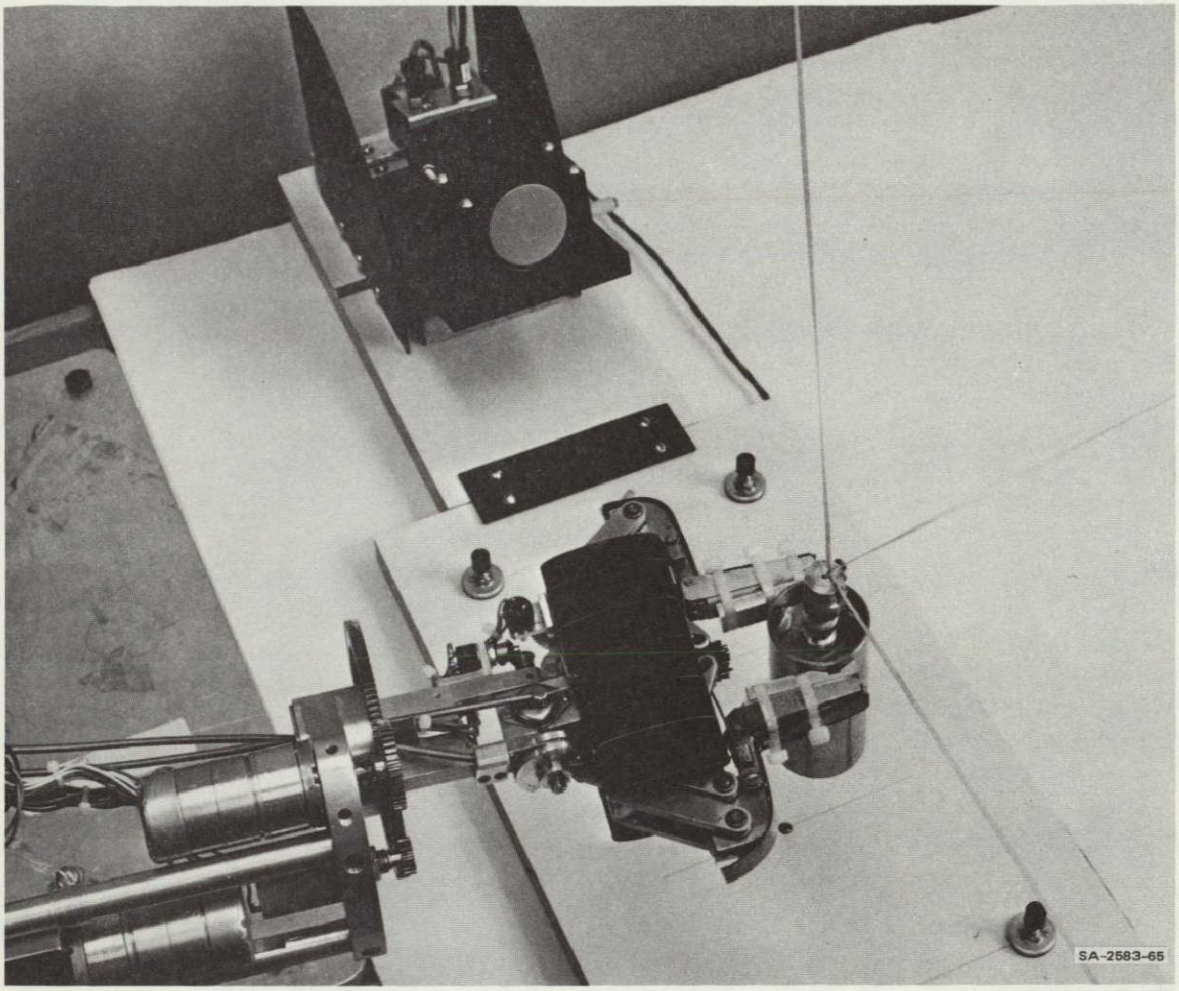

FIGURE 43 EXPERIMENTAL SETUP WITH POSITION SENSING STRINGS AND TASK BOARD

manipulator joint angles, orthogonal position and velocity of the tool, and depth of insertion in the task board receptacle. The transformations required to convert the position and velocity provided in the curvilinear coordinates of the sensors into orthogonal position and true vector velocity are described in Appendix H.

Output from the computer system is in the form of a printed listing of results and a formatted magnetic tape. Figure 44 shows a sample listing of position and velocity measures and the joint angles. The

tape provides a compact record of the experiment and allows rapid reprocessing by a computer, without reconversion of the various inputs. Simple results can be obtained from the output listing, but because of the large quantity of information obtained (23 numbers for each 0.1 second of experiment time), any involved data searches will utilize the tape output.

C. Preliminary Results

A short series of preliminary experiments were performed using the Rancho manipulator and the peg-in-the-hole task board shown in Figure 38. These experiments represented a developmental effort and were somewhat crude in terms of controls and rigid experimental practice. Also, at the time the data were taken, noise was present in the tachometer circuits of the position sensors. However, even with these limitations, the data obtained are useful in coarse investigations of manipulator performance.

Following the interpretation advanced by Annett, Golby, and Kay (1958), the time versus distance from the hole was averaged for all the experimental runs of equal difficulty. Table 18 lists the mean and standard deviations for the runs in each category. As can be seen, the increased time required for increased precision is incurred in the last several inches of movement. The definition of the final adjustment area cannot be determined more closely from the developmental experiments cited here. However, more detailed experimentation has been performed and it is hoped that a final adjustment area can be firmly identified.

The comprehensive data obtained from the data taker described above lends itself to manipulator system performance evaluation. A plot of

DATA RUN NUMBER 3

TIME SEC.	X	Y	Z	VX	VY	VZ	VMAG	DCHAN	MJ1	SJ1	MJ2	SJ2	MJ3	SJ3	MJ4	SJ4	MJ5	SJ5	MJ6	SJ6	MJ7	SJ7
	DOUGTHREE	INCHES		INCHES PER SECOND				IN.	DEGREES													
.1	8.1	.5	4.5	0.0	0.0	0.0	0.0	2.526	-4.5	-4.9	-3.3	-3.6	-2.2	-1.8	91.7	92.1	56.5	57.3	-73.7	-50.0	23.3	22.9
.2	8.1	.5	4.8	0.0	0.0	0.0	0.0	2.523	-4.7	-4.7	-3.3	-3.5	-2.1	-1.8	91.9	92.8	56.5	57.3	-73.7	-50.0	23.4	23.1
.3	8.0	.5	4.8	0.0	0.0	0.0	0.0	2.523	-4.7	-4.9	-3.3	-3.8	-2.1	-2.0	91.9	92.1	56.5	57.3	-73.7	-50.0	23.3	23.9
.4	8.1	.5	4.8	0.0	0.0	0.0	0.0	2.523	-4.7	-4.9	-3.3	-3.8	-2.1	-2.0	91.9	92.1	56.5	57.3	-73.7	-50.0	23.3	23.9
.5	8.0	.5	4.8	0.0	0.0	0.0	0.0	2.523	-4.7	-4.9	-3.3	-3.8	-2.1	-2.0	91.7	92.1	56.5	57.3	-73.7	-50.0	23.3	23.9
.6	8.0	.5	4.8	0.0	0.0	0.0	0.0	2.523	-4.7	-4.9	-3.3	-3.8	-2.1	-2.0	91.7	92.1	56.5	57.3	-73.7	-50.0	23.3	23.9
.7	8.0	.5	4.8	0.0	0.0	0.0	0.0	2.523	-4.7	-4.9	-3.3	-3.8	-2.1	-2.0	91.7	92.1	56.5	57.3	-73.7	-50.0	23.3	23.9
.8	8.0	.5	4.8	0.0	0.0	0.0	0.0	2.528	-4.7	-5.3	-3.3	-3.8	-2.1	-2.0	91.7	92.1	56.5	57.3	-73.7	-49.9	23.5	23.9
.9	8.0	.5	4.8	0.0	0.0	0.0	0.0	2.523	-4.7	-4.9	-3.3	-3.8	-2.1	-2.0	91.7	92.1	56.5	57.3	-73.7	-50.0	23.3	23.9
1.0	8.0	.5	4.8	0.0	0.0	0.0	0.0	2.528	-4.7	-5.0	-3.3	-3.6	-2.1	-2.0	91.9	92.1	56.5	57.3	-73.7	-50.0	23.3	23.9
1.1	8.0	.5	4.9	.0	.0	.3	.3	2.522	-4.4	-4.9	-3.1	-3.8	-2.1	-2.0	92.5	92.3	56.5	57.1	-73.7	-50.0	23.3	23.9
1.2	8.1	.6	5.6	.1	.8	9.6	9.6	.005	-3.5	-4.7	-3.1	-3.9	-2.5	-2.3	95.1	94.1	55.0	56.5	-73.7	-50.2	24.3	24.3
1.3	7.8	.8	7.2	-5.7	2.4	12.9	14.3	.005	-2.1	-3.5	-2.8	-3.8	-3.8	-3.1	97.1	97.6	52.4	53.4	-73.9	-50.2	26.6	26.7
1.4	5.5	1.1	7.7	-18.8	3.0	-.3	19.0	.005	-.1	-1.2	-2.8	-3.9	-6.3	-5.8	97.0	97.3	51.5	51.7	-73.9	-50.2	27.6	28.5
1.5	3.7	1.5	7.1	-21.0	1.2	.6	21.0	.006	1.8	.7	-2.8	-3.9	-9.6	-8.9	96.2	96.3	51.5	52.2	-74.1	-50.3	27.7	28.7
1.6	1.9	1.2	6.6	-16.9	.1	-5.0	17.6	.005	3.2	2.4	-2.8	-3.9	-12.7	-11.9	94.5	94.9	51.5	51.9	-73.9	-50.3	28.5	29.2
1.7	.2	.0	5.9	-15.4	-2.4	-5.3	16.4	.005	3.5	2.7	-3.1	-3.9	-15.8	-15.7	93.7	93.7	51.5	51.9	-73.9	-50.3	28.7	29.9
1.8	-.6	-.1	5.6	-9.5	-2.3	-4.7	10.9	.005	3.4	2.7	-3.3	-3.8	-17.7	-17.1	93.0	92.9	51.5	51.9	-74.1	-50.3	28.8	29.9
1.9	-.8	.6	4.8	-1.2	-1.5	-7.0	7.3	.005	2.8	2.4	-3.3	-3.9	-17.8	-17.8	92.2	92.4	51.6	52.0	-73.9	-50.3	28.8	29.9
2.0	-.7	.6	4.7	1.2	-.3	-1.0	1.6	.005	2.2	1.6	-3.3	-3.9	-17.7	-17.8	92.0	92.3	52.2	52.5	-74.1	-50.3	28.8	30.1
2.1	-.4	.5	4.7	2.2	-.0	-.2	2.2	.005	1.8	1.3	-3.3	-3.8	-17.5	-17.4	91.9	92.3	52.2	52.8	-74.1	-50.2	28.8	30.1
2.2	-.3	.5	4.7	1.4	.0	-.2	1.4	.005	1.5	1.2	-3.3	-3.8	-17.2	-17.1	91.8	92.1	52.2	52.8	-74.1	-50.2	28.8	30.1
2.3	-.1	.6	4.7	1.1	-.0	-.0	1.1	.005	1.5	.7	-3.3	-3.6	-16.9	-16.8	92.0	92.3	52.2	52.8	-74.1	-50.2	28.8	30.1
2.4	-.1	.6	4.7	.4	-.0	-.0	.4	.005	1.4	.7	-3.1	-3.8	-17.1	-17.0	92.2	92.4	52.2	52.8	-74.1	-50.2	28.8	30.1
2.5	-.0	.5	4.7	1.4	-.1	-.1	1.4	.005	.9	.7	-3.3	-3.6	-16.9	-16.8	92.5	92.4	52.2	52.8	-73.9	-50.2	28.8	30.1
2.6	.1	.5	4.7	1.2	-.3	-.2	1.3	.005	.8	.2	-3.3	-3.6	-17.1	-17.0	92.8	92.8	52.2	52.8	-74.1	-50.2	28.8	30.1
2.7	.2	.5	4.7	.5	-.4	-.4	.7	.005	.2	-.4	-3.3	-3.8	-17.1	-17.0	93.3	93.6	51.9	52.5	-74.1	-50.2	28.8	30.1
2.8	.2	.4	4.5	-.1	-.9	-1.8	2.0	.247	-.1	-.8	-3.3	-3.8	-16.9	-17.0	93.4	93.4	51.6	52.5	-74.1	-50.2	28.8	30.1
2.9	.2	.4	4.4	-.4	-.5	-.5	.8	.273	-.2	-.5	-3.3	-3.8	-17.2	-17.0	93.4	93.4	51.5	52.0	-74.0	-50.3	28.8	30.1
3.0	.2	.3	4.4	-.2	-.3	-.7	.7	.340	-.2	-.7	-3.3	-3.8	-17.1	-17.0	93.1	93.4	51.5	52.0	-74.2	-50.3	28.8	30.1
3.1	.1	.3	4.3	-.2	-.2	-.6	.7	.429	-.4	-.7	-3.3	-3.6	-16.9	-17.0	92.5	92.8	51.6	52.2	-74.2	-50.3	28.8	30.1
3.2	.1	.3	4.2	-.0	-.0	-.6	.6	.470	-.4	-.5	-3.3	-3.6	-16.8	-16.8	91.6	92.4	51.9	52.5	-74.5	-50.5	28.8	30.1
3.3	.1	.4	4.2	-.0	.4	-.4	.6	.494	-.2	-.5	-3.3	-3.6	-16.4	-16.5	90.6	91.8	52.2	53.0	-74.7	-50.3	28.8	30.1
3.4	.1	.4	4.2	-.0	.1	-.5	.5	.527	-.4	-.1	-3.3	-3.5	-16.1	-16.2	90.0	91.2	52.4	53.0	-74.8	-50.3	28.8	30.1
3.5	.2	.4	3.9	-.2	-.2	-5.6	5.6	.967	-.6	-.1	-3.3	-3.5	-16.1	-16.2	89.2	90.3	52.6	53.3	-74.8	-50.3	28.8	30.2
3.6	.0	.3	3.1	-.9	-1.0	-4.7	4.9	1.622	-.8	-.1	-3.3	-3.5	-16.1	-15.9	89.1	89.5	52.6	53.4	-75.2	-51.1	28.7	30.2
3.7	.0	.3	3.1	.1	-.0	-.6	.6	1.622	-.8	-1.4	-3.1	-3.6	-16.0	-15.9	88.9	89.7	52.6	53.1	-75.2	-51.3	28.5	30.2
3.8	.0	.3	3.1	-.1	-.0	-.2	.3	1.622	-.8	-.6	-3.2	-3.3	-16.0	-16.0	89.1	89.5	52.6	53.1	-75.2	-51.3	28.5	30.2
3.9	.0	.3	3.1	0.0	0.0	0.0	0.0	1.622	-.6	-.5	-3.1	-3.6	-16.0	-16.0	89.4	89.7	52.6	53.3	-75.2	-51.3	28.5	30.2
4.0	.0	.3	3.2	.1	.1	2.1	2.1	1.478	-.4	-.5	-3.3	-4.3	-16.1	-15.9	91.3	90.2	52.6	53.1	-75.2	-51.4	28.5	30.2

FIGURE 44 OFF-LINE PRINTOUT FOR A PEG INSERTION TASK

Shown as a function of time are the true position (X, Y, Z), true velocity (VX, VY, VZ), velocity magnitude (VMAG), insertion depth (DCHN), and master and slave joint angles (MJ1 TO MJ7 and SJ1 to SJ7) in degrees

Table 18

PRELIMINARY DATA FROM PEG-IN-HOLE TASK

(The inside diameter of the hole is 2.0 inches)

Peg Diameter (inches)	Movement Distance (inches)	I_d (bits)	Time to Reach ( ) from Hole			Time to Enter Hole (seconds)	Number of Runs
			2 inches	1.5 inches	1 inch		
1.00	16	5	3.3 (σ = 0.234)	3.48 (σ = 0.173)	3.73 (σ = 0.189)	8.93 (σ = 2.43)	6
1.00	8	4	2.11 (σ = 0.355)	2.24 (σ = 0.377)	2.34 (σ = 0.403)	5.02 (σ = 0.891)	6
1.875	8	7	2.10 (σ = 0.511)	2.25 (σ = 0.515)	2.40 (σ = 0.515)	15.55 (σ = 8.02)	6
1.96	4	9	1.0	1.15	1.32	~ 30	2

time to reach the final adjustment area as a function of starting distance, as seen in Figure 45, reflects the speed of the manipulator system and the confidence of the operator. Few precision movements appear in this movement range. Faster or more tightly controlled systems will reach the final area sooner and will have less variation with distance.

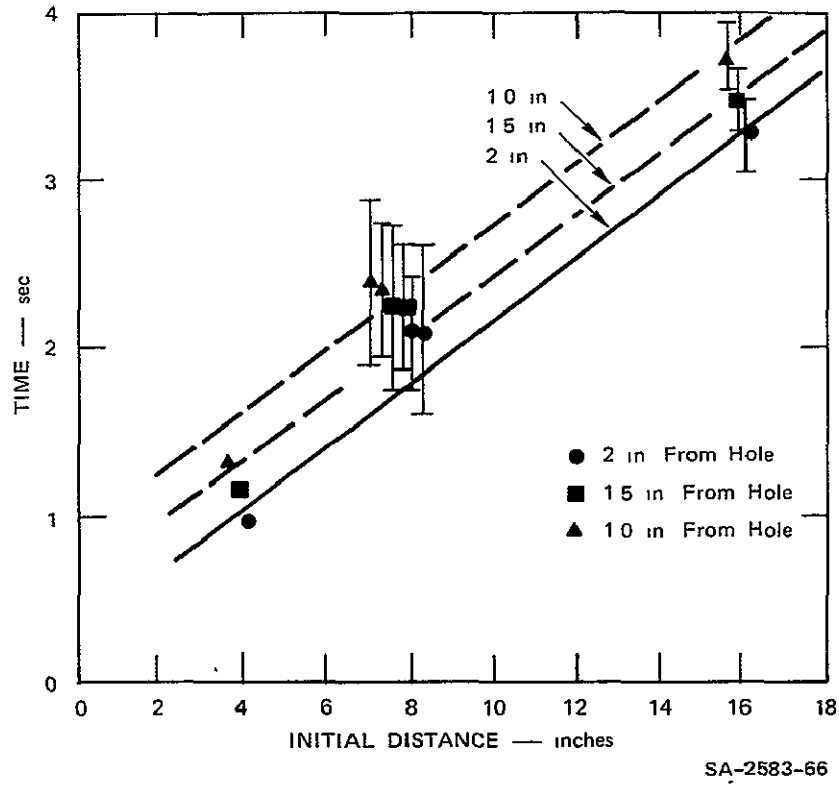

FIGURE 45 TIME TO APPROACH HOLE

The length of the vertical bars is two standard deviations

Investigating the end effector velocity as a function of distance reveals details of the strategy employed by the operator. Figure 46 shows a plot of velocity in the x direction (the major axis of motion in this experiment) versus displacement along the x axis for three trials.

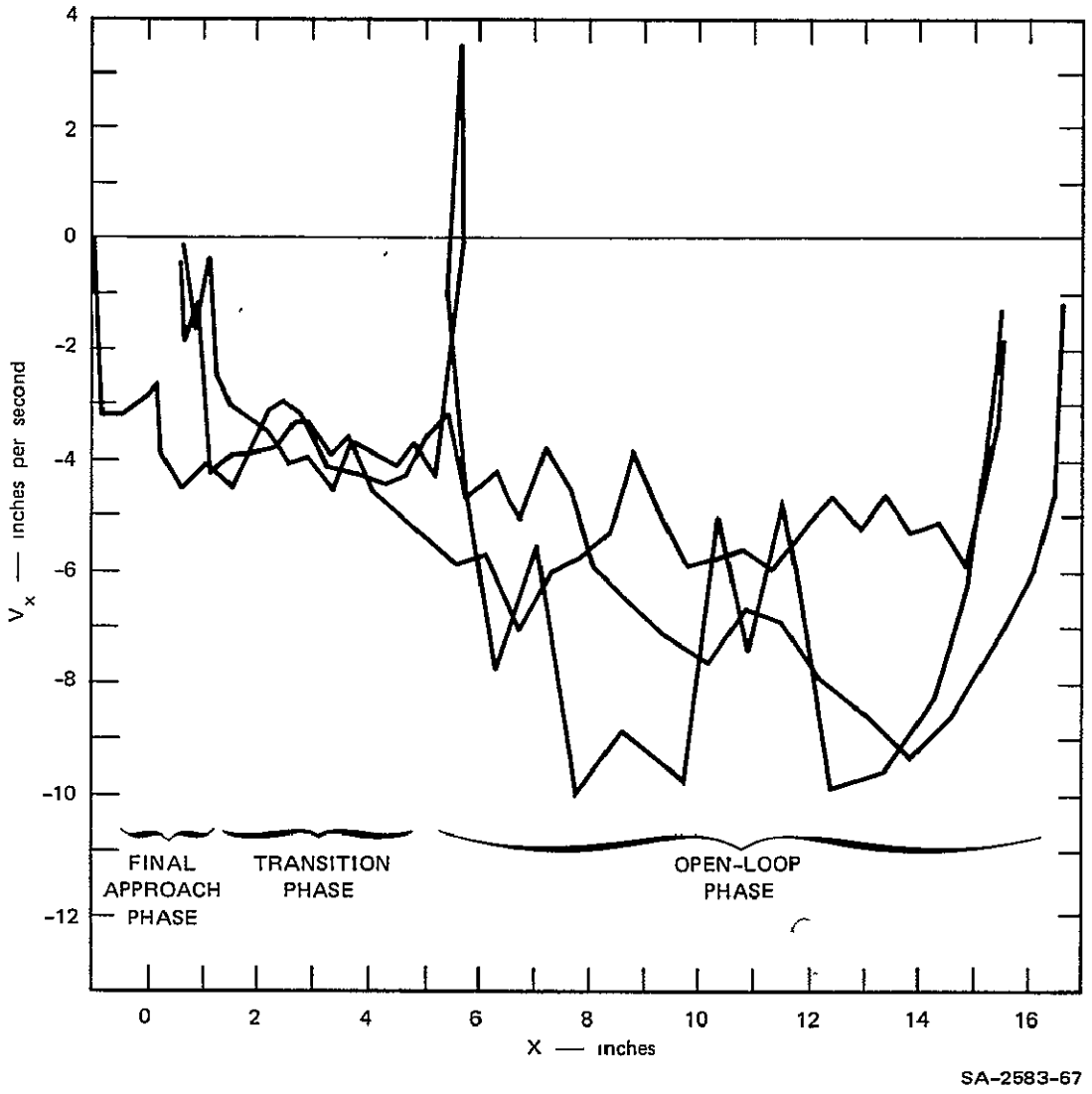

FIGURE 46 PHASE PLANE PLOT FOR THREE PEG-IN-HOLE INSERTIONS

The task was to place a 1 00-inch peg in a 2 00 inch hole from a distance of 16 inches

The origin is chosen to correspond to the center of the receptacle. Three general areas are marked on this graph to identify the strategy the operator is using. The initial strategy is essentially an open loop movement to "near" the receptacle. The peaks in velocity are partially a result of the kinematics of the manipulator system. A smooth movement involving seven joints results in a varying velocity at the end effector.

Some of the jerkiness is due to the lack of smooth response in the system under test. The remainder is due to noise in the velocity measurement system.

The end of the initial open-loop movement strategy occurs at approximately six inches from the receptacle. One of the runs indicates a reversal in velocity at this point. The servo-lag in the manipulator was such that the operator was leading the slave by a considerable margin. At the point of reversal, the operator was trying to "catch" the slave to reassume tight control. The other runs also indicate a slowing of the motion as the operator regains tight control.

From this point to about one inch from the receptacle, the average velocity was slightly lower, reflecting the second area of strategy. The operator was in firm control of the system but was still approaching the receptacle.

At about one inch from the receptacle, the operator enters a terminal approach phase. The x velocity decreases while the vertical velocity becomes large. The attempt is made to insert the peg in the hole.

Investigation of the joint angle records shows this even more clearly. Figure 47 shows joints one, two, four, and five for a typical task. The first two joints are the shoulder, the next the elbow, and the last wrist rotation of the manipulator. These angles are plotted as a function of time with the pertinent phases of the trajectory indicated. The servo delay in this particular system is readily seen by comparing master commands with slave response. The various command changes and trajectory corrections can also be seen. The initial open loop strategy is characterized by high speed transit in a not well controlled manner. In the transition phase, velocity is lower and about

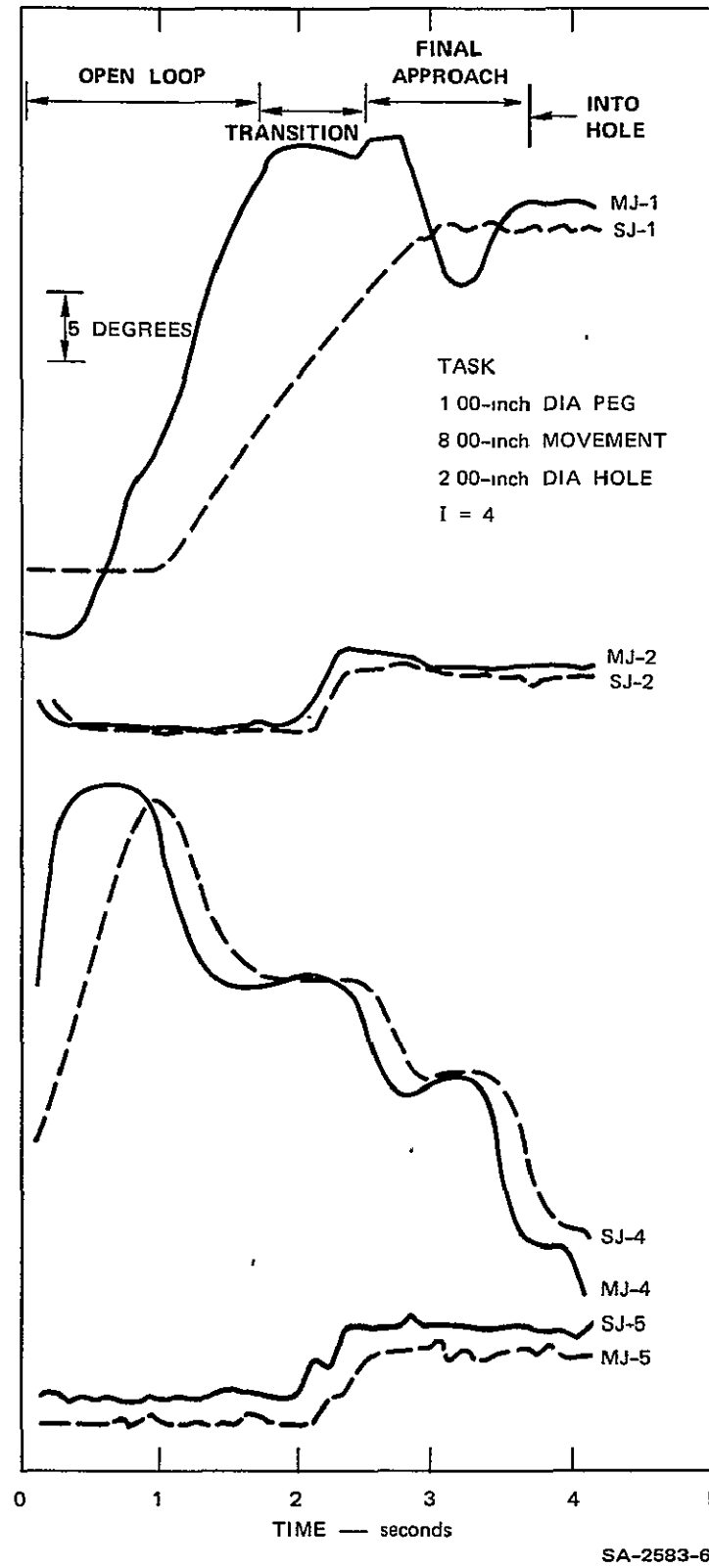

FIGURE 47 JOINT ANGLE RECORD FOR PEG-IN-HOLE INSERTION

the same for all runs. In the final approach phase, velocity decreases and fine adjustments are made based on the operator's evaluation of overshoot or undershoot to the hole.

Investigations of this sort, when completed in more and better detail will eventually lead to a firmer understanding of the process of manipulation. The determination of final areas of adjustment will lead to more efficient computer augmentation on the partial task scale. The recognition of how the operator determines the limits of the various types of moves (the transition between initial open loop and approach trajectories, for instance) will contribute to the design of feedback and operator training programs to emphasize the desirable aspects. The definition of tasks, based on the manner in which they are actually performed will enhance the capabilities of the systems planner to predict response to new environments.

Appendix A

DETAILED DESCRIPTION OF THE SRI END EFFECTOR

Appendix A

DETAILED DESCRIPTION OF THE SRI END EFFECTOR

A. Tactile Jaws

The method of operation of the two tactile sensing jaws has been previously discussed in Section IV of this report. The construction details of the jaws, the external touch sensing plates, and the jaw sensor matrices are discussed and illustrated in Figures A-1 to A-8.

B. Jaw Actuation

The jaws are actuated by a conventional motor driven bevel-gear/spur-gear drive train, best understood by referring to Figures A-9 to A-12.

C. Force Sensing Wrist

The method of operation of the six-axis force sensing wrist has been previously discussed in Ref. 5 and is illustrated in Figures A-13 to A-19.

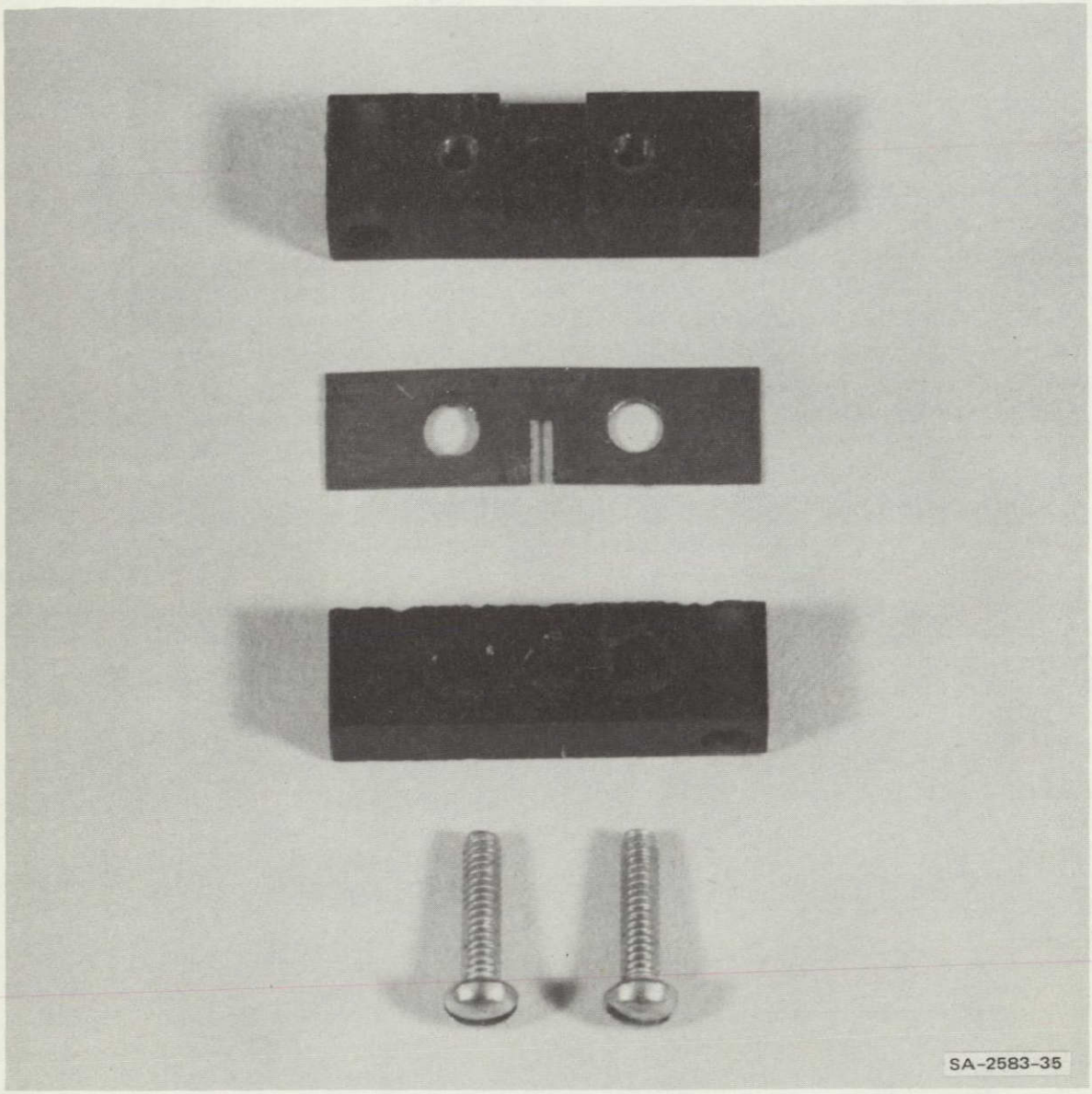

FIGURE A-1 BASIC PROPORTIONAL TACTILE SENSING UNIT

The basic sensor is composed of three parts (from top): sensor mounting block, aperture plate, and cover plate. The basic sensor is used in both the external and jaw sensors. The sensor mounting block has a recess to accommodate a moveable light shutter. Centered in this recess is a hole to accommodate a light emitting diode. The aperture plate has a slit 1/32-inch wide which when combined with the notch in the shutter, forms a square aperture 1/32-inch on a side. The cover plate has a hole in line with both the shutter and LED to accommodate a phototransistor. The three pieces are attached by means of screws to form one complete assembly, which is then bolted to the jaw body via two mounting holes. The single unit shown here is for an external sensor. The sensing elements for the jaw sensing buttons are identical except that there are three sensors per sensing block.

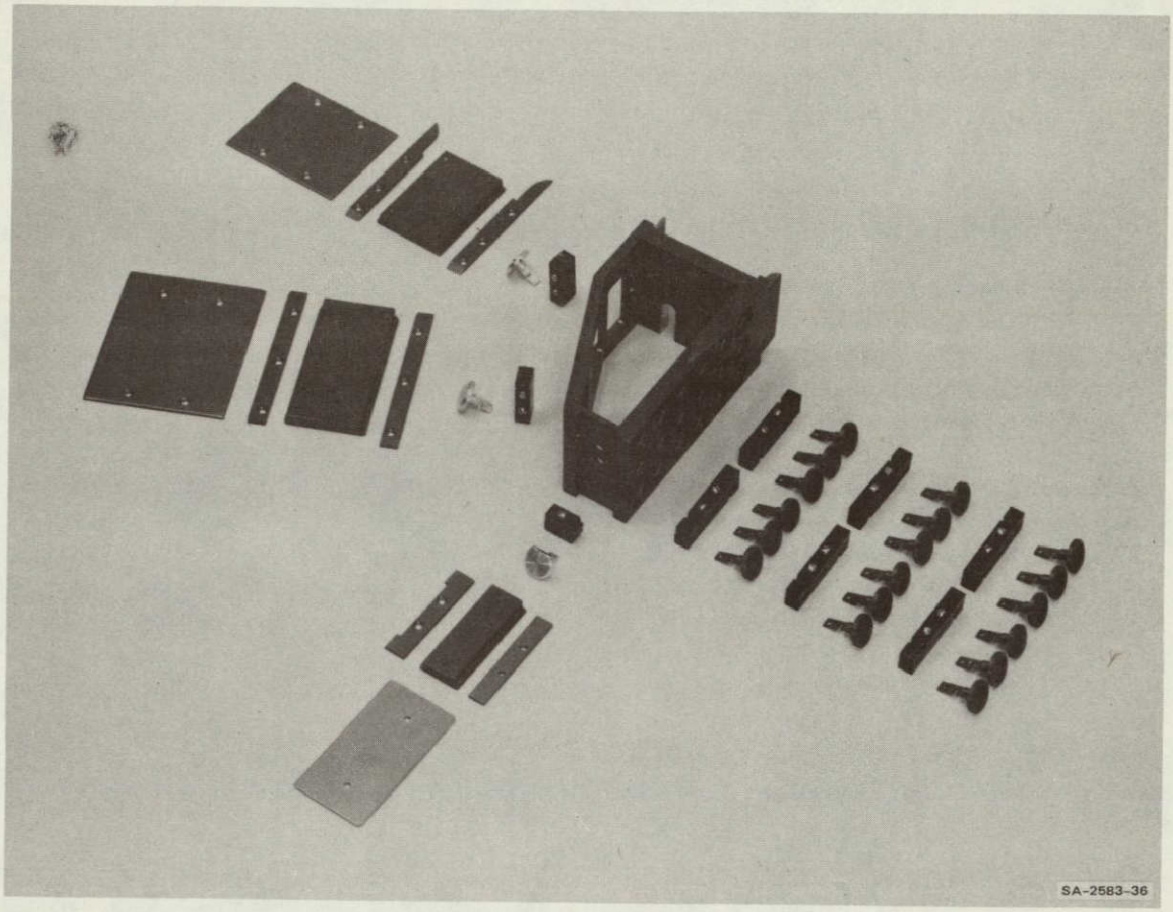

FIGURE A-2 LAYOUT VIEW: RIGHT JAW BODY AND ASSOCIATED PARTS

Extending radially to the right are the parts that make up the jaw sensing button proportional sensors. From the center outward are six proportional tactile sensing blocks composed of three sensors each and eighteen sensor buttons with attached shutter vanes. Together the buttons and the sensor blocks make up the tactile sensing elements. Milled in the face of the jaw body are circular holes which accommodate both the compliant elements (not shown here) and the sensing buttons. Extending radially outward from the top left are the parts that constitute the proximal exterior sensor. From the center outward are tactile sensing block, sensing button with attached light vane, top mesa hold-down, sensor mesa, bottom mesa hold-down, and proximal exterior sensing plate. Extending radially outward from the left middle and the left bottom are the parts that make up both the distal exterior sensing mechanism and the jaw-tip sensing mechanism, respectively. These parts are identical in function to the proximal exterior sensing mechanism. The right tong and left tong are identical in construction and are mirror images of one another. The arch shaped hole in the rear of the jaw body accommodates the electrical cable.

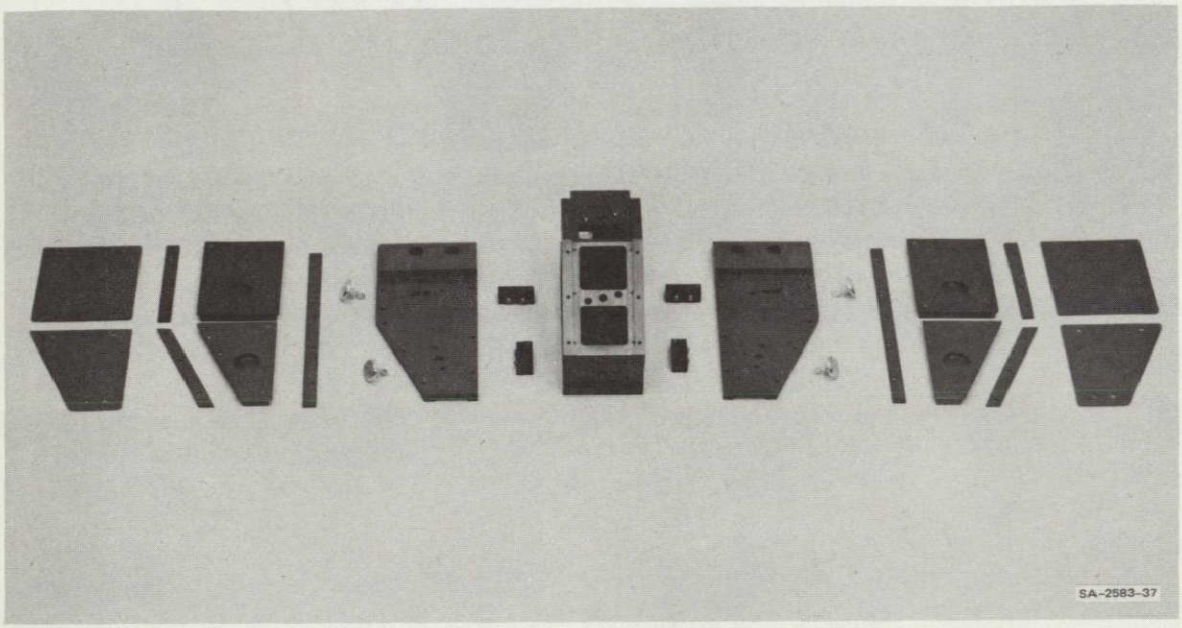

FIGURE A-3 LAYOUT VIEW: TOP AND BOTTOM EXTERIOR SENSING MECHANISMS

Extending from the tong body to the right are the parts that make up the external top sensors. They are, in order, proportional tactile sensing blocks, top cover plate, sensing buttons with attached light vanes, combined proximal and distal mesa hold down strip, proximal and distal sensor mesas, associated mesa hold down strips, and exterior sensing plates. Extending from the tong body to the left are the parts constituting the bottom exterior sensors. These parts are identical in function to the top parts. The milled rectangular holes in the jaw body are for access during assembly. The two holes in both the top and bottom cover plates are to accommodate pins to which the links are later attached. The recessed holes in the mesa plates are to accept the heads of the sensing buttons and thereby prevent the mesa plates from slipping.

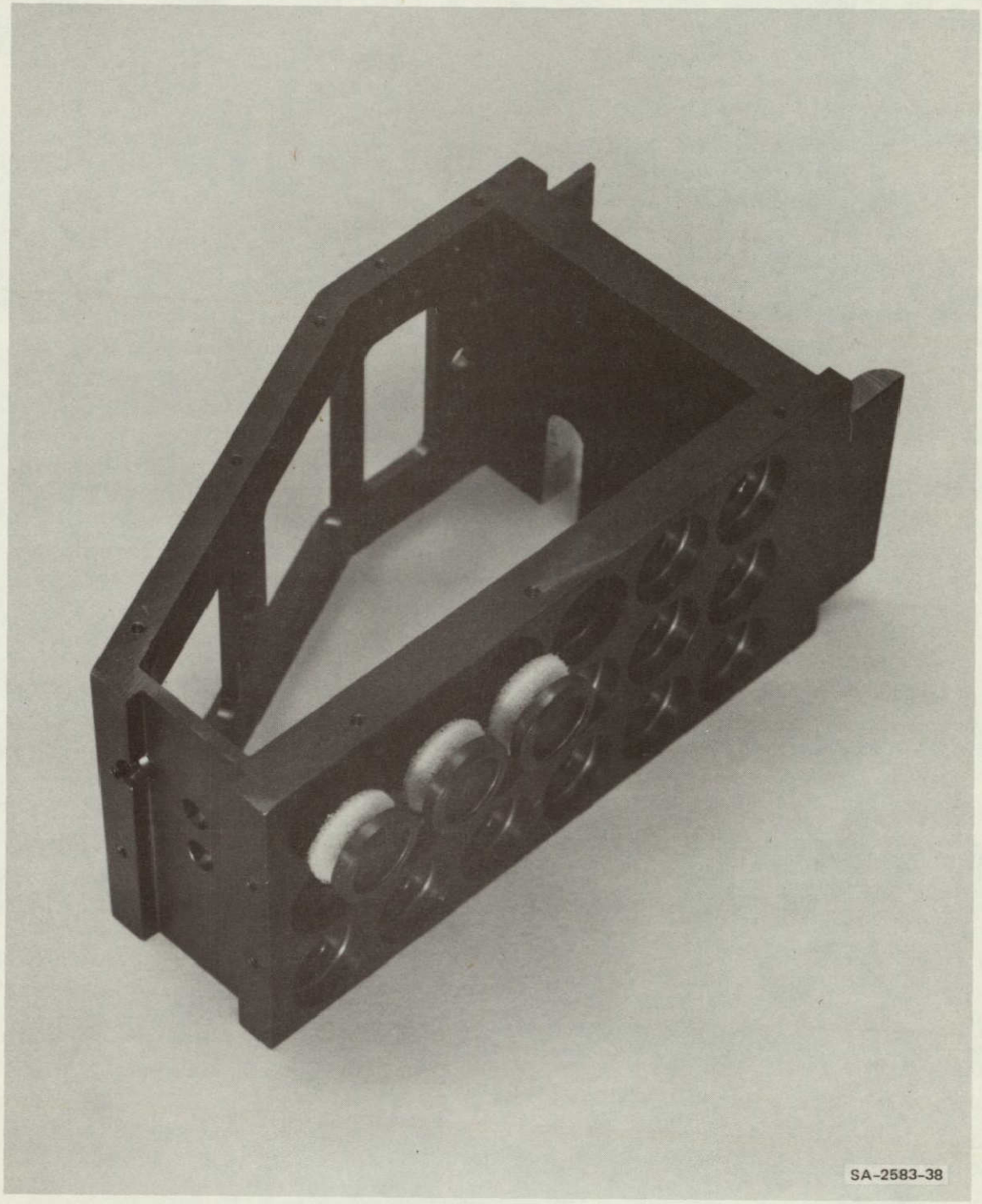

FIGURE A-4 SENSOR BUTTONS WITH COMPLIANT ELEMENTS

This figure shows the sensor buttons inserted into the jaw body through donut shaped compliant elements. The compliant elements may be of foam or molded rubber and may be of uniform or nonuniform cross section, depending on the desired force characteristics. The milled circular holes in the head of the sensor buttons are provided for rubber inserts that increase the gripping capability of the end effector.

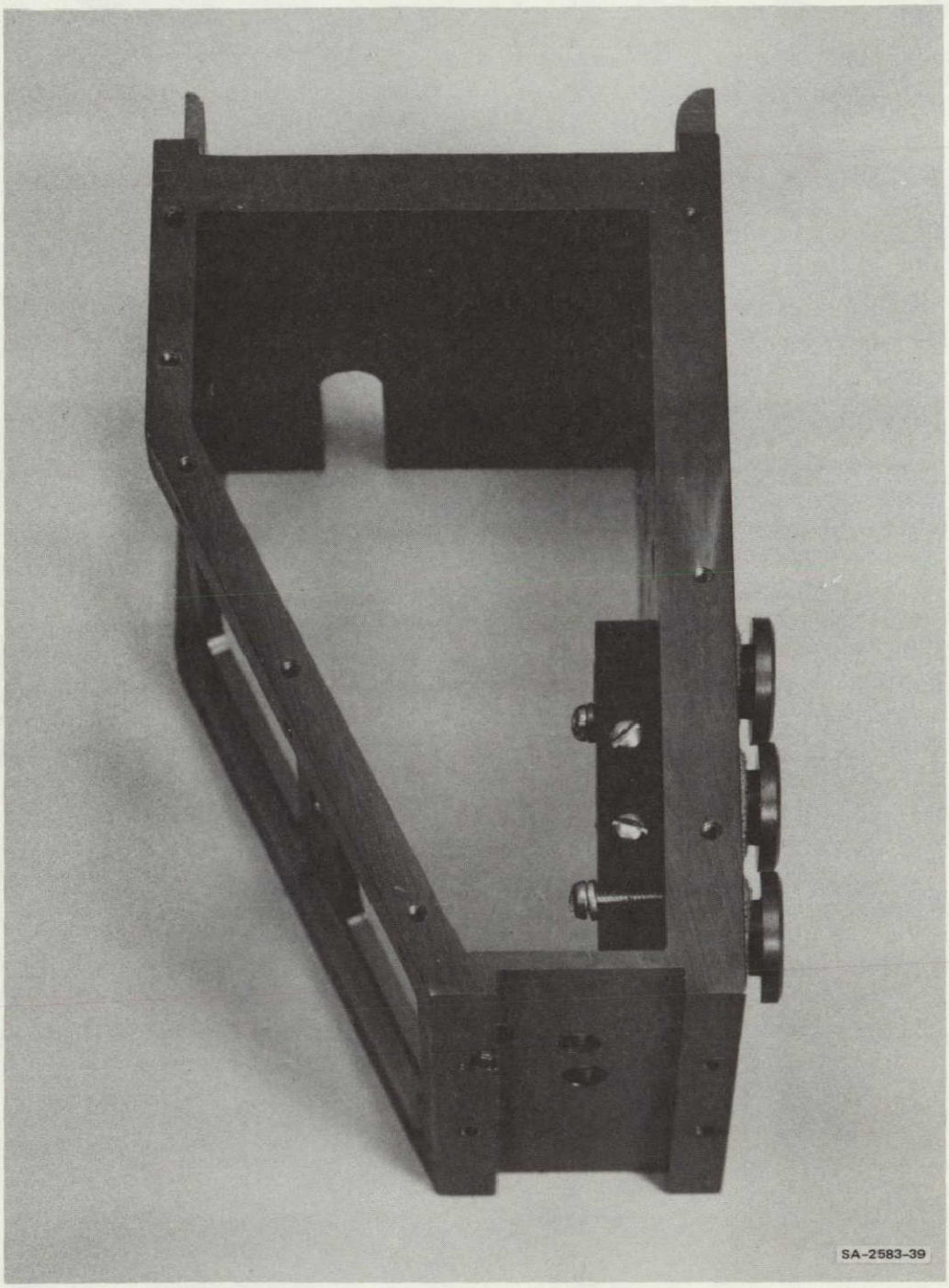

FIGURE A-5 ASSEMBLED SET OF THREE PROPORTIONAL TACTILE SENSORS

This figure shows the basic tactile sensing block bolted to the rear of the body with the buttons and attached light vanes protruding through the jaw body into the sensor block. The phototransistors and LEDs are not shown. When fully assembled, the buttons protrude all the way through the sensing element and are prevented from popping out by means of small retaining pins.

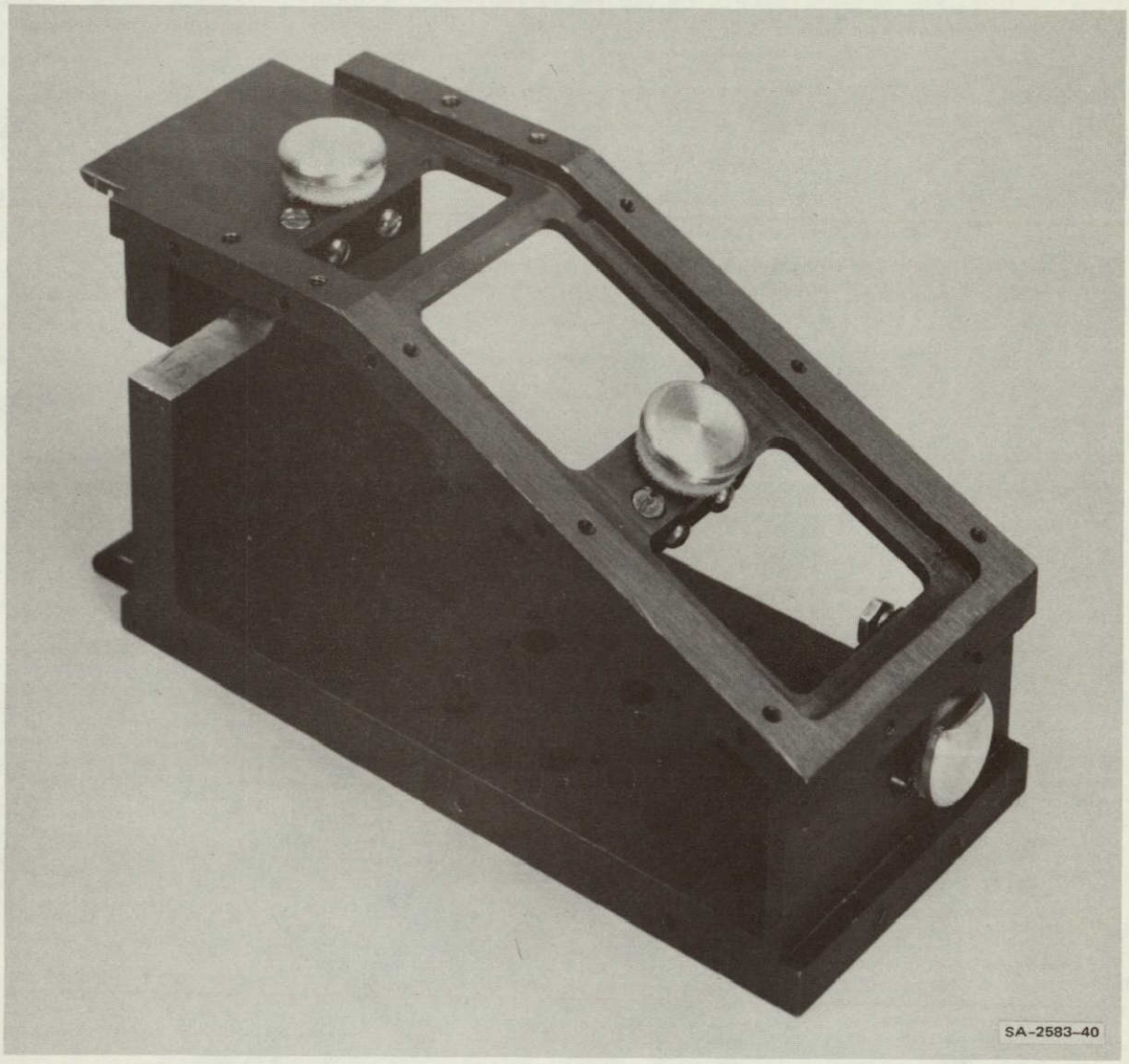

FIGURE A-6 FULLY ASSEMBLED EXTERNAL SENSING MECHANISMS

This figure shows the proximal, distal, and jaw-tip sensors fully assembled with sensing button, compliant element, and sensing element. The sensors are assembled to the top and bottom plates in exactly the same manner as shown here.

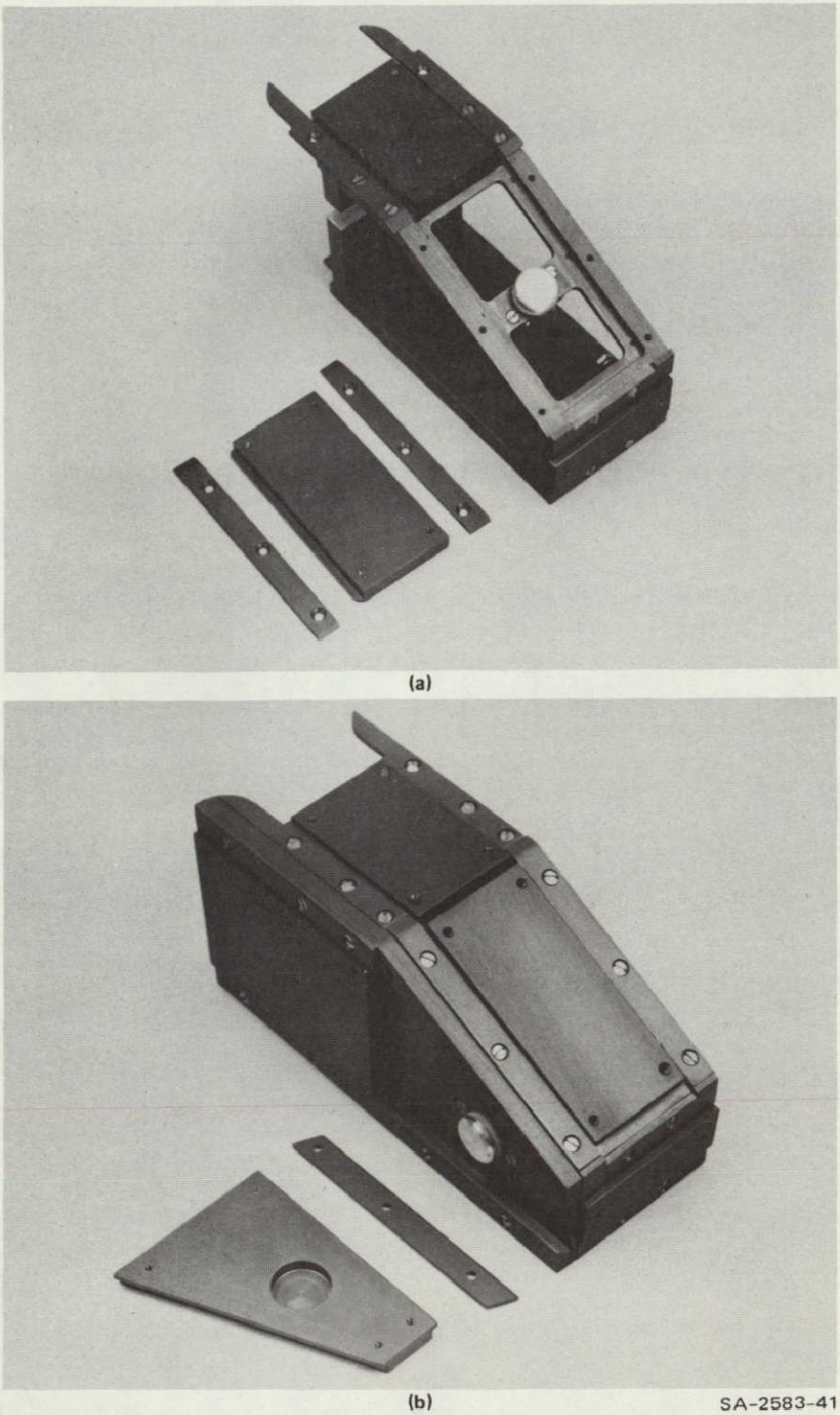

FIGURE A-7 FINAL ASSEMBLY OF THE EXTERIOR AND TOP SENSORS

View (a) shows both the proximal and jaw-tip sensors fully assembled with sensing mechanisms, mesas, and mesa hold downs. The parts to the left are the mesa and associated hold downs for the distal sensor and are about to be assembled onto the sensing mechanism. View (b) shows the parts to the top distal sensor just before final assembly. The final step will be the assembly of the sensor plates to the mesa. In this view the bottom cover plate and associated sensors have been omitted.

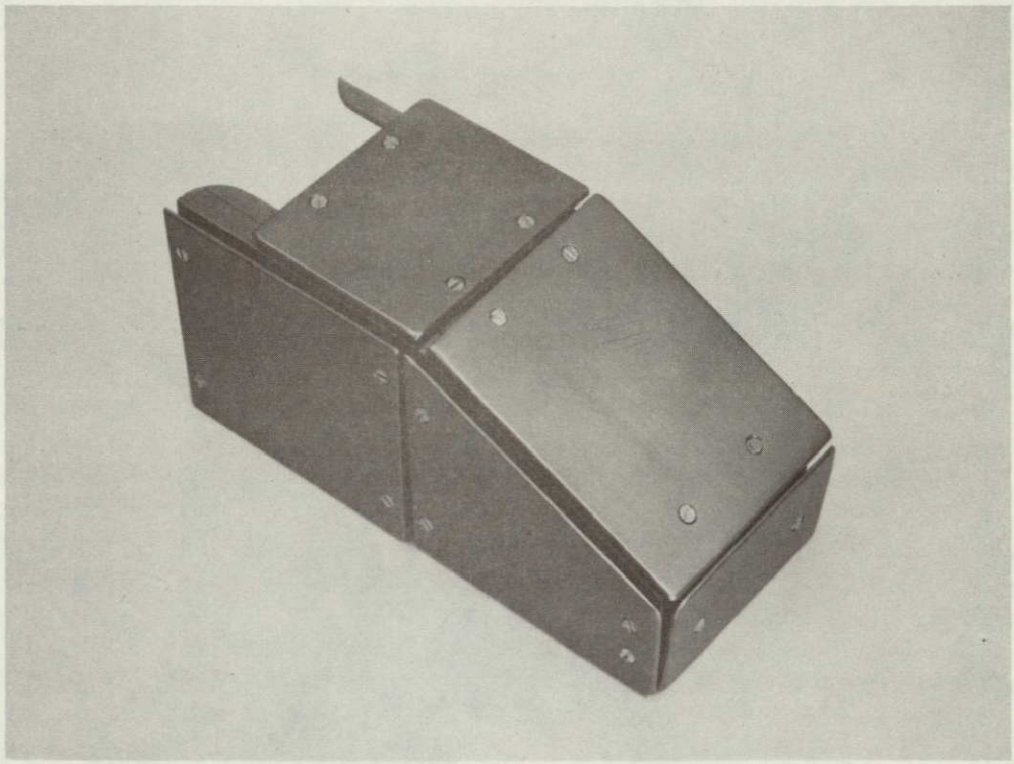

(a)

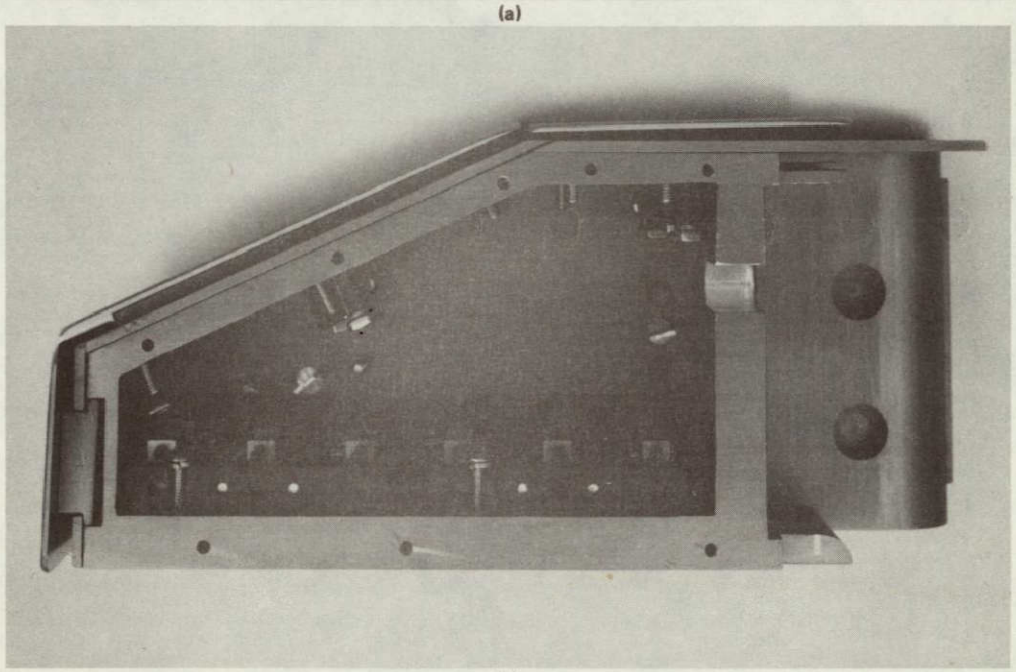

(b)

SA-2583-42

FIGURE A-8 COMPLETED ASSEMBLY OF JAW BODY

View (a) shows the completed assembly with the sense plates covering the entire surface of the tong. View (b) shows an interior view of the same assembly showing all of the sensing mechanisms as well as the two holes for the pins that connect the jaws to the wrist and the bottom plate with all its associated sensors.

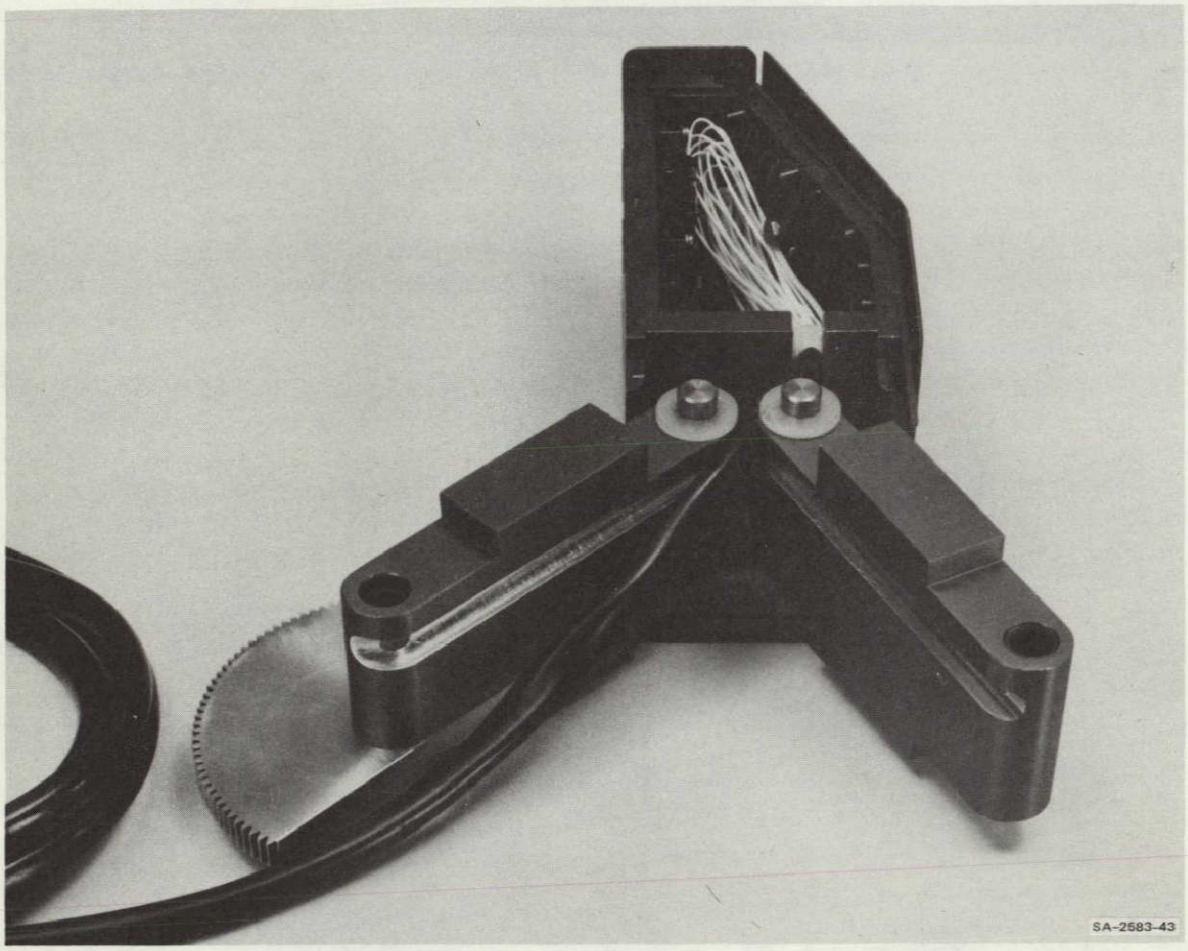

FIGURE A-9 ASSEMBLY OF JAW TO LINKS

The link pins are placed into holes in one of the jaw cover plates. This is followed by the placement of nylon washers on the pins, then links over the pins, then a second nylon washer, and finally the top cover plate (not shown here). Notice that the cable is prevented from tangling with the environment by milled slots in the links in which it lies. The gear shown here is one of a pair of drive gears used to operate the parallel operating jaws. The holes through which the pivot pins fit are lined with a thin nylon sleeve to reduce friction.

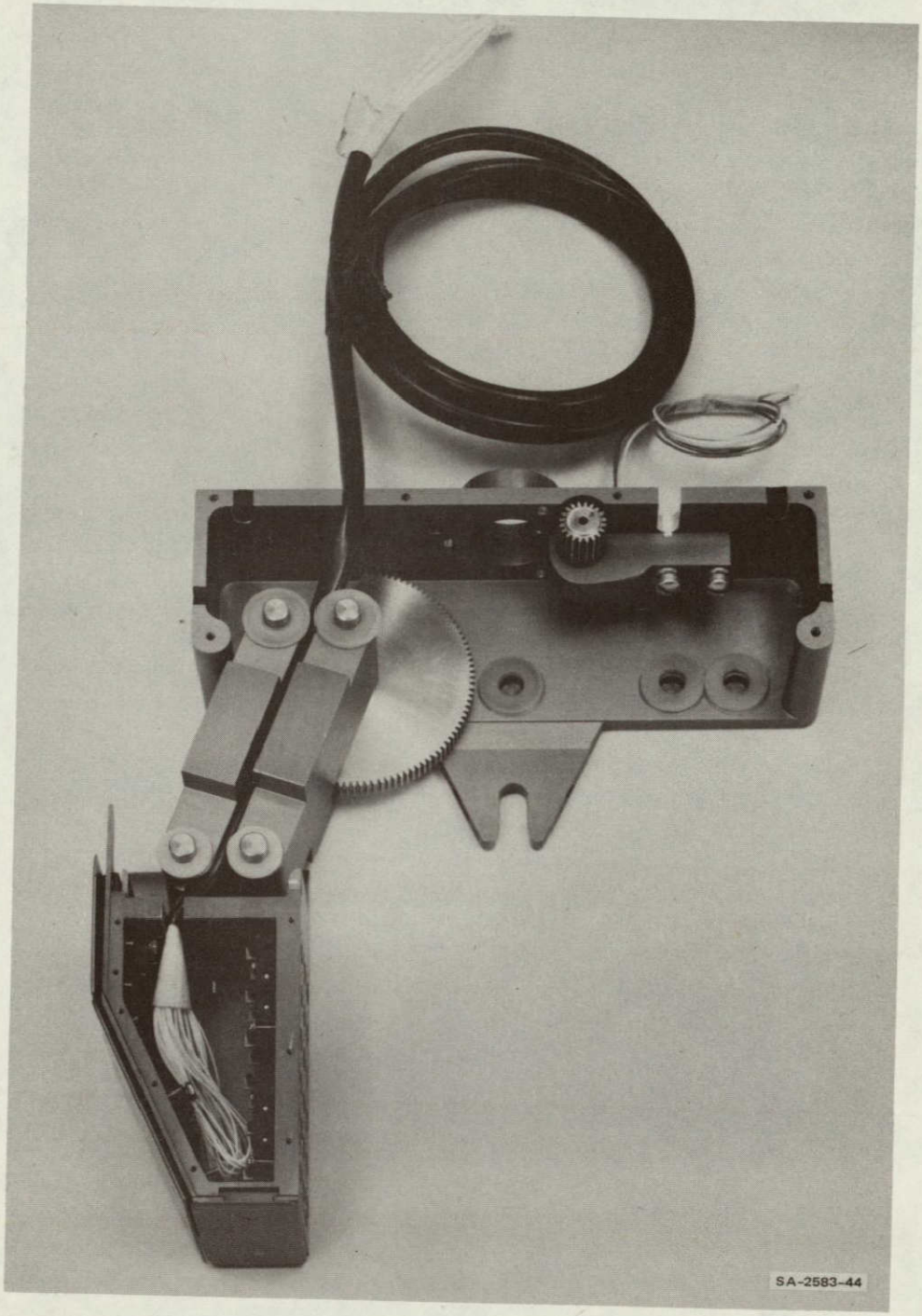

FIGURE A-10 ASSEMBLY OF JAW INTO DRIVE TRAIN HOUSING

The jaw and associated links are attached to the drive train housing by means of a second set of pins. The housing is provided with a small rotary potentiometer, a milled T-handle tool holder, and access for cabling. The jaws are prevented from opening too far by round milled stops on the sides of the gear box housing.

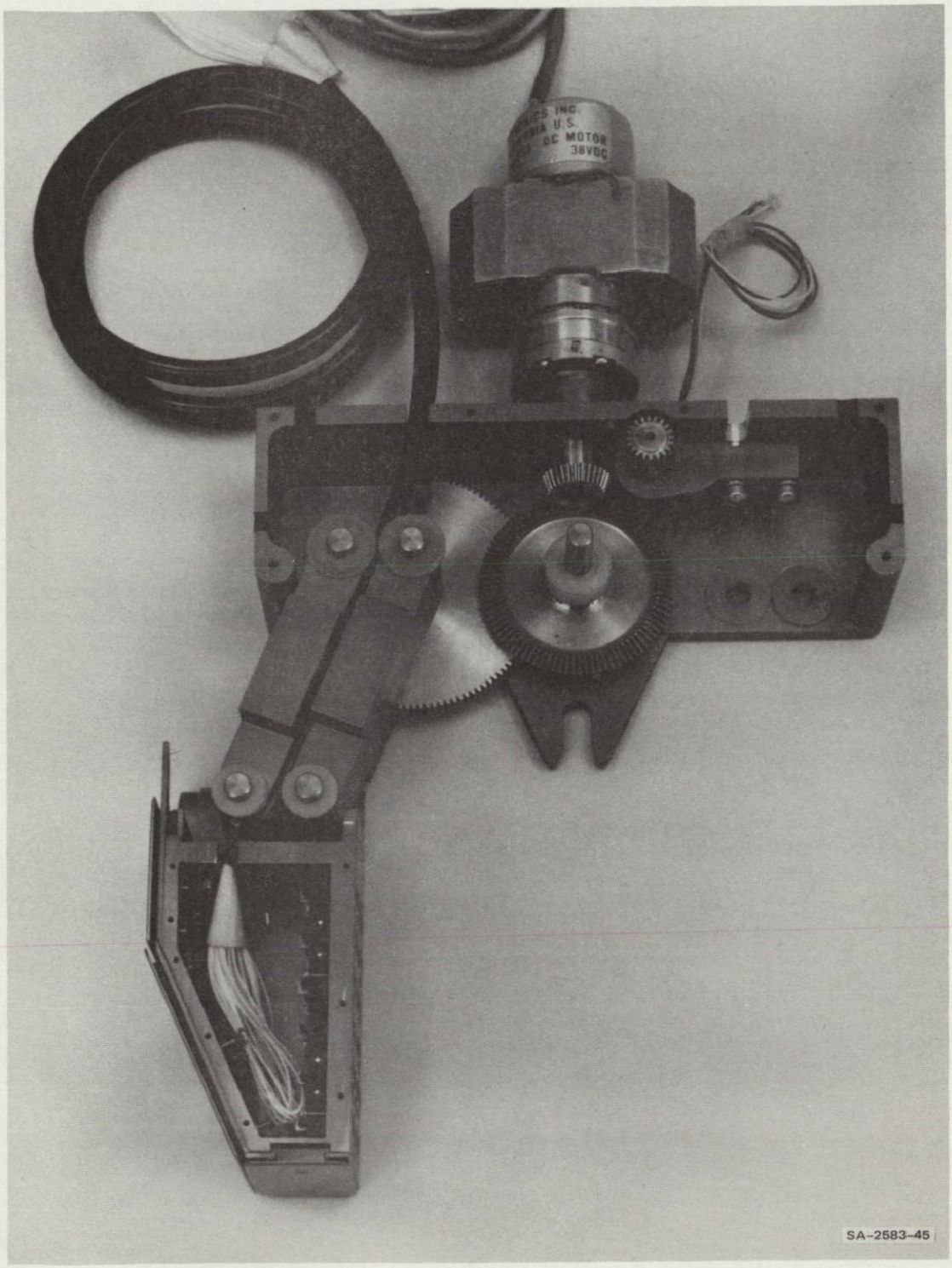

FIGURE A-11 ASSEMBLY OF MOTOR AND DIFFERENTIAL DRIVE MECHANISM

The drive train consists of a motor to which is attached a beveled pinion gear. The pinion gear engages with a second beveled gear to which is rigidly attached a spur gear. The spur gear in turn engages with the drive gear attached to the drive link.

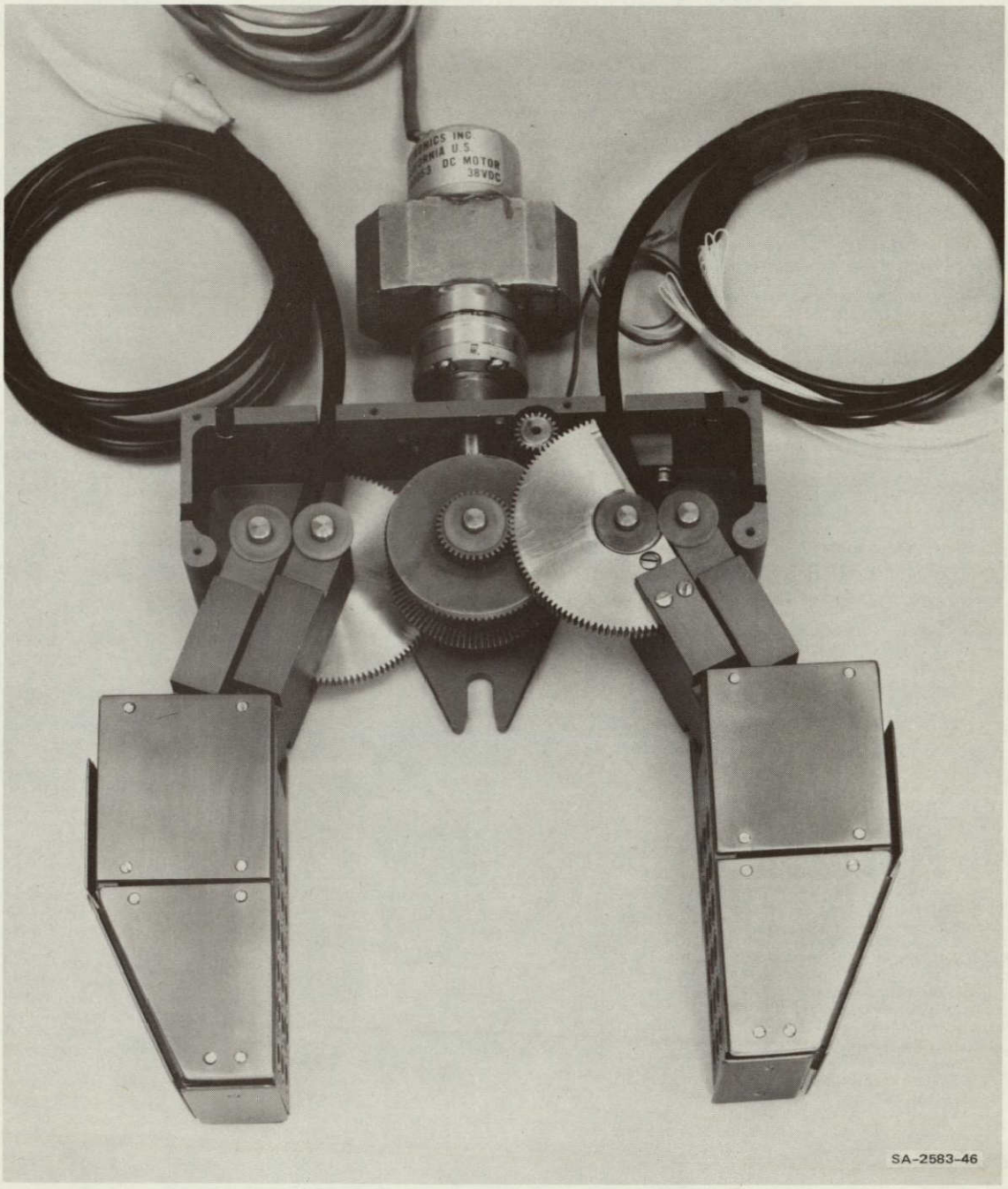

FIGURE A-12 COMPLETE ASSEMBLY: JAWS, LINKS, AND DRIVE TRAIN MECHANISM

This figure shows a second counter-rotating beveled-gear/spur-gear which acts as the drive mechanism for the second tong. The jaw is shown completely assembled except for the top cover plate. The top cover plate has holes that accommodate the free ends of the gear and link pivot pins and is bolted down over the top of the gear train housing.

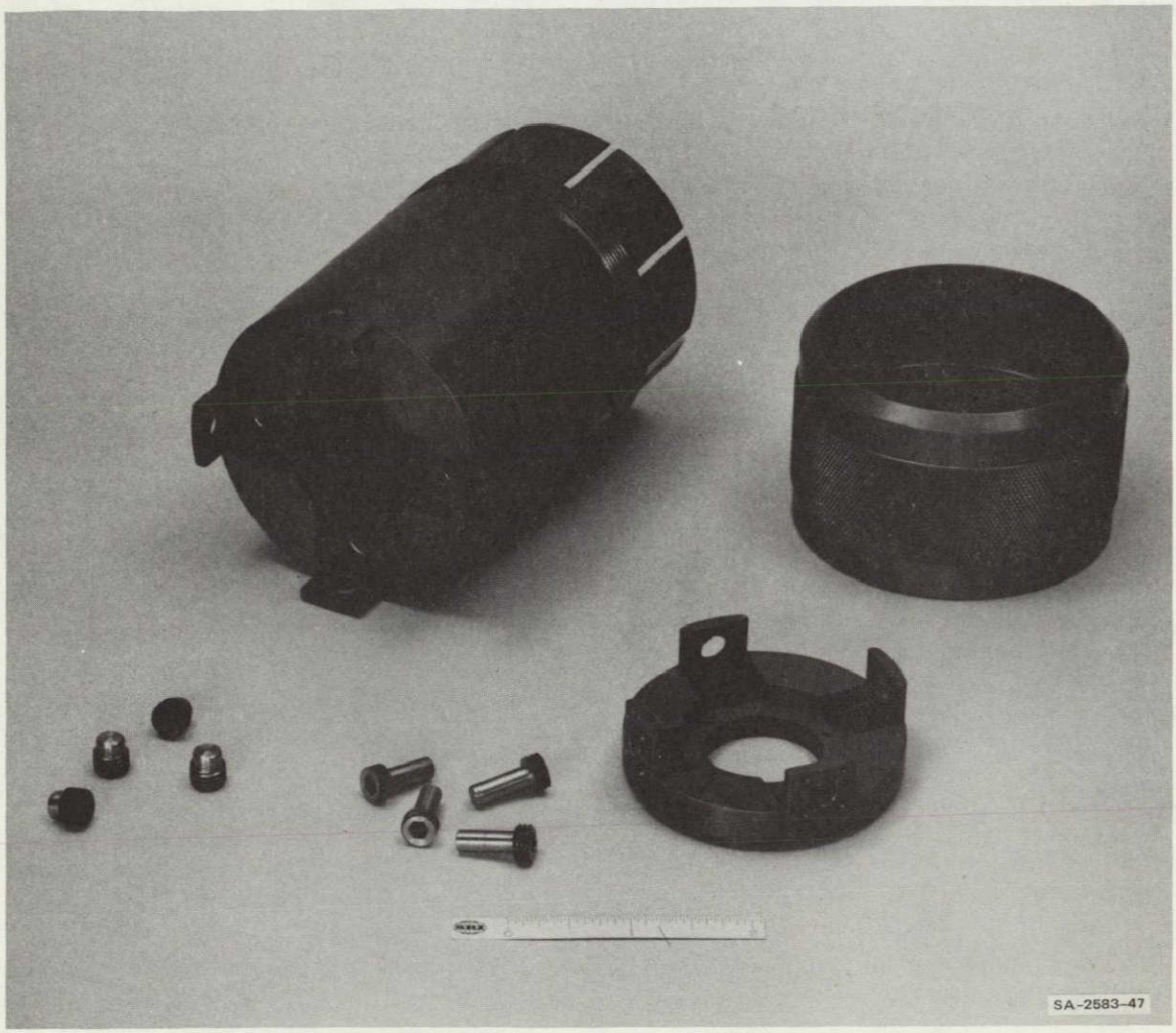

FIGURE A-13 WRIST SENSOR LAYOUT

The parts are: distal wrist sensor housing—(bottom right), sense pins—(bottom middle), locating pins—(bottom left), proximal wrist sensor housing with attachment collet—(top left), and tightening ring for attachment collet—(top right).

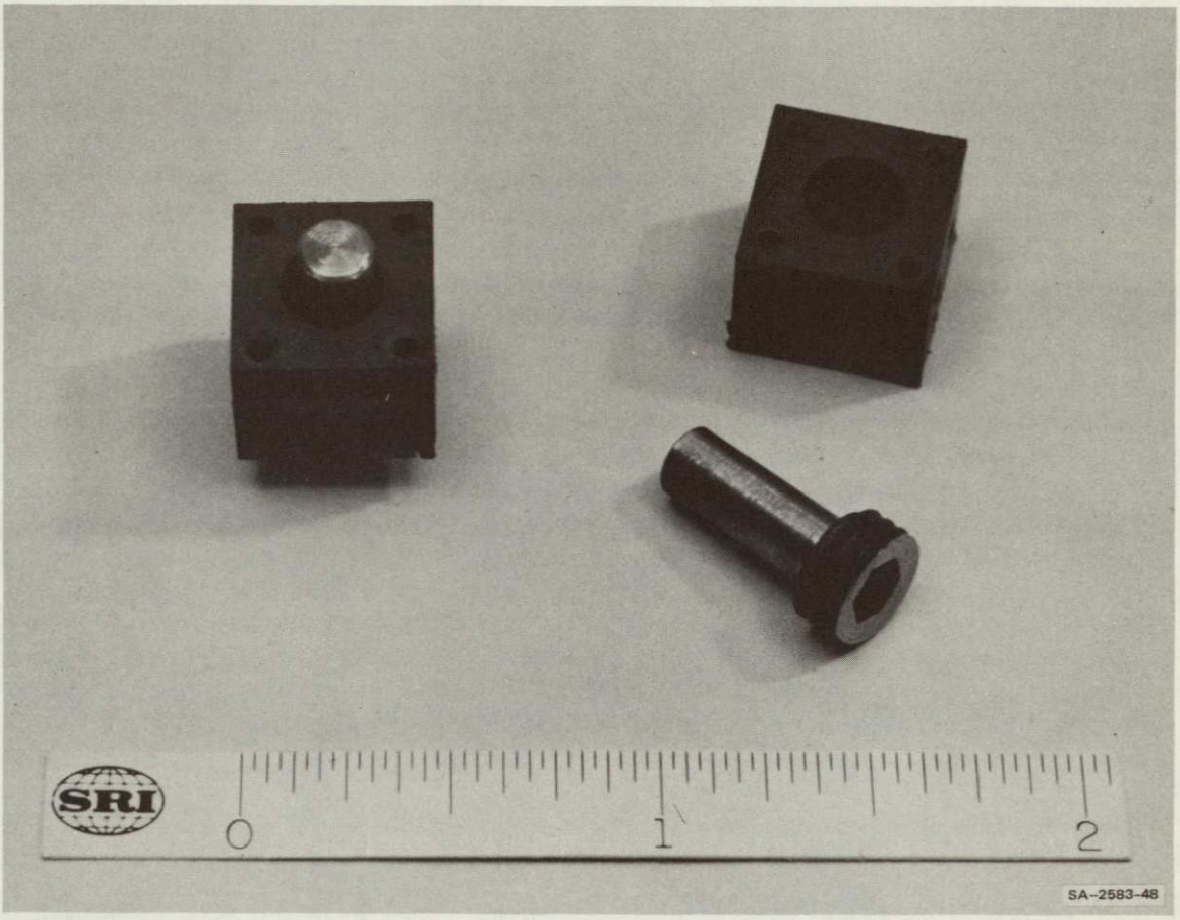

FIGURE A-14 SIX-AXIS WRIST SENSOR: BASIC SENSING ELEMENT

The basic sensing element consists of a small polyvinyl chloride plastic cube (top right) and a mating sense pin (bottom right). The block has a hole to accommodate the sense pin. This hole is surrounded by four smaller holes used for mounting to the distal sensor housing. Into each face of the cube are drilled small holes that accommodate LEDs and phototransistors. These holes are arranged so that numerous light paths are formed across opposite faces of the cube. In normal operation (left), the sense pin attached to the proximal sensor housing is allowed to protrude through the cube attached to the distal sensor housing. As one part moves in relation to the other through a compliant member, the sense pin simultaneously obscures some light paths and opens others. It is these signals that are used to sense the three forces and the three torques.

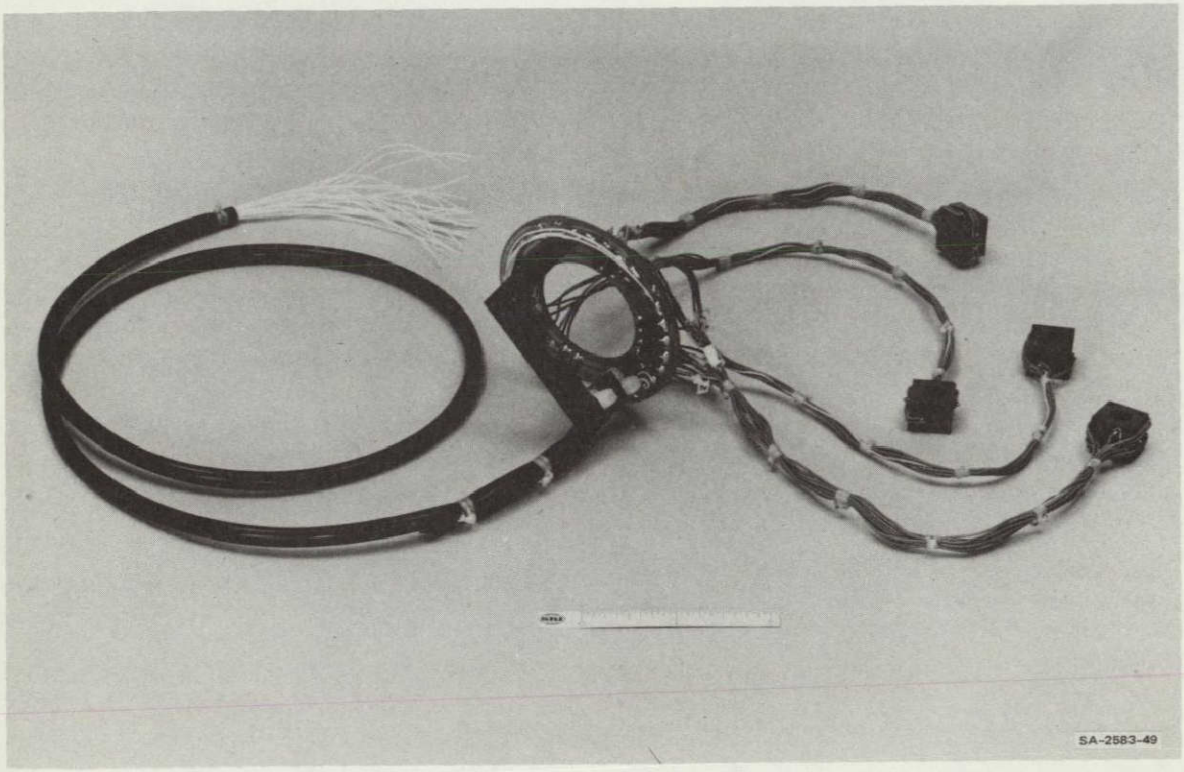

FIGURE A-15 SIX-AXIS WRIST SENSOR: METHOD OF WIRING

In this figure, four sensing elements are shown wired to a circular printed circuit board on which various electronic components are mounted.

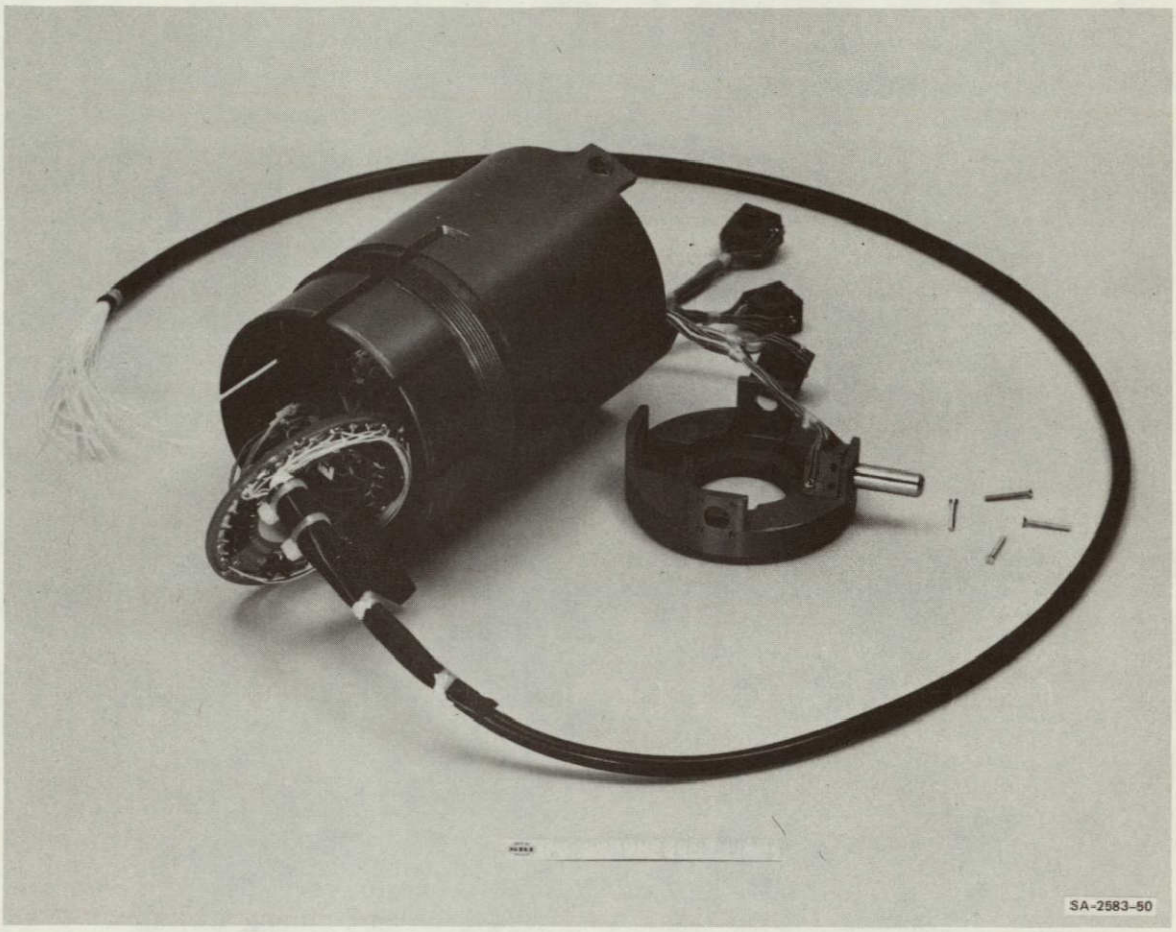

FIGURE A-16 ATTACHMENT OF SENSING BLOCKS

The four sensing blocks are attached to the distal wrist sensor housing in the following manner: a dowel pin is inserted into one of the holes of the distal wrist sensor housing so that it protrudes into the interior. The wired sensor block is then axially located on this pin and bolted down. The pin is then removed, thus insuring precise axial alignment of both holes.

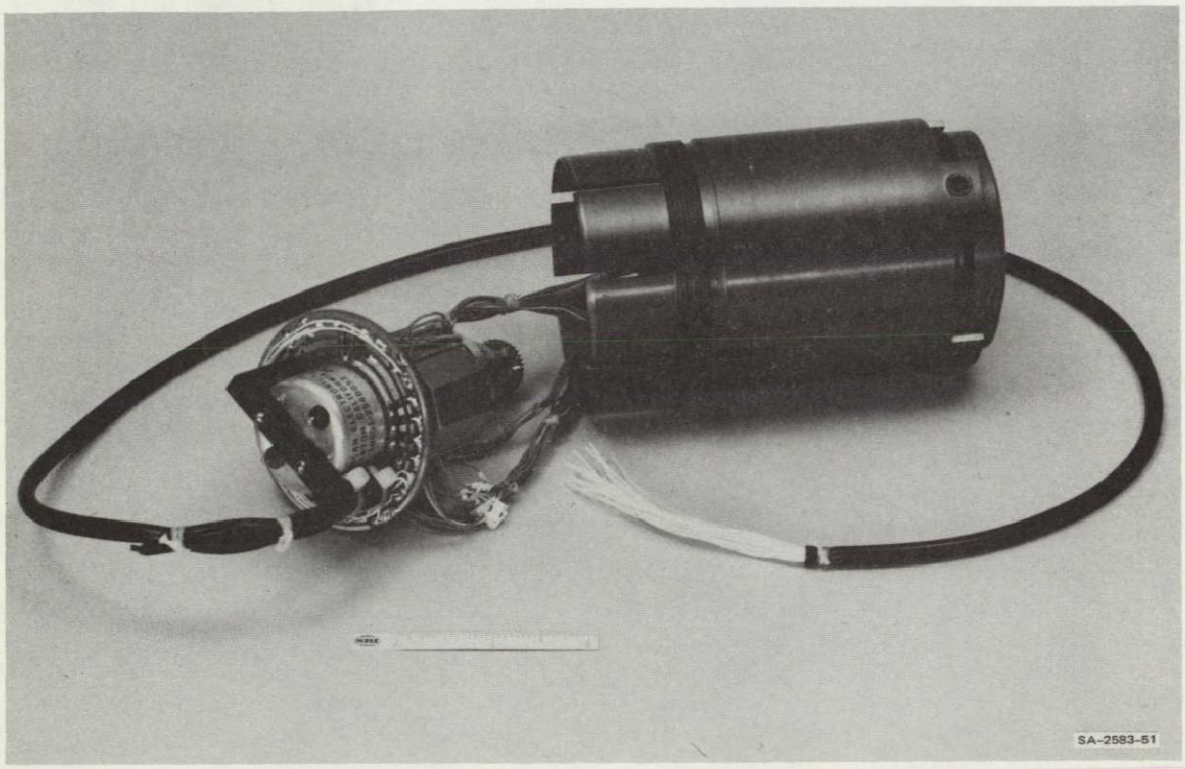

FIGURE A-17 MOTOR ATTACHMENT

This figure shows the distal sensor housing together with the four sensing blocks attached to the proximal sensor housing. Also note that the circular printed circuit board is mounted so that it fits around and is bolted down to the motor.

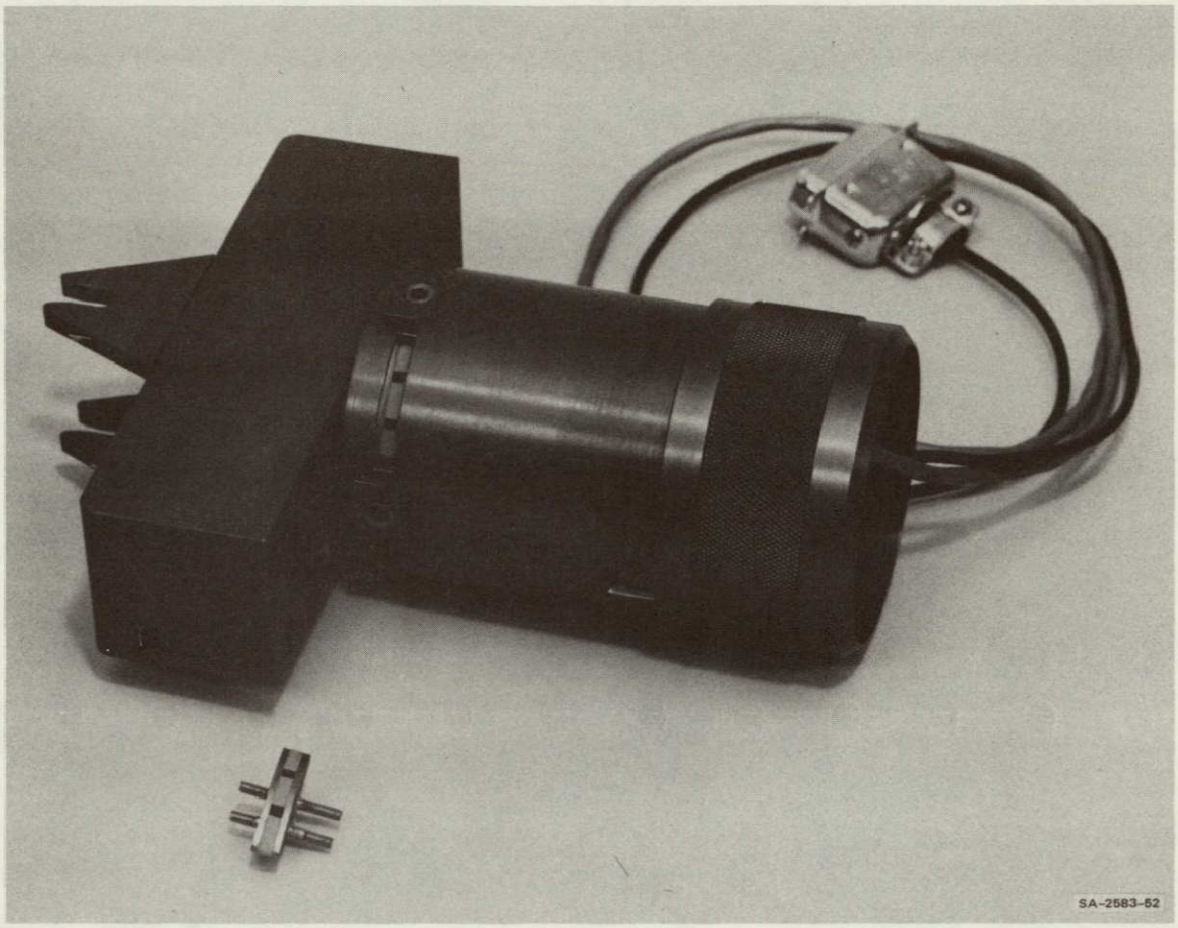

FIGURE A-18 COMPLETED WRIST SENSOR AND COMPLIANT ELEMENT

Here the completed wrist sensor is shown attached to the drive train housing. In the foreground is one of the specially constructed compliant elements of which there are four. It is made of steel plates between which is molded segments of J-RTV rubber. The elements and sensor are designed so that a 20-lb load will cause maximum deflection. One of the unique features of this design is that different compliant elements molded out of different types of RTV may be used to obtain different force ranges.

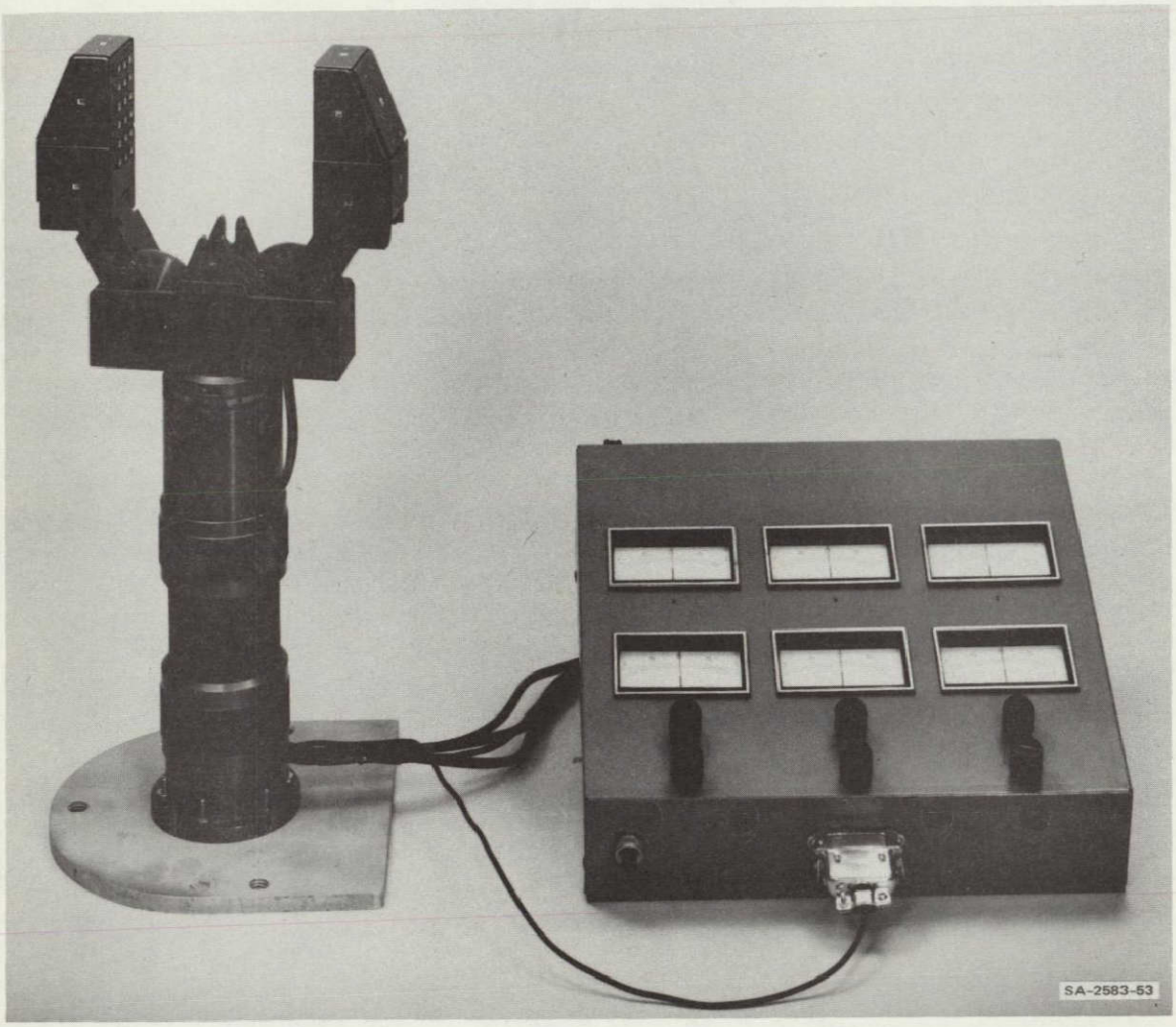

FIGURE A-19 COMPLETED END EFFECTOR

This figure shows the jaws, drive links, gear train housing, and wrist sensor with attachment collet attached to a mechanical fuse which is, in this case, an ordinary aluminum beverage can. This in turn is attached to another collet with a flange. Shown on the right is a meter box containing six meters—one meter for the force along each axis and one meter for each of the three torques about those axes. This meter box may be used to investigate what forces and torques are required to perform a task by the manipulator.

Appendix B

COMPUTER PROCESSING OF THE COMPENSATORY TRACKING DATA

Appendix B

COMPUTER PROCESSING OF THE COMPENSATORY TRACKING DATA

The LINC-8 computer accumulates 36-bit (triple-precision) sums of the analog inputs, S_k, (which are sampled to 9 bits) where

$$S_k = \sum_{i=1}^{64\ RTIM} INPUT_k(i)$$

Similarly it accumulates 36-bit sums of the input cross-products, P_{Jk}, where

$$P_{Jk} = \sum_{i=1}^{64\ RTIM} INPUT_J(i)\ INPUT_k(i) \quad .$$

Here k ($1 \leq k \leq 16$) and j ($1 \leq j \leq k$) are channel numbers, and 64 RTIM is the total number of 1/30-second steps taken in a given test run. The computer generates three sums-of-sines command signals of the form

$$C_k(i) = \sum_{\ell=1}^{10} C_{k\ell} \sin\left(\frac{2\pi F_{k\ell}}{64\ RTIM} i + \varphi_{k\ell}\right) \quad .$$

where $C_{k\ell}$ is the amplitude coefficient for the k^{th} command signal $F_{k\ell}$ is the frequency for the k^{th} command signal, $\varphi_{k\ell}$ is the initial phase shift, and the sine function is approximated by a function table having 64 entries.

While a tracking run is in progress, the computer saves all the input numbers, $INPUT_k(i)$, on a disk scratch file to obtain Fourier sums at the command signal frequencies after the test run has been completed. The Fourier sums for each channel, k, and at each command frequency, $F_{k\ell}$, are

$$A_{k\ell} = \sum_{i=1}^{64\ RTIM} \sin\left(\frac{2\pi\ F_{k\ell}}{64\ RTIM}\ i\right) INPUT_k\ (i)$$

and

$$B_{k\ell} = \sum_{i=1}^{64\ RTIM} \cos\left(\frac{2\pi\ F_{k\ell}}{64\ RTIM}\ i\right) INPUT_k\ (i) \quad .$$

These data, on punched paper tape, serve as the input for a second computer program that provides the usable output. This FORTRAN program first converts the numbers into the correct units by multiplying by the correct scale factor. The means and standard deviations are computed from the scaled sums, products, and Fourier coefficients as follows

$$MEAN_k = S_k$$

$$SD_k = \sqrt{P_{kk} - S_k^2} \quad .$$

The between-signal correlation coefficients, r_{jk}, are

$$r_{jk} = \frac{\sqrt{P_{jk} - S_j S_k}}{SD_j\ SD_k} \quad .$$

To calculate a subject's gain and phase shift at each of the command signal frequencies, both the error, E, and the response, R, must be known. The magnitude and phase of the error components, $E_{k\ell}$, are

$$\left|E_{k\ell}\right| = \sqrt{A_{k\ell}^2 + B_{k\ell}^2}$$

$$\angle E_{k\ell} = \tan^{-1} (A_{k\ell}/B_{k\ell}) \quad .$$

To obtain the magnitude and phase components for the subject's response, $R_{k\ell}$, the command signal must be known. The command amplitudes were measured in a test run with zero response signal and built into the FORTRAN analysis program. By using the command amplitude, $C_{k\ell}$, the response is calculated by the complex number subtraction

$$R_{k\ell} = C_{k\ell} - E_{k\ell} \quad ,$$

and the magnitude and phase of $R_{k\ell}$ are computed in the same way that they are computed for $E_{k\ell}$. Finally, the gain and phase shift of the subject at each command frequency are calculated and printed out:

$$GAIN_{k\ell} = \frac{\left|R_{k\ell}\right|}{\left|E_{k\ell}\right|}$$

$$PHASE_{k\ell} = \angle R_{k\ell} - \angle E_{k\ell} \quad .$$

The gain in decibels is determined by the formula

$$GAIN\ (dB)_{k\ell} = 20 \log\ GAIN_{k\ell} \quad .$$

The gain and phase shift plotted as a function of frequency become the "Pilot-vehicle Describing Function" of McRuer et al. (1965). From this describing function several derived measurements are obtained. The gains and phases from the five highest and five lowest of the frequencies are averaged together to produce the "Hi" and "Low" frequency gain and "Hi" and "Low" frequency phase listed in Table B-1. The "Hi" and "Low" frequency crossovers are obtained by least-mean-square fitting of straight lines to the five highest and lowest frequency gains and determining the intercept frequency at zero hertz. The equivalent time delay is obtained by a least-mean-square fit of the model $\exp(-st/\tau)$, to the phase shifts at the five highest frequencies to estimate the operator time delay parameter τ, of the McRuer et al. Simple Crossover Model (1965).

In the remnant analysis, the Fourier sine and cosine coefficients, A_{ke} and B_{ke}, for the k^{th} axis error are determined at the remnant frequencies. These are a set of frequencies different from those of any of the command signals and hence orthogonal. The remnant amplitude is the ratio of these coefficients to the total power in k^{th} command, or

$$\text{REMNANT}_{ke} = 10 \log \frac{\left(A_{ke}^2 + B_{ke}^2\right)}{10 \sum_{\ell=1} C_{k\ell}} .$$

In addition, the mean square error accounted for in the k^{th} variable by the frequencies of the k^{th} variable is computed by summing ten terms:

$$\text{MSE accounted for} = \sum_{e=1}^{10} A_{ke}^2 + B_{ke}^2$$

The high and low frequency portions are computed by summing the lowest five and highest five frequencies of this sum.

```
STEVE, 1/14/74, RUN 14                                                    NUMBER OF
                                                                        LAST VARIABLE
MEDIUM BANDWIDTH, 3-AXIS COMMAND                                      PRINTED ON LINE

..............MEAN.....SD....UNITS
X - AXIS        -8.42    2.25  CM.                                              2
Y - AXIS        -9.22    2.10  CM.                                              4
Z - AXIS        -9.04    3.29  CM.                                              6
JOINT 1        -14.08     .33  DEGREES                                          8
JOINT 2         53.05     .44  DEGREES                                         10
JOINT 3        144.32     .42  DEGREES                                         12
JOINT 4        109.60     .40  DEGREES                                         14
JOINT 5        -65.98     .36  DEGREES                                         16


CORRELATION COEFFICIENTS, R(I,J)

   .002                                                                        17
   .089  -.317                                                                 19
   .013   .032  -.005                                                          22
  -.003  -.041   .024   .145                                                   26
  -.020  -.039   .015  -.126   .197                                            31
  -.006  -.016  -.016   .139   .098   .135                                     37
  -.003   .010  -.033  -.273   .150   .007   .081                              44


X - AXIS   ANALYZED AT THE X - AXIS   FREQUENCIES

  FREQ    GAIN       GAIN     PHASE
  (HZ)               (DB)     (DEG)
 .0183   32.645     30.28    -75.01                                            47
 .0293   24.125     27.65    -73.35                                            50
 .0476   13.300     22.48    -61.51                                            53
 .0732   14.078     22.97    -64.06                                            56
 .1282    8.884     18.97    -86.17                                            59
 .1721    6.932     16.82   -100.93                                            62
 .3040    2.954      9.41   -118.60                                            65
 .4871    1.587      4.01   -134.32                                            68
 .9192     .614     -4.24   -154.89                                            71
1.6113     .414     -7.67   -182.04                                            74
MEAN SQUARE FORCING FUNCTION                    212.87 CM*CM
X - AXIS  MEAN SQUARE ERROR (MSE)                 5.06 CM*CM      100.00 PCT
MSE ACCOUNTED FOR BY X - AXIS  FREQUENCIES         3.06 CM*CM       60.52 PCT   76
 BY LOW FREQUENCIES ONLY                            .88 CM*CM       17.34 PCT   78
 BY HIGH FREQUENCIES ONLY                          2.19 CM*CM       43.18 PCT   80
LOW FREQUENCY GAIN                  24.47 DB                                    81
LOW FREQUENCY CROSSOVER           3.4852 HZ                                     82
LOW FREQUENCY PHASE               -72.02 DEGREES                                83
HI FREQUENCY GAIN                    3.67 DB                                    84
HI FREQUENCY CROSSOVER               .7201 HZ                                   85
HI FREQUENCY PHASE               -138.15 DEGREES                                86
EQUIVALENT TIME DELAY               .175 SEC                                    87


X - AXIS   ANALYZED AT THE REMNANT    FREQUENCIES
  FREQ   AMPLITUDE
  (HZ)     (DB)
 .0110    -47.18                                                              88
 .0256    -46.59                                                              89
 .0513    -49.04                                                              90
 .0696    -43.96                                                              91
 .1062    -55.37                                                              92
 .1794    -46.65                                                              93
 .3406    -46.51                                                              94
 .6152    -43.65                                                              95
 .9851    -44.04                                                              96
2.0105    -62.89                                                              97
X - AXIS  MEAN SQUARE ERROR (MSE)                 5.06 CM*CM      100.00 PCT
MSE ACCOUNTED FOR BY REMNANT   FREQUENCIES          .05 CM*CM        .94 PCT   99
 BY LOW FREQUENCIES ONLY                            .02 CM*CM        .41 PCT  101
 BY HIGH FREQUENCIES ONLY                           .03 CM*CM        .53 PCT  103
```

FIGURE B-1 COMPUTER ANALYSIS OF A THREE-AXIS TRACKING RUN

```
Y - AXIS   ANALYZED AT THE Y - AXIS   FREQUENCIES

  FREQ     GAIN        GAIN      PHASE
  (HZ)                 (DB)      (DEG)
 .0146     24.093      27.64     -71.04                                          106
 .0330     12.871      22.19     -48.41                                          109
 .0623     10.947      20.79     -54.06                                          112
 .0916      6.170      15.81     -67.10                                          115
 .1501      5.786      15.25     -83.66                                          118
 .2454      3.261      10.27    -107.23                                          121
 .4065      2.054       6.25    -124.71                                          124
 .6482       .954       -.41    -140.86                                          127
 .9998       .427      -7.39    -169.91                                          130
2.1497       .294     -10.65    -242.21                                          133
MEAN SQUARE FORCING FUNCTION                          60.68 CM*CM
Y - AXIS  MEAN SQUARE ERROR (MSE)                      4.39 CM*CM       100.00 PCT
MSE ACCOUNTED FOR BY Y - AXIS  FREQUENCIES             2.09 CM*CM        47.66 PCT    135
 BY LOW FREQUENCIES ONLY                                .66 CM*CM        14.99 PCT    137
 BY HIGH FREQUENCIES ONLY                              1.44 CM*CM        32.67 PCT    139
                                                                                     140
LOW FREQUENCY GAIN                    20.33 DB                                      141
LOW FREQUENCY CROSSOVER               2.1821 HZ                                     142
LOW FREQUENCY PHASE                  -64.85 DEGREES                                 143
HI FREQUENCY GAIN                      -.39 DB                                      144
HI FREQUENCY CROSSOVER                 .6492 HZ                                     145
HI FREQUENCY PHASE                  -156.98 DEGREES                                 146
EQUIVALENT TIME DELAY                  .203 SEC


Y - AXIS   ANALYZED AT THE REMNANT   FREQUENCIES
  FREQ   AMPLITUDE
  (HZ)     (DB)
 .0110    -31.59                                                                  147
 .0256    -36.86                                                                  148
 .0513    -45.59                                                                  149
 .0696    -45.22                                                                  150
 .1062    -37.57                                                                  151
 .1794    -41.32                                                                  152
 .3406    -43.07                                                                  153
 .6152    -44.40                                                                  154
 .9851    -48.56                                                                  155
2.0105    -50.35                                                                  156
Y - AXIS  MEAN SQUARE ERROR (MSE)                      4.39 CM*CM       100.00 PCT
MSE ACCOUNTED FOR BY REMNANT   FREQUENCIES              .08 CM*CM         1.82 PCT    158
 BY LOW FREQUENCIES ONLY                               .07 CM*CM         1.56 PCT    160
 BY HIGH FREQUENCIES ONLY                              .01 CM*CM          .25 PCT    162


Z - AXIS   ANALYZED AT THE Z - AXIS   FREQUENCIES

  FREQ     GAIN        GAIN      PHASE
  (HZ)                 (DB)      (DEG)
 .0220     19.270.     25.70     -55.02                                          165
 .0403     10.853      20.71     -50.15                                          168
 .0549     12.385      21.86     -53.59                                          171
 .0842      7.329      17.30     -72.41                                          174
 .1355      5.348      14.56     -89.29                                          177
 .2087      3.848      11.71    -106.43                                          180
 .3552      1.741       4.82    -119.52                                          183
 .5640      1.050        .42    -141.40                                          186
1.0583       .555      -5.12    -174.65                                          189
1.9299       .324      -9.80    -273.22                                          192
MEAN SQUARE FORCING FUNCTION                        202.42 CM*CM
Z - AXIS  MEAN SQUARE ERROR (MSE)                     10.82 CM*CM       100.00 PCT
MSE ACCOUNTED FOR BY Z - AXIS  FREQUENCIES             6.25 CM*CM        57.74 PCT    194
 BY LOW FREQUENCIES ONLY                               2.24 CM*CM        20.66 PCT    196
 BY HIGH FREQUENCIES ONLY                              4.01 CM*CM        37.08 PCT    198
LOW FREQUENCY GAIN                    20.03 DB                                      199
LOW FREQUENCY CROSSOVER               1.6174 HZ                                     200
LOW FREQUENCY PHASE                  -64.09 DEGREES                                 201
HI FREQUENCY GAIN                      .40 DB                                       202
HI FREQUENCY CROSSOVER                 .6379 HZ                                     203
HI FREQUENCY PHASE                  -163.04 DEGREES                                 204
EQUIVALENT TIME DELAY                  .253 SEC                                     205


Z - AXIS   ANALYZED AT THE REMNANT   FREQUENCIES
  FREQ   AMPLITUDE
  (HZ)     (DB)
 .0110    -40.11                                                                  206
 .0256    -45.35                                                                  207
 .0513    -56.64                                                                  208
 .0696    -46.58                                                                  209
 .1062    -43.27                                                                  210
 .1794    -46.80                                                                  211
 .3406    -43.18                                                                  212
 .6152    -42.55                                                                  213
 .9851    -47.38                                                                  214
2.0105    -56.21                                                                  215
Z - AXIS  MEAN SQUARE ERROR (MSE)                     10.82 CM*CM       100.00 PCT
MSE ACCOUNTED FOR BY REMNANT   FREQUENCIES              .07 CM*CM          .64 PCT    217
 BY LOW FREQUENCIES ONLY                               .04 CM*CM          .37 PCT    219
 BY HIGH FREQUENCIES ONLY                              .03 CM*CM          .27 PCT    221
```

FIGURE B-1 COMPUTER ANALYSIS OF A THREE-AXIS TRACKING RUN (Concluded)

Appendix C

INFRARED POSITION SENSOR

Appendix C

INFRARED POSITION SENSOR

The infrared position sensor initially described by Hill and Sword (1973), Appendix A) was developed further during this project. A block diagram of the new system is shown in Figure C-1. All oscillators, amplifiers, and detectors for this system are included in the single electronics package shown in Figure C-2. This package has its own power supplies and an LED display that corresponds to the physical layout of the intersecting beams, located on the front panel. Analog signals that are proportional to the reflected light at each intersection and that correspond to the on-off (binary) signals are supplied through a back-panel connector. A potentiometer, located on the panel, allows the operator to set the threshold for converting the analog to the binary signals.

Preliminary experiments with the system included measuring (1) the optimum focus and maximum strength of the light beams, and (2) the optimum focus and maximum receptivity of the phototransistor "eyes." To make these measurements, we mounted the infrared position sensor on one edge of an XY plotter table. The movable carriage used a raster scan to search the area in front of the sensor. By mounting a light sensor or emitter on the movable carriage and controlling the up-down position of the pen from the detector output, we plotted field strengths. An example of such a field-strength plot is given in Figure C-3. Here a phototransistor with a small window (1-mm diameter) was swept slowly through the field on a raster scan. The period of the vertical sweep is about 10 seconds; the period of the horizontal sweep is about 10 minutes. The plot of Figure C-3 reveals that two side lobes (not designed into the

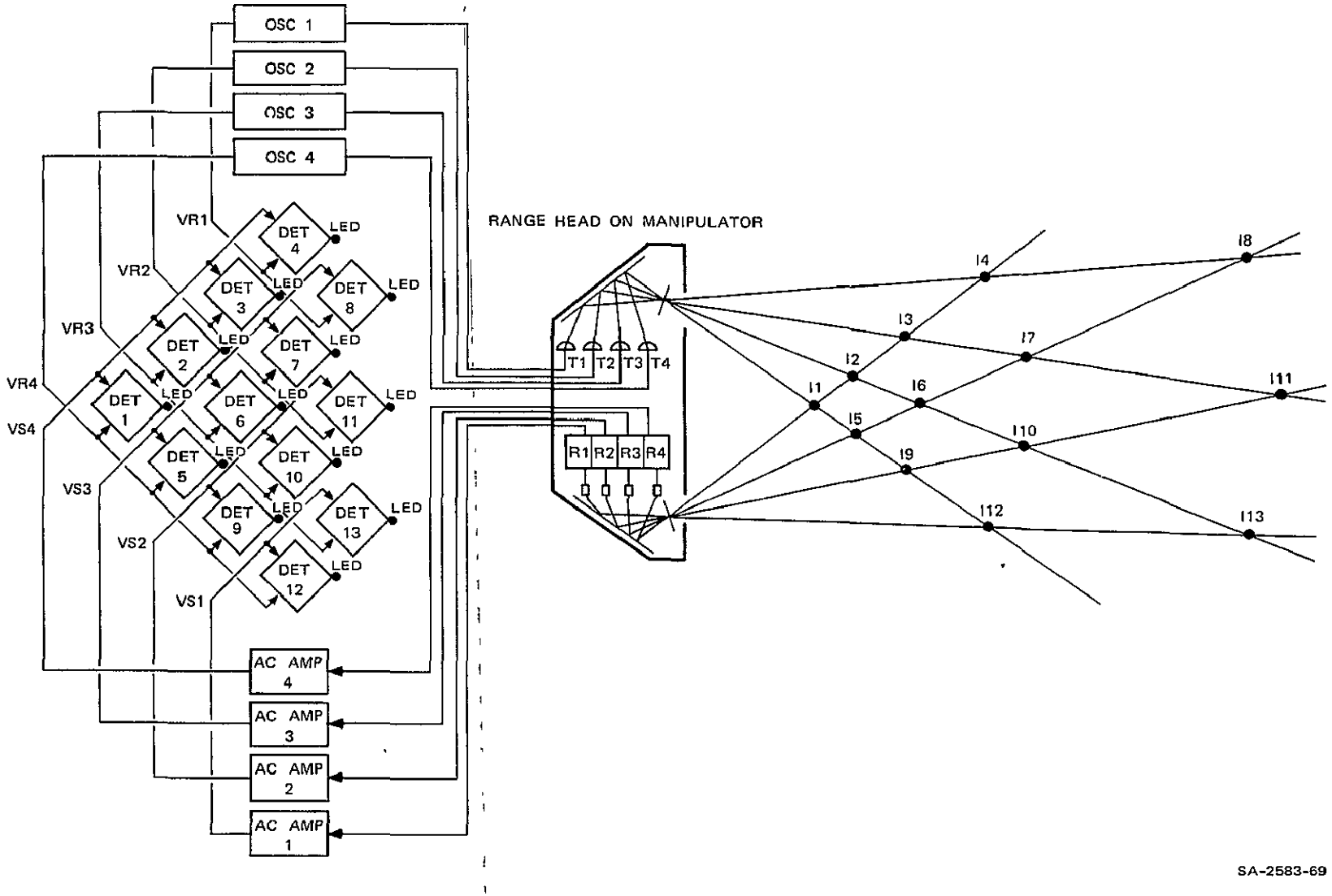

FIGURE C-1 BLOCK DIAGRAM OF RANGE SENSOR

Objects at certain intersections from I1 to I13 reflect light from transmitter T to Receiver R The syncronous detectors, DET, driven by both an oscillator and an amplified signal, light corresponding lamps marked LED

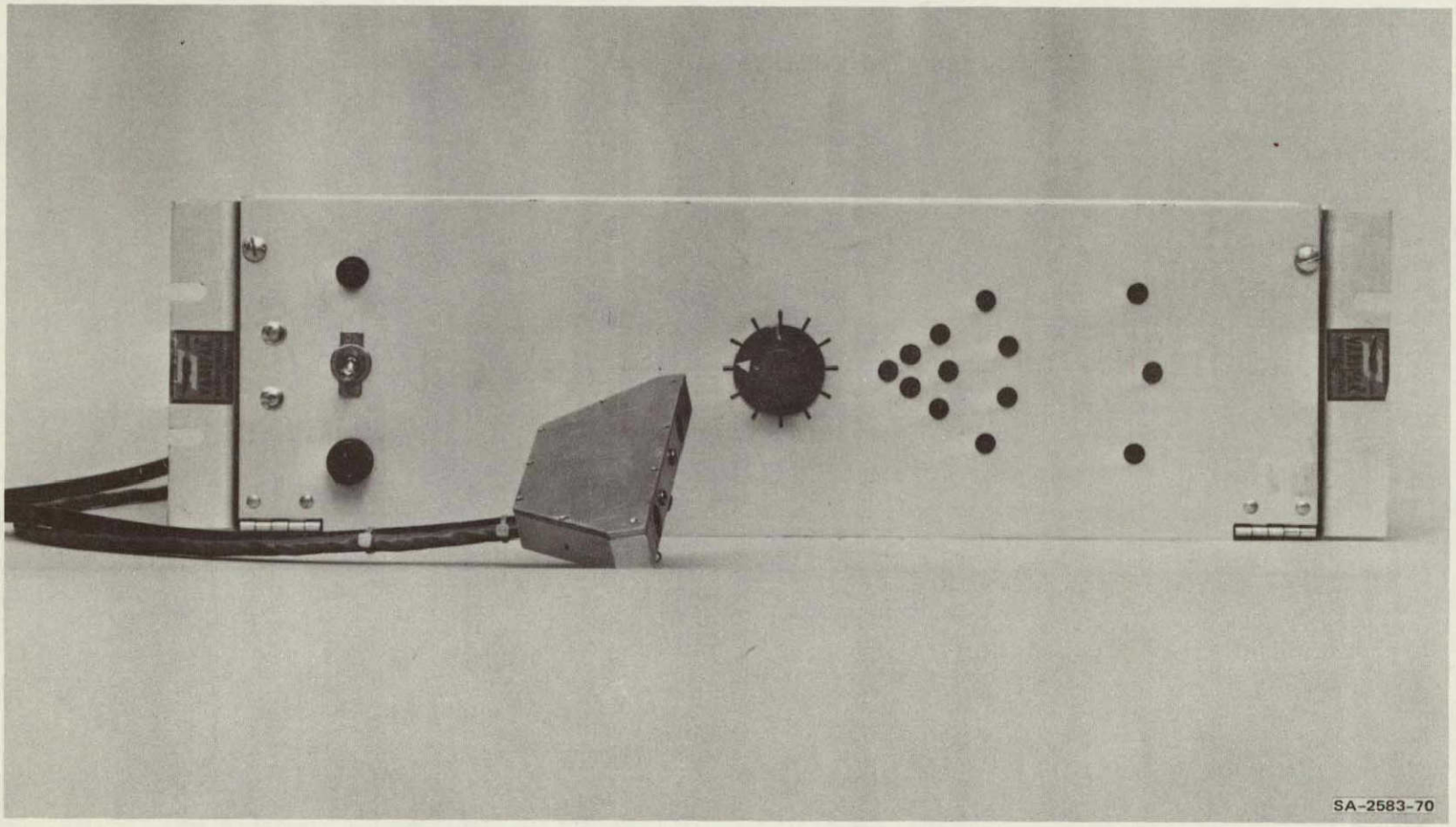

FIGURE C-2 RANGE HEAD WITH SELF CONTAINED ELECTRONICS PACKAGE

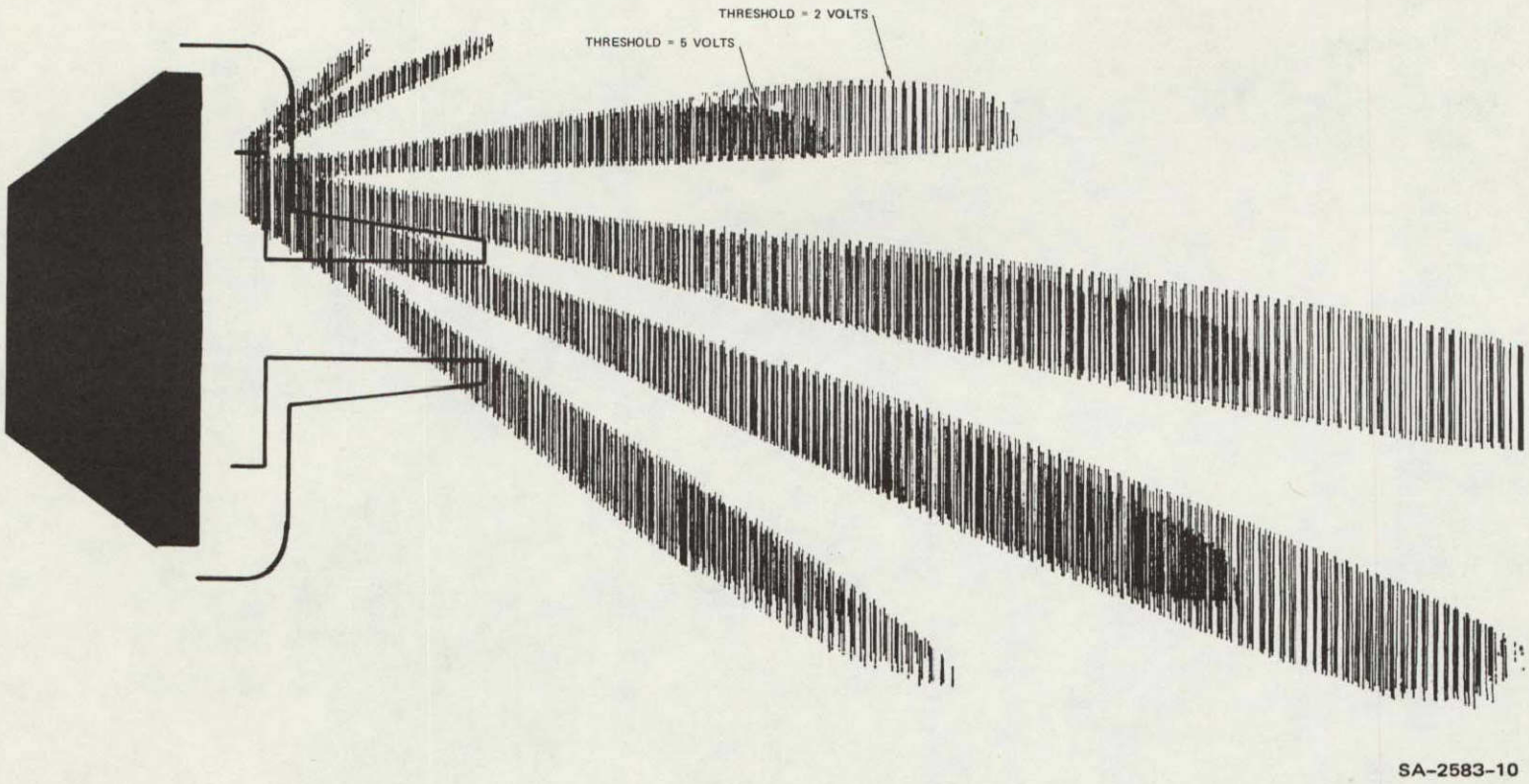

FIGURE C-3 FIELD STRENGTH PATTERN OF INFRARED LIGHT SOURCES

light-emitting system) are present at the top of the picture, and that the image plane of the light emitters is 2.2 inches in front of the sensor housing. Using these procedures, it should be possible to map and control the receptive areas of the position sensor for best use in manipulation tasks.

Appendix D

MANIPULATION BASED ON SENSOR DIRECTED CONTROL · AN INTEGRATED END EFFECTOR AND TOUCH SENSING SYSTEM

Paper presented to the 17th
Annual Human Factors Society Convention,
Washington, D.C.,

October 16-18, 1973

MANIPULATION BASED ON SENSOR-DIRECTED CONTROL AN INTEGRATED END EFFECTOR AND TOUCH SENSING SYSTEM*

J. W. Hill and A J Sword

Stanford Research Institute, Menlo Park, California 94025

ABSTRACT

This paper describes a hand/touch sensing system that, when mounted on a position-controlled manipulator, can greatly expand the kinds of automated manipulation tasks that can be undertaken Because of the variety of coordinate conversions, control equations, and completion criteria, control is necessarily dependent upon a small digital computer The sensing system is designed both to be rugged and to sense the necessary touch and force information required to execute a wide range of manipulation tasks The system consists of a six-axis wrist sensor, external touch sensors, and a pair of matrix jaw sensors Details of the construction of the particular sensors, the integration of the end effector into the sensor system, and the control algorithms for using the sensor outputs to perform manipulation tasks automatically are discussed

INTRODUCTION

Current industrial robots are devices that move from position to position under preprogrammed control Semmerling (1972) describes them as follows

> easily programmable, operatorless handling devices that can perform simple, repetitive jobs that require few alternative actions and minimum communication with the work environment They are unable to think, see, hear, smell, or taste, and only in some instances can they be given a rudimentary sense of feel.

Whenever there are sufficient variations in the positions of objects to be picked up or motion constraints on an object to be moved, the conventional, position-controlled manipulator cannot carry out the task. Research at SRI and other laboratories in the United States and in Japan has begun to show how touch and force sensing in robots, together with the proper control system (usually based on a small computer), can be used to solve these problems and to make robots more useful

Table 1 lists several areas in which touch sensing can be used to expand the range of manipulation tasks Each of these uses requires particular touch sensors and a particular control algorithm for accomplishing the task Thus, in designing a touch sensing system for automatic manipulation, both the quantities to be sensed and the type of control algorithms available must be considered The sensing system described in this paper includes sensors that can be used in all of the tasks in Table 1

Table 1

USES OF TOUCH INFORMATION

Correcting position errors
- Bringing mating parts together
- Starting pins into holes
- Locating surfaces, corners, edges, and the like

Acquisition
- Aligning jaws to objects
- Extracting one part from a bin of parts

Constrained motion
- Sliding parts
- Final insertion of pins into holes
- Turning cranks, or hinged doors

Error detection
- Collisions
- Acquisition failures
- Task completion failures

Training (or programming) the manipulator by pushing on hand
- Steering through tasks
- Setting force levels

Classification of objects
- Size
- Weight
- Shape
- Motion constraints

TOUCH CONTROLLED MANIPULATION

To assemble parts, information from touch sensors can be used to steer the hand as it closes and moves A simple example of this procedure is that of aligning the hand to an object without disturbing it, as illustrated in Figure 1. This alignment procedure may be required either to pick up an object without knocking it over or to calibrate the hand to part of any object for subsequent mating of parts to that object. For such purposes, sufficiently sensitive sensors are needed on the gripping surfaces of the fingers to detect finger contact with an object without pushing it away

*This work was supported by the National Aeronautics and Space Administration, under Contracts SNSN-63 and NAS2-7507, and by the National Science Foundation, under Grant GI-38100x.

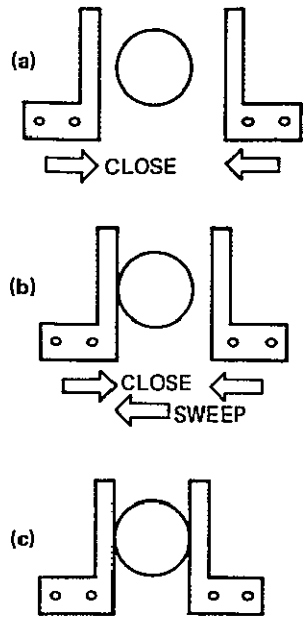

FIGURE 1 ALIGNING FINGERS TO OBJECT

Jaw closes (a) until light touching contact is made (b) Then entire hand is moved at jaw closing speed until both tongs contact object (c)

As the improperly centered fingers shown in Figure 1(a) close on the object, contact against one finger is made The computer control system must then cause the hand to sweep in a direction from one finger to another, in a coordinate system determined by the hand, while the fingers continue to close [Figure 1(b)] Closing and sweeping proceed until both fingers contact the object, as shown in Figure 1(c) At this point, the control system must terminate the grasping process and activate the next step in the assembly algorithm This example shows that several separate abilities are required for successful manipulation based on touch control

- Motion in different coordinate systems
- The ability to steer the hand relying on touch
- Determination of critical forces for carrying out the task.
- Determination of task completion criteria based on touch
- The means for measuring these critical forces.

In the following four sections, the implications of the above requirements are briefly discussed, and their importance to the design of a general purpose end effector with a built-in touch sensing system is described

Coordinate Systems

Before describing how sensors are used to control the manipulator, it is necessary to define the coordinate systems in which the manipulator must move. Any manipulator is controlled in an arm coordinate system that is uniquely determined by its own geometry, there are as many coordinates as there are movable joints in the manipulator Arm coordinates, however, are of little use in the automatic manipulation tasks of interest here. To assemble parts, it is necessary to move the manipulator holding the daughter part in the coordinate system of the mother part On the other hand, when maneuvering in the working area, it is necessary to move in the coordinate system of the work space This is particularly useful when maintaining the hand at a certain height above the floor and tables and still being able to slide objects across them By placing parts on a motorized turntable, and by using jigs and fixtures, it is possible to cause the coordinate system of the mother part to coincide with that of the work space, thus simplifying the manipulator control problem. Similarly, by either carefully designing the end effector to mate with the daughter part or by designing jigs to hold or align the part as it is being picked up, the coordinate systems can be fixed with respect to one another, again simplifying the control equations

The two most important coordinate systems in which the arm must be able to move for automatic-controlled assembly operations are therefore workspace coordinates and hand coordinates These are illustrated in Figure 2. The mathematics for moving a manipulator in these coordinate systems for particular applications has been discussed by both Whitney (1969) and Paul (1972)

Control Algorithms

To perform useful tasks, the information from touch sensors must be used to control the position of the manipulators When the hand is close to the area of the object to be picked up, the motion of the hand must be steered by the actuation of sensors so that (1) the object will not be knocked about and (2) a secure grip will be maintained.

The situation can be compared to the hypothetical requirement that a yardman in a railroad switchyard walk up to a 100-ton engine and push it along the track with his bare hands. The problem can be solved simply by installing the throttle (a proportional touch sensor) on the front of the engine within reach of the yardman. By exerting a pound or so of force on the throttle, he can then move the 100-ton engine. The harder he pushes, the faster the engine will go

Similarly, the "power steering" required for the self-centering grip shown in Figure 1 causes the hand to sweep left or right, depending on whether the left or right gripping surface of the finger is pushed The harder the push, the faster the hand should sweep. To accomplish this task, the control algorithm must move the joints of the manipulator in a particular

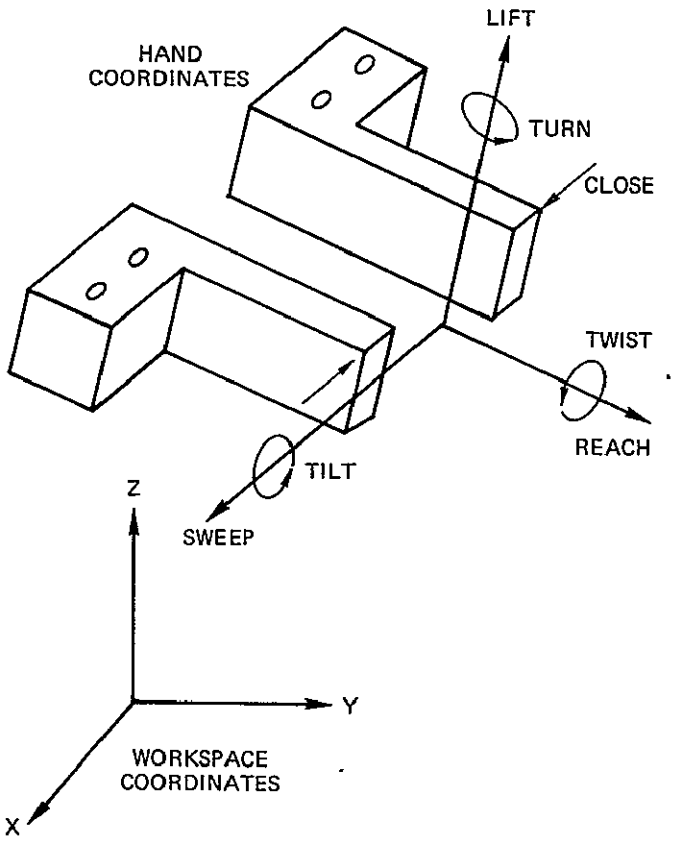

FIGURE 2 TWO IMPORTANT COORDINATE SYSTEMS

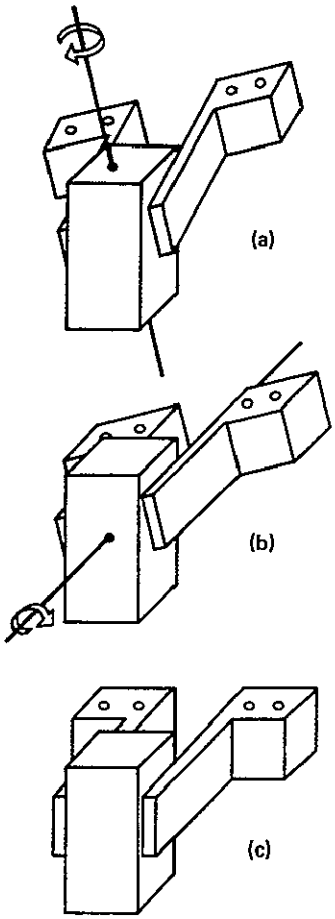

FIGURE 3 ROTARY ALIGNMENT TO OBJECT

As the jaws close, the hand is driven first to turn (a) and then to tilt (b) by signals derived from proportional force sensors on jaw surfaces to achieve desired orientation (c) for grasping

coordinated fashion in response to the proportional inputs from touch sensors on the inside surface of the jaw Like power steering, a small force will cause an otherwise immobile manipulator to move freely

A second example of an acquisition strategy illustrating a particularly desirable combination of sensor-directed motions is shown in Figure 3 After sweeping, the hand is directed to move about the turn and tilt axes by signals from touch sensors on the gripping surfaces of the jaws This strategy is useful for acquiring objects without moving them or for determining the position, size, and orientation of an imprecisely known object The task requires sensing both small, proportional torques used to drive the turn and tilt axes and the light proportional pressure developed on the inside surface of the tongs used to drive the sweep axis The closing of the hand generates these forces, and task completion is indicated by the attainment of some threshold gripping force For this task, the most appropriate location for sensors is on the inside surfaces of the jaws

A different example, a placement task, is illustrated in Figure 4 Here the task is to push a block into a mating corner The control problem is simplified both by the proper alignment of the coordinates of the mother part with the work-space coordinates and the proper alignment of hand coordinates to block coordinates using the previous acquisition strategy The first step in the placement task [Figure 4(a)] involves the assumption of the parent-part coordinates by the end effector This is done by allowing the hand to tilt and turn to nullify torques that build up as the block is lowered to and pressed against the parent surface. When a threshold reach force builds up, the first portion of the task is complete, and the hand must then be controlled to lift, to maintain reach pressure, and to nullify twist torque This brings the second block face to mate with the second parent surface [Figure 4(b)] When a threshold lift force is obtained [Figure 4(c)], the task is complete. The jaws are then opened while holding the hand in its position

Control Equations

Control of the manipulator to assume various positions, to move at different rates, and to apply forces, is accomplished by selecting and implementing the

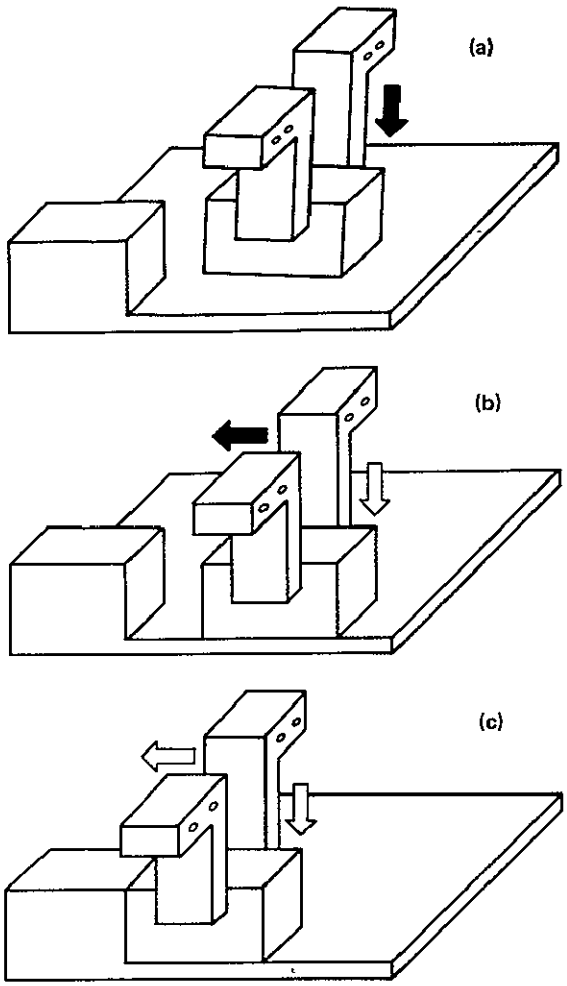

FIGURE 4 AUTOMATIC PLACEMENT OF BLOCK

Block is placed flat against a surface (a) by lowering it until contact force is measured at wrist and then rotating hand on two axes to null misalignment torques As downward pressure is maintained (light arrow in b) on block, it is slid left (dark arrow in b) until sufficient contact force is built up (c)

proper control equation for each of the coordinate axes The well-known equation for position is

$$\text{Rate} = K_p (P_c - P) \quad , \tag{1}$$

where K_p is the position gain, P_c is the commanded position, and P is the actual position. For control in hand coordinates, Rate, P_c and P can be considered to be 1 x 7 matrices that specify the corresponding rates or positions of the seven hand coordinates. To obtain sliding along a particular axis, the control equation is more simply expressed as

$$\text{Rate} = R_c \quad , \tag{2}$$

where R_c is the command rate matrix To control force, the general force generating equation is

$$\text{Rate} = K_f (F_c - F) \tag{3}$$

If K_f, the force gain, is zero, the hand is stiff and will not respond to external forces if K_f is large, then the hand moves quickly to generate or respond to external forces If the command force vector, F_c, is zero, the hand moves freely wherever it is pushed If F_c is not zero, the hand moves until forces are developed on particular force sensors (F) that match F_c There can be one or many more than seven force sensors

It is useful to combine Eqs (1), (2), and (3) into the general control equation given below

$$\text{Rate} = K_p (P_c - P) + R_c + K_f (F_c - F) \tag{4}$$

By properly choosing the gains in Eq (4), the hand can be made to perform the following actions simultaneously

- To push on one axis
- To move on another at a fixed rate.
- To hold a third fixed
- To make the remaining four axes passive to external forces or torques

Performing the sequences of tasks previously shown in Figures 3 and 4 requires (1) a sequence of different control equations based on Eq (1),, and (2) proportional sensors to measure those forces pertinent to the task.

Completion Criteria

To determine when the transition from one set of control equations to another should be made, completion criteria must be established and continuously tested Some examples of these criteria, based on force sensing, are given in the previous tasks (Figures 1, 3, and 4). In general, many different completion conditions must be specified during any manipulation task Equally important to subtask completion are those criteria that indicate improper operation of the system. Examples of both kinds of criteria are given in Table 2

With each control equation, it is necessary to specify both a list of completion criteria and the new actions and control equations to be used if any of these criteria are met This suggests that a branching structure associated with a computer language is required to specify both the manipulation task and any required emergency procedures. These procedures should cause the hand to stop in midtask and should inform the human supervisor of any difficulties and their symptoms

Table 2

EXAMPLES OF COMPLETION CRITERIA

Workspace coordinates
* Exceeded work space
* Entered obstacle area
• Height greater than 52 inches
• Incremental height greater than 6 inches

Arm coordinates
* Exceeded allowable range
* Elbow torque greater than 50 foot-pounds
• Wrist increment greater than 90°

Hand coordinates
* Excess hand force
• Grip greater than zero
• Squeeze less than 10 pounds
• Reach increment greater than 5 inches
• Lift greater than 15 pounds

Individual sensors
• Any touch sensor on
• Right fingertip force greater than 0.1 ounce
• Both jaw forces greater than 1 pound

Elapsed time
* Time greater than preset limit

Note: Asterisks denote emergency criteria, and bullets denote operational criteria.

MEANS OF MEASURING THE CRITICAL FORCES

To carry out the above manipulation tasks, various contacts with and pushes against objects in the environment must be sensed. Several methods of sensing these forces using manipulators are described in the following paragraphs.

Joint Forces

The force or torque at each joint in the manipulator can be sensed by measuring either the motor current in electric systems or the back pressure in hydraulic systems. This is particularly easy in electrically driven manipulators because the torque motor itself is used as the sensor, thus requiring no additional sensors.

The use of joint forces as measures of contact between the object and the end effector is limited by several factors. Joint forces are contaminated by the weight of both the manipulator segments and the load. In addition, when the arm is in motion, changing acceleration forces, changing centripetal forces, and reaction forces developed due to motions in other joints, all further contribute to the joint force contamination.

Joint force measurements are also limited by the back-drive friction of the individual joints. Depending on the gearing, more than 10 percent of the force exerted by a given joint is likely to be required to back-drive that joint. Though capable of driving 10 pounds, such a joint could sense only 1 pound. A force applied to the hand may back-drive some joints (the freest ones) but not others, thus giving false information concerning the applied force vector.

In spite of these limitations, Goto (1972) has used joint forces to pack blocks tightly on a pallet. Inoue (1971) compensated joint forces for gravity loading by measuring and storing static joint forces before task initiation. Using changes in the joint force, he programmed a manipulator to insert a pin into a hole and to turn a crank. Considerably refining the technique, Paul (1972) compensated joint forces for both gravity and acceleration loading and demonstrated several placing and sliding tasks. Another use of joint forces is the detection of collisions against an obstacle. Restricting the use of joint forces to the range from 30 to 100 percent of a joint's maximum force capability should avoid many of the complexities of compensation and back-drive limitations.

Separate Sensing Couple

Another means of measuring contact between the end effector and the environment is to measure the force couple at some point on the manipulator. The force couple consists of a torque vector and a force vector. Together, these forces completely describe the reaction force at the point where the manipulator is cut. The obvious place to make this measurement is between the end effector and the last joint of the arm, as suggested by Scheinmann (1969). Here the sensing is in close proximity to the load and, because the factors influencing the signals from external contact are due only to the gravity and acceleration loading from the combined hand-object mass, the sources of contamination are significantly reduced.

Thus, in moving from the joints to the wrist, the sensing problem becomes greatly simplified. The major portion of the weight and the varying geometry are both removed from the sensing scheme. Assuming the weight of the end effector to be one-tenth the weight of the arm, wrist sensing rather than joint sensing expands the useful force range by a factor of 10, allowing smaller forces to be measured. A wrist sensor for computer control of an arm was used by Groome (1972) to permit sliding a pin in a closely toleranced hole and aligning the wrist to a flat object.

Touch Sensing

The most sensitive and direct method of measuring contact between an object and the end effector is to mount sensors on the outer surfaces of the end effector. Such sensing plates can have a mass of only a few grams, and they in no way reduce the magnitude of the forces applied to the arm. With such a low mass, it is not necessary to compensate for either gravity or arm acceleration, and forces on the order of grams can be sensed directly. Uncompensated touch sensors are easily 1000 and 100 times, respectively, more

sensitive to measuring contact forces than compensated joint and wrist sensing.

Using touch sensors on the inside of the jaw, it is possible to pick up lightweight objects automatically without disturbing them. This was done by Goto (1972), Hill and Sword (1973), Inoue (1971), Ernst (1962), and Paul (1972) by compensating in various ways to reduce errors in positioning either the object or the hand. Using touch sensors on the outside of the fingers, Goto (1972) was able to package small boxes on a pallet.

DESIGN OF A HAND WITH TOUCH AND FORCE SENSING

The hand system shown in Figure 5 was designed based on (1) the requirement to perform automatic manipulation and assembly tasks using touch sensing and (2) the limitations of the sensing systems previously discussed. The system consists of the following integrated parts:

- Six-axis wrist sensor
- Motor driven hand
- External touch sensing plates
- Jaw sensor matrices
- T-handle tool holder.

In addition, jaw position potentiometer signals and jaw motor drive current signals are available. These signals will allow the control computer to sense and control both the jaw opening and the total jaw gripping force.

Wrist Sensor

The wrist sensor measures both the three components of force, which correspond to the reach, lift, and sweep directions, and the three components of torque, corresponding to the twist, turn, and tilt directions (Figure 2). The wrist sensor is situated at the base of the drive housing, and its operation is based upon deflection across the deformable suspension located at the hand-wrist junction.

The key elements of the wrist sensor are the four sensing blocks arranged as shown in Figure 6. Each block consists of several light-emitting diode (LED)/

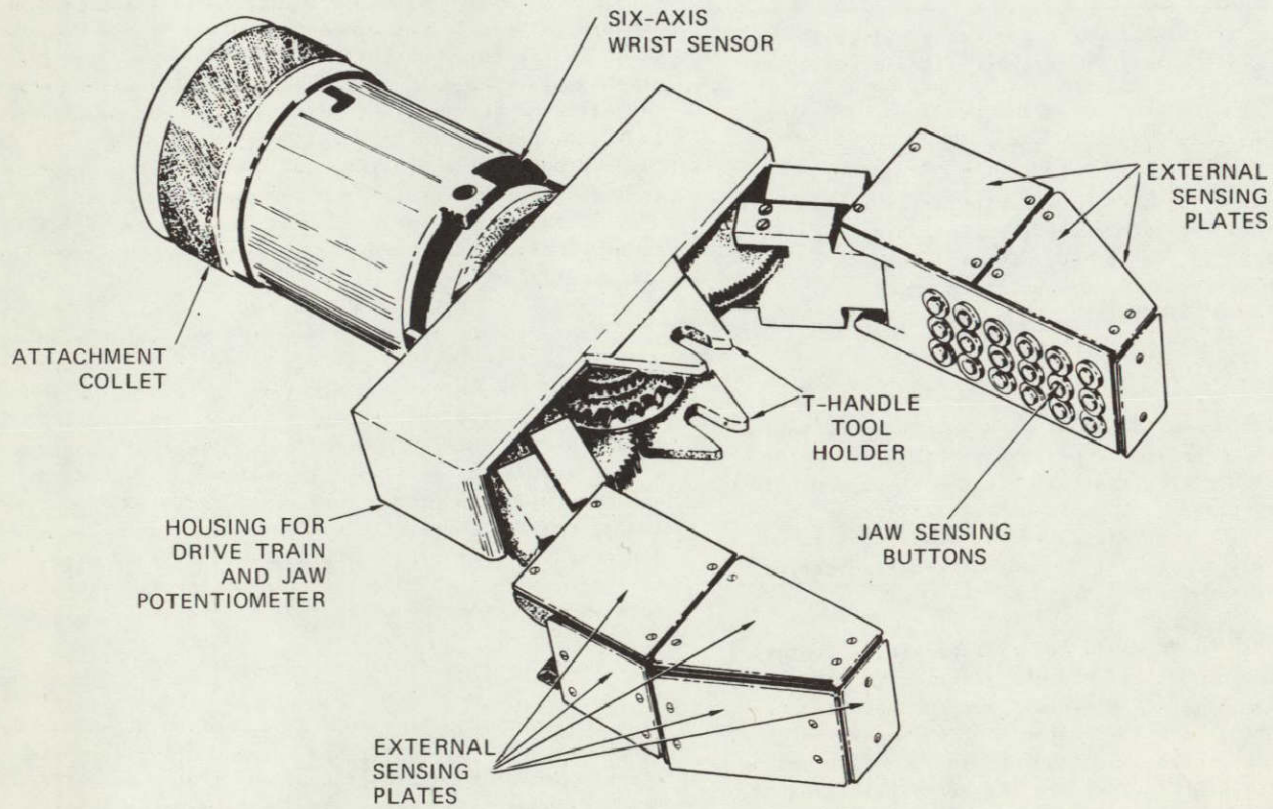

FIGURE 5 END EFFECTOR WITH PROPORTIONAL TACTILE AND SIX-AXIS WRIST SENSOR

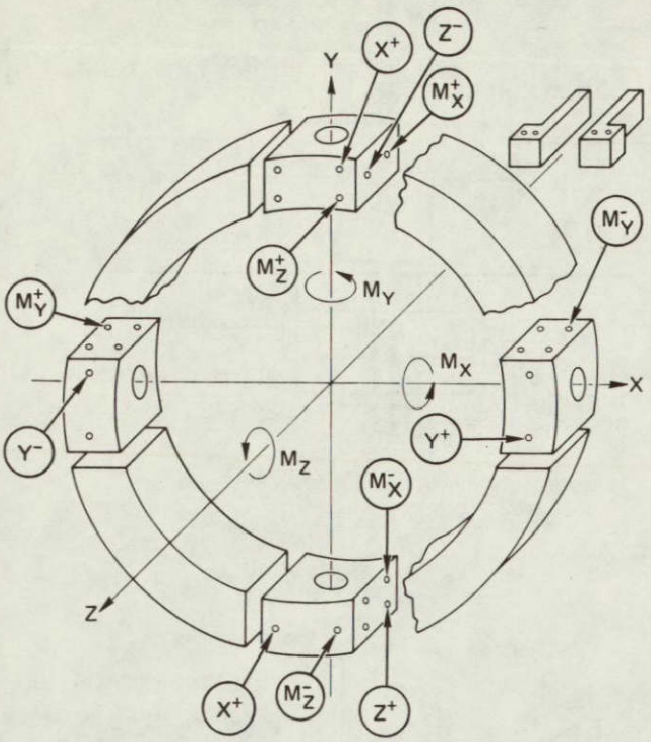

FIGURE 6 SIX-AXIS WRIST SENSOR GEOMETRY

phototransistor light paths, which are broken by pins attached to the hand yoke. The motion of these pins will change the position of the shadow cast upon the square light-sensitive area of the phototransistors by the edge of the pin. Electrical signals corresponding to the three forces and three torques are obtained directly by subtracting the two constituent photocurrents.

A useful feature of this system is that the weight of the hand drive motor balances the weight of the jaws, as shown in Figure 7. Thus, the torques measured at the wrist sensor do not reflect hand weight. Proper balancing permits manipulation with lighter loads. This is similar to the mathematical compensation previously described, except that it is done prior to sensing and hence does not require such highly linear sensors.

Touch Sensors

The seven external sensing plates that cover each jaw activate proportional sensing elements. These plates are uniformly sensitive to force over their surface and deflect approximately 1 mm under load conditions. Since the sensors were incorporated directly into the jaw, they are very rugged. Because of the experimental nature of the hand, the external sensing plates seen in Figure 5 were designed to be replaceable and can be constructed of hard rubber or metal. The force range for each sensor depends upon a compliant element that can be easily changed to vary the full scale sensitivity from 5 g to 5 kg. Since the sensors are linear over a 100- to -1 range of force,

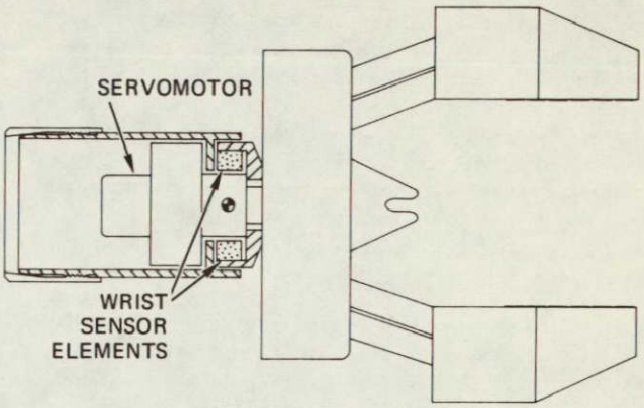

FIGURE 7 WRIST INTERIOR SHOWING HOW WEIGHT OF SERVOMOTOR BALANCES WEIGHT OF HAND

a single sensitivity can be used for different tasks. The addition of composite or nonlinear compliant elements will permit the force range to be expanded greatly.

Integral to the inside surface of each jaw is a 3 x 6 matrix of sensing buttons, each with the same properties as the external sensing plates, as shown in Figure 8. With this array of sensors, it is possible to derive simply control signals that will permit turn, twist, and sweep during jaw closure to be governed by the contours of the object, as previously shown in Figure 3. The tactile information from the jaw sensor matrix can be used to find the location of objects in the jaws and to compensate for faulty positioning by motions in reach and lift.

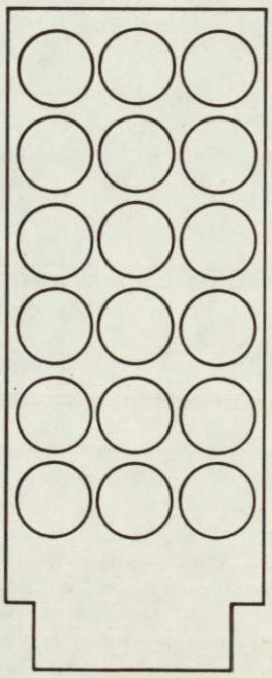

FIGURE 8 THREE-BY-SIX SENSOR ARRANGEMENT ON INSIDE SURFACES OF JAWS (FULL SIZE)

Finally, the base of the jaw contains deep notches for attachment of tools directly to the wrist. A switch in the wrist indicates that the T-handle is firmly seated and that the tool can be grasped. The inside jaw sensors signal when proper grasp has been achieved and the tool firmly grasped. Then, using the wrist sensor, forces on the tool can be detected, and further sensor-controlled manipulations can be performed.

The configuration of the touch sensors within one jaw is shown in the cross section of Figure 9. Transduction from external force to electrical signal occurs in two stages. First, a compliant washer in each sensor determines the deflection of a light vane from the external force. Then, the vane controls the light falling on a phototransistor, as shown in Figures 10 and 11.

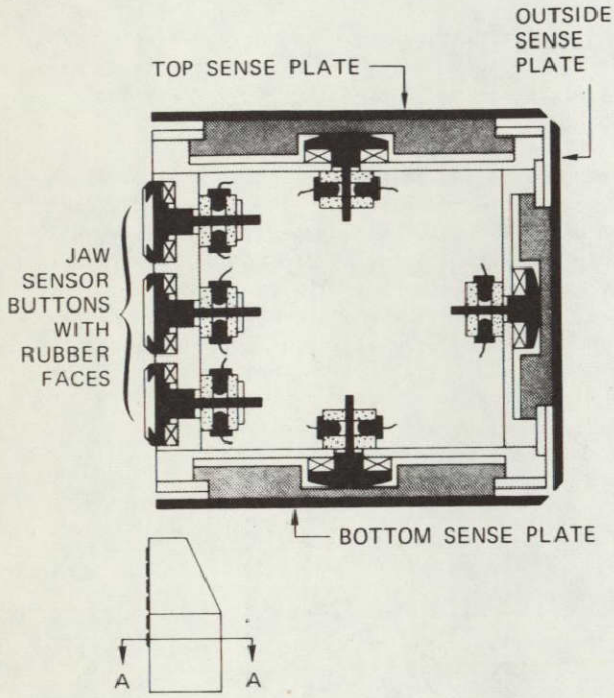

FIGURE 9 CROSS SECTION THROUGH JAW
Section is shown at line A-A of insert.

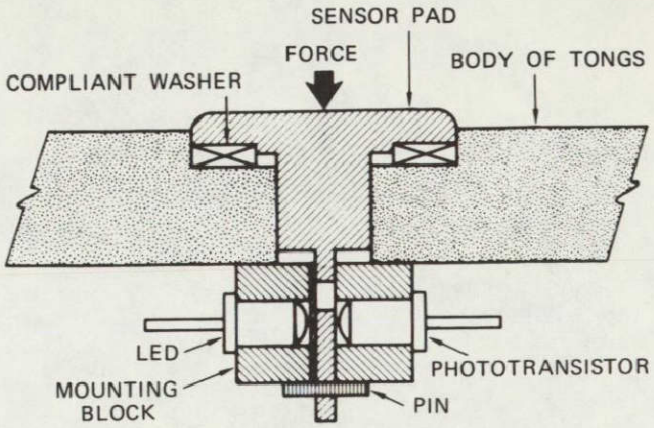

FIGURE 10 CROSS SECTION OF SENSOR WITH COMPACT SHUTTER

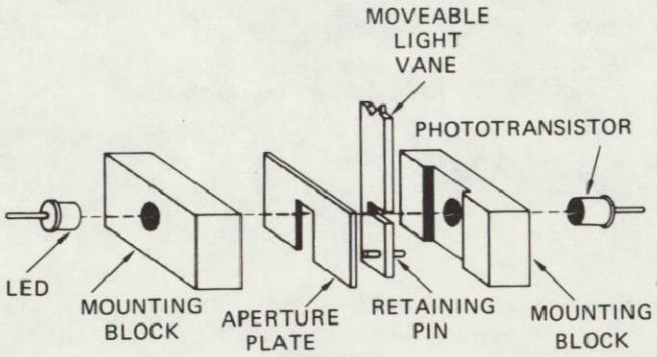

FIGURE 11 EXPLODED DRAWING OF SHUTTER

REFERENCES

Ernst, H. A. MH-1, A Computer Operated Mechanical Hand. In 1962 Spring Joint Computer Conference, AFIPS Conference Proceedings, Vol. 21, pp. 39-51, National Press, May 1962.

Goto, T. Compact Packaging by Robot with Tactile Sensors. Proceedings of the Second International Symposium on Industrial Robots. IIT Research Institute, Chicago, Illinois, 1972.

Groome, R. C., Jr. Force Feedback Steering of a Teleoperator System. MIT Charles Stark Draper Lab, Report T-575, Cambridge, Massachusetts, August 1972.

Hill, J. W. and Sword, A. J. Studies To Design and Develop Improved Remote Manipulation Systems. NASA Contractor Report CR-2238, NTIS, Springfield, Virginia, April 1973.

Inoue, H. Computer Controlled Bilateral Manipulator. Bulletin of the Japanese Society of Mechanical Engineers, Vol. 14, p. 199-207, 1971.

Paul, R. Modelling, Trajectory Calculation and Servoing of a Computer Controlled Arm. Stanford Artificial Intelligence Project Memo AIM-177, Stanford University, Stanford, California, November, 1972.

Scheinman, V. D. Design of a Computer Controlled Manipulator. Stanford Artificial Intelligence Project Memo AIM-92, Stanford University, Stanford, California, June 1969.

Semmerling, W. Robots are Here. Assembly Engineering, Vol. 15, p. 42-49, April 1972.

Whitney, D. E. Resolved Rate Control of Manipulators and Human Prostheses. IEEE Transactions on Man-Machine Systems, Vol. MMS-10, p. 47-53, June 1969.

Appendix E

CONTROL OF PROSTHETIC DEVICES WITH SEVERAL DEGREES OF FREEDOM

Paper presented to the
17th Annual Human Factors Society Convention,
Washington, D.C.

October 16-18, 1973

CONTROL FOR PROSTHETIC DEVICES WITH SEVERAL DEGREES OF FREEDOM*

A. J. Sword and J. W. Hill

Stanford Research Institute, Menlo Park, California 94025

ABSTRACT

One of the major factors limiting the use of multijointed prosthetic devices is that as the severity of disablement increases, the number of joints to be replaced and controlled also increases. Along with this problem there is a corresponding decrease in the number of available control sites This paper shows how this problem can be solved using a method of coordinated control of a multidegree-of-freedom prosthesis. By using a single proportional analog input, together with a digital control input, an arm prosthesis can perform useful movements heretofore impossible with conventional myoelectric control techniques. In addition, more sophisticated motions can be made when tactile sensors are incorporated into the control scheme. Finally, the paper demonstrates the generality of the approach and the feasibility of extension of this control scheme to other types of prosthetic devices.

INTRODUCTION

The Problems of Present Prosthetic Control

When the normal human being decides to initiate a manipulation task, he sets in motion a complex set of neuromuscular functions. It is well known that the completion of the task requires the simultaneous and unequal activation of a large number of muscles whose contractions are coordinated in a complex fashion both in degree and in time. However, the person is conscious only of his desired goal, not of his complex muscle movements. If one were to monitor muscle activity in the arm and hand, he would find that the degree of contraction of the muscles is a complex function of the time since task initiation. In fact, to attempt to accomplish a task by consciously commanding individual muscles would either render the task impossible or tire the normal person so much that task completion would no longer be worthwhile.

A similar problem arises for the amputee. A conventional method of prosthetic/orthotic control takes the form shown in Figure 1. This figure shows that as the desire to control more degrees of freedom grows, a corresponding increase in the available number of control sites is required Furthermore, a conscious human intelligence must individually and proportionally control each muscle site and integrate all their actions to perform a single, coordinated movement. Clearly, this can become quite taxing, and the value of performing a task can be quickly overshadowed by the effort that must be expended to complete it. In addition, it has been proven to be difficult for the wearer of a prothesis to train individually specific muscles or muscle groups and to generate signals that are sufficient to control a prosthesis (Radonjic and Long, 1969). The situation is further complicated by the fact that the muscle sites used for control may turn out to be the same muscles required for the execution of a simultaneous activity with another part of the body.

This limitation--coupled with the fact that as the severity of the disability increases, the desired number of degrees of freedom increases and the number of available myoelectric control sites decreases--indicates that the present method of prosthetic control is not sufficient or useful for functions other than extremely primitive ones

Background

Many previous attempts have been directed toward developing various coordinated/multimoded prosthetic devices. The "Heidelberg Arm" was one of the early multifunctional prostheses Its primary difficulty was a control system so complex that it required the complete attention of the amputee (Hoerner, 1958) Another attempt was the "Swedish Arm," which tried to conceal the control problem from the amputee. Using the "Swedish Arm," Lawrence (1972) employed pattern recognition techniques on the natural myoelectric activity of the amputation stump to determine which modes were commanded The problem with this design is that most pattern recognition techniques require significant amounts of data processing. In a similar context, Whitney (1969) proposed a matrix coordinate conversion method that would allow the terminal device to move in an arbitrary straight line that is defined in terms of those axes relevant to the task environment. Again, the objection with Whitney's scheme is that considerable data processing in the form of vector operations is required. Two attempts to develop a multimoded prosthetic device are the "Belgrade Hand" ("Externally Powered Terminal Devices," 1969) and the "Berkeley Arm" (Carlson, 1971). Each of these devices has the advantage of using musculoskeletal control, thus

*The work described herein, although a direct offshoot of work performed for the National Aeronautics and Space Administration under Contract NAS2-6680, was supported by Stanford Research Institute internal R&D funds The equipment used was provided under the NASA contract.

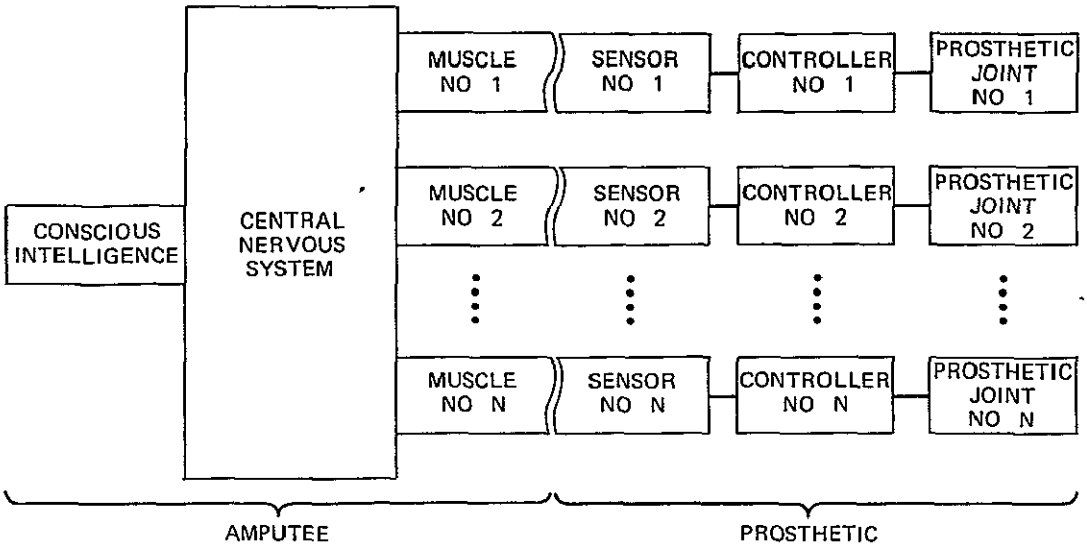

FIGURE 1 CONVENTIONAL MODE OF PROSTHETIC CONTROL

overcoming many of the previous objections to the myoelectric control technique. The "Belgrade Hand" uses a single motor to drive two different modes of prehension--palmar and lateral, the "Berkeley Arm" has three degrees of freedom and provides the following four different modes:

- Wrist flexion coupled with elbow flexion such that the terminal device moves in a parallel path in space.
- Wrist rotation coupled with elbow flexion.
- Independent wrist flexion.
- Independent wrist rotation.

The problem with each of these prostheses is that, because of the nature of their design, only those motions that have been built in are available to the amputee.

A DIFFERENT APPROACH TO PROSTHETIC CONTROL

A more fruitful approach to prosthetic control can result from a consideration of how a human being controls his natural appendages. As previously mentioned, the person is conscious only of his desire to perform a given task, not of the individual muscle commands necessary to complete the task. It thus seems reasonable that what is needed in a prosthetic controller is a method of mapping a single signal into a set of control signals related to one another in a coordinated fashion.

A method of achieving this objective is shown in Figure 2. This method differs from that of Figure 1 in several respects. Most importantly, it requires the conscious control of only two muscles, rather than the greater number required by conventional control techniques. One muscle signals the controller, selecting the way in which the second muscle signal is to be used in moving the prosthetic device. The key to this approach lies in the coordinated motion controller, which has the ability to accept only a few signals and to perform one to many transformations.

Laboratory Implementation of the Control Scheme

Such a mapping of one signal into many coordinated signals can be accomplished by means of the control scheme shown in Figure 3. The control algorithm,

$$C = pM$$

requires only a single proportional analog input. The scalar input, p, is operated upon by a motion vector, M, consisting of one element for each available degree of freedom, and that operation results in a set of analog command signals, C, which are in the same proportion as in the motion vector.

The coordination algorithm was simulated on the laboratory LINC-8 computer control system shown in Figure 4. The control algorithm accepts both a single proportional analog control signal generated by the transducer worn by the person and a command signal generated via a Teletype. Using these inputs, the control algorithm generates seven separate, coordinated control outputs. These outputs were used to control a simulated prosthetic device: a modified, seven-jointed Rancho manipulator, Model 8A. The manipulator joints and their anthropomorphic equivalents are shown in Figure 4.

Experimentation with this system resulted in the determination of several motion vectors that allowed demonstration of various coordinated motions. These motions and the number of required degrees of freedom (dof) were:

- Reaching out while keeping the forearm level (2 dof).

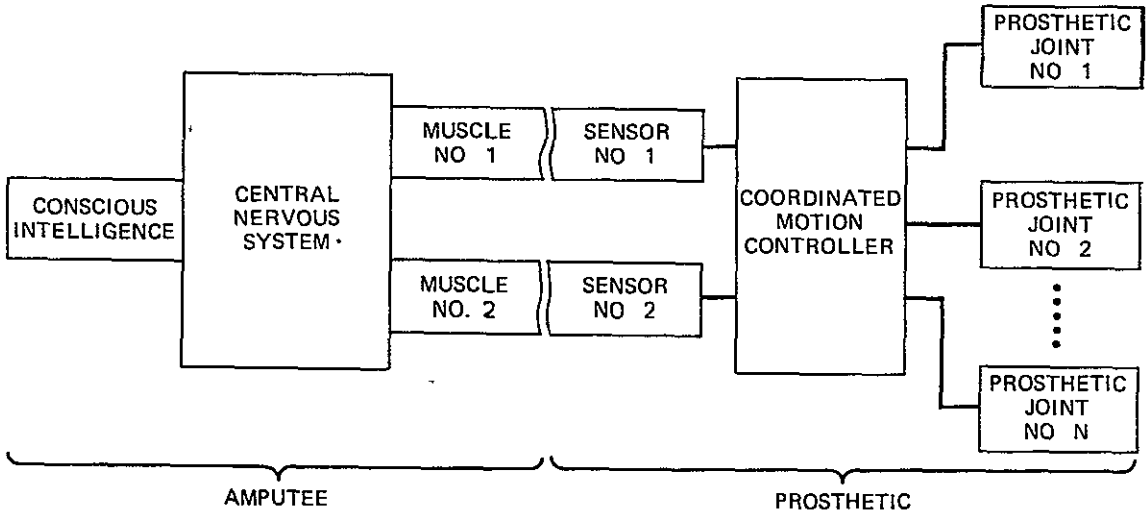

FIGURE 2 A DIFFERENT METHOD OF PROSTHETIC CONTROL

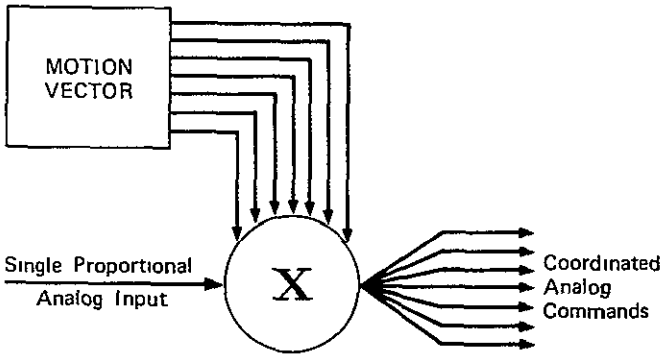

FIGURE 3 THE COORDINATED MOTION SCHEME

- Abducting the shoulder while keeping the hand stationary (4 dof).
- Rotating the humerus while keeping the wrist level (5 dof).
- Feeding, coupled with wrist rotation (5 dof).
- Reaching the hand across the chest (6 dof).

In addition, more complex compound motions could be obtained by properly sequencing two or more simple motions, each requiring a single motion vector. As an example, consider the reach-out motion. If the feeding motion is followed by the reach-out motion, a motion similar to that of brushing the teeth is obtained. Alternatively, if the reach-behind-the-back motion (itself a compound motion) is followed by the reach-out motion, then a toileting motion is obtained. In the laboratory, both a toileting motion and a motion that causes the hand to reach toward and to touch the shirt pocket have been demonstrated. The reach-to-pocket motion consists of a shoulder abduction motion followed by a reach-across-the-chest

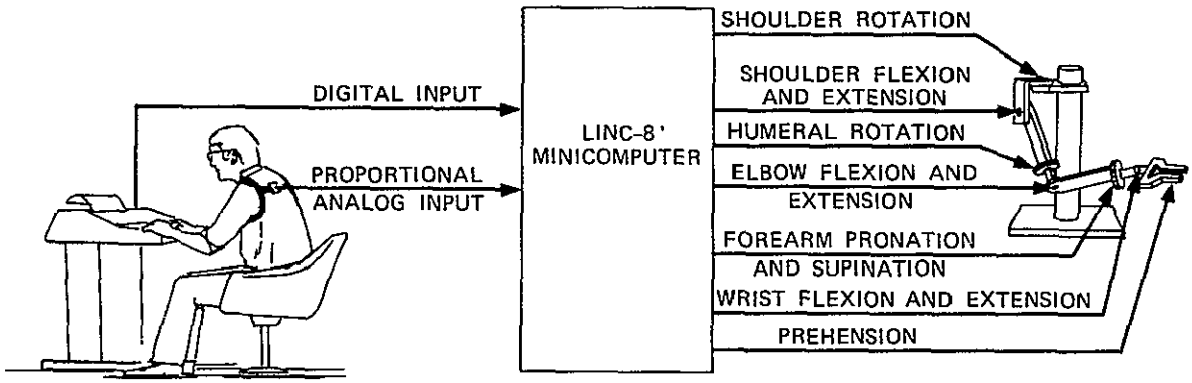

FIGURE 4 IMPLEMENTATION OF THE COORDINATED MOTION CONTROLLER

motion Thus, any individual simple motion can assume a multiplicity of uses that are dependent upon the particular sequencing chosen.

Proportional Control Signal

Proper proportional control site selection is of extreme importance to the resulting coordinated motion. A control site should provide proportional control, be sensitive to small movements, be in a position that can be readily hidden by clothing, and be insensitive to unrelated body movements. Any transducer mounted on this control site should be cosmetic in appearance; insensitive to various body and environmental conditions, such as perspiration, temperature, and humidity; and not fatiguing under normal usage.

Some of the available control sites are shown in Figure 5. Of these, the shoulder separation site was selected. The transducer selected was a specially fabricated linear potentiometer, shown in Figure 6, which was used to detect musculoskeletal movement. One side of the double slider mechanism contacts a 1/8-inch strip of commercially available resistive material, and the other side contacts a narrow copper strip. This unique construction allows the 0.2-inch-thick transducer to be unobtrusive while detecting movements over a range of 4-1/2 inches Further refinements could reduce the thickness even further.

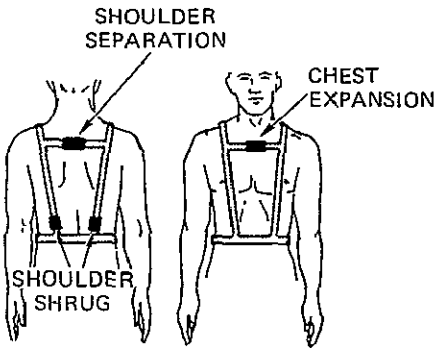

FIGURE 5 SOME AVAILABLE MUSCULOSKELETAL CONTROL SITES

Use of this transducer in the laboratory consisted of mounting it on a shoulder harness that incorporated a narrow elastic band. Tension was then adjusted such that when the person was in a relaxed state, the transducer slider mechanism was at its midpoint. With this scheme, the person could control the coordinated motion accurately without experiencing any fatigue. In addition, small, extraneous body movements did not couple with the coordinated motion. Since the transducer measured a mechanical quantity, no difficulties were encountered with bodily or environmental conditions.

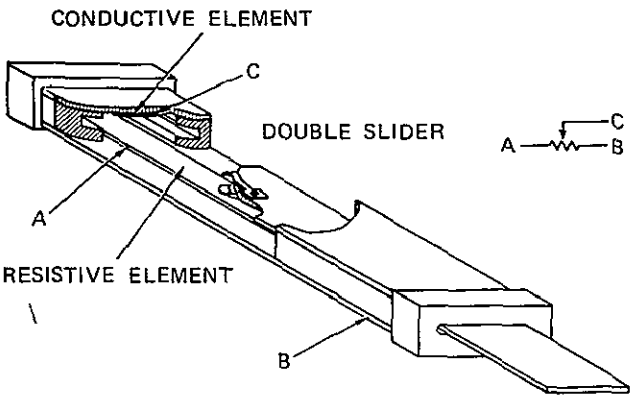

FIGURE 6 A SINGLE PROPORTIONAL INPUT TRANSDUCER

Motion Vector Determination

A general purpose method was employed to determine each of the motion vectors used to produce the coordinated motions enumerated above. In each case, the initial step was the determination of the absolute joint angles as a function of time for each desired motion. This was accomplished by using a small digital computer to record the signals from a Rancho master brace while it was being moved through the desired motion. These data were then plotted and examined.

One such plot for the eating motion is shown in Figure 7. Examination of this figure reveals that, except for the starting and finishing phases of the motion, the joint angle functions could be approximated by a straight line. In this way, the linearized movement of Figure 7(b) was obtained such that the starting and finishing joint angles of each joint remained the same as in the original data. Using the linearized data, the joint that experienced the greatest net change was determined. This joint, depending upon whether the function had increased or decreased, was assigned a +1 or a -1 entry in the motion vector. The remainder of the joint functions were then scaled against this entry, and appropriate fractional entries lying within the range of ± 1 were entered in the motion matrix for each joint Thus, when the motion matrix is applied to the proportional input, one joint experiences the full magnitude of the input signal, whereas the other joints experience some fraction of the signal. This results in the desired coordinated motion.

This procedure seems to be adequate, except in the case--shown in Figure 8(a)--of a joint angle recording for the reach-behind-the-back motion. This figure shows that during the motion, Joints 1 and 2 (shoulder rotation and shoulder flexion) are not monotonic functions, and thus, the previously used linearization scheme cannot be applied. Instead, the motion is divided into two separate, piecewise-linear motions, as shown in Figure 8(b), and a motion vector is determined for each.

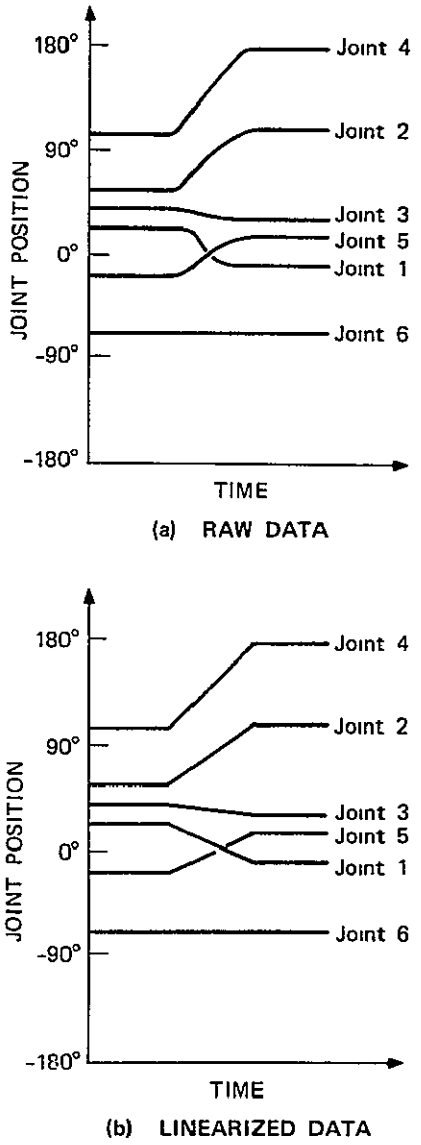

FIGURE 7 JOINT POSITIONS DURING THE EATING MOTION

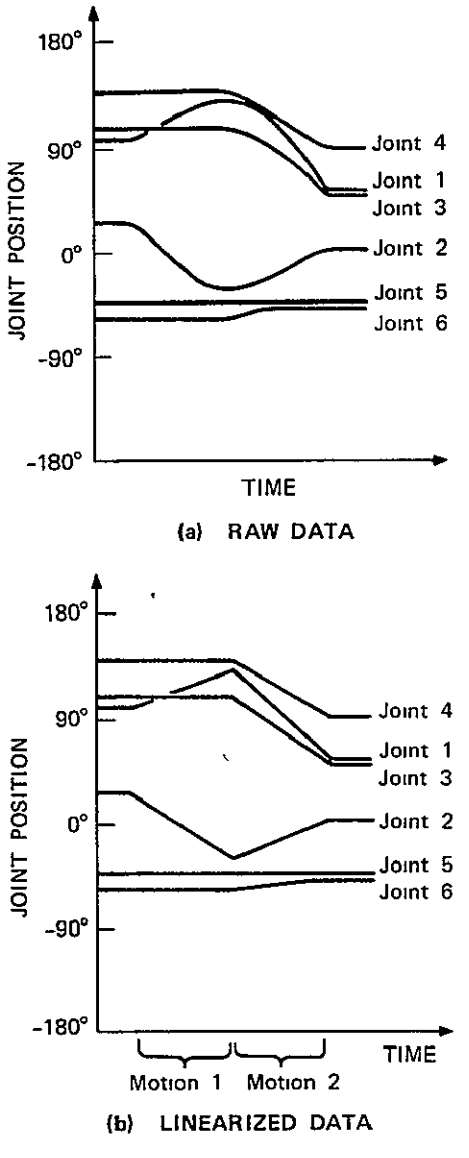

FIGURE 8 JOINT POSITIONS DURING THE REACH-BEHIND-THE-BACK MOTION

This and other compound motions were demonstrated in the laboratory using a Teletype to change the motion vectors. This was accomplished by stopping the arm partway through the motion, changing the vector, and then resuming the motion. This procedure worked reasonably well and allowed verification that the subdivision of a compound motion into two or more simple motions was valid, and did yield the desired motion. However, this procedure was extremely awkward in that the operator was required to judge the point at which the vector should be changed, and real-time operation was interrupted.

This highlights an area in which further work is necessary. If a set of completion criteria can be established such that when they are satisfied, a new motion vector will be applied, then it will be possible to change the motion vectors automatically, independent of human judgment, while maintaining smooth operation. This set of completion criteria might be based on the time since the initiation of the motion, the ratios of joint angles, the positions of certain critical joints, or combinations of these factors. If this can be accomplished, then any motion, regardless of how complex, can be performed using a single analog input in the present control scheme.

Microcomputer Controller

Two of the major drawbacks to the realization of this control scheme in a commercially feasible control system are the relatively large size of a minicomputer and its expense. An attempt is currently being made to circumvent these problems through the use of a microcomputer.

Recent advances in integrated circuit technology have brought with them commercially available computer components (Intel Corporation Catalog, 1973)

that, due to their small sizes and low power requirements, are prime candidates for a prosthetic controller. The heart of this system is the four-bit central processor unit (CPU) with a 10.8-microsecond instruction cycle time. These CPUs are small (0.8 × 0.3 × 0.1 inch), they can be driven with flashlight batteries, they have an instruction repertoire of 45 instructions, and they cost under $30 each in small quantities. In addition, they are directly compatible with both read-only and random-access memory chips (ROMs and RAMs). The memory chips are of this same small size, and in small quantities cost $15 each.

To demonstrate the feasibility of substituting a microcomputer set that could perform all of the functions of the minicomputer controller, the microcomputer shown in Figure 9 has been constructed.

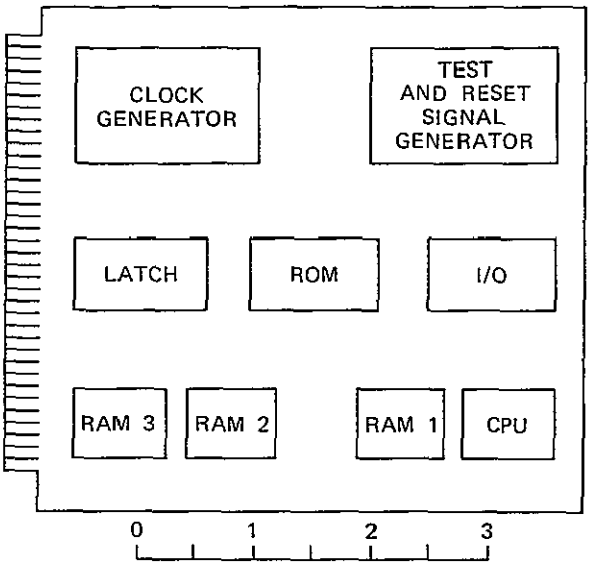

FIGURE 9 CONFIGURATION OF THE MICROCOMPUTER CONTROLLER

Scale in inches

If such a controller should ever be made commercially available, then the three integrated circuit chips shown as latch, ROM, and I/O chips in Figure 9 could be replaced with a single chip of the same dimensions as the CPU chip, thus further reducing the size and cost of the controller

The functional implementation of the present control scheme on the microcomputer set of Figure 9 takes the form shown in Figure 10 In this scheme, both the single proportional control signal and the control algorithm are substantially identical to those previously discussed The major differences lie with the computer itself and with the form of the digital input signal.

The microcomputer implementation of the control scheme will consist of a small driver program stored together with approximately 15 different motion vectors in read-only memory The Teletype of Figure 4 will be removed from the system and will be replaced

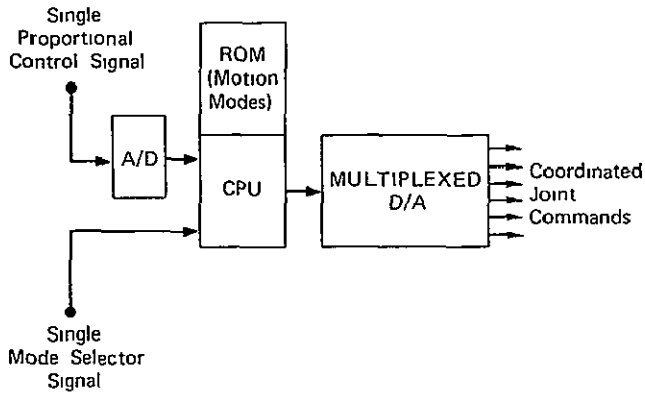

FIGURE 10 FUNCTIONAL IMPLEMENTATION OF THE CONTROL ALGORITHM

The proportional input from the shoulder sensor generates the different joint motions in accordance with the motion vector previously selected by the mode selector signal

by a separate command signal The digital command signal will be used to effect the selection of various coordinated motions, which can be either simple or compound and which will take the form of a one-bit binary signal This signal might be generated by a simple switch that is activated by a shoulder shrug, as shown in Figure 5. The command signal could be interpreted as a variety of Morse code, with the duration of each "on" pulse determining whether that pulse was a dot or a dash. Alternatively, if two shoulder shrug signals were used, then one shoulder could be assigned to correspond to the "dot" signal and the other to the "dash." Although this scheme adds complexity to the harness, it reduces the software burden.

THE USE OF SENSORY FEEDBACK

In discussing human perception, Johnson (1969) has described the following coordinated control scheme

> Hammering a nail is a formal procedure with informal variations it is a behavioral style ... [The carpenter] is participating in a multiple-loop process and will establish, without conscious effort, a predictive model of the properties of each impact. Any variation from the expected pattern--such as one that might indicate the bending of the nail or the approach to a hard knot--will be immediately apparent to him because his style will be changed by it. He "senses" it, not because something has been done to him as a raw input from the outside, but because change in the environment has intervened in a loop process in which he is actively engaged, and it has altered the properties of the loop.

This control scheme is a formal, goal-oriented procedure that is proportionally controlled and flexible and that appears to be realizable. What is absent are those informal variations that transform the formal procedure into a behavioral style. The essential

aspect of introducing variation into formal procedure is that of sensory input. Sensory input allows a control system to detect subtle variations of a changing environment so that it can adapt to these changes. Since man cannot adapt to a change of which he is unaware, it would be quite unreasonable to expect a machine to do so.

Sensory feedback signals can be used in either or both of two fashions; they can be fed back to the person, thus requiring that he evaluate them and initiate some action, or they can be fed back to the control system such that the resulting action is invisible to the person. In a prosthetics application, a combination of the two may be the optimal use of sensory feedback.

Mann and Reimers (1969) have had some success in providing kinesthetic feedback of the elbow position of the "Boston Arm" to the amputation stump using a cutaneous display scheme. Bach-y-Rita and Collins (1969) have proposed a display format whereby kinesthetic feedback of the five relative forearm angles could be provided to the amputation stump. This type of sensory feedback might well prove to be extremely advantageous in sensing many of the gross motions of a many degrees-of-freedom prosthetic device. Thus, a wearer performing the eating motion described above might be able to sense the gross position of the prosthesis without depending upon visual feedback. This would allow him to focus less attention on prosthetic control and to engage in other activities, such as dinner conversation.

The method of providing feedback via cutaneous stimulation does not seem particularly well suited to detecting many of the finer sensations upon which adaptation to the environment is based. Instead, signals from small, sensitive tactile sensors or other types of sensors can be input directly to the microcomputer controller. With this ability to sense the most subtle quantities directly, the prosthetic controller can assume a more active role in relieving the wearer of the burden of control. Kato et al. (1969) have used tactile sensors in a prosthetic controller to grab an object automatically when it is touched and to hold an object without crushing it.

In the technology of remote manipulation and automation, signals from tactile sensors have been used as inputs to computer algorithms to perform various manipulation tasks. Much of this technology can be successfully utilized in a prosthetic controller. As an example, consider the shoulder disarticulation amputee who desires to pick up a glass of water. If he uses his single proportional input to control the reach-out motion, then the arm moves out and the forearm remains level. If the amputee happens to be sitting slightly to the left or to the right of the glass, then, although the terminal device may touch the glass, it might be slightly misaligned such that proper prehension is not possible. If this brief touch could initiate a simple alignment algorithm, then the amputee could successfully retrieve the glass without moving his entire body. Thus, once again, sensory input can be used to reduce further the level of conscious effort required. In addition, such sensory input signals might prove to be invaluable elements of the set of completion criteria used to determine when motion vectors should be changed.

GENERALITY OF APPROACH

The single-input prosthetic controller demonstrated is an extremely general one. It is quite reasonable to expect that this controller will perform useful coordinated motions in response to a single, proportional, goal-oriented signal, regardless of the device to be controlled. In fact, whether it controls a device having two degrees of freedom or many more than seven degrees of freedom, the control scheme remains identical. The only difference in the latter case is the increased size of the vectors involved and the greater number of sensory input signals that may require processing. Thus, with an increasing number of degrees of freedom, the control scheme should be expected to exceed the degree of complexity that a microcomputer controller can conveniently process. The only requirement levied on the use of this controller is that the degrees of freedom that it is intended to control should be related in a functional manner such that their simultaneous control appears logical.

Historically, the role of an above-knee prosthesis has been a passive one. Kato and Minowa (1972) have been successful in devising a control scheme for an externally powered above-knee prosthesis having a single degree of freedom. Their control scheme is based on a classification of terrain (e.g., flat, graded, staircase) and the walking speed of the amputee. The continuums of terrain and walking speed have each been lumped into three categories. If both a powered ankle joint and a coordinated motion controller equipped with appropriate sensory inputs were to be added to this system, an amputee could conceivably walk and make undetected transitions into running or climbing on uneven terrains without being as conscious of the control problems.

When trying to replace the functions of the human hand, the enormity of the control problem becomes more obvious. The human hand possesses 22 separate degrees of freedom. A coordinated motion controller would significantly alleviate the control problem, and many of the common hand functions could be obtained with a single input signal. Here the problem that persists is one of mechanical design.

As a final example, consider the case of the bilateral amputee. Many of his desired abilities are based on holding an object stationary in one hand while performing some operation with the other. It then appears logical to view the two arms as a single system having 14 degrees of freedom Even the most limited repertoire of coordinated motions would be of enormous benefit to this type of amputee.

REFERENCES

Bach-y-Rita, P., and Collins, C. C , Sensory substitution and limb prosthesis. Proceedings of Third International Symposium on External Control of Human Extremities, Dubrovnik, Yugoslavia, August 1969, pp. 9-21.

Carlson, L. E., Multi-mode control of an above-elbow prosthesis. Technical Report 61, Biomechanics Laboratory, University of California, Berkeley, California, September 1971.

Externally powered terminal devices. Report of the Seventh Workshop Panel on Upper-Extremity Prosthetics, Committee on Prosthetics Research and Development, Santa Monica, California, July 1969.

Hoerner, E F., Heidelberg pneumatic arm prosthesis. Arch. Phys. Med and Rehab., July 1958, Vol. 39, pp. 411-416.

Intel Corporation catalog. Intel Corporation, Santa Clara, California, February 1973.

Johnson, A. R , Self-organizing control in prosthetics. Proceedings of Third International Symposium on External Control of Human Extremities, Dubrovnik, Yugoslavia, August 1969, pp. 1-8.

Kato, I , and Minowa, K., A way of the above-knee prosthesis control. Presented at the Fourth International Symposium on External Control of Human Extremities, Dubrovnik, Yugoslavia, August 1972.

Kato, I., Yamakawa, S , Ichikawa, K., and Sano, M., Multifunctional myoelectric hand prosthesis with pressure sensory feedback system. WASEDA HAND 4P, Proceedings of Third International Symposium on External Control of Human Extremities, Dubrovnik, Yugoslavia, August 1969, pp 155-170.

Lawrence, P., Herberts, P., and Kadefors, R., Experiences with a multifunctional hand prosthesis controlled by myoelectric patterns. Presented at the Fourth International Symposium on External Control of Human Extremities, Dubrovnik, Yugoslavia, August 1972.

Mann, R. W., and Reimers, S. D , Kinesthetic sensing for the EMG controlled "Boston Arm." Proceedings of Third International Symposium on External Control of Human Extremities, Dubrovnik, Yugoslavia, August 1969, pp. 231-243.

Radnjic, D., and Long, C., II, Why myoelectric control is so difficult Proceedings of Third International Symposium on External Control of . Human Extremities, Dubrovnik, Yugoslavia, August 1969, pp. 59-67.

Whitney, D E., Resolved rate control of manipulators and human prostheses. IEEE Transactions on Man-Machine Systems, June 1969, Vol. MMS-10, pp. 47-53.

Appendix F

COMPARISON OF SEVEN PERFORMANCE MEASURES IN A TIME-DELAYED MANIPULATION TASK

The paper, consisting of the following abstract, the contents of Section II of this report, and the matching references from the Bibliography, was presented at the Tenth Annual Conference on Manual Control held at Wright-Patterson Air Force Base, Ohio, April 9-11, 1974. The paper will be published with the conference proceedings as a technical report by the Air Force Flight Dynamics Laboratory.

COMPARISON OF SEVEN PERFORMANCE MEASURES IN A TIME-DELAYED MANIPULATION TASK*

John W. Hill
Stanford Research Institute
Menlo Park, California 94025

ABSTRACT

Real-time performance data was collected during a pick-up task carried out with Rancho master-slave manipulator using a minicomputer-based data taker. Motions on all seven master and all seven slave joints as well as instantaneous electrical power consumed were continuously monitored. In addition to the usual task-time measurements, computer algorithms to integrate the energy consumed and to count and time the number of moves were implemented. In addition to these measures, several derived measures as the fraction of time moving (MRATIO) and mean time per move (MBAR) were obtained in an off-line analysis. A major goal of these experiments is to compare the seven different measures of performance to determine which are best for evaluating particular experimental conditions. Preliminary results of the time delay experiment indicate that two new measures, MRATIO and MBAR, are almost an order of magnitude more sensitive than task time, the conventional measure, in determining performance changes with transmission delays in the range from 0.0 to 1.0 second. Taking advantage of the operator's move-and-wait strategy, we also show how the energy consumed in carrying out a task can be reduced by a factor of three in the one-second transmission-delay case.

---

*This work was supported by the National Aeronautics and Space Administration under Contract NAS2-7507 to SRI.

Appendix G

LINC-8 AUTOMATED PERFORMANCE MONITORING SYSTEM

Appendix G

LINC-8 AUTOMATED PERFORMANCE MONITORING SYSTEM

A performance monitor package was created to study (1) the complex move-and-wait strategy and (2) the movement and waiting times with different transmission delays, different visual and tactile feedback, and different arms. The performance monitor can measure and tabulate the movement and waiting times with considerably greater accuracy and reliability than can a human observer with a stopwatch

The performance monitor package consists of an on-line program for data logging and several off-line programs for numerical analysis. During the experimental runs, a high-speed disk memory logs on-line data. Upon completion of the experiment, contents of the disk are copied to magnetic tape for permanent storage. Different off-line programs are used to search the log and to extract the desired performance indices. This Appendix gives the description of the components of this performance measuring system which is based on a LINC-8 Computer.

A. Using the On-Line Performance Logger

The control codes available to the experimenter for accumulating and logging data are shown in the control tree of Figure G-1. A typical control sequence for logging two replications of an experiment is shown in Figure G-2, where information typed by the operator is underlined.

B. Operation of the On-Line Performance Logger

The on-line performance logger detects the beginning and end of moves by using derivatives of the individual joint angles. In total, 14

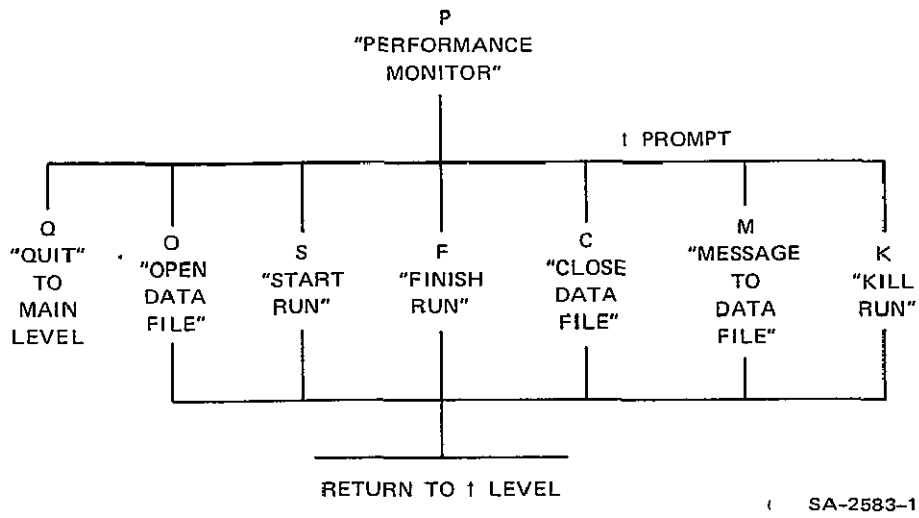

FIGURE G-1 COMMAND STRUCTURE FOR THE ON-LINE PERFORMANCE LOGGER

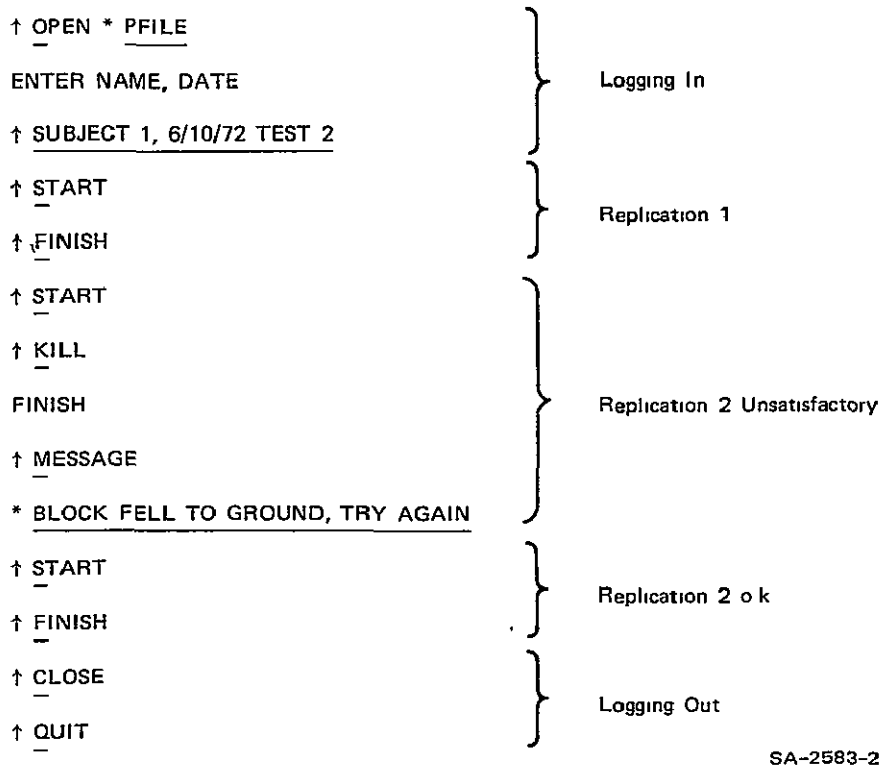

FIGURE G-2 TYPICAL PERFORMANCE LOGGER CONTROL SEQUENCE

derivatives (seven master and seven slave joint angles) are updated and digitally filtered every 1/30 of a second. If any of the master or slave joints exceeds a predetermined threshold for motion during a 1/30-second period, a note of the fact is made in separate master and slave move detection queues. These queues (software shift registers) record whether or not a move was detected during 12 successive 1/30-second intervals. From these intermediate data, decisions are made to determine whether a master or slave move has begun or ended. The flow chart of the performance monitor is given in Figure G-3. The criteria for detecting the beginnings and ends of moves that have proved successful are defined below:

- Move criterion--A move begins when the velocity threshold is exceeded during the current 1/30-second interval and will be exceeded on five of the next 12 intervals.
- Done criterion--A move is done when the velocity threshold is not exceeded during the current interval and will not be exceeded more than once in the next 12 intervals.

Two total task measurements are also obtained. The on-line program counts the number of 1/30-second intervals taken to complete a task and logs the total at the end to permit the calculation of task duration. Additionally, it accumulates the current delivered by the 24-volt servo power supply every 1/30 second and logs the total at the end of the run to permit calculation of the total energy consumed. The first three numbers following the "/" symbol are the triple precision accumulation of the current, and the next two are the double precision accumulation of the task time.

Messages entered during the run are printed directly in the data log. Entering the "kill" message during a run causes a "?" symbol to print out on the data log and further logging to cease. The meanings of the various symbols used in the data log are given in Table G-1. An example of the data log for Run Number 1 of Subject SM is given in Figure G-4. The first number and symbol, 0036 >, represents the one-second time delay in thirtieths of

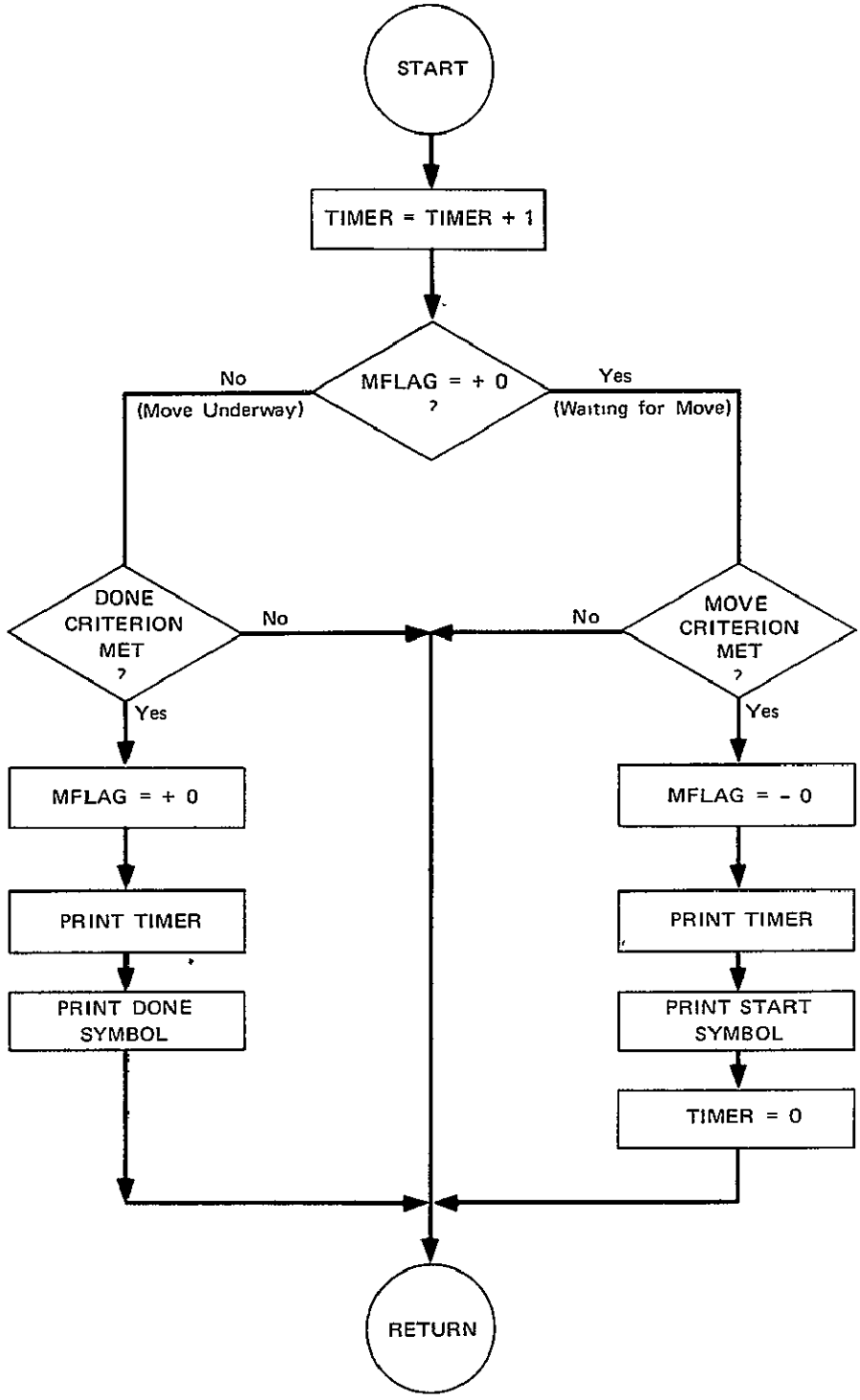

FIGURE G-3 PERFORMANCE LOGGER MOVE DETECTION ALGORITHM

Table G-1

SYMBOLS USED BY ON-LINE PERFORMANCE LOGGER

Symbol	Meaning
$	Master move detected, counter = 0
#	Master move ended
@	Automatic move initiated, counter = 0
↑	Slave move detected
•	Slave move ended
"carriage return"	Counter before automatic or manual move begun
>	Time delay
/	Power and time printout follow
?	Kill feature initiated; ignore data from this run
*	Identifying message follows
"end of record"	End of replication.
"end of file"	End of run

```
*SUBJECT SM BLOCK PICKUP AND DROP
0036>0036
0000$0043↑0052#0110•0111
0000$0020#0043↑0063•0073
0000$0017#0043
0000$0000↑0024•0043↑0046#0077
0000$0011•0027#0106↑0146•0157
0000$0043↑0254#0316
0000$0001•0034#0042↑0100•0154
0000$0017#0046
0000$0000↑0020#0066
0000$0004•0024#0045↑0060
0000$0010•0040↑0042#0101•/0000 0014 2277 0000 1626
```

FIGURE G-4 EXAMPLE OF DATA LOG

a second (in octal). On the last line, the first three numbers after the "/" are the accumulated current, and the next two are the accumulated run time in thirtieths of a second (octal).

C. Off-Line Timing Program

A computer program for obtaining particular performance figures from the data log has been developed. The indices obtained and the means of obtaining each of them is given in Table G-2.

Table G-2

PERFORMANCE INDICES

Symbol	Definition	Method of Obtaining Measurement
N_m	Number of master moves	Counting the number of "#" symbols
N_s	Number of slave moves	Counting the number of "." symbols
E_t	Task energy	$\frac{V}{Rate}$ times the current accumulator
T_t	Task time	$\frac{1}{Rate}$ times clock accumulator
T_m	Total moving time	$\frac{1}{Rate}$ times sum of master move times; the master move time for each move precedes the "#" symbol.
R_m	Moving ratio	T_m divided by T_t
$\bar{M}_m$	Mean movement time	T_m divided by N_m

The printout from the timing program for two subjects is shown in Figure G-5. Each of the data files analyzed consists of 11 replications

```
.........................
EXAMIN*SM3

SUBJECT SM BLØCK PICKUP AND DRØP
TIME DELAY = 1.00
```

RUN	M-MØVES	S-MØVES	ENERGY	TIME	MTIME	MRATIØ	MBAR
1	11	10	1.41	30.5	13.9	.456	1.26
2	11	12	1.91	35.4	13.4	.380	1.22
3	10	8	1.21	27.4	12.0	.436	1.20
4	50	41	5.58	118.4	47.4	.400	.94
5	20	17	3.29	58.0	27.3	.471	1.36
6	9	8	1.55	30.4	16.3	.536	1.81
7	27	24	3.69	69.0	32.7	.474	1.21
8	23	17	3.77	63.5	29.4	.464	1.28
9	10	8	1.28	25.7	10.8	.419	1.08
10	8	5	1.35	29.2	16.9	.578	2.11
11	52	44	8.41	159.1	68.2	.428	1.31
AVG	20.99	17.63	3.04	58.8	26.2	.446	1.24

```
.........................
EXAMIN*LM3

SUBJECT LM BLØCK PICKUP AND DRØP
TIME DELAY = 1.00
```

RUN	M-MØVES	S-MØVES	ENERGY	TIME	MTIME	MRATIØ	MBAR
1	50	46	6.44	130.8	66.4	.507	1.32
2	10	13	1.41	30.7	17.0	.552	1.70
3	13	9	1.40	28.3	11.1	.390	.85
4	29	29	4.59	97.7	30.9	.316	1.06
5	16	14	1.84	37.7	15.6	.415	.97
6	27	22	3.48	68.4	38.0	.555	1.40
7	10	6	1.46	29.9	16.4	.548	1.64
8	19	16	2.34	46.1	21.4	.464	1.12
9	12	11	1.72	35.3	17.9	.508	1.50
10	9	9	1.52	30.9	17.6	.568	1.95
11	21	16	2.37	52.0	20.9	.402	.99
AVG	19.64	17.36	2.60	53.5	24.8	.464	1.26

```
.........................
```

FIGURE G-5 PRINTOUT OF TIMING ANALYSIS

of a pickup and drop task carried out with a time delay of one second. The performance indices are printed out in the same order as they are defined in Table G-2. Times are in seconds and energy is in kilowatt seconds.

D. Off-Line Histogram Program

In order to investigate changes in the operator's strategy under experimental conditions such as time delays, we wrote a program to obtain the distribution of move times. The algorithm is essentially that of the well-known "pulse-height analyzer."

In the move-time analyzer there are 51 bins for accumulating counts. When a master move (indicated by a "#" in the data log) is found, the appropriate bin is incremented by one to count the move. The first bin is for move durations of 1/30, 2/30, and 3/30 second (0.03 to 0.1 second); the second bin is for durations of 4/30, 5/30, and 6/30 second (0.13 to 0.2 second); and so the bins continue to the highest bin which accumulates all moves greater than 150/30 seconds (5 seconds). After all the desired data logs are searched, a printout of the bins can be requested.

An example of using the program and its resultant output is shown in Figure G-6. Here the data analyzed are the same as those of Figure G-5. As Figure G-6 indicates, there were 22 test runs and 447 master moves; the mean value of the ensuing distribution is 1.257 second. Following the totals is printout of the bin totals. The first number on each line is the bin count, and the second is the lower bound of each bin in seconds. The bin counts are illustrated graphically by printing one space for each move in the bin followed by an asterisk.

As in Figure G-6, whenever a moderate number (447) of moves is tabulated in this way, the distribution is noisy. For purposes of comparing two distributions to see how they differ, it is desirable to smooth the

```
HISTOGRAM FROM*SM3
DELAY = 1.00
..........AND FROM*LM3
..........AND FROM*H\ E

      22 RUNS      447 M-MOVES    1.257 SEC=MBAR


--------+---------+---------+---------+---------+---------+---------+---------+---
  0  .0 *
 13  .1              *
 27  .2                        *
 29  .3                          *
 37  .4                                    *
 27  .5                        *
 37  .6                                    *
 26  .7                       *
 29  .8                          *
 29  .9                          *
 24 1.0                     *
 19 1.1                  *
 20 1.2                   *
 14 1.3              *
 14 1.4              *
 15 1.5               *
  9 1.6         *
  5 1.7      *
  8 1.8        *
  2 1.9   *
  5 2.0     *
  1 2.1 *
  2 2.2  *
  4 2.3    *
  1 2.4 *
  3 2.5   *
  3 2.6   *
  1 2.7 *
  0 2.8 *
  2 2.9  *
  3 3.0   *
  4 3.1    *
  5 3.2     *
  2 3.3  *
  2 3.4  *
  1 3.5 *
  1 3.6 *
  2 3.7  *
  0 3.8 *
  1 3.9 *
  3 4.0   *
  1 4.1 *
  1 4.2 *
  1 4.3 *
  2 4.4  *
  0 4.5 *
  0 4.6 *
  1 4.7 *
  1 4.8 *
  1 4.9 *
  9 5.0         *
--------+---------+---------+---------+---------+---------+---------+---------+---
```

FIGURE G-6 USE AND OUTPUT OF THE HISTOGRAM PROGRAM

distribution mechanically rather than by hand. As an option, the user may apply the smoothing function

$$S_i = \tfrac{1}{4} C_{i-1} + \tfrac{1}{2} C_i + \tfrac{1}{4} C_{i+1}$$

which causes each bin in the smoothed function S_i, to contain half the counts in the same bin of the original function, C_i, and one-quarter the counts in each neighboring bin, C_{i+1} and C_{i-1}. The results of applying this smoothing function to the distribution obtained in Figure G-6 are shown in Figure G-7.

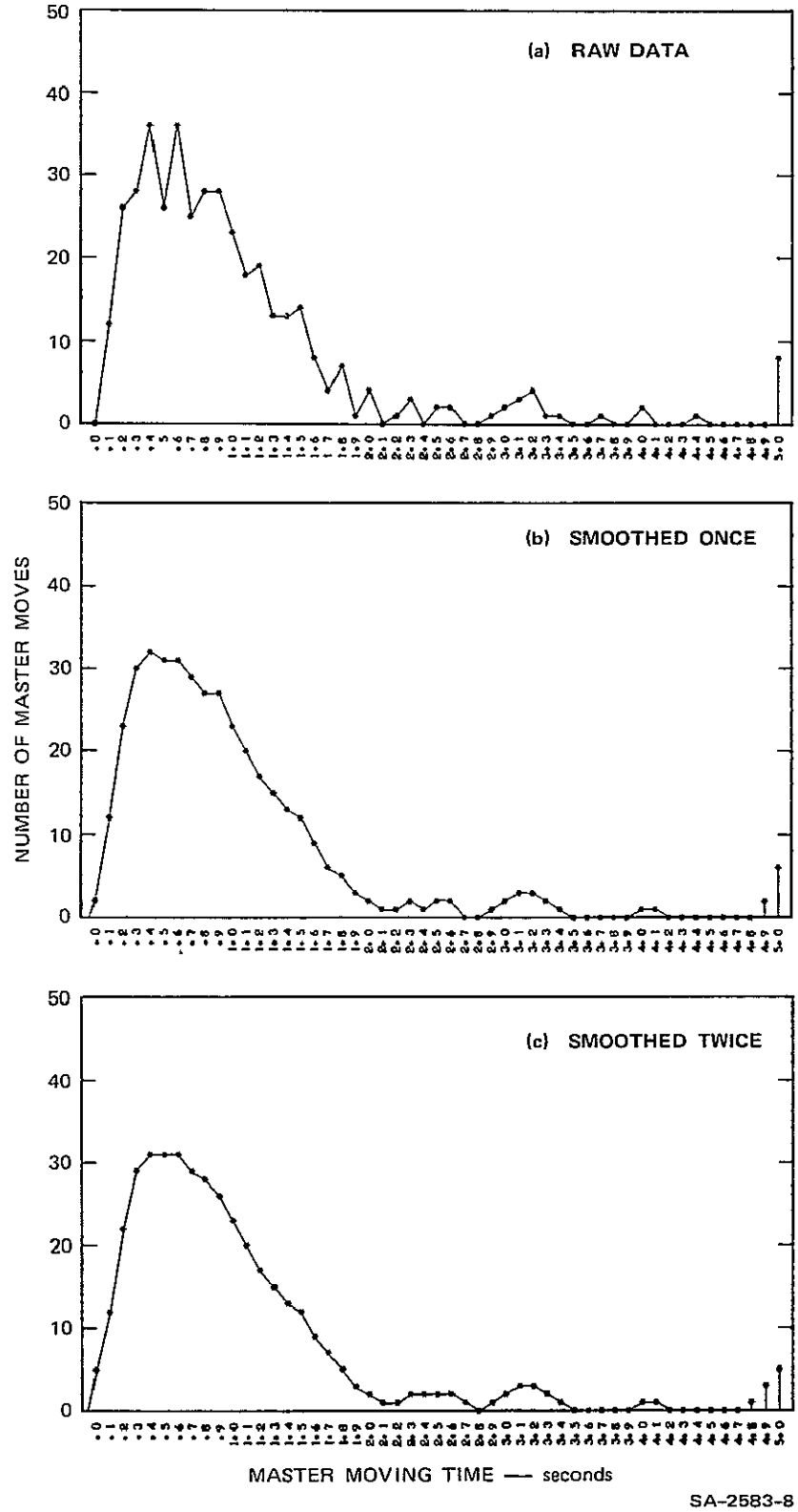

FIGURE G-7 EFFECT OF SMOOTHING ON DISTRIBUTION OF MASTER MOVING TIMES

Appendix H

STRING TENSIONER TRANSFORMATIONS

Appendix H

STRING TENSIONER TRANSFORMATIONS

The use of three orthogonal strings to measure the position of the end effector during a task, as previously described in Section VII, only gives approximate results. Calculations show that in motions of 10 inches with strings 60 inches long, errors in position of several inches can be incurred by assuming orthogonality. Reducing the working area and centering it on the origin can make the assumption of orthogonality a reasonable assumption. For example, in a 10-inch cube centered on the origin and 60 inch strings, position and velocity errors of less than 10 percent can be expected at the edges of the working area. However, we wished to place the origin of the coordinate system on one edge of the task for high-accuracy measurements at the origin and follow trajectories beginning up to 20 inches from the origin. In this case, position and velocity errors exceeding 17 percent will occur. Transformations were used to correct these curvilinear measurements.

An implementation of the transformations in the form of a FORTRAN subroutine is shown in Figure H-1. The call to the subroutine is with string positions x, y, and z, and string velocities Vx, Vy, and Vz (curvilinear coordinates). The return is with orthogonal position XG, YG, and ZG, and true vector velocity VXG, VYG, and VZG. The indicator IBAD, which is included as a system debugging check, is a flag for bad data.

Using a computer simulation of the string system and the FORTRAN subroutine, transformation accuracy did not require extreme accuracy in string length or placement of the tensioners. A 1-percent error in

```
      SUBROUTINE GEOM(X,Y,Z,VX,VY,VZ,XG,YG,ZG,VXG,VYG,VZG,IRAD)
C     THIS SUBROUTINE ACCEPTS THE LENGTHS OF THE MEASUREMENT STRINGS AS
C     GIVEN FROM THE DATA TAKER AND RETURNS X,Y,Z POSITIONS AND
C     VELOCITIES TRANSFORMED TO ORTHOGONAL COORDINATES.
C     A DATA CARD MUST BE INCLUDED IN THIS SUBROUTINE, CONTAINING THE
C     LOCATION OF THE STRING MOUNTING POINTS REFERENCED TO THE
C     ORIGIN.  (STRING X IS AT (X0,0,0), ETC.)
C     RETURN IS AT SG WITH XG,YG,ZG, AND VXG,VYG,VZG.
C     MATRIX A CONTAINS THE TRANSFORMATION MATRIX FOR VELOCITIES.
C     MATRIX B CONTAINS THE INVERSE OF A.
      DIMENSION A(3,3)
      DIMENSION B(3,3)
      DATA X0,Y0,Z0/108.06,67.06,61.375/
      IRAD=1
      SX=X0-X
      SY=Y0-Y
      SZ=Z0-Z
      C1=SX**2-X0**2-SY**2+Y0**2
      C2=SX**2-X0**2-SZ**2+Z0**2
      D=1.+(X0**2)*(1./Y0**2+1./Z0**2)
      E=(C1/Y0**2+C2/Z0**2-2.)*X0
      C=C1**2/(4.*Y0**2)+C2**2/(4.*Z0**2)-SX**2+X0**2
      XTEST=E**2-(4.*D*C)
      IF(XTEST.GT.0.) GO TO 5
      IRAD=2
      GO TO 55
    5 XG=(-E-SQRT(XTEST))/(2.*D)
      YG=(X0/Y0)*XG+C1/(2.*Y0)
      ZTEST=SX**2-X0**2-C1**2/(4.*Y0**2)+(X0*(2.-C1/Y0**2))*XG-(1.+X0**2
     1/Y0**2)*XG**2
      IF(ABS(ZTEST).GT..001) GO TO 1
      ZG=0.0
      GO TO 35
    1 ZG1=SQRT(ZTEST)
C     CHECK FOR CALCULATED POINTS RETURNING CORRECT STRING LENGTHS.
      S2T=SQRT(XG**2+YG**2+(Z0-ZG1)**2)
      IF(SZ-S2T-.001) 20,2,30
    2 ZG=ZG1
      GO TO 35
    3 ZG=-ZG1
   35 TX=ATAN(YG/(X0-XG))
      TY=ATAN(ZG/(Y0-YG))
      TZ=ATAN(XG/(Z0-ZG))
      PX=ATAN(ZG/SQRT((X0-XG)**2+Y0**2))
      PY=ATAN(XG/SQRT((Y0-YG)**2+ZG**2))
      PZ=ATAN(YG/SQRT((Z0-ZG)**2+XG**2))
      A(1,1)=COS(PX)*COS(TX)
      A(1,2)=-COS(PX)*SIN(TX)
      A(1,3)=-SIN(PX)
      A(2,1)=-SIN(PY)
      A(2,2)=COS(PY)*COS(TY)
      A(2,3)=-COS(PY)*SIN(TY)
      A(3,1)=-COS(PZ)*SIN(TZ)
      A(3,2)=-SIN(PZ)
      A(3,3)=COS(PZ)*COS(TZ)
      DET=A(1,1)*A(2,2)*A(3,3)+A(1,2)*A(2,3)*A(3,1)+A(1,3)*A(2,1)*A(3,2)
     1-A(1,3)*A(2,2)*A(3,1)-A(1,2)*A(2,1)*A(3,3)-A(1,1)*A(2,3)*A(3,2)
      ABDET=ABS(DET)
      IF(ABDET.GT.0.) GO TO 45
      IRAD=3
      GO TO 55
   45 CONTINUE
      B(1,1)=(A(2,2)*A(3,3)-A(2,3)*A(3,2))/ABDET
      B(1,2)=-(A(1,2)*A(3,3)-A(1,3)*A(3,2))/ABDET
      B(1,3)=(A(1,2)*A(2,3)-A(1,3)*A(2,2))/ABDET
      B(2,1)=-(A(2,1)*A(3,3)-A(2,3)*A(3,1))/ABDET
      B(2,2)=(A(1,1)*A(3,3)-A(1,3)*A(3,1))/ABDET
      B(2,3)=-(A(1,1)*A(2,3)-A(1,3)*A(2,1))/ABDET
      B(3,1)=(A(2,1)*A(3,2)-A(2,2)*A(3,1))/ABDET
      B(3,2)=-(A(1,1)*A(3,2)-A(1,2)*A(3,1))/ABDET
      B(3,3)=(A(1,1)*A(2,2)-A(1,2)*A(2,1))/ABDET
      VXG=VX*B(1,1)+VY*B(1,2)+VZ*B(1,3)
      VYG=VX*B(2,1)+VY*B(2,2)+VZ*B(2,3)
      VZG=VX*B(3,1)+VY*B(3,2)+VZ*B(3,3)
   55 RETURN
      END
```

FIGURE H-1 FORTRAN SUBROUTINE FOR STRING TENSIONER TRANSFORMATIONS

string length results in less than 0.5 percent error in position and velocity.

The position and velocity sensors together with the transformations were checked out with a known circular trajectory generated by a low-speed gear motor and 12-inch beam. The results indicate that position measurements can be made to about ± 0.05 inch and velocity measurements to about ± 0.1 inch per second.

REFERENCES

Annett, J., Golby, C. W., and Kay, H., The Measurement of Elements in an Assembly Task--The Information Output of the Human Motor System, Quart. J. exp. Psychol., 1958, 10, 1-11.

Black, J. D., Jr., "Factorial Study of Remote Manipulation with Transmission Time Delay," Report DSR 70283-16, Engineering Projects Laboratory, Department of Mechanical Engineering, Massachusetts Institute of Technology (December 1970).

Blackmer, R. H., et al., "Remote Manipulators and Mass Transfer Study," Technical Report AFAPL-TR-68-75 (AD 843767 from NTIS), Air Force Aero Propulsion Laboratory, Wright-Patterson Air Force Base, Ohio (November 1968).

Draper Labs, "Development of Multi-Moded Remote Manipulator Systems," Quarterly Progress Report 5, NASA Contract SNPN-54, Charles Stark Draper Laboratories, Massachusetts Institute of Technology (July 1972).

Ferrell, W. R., "Remote Manipulation with Transmission Delay," IEEE Transactions, Vol. HFE-6, pp. 24-32 (September 1965).

Fitts, P. M., The Information Capacity of the Human Motor System in Controlling Amplitude of Movement, J. exp. Psychol., Vol. 47, pp. 381-391, June 1954.

Fornoff, H., and Thornton, W. G., Experimental Evaluation of Remote Manipulator Systems, E. Heer, Editor, Remotely Manned Systems, California Institute of Technology, 1972.

Hill, J. W., and A. J. Sword, "Studies to Design and Develop Improved Remote Manipulator Systems," NASA Contractor Report CR-2238, National Aeronautical and Space Administration, Washington, D.C. (April 1973).

Jex, H. R., J. D. McDonnell, and A. V. Phatak, "A 'Critical' Tracking Task for Manual Control Research," IEEE Trans., Vol. HFE-7, pp. 138-144 (1966).

McRuer, D. T., D. Graham, E. Krendel, and W. C. Reisener, "Human Pilot Dynamics in Compensatory Systems; Theory, Models, and Experiments with Controlled Element and Forcing Function Variations," AFFDL TR 65-15, DDC Document No. AD 470 337 (July 1965).

A. B. Rechnitzer and W. Sutter, "Naval Applications of Remote Manipulation," paper presented at the First National Conference on Remotely Manned Systems, California Institute of Technology, Pasadena, California (September 1972).

Sheridan, T. B., and W. R. Ferrell, "Remote Manipulative Control with Transmission Delay," IEEE Transactions, Vol. HFE-4, pp. 25-29 (September 1963).

Vykukal, H. C., R. F. King, and W. C. Vallotton, An Anthromorphic Master-Slave Manipulator System, E. Heer, Editor, Remotely Manned Systems, California Institute of Technology, 1972.